

AB INITIO STUDIES OF A PENTACYCLO-UNDECANE CAGE LACTAM

by

Thishana Singh

Submitted in fulfilment of the requirements for the degree of PhD

in the School of Chemistry,

Faculty of Science and Agriculture,

University of Kwazulu-Natal, Durban, 2011

DECLARATION 1 - PLAGIARISM

I,, declare that

1. The research reported in this thesis, except where otherwise indicated, is my original research.
2. This thesis has not been submitted for any degree or examination at any other university.
3. This thesis does not contain other persons' data, pictures, graphs or other information, unless specifically acknowledged as being sourced from other persons.
4. This thesis does not contain other persons' writing, unless specifically acknowledged as being sourced from other researchers. Where other written sources have been quoted, then:
 - a. Their words have been re-written but the general information attributed to them has been referenced
 - b. Where their exact words have been used, then their writing has been placed in italics and inside quotation marks, and referenced.
5. This thesis does not contain text, graphics or tables copied and pasted from the Internet, unless specifically acknowledged, and the source being detailed in the thesis and in the Reference section.

Signed

.....

DECLARATION 2 – PUBLICATIONS

DETAILS OF CONTRIBUTION TO PUBLICATIONS that form part and/or include research presented in this thesis (include publications in preparation, submitted, *in press* and published and give details of the contributions of each author to the experimental work and writing of each publication)

Publication 1

T. Singh, K. Bisetty and H.G. Kruger; A Computational Study of the Mechanism of Formation of the Penta-Cyclo undecane (PCU) Cage Lactam, Trends and Perspectives in Modern Computational Science, Volume 7, 2006, pp. 511-514

Signed: _____

APPROVED FOR FINAL SUBMISSION

Supervisor: Prof. H.G. Kruger (Ph.D.)

Co-supervisor: Prof. K. Bisetty (Ph.D.)

Date

ACKNOWLEDGEMENTS

I would like to thank my supervisors Professors H.G. Kruger and Prof. K. Bisetty for their constant assistance, guidance, patience and much appreciated words of encouragement throughout the duration of this research project.

My sincere gratitude also goes to:

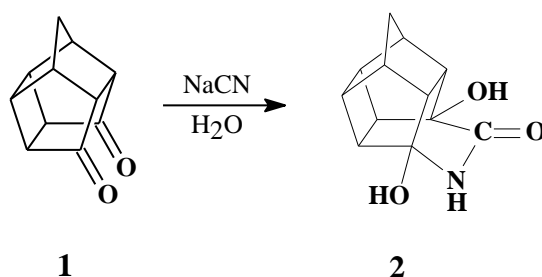
- (i) My friends and colleagues at the Durban University of Technology, Department of Chemistry, for their support, encouragement and assistance.
- (ii) The National Research Foundation (NRF), the Durban University of Technology's Centre for Research Management and Post Graduate Department of Studies for financial assistance.
- (iii) The Centre for High Performance Computing (CHPC) in Cape Town for the generous use of computer time on the e1350 IBM and the Sun clusters.
- (iv) The University of Kwazulu-Natal, Westville Campus, School of Chemistry for the office space during the period of my study leave.
- (v) Dr Bahareh Honarpavar for her assistance with the solvent calculations. Dr Glenn Maguire for painstaking proof-reading and the valuable suggestions for improving the dissertation.

A special thanks to my parents for their continuous support and encouragement throughout the duration of my studies.

"Jai Shree Krishna"

ABSTRACT

This study involved the application of computational techniques to determine the mechanistic pathways for the one-pot conversion of a pentacyclo-undecane (PCU) dione **1.1** to a pentacyclo-undecane cage lactam **1.2**.



A series of proposed mechanisms for this unique conversion was based on chemical intuition. Accordingly, *ab initio* quantum mechanical and a Density Functional (DFT) level of theory were employed to study the mechanistic pathways of the reaction. The primary goal of this study was to compute the relative difference in energies for the reactants, intermediates, transition states and products of the proposed reactions routes. The energy values calculated were used to obtain theoretical insight about the thermodynamic and kinetic preferences for the reaction. All calculations were performed using the Gaussian 09 series of programs; the visualisation platform was GaussView.

To save time with the labourious determination of the many possible intermediates and transition states, initial geometry optimisations were performed at the Hartree-Fock (HF) level of theory using the 6-31+G(d) basis set. In addition, most of the transition structures were established using the relaxed scan technique to obtain a suitable starting structure.

Full geometry optimisations were performed at the B3LYP level of theory using the 6-31+G(d) basis set. Transitions states were verified by using second-derivative analytical vibrational frequency calculations and the visual inspection of the movement of atoms associated with the transition. Further verification whether a specific transition state indeed connects a specific “reagent” with the next intermediate or product was obtained by intrinsic reaction coordinate (IRC) calculations.

A total of 10 local minima structures and 20 transition structures detailing 4 reaction mechanisms are presented and discussed in this study. The calculations were performed in the gas phase and then modelled in water, methanol, acetonitrile, dimethyl sulphoxide, carbon tetrachloride and dichloromethane to simulate solvent effects.

It has been established from previous experimental work that the reaction proceeds through a cyanohydrin intermediate which in all probability represents the rate determining step. Analysis of the theoretical data suggests that the computationally determined rate-determining step agrees with the experimentally suggested rate-determining step.

TABLE OF CONTENTS

Declaration 1 - PLAGIARISM	ii
Declaration 2 – PUBLICATIONS	iii
APPROVED FOR FINAL SUBMISSION	iii
Acknowledgements	iv
Abstract	v
Table of contents	vii
List of figures	ix
List of tables	xii
Chapter 1	1
INTRODUCTION	1
1.1 Computational Chemistry	1
1.2 Pentacyclo-undecane (PCU) Cage Compounds	2
1.3 Lactam formation	4
1.4 Proposed mechanisms	5
1.5 Aim of this study	8
Chapter 2	10
THEORETICAL TOOLS	10
2.1 Molecular Mechanics	10
2.2 Electronic Structure Theory	11
2.2.1 Semi-Empirical Models	12
2.2.2 The <i>Ab Initio</i> Method	13
2.2.3 Electron Correlation Methods	18
2.2.4 Basis Sets	24
2.3. Geometry Optimisation	27
2.3.1. Locating minima.....	29
2.3.2. Locating maxima	29
2.4. Frequency calculations and thermochemistry	34

2.5. Solvation studies	36
Chapter 3.....	42
Computational Details.....	42
3.1 The Gaussian 09 Program	42
3.2 The GaussView Program	43
3.3 The Relaxed Scan Calculation	44
3.4 Keywords used in G09	44
Chapter 4.....	49
The Computational Model.....	49
4.1 Computational model and calculation details for the stationary points	49
4.2 Computational model and calculation details for the transition state structures	50
4.3 Computational model and calculation details for the addition of solvents	53
Chapter 5.....	54
RESULTS AND DISCUSSION.....	54
5.1 Introduction	54
5.2 Mechanism 1	55
5.2.1 Mechanism 1 with different solvents.....	92
5.3 Mechanism 2	95
5.3.1 Mechanism 2 with different solvents.....	109
5.4 Mechanism 3 – Route 1.....	111
5.4.1 Mechanism 3-route 1 with different solvents	123
5.5 Mechanism 3 – Route 2.....	125
5.5.1 Mechanism 3route 2 with different solvents	138
Chapter 6.....	140
CONCLUSION	140
APPENDIX 1.....	143
Thermochemical data for 5.1 extracted from the frequency output file.....	143

Energy for 5.1 extracted from the frequency output file.....	143
Scheme of reaction for mechanism 1	145
Attempts to model Transition Structure 5.3.2 with HCN	151
APPENDIX 2.....	166
Scheme of reaction for mechanism 2	167
Attempts to model Transition Structure 5.17 with HCN	173
APPENDIX 3.....	187
Scheme of reaction for mechanism 3-route 1.....	188
Scheme of reaction for mechanism 3-route 2.....	207
References.....	225

SUPPLEMENTARY MATERIAL:

A CD accompanying this thesis includes the following:

- Text containing Chapters 1-6 (including References).
- Cartesian coordinates of all the 3D structures from Chapter 5.
- Frequency calculations of the TS's.

LIST OF FIGURES

Scheme 1	Conversion of the dione to the cyclic PCU ether 11 ^{36,34,37}	5
Scheme 2	Summary of the two proposed routes for the conversion of the cyclic ether 11 to the dihydroxylactam 2 ^{36,34,37}	7
Figure 2.1	Schematic representation of energy contributions in an MM system	10
Figure 2.2	Electron configuration diagram illustrating RHF and UHF	17
Figure 2.3	3D presentation of a typical PES ⁹⁶	28
Figure 2.4	Reaction coordinate diagram for the bimolecular nucleophilic substitution (S _N 2) reaction between bromomethane and the hydroxide anion ⁹⁷	30
Figure 2.5	Illustration of the LST and QST methods; energy maxima and minima are denoted by * and •, respectively. ⁵⁷	32
Figure 5.1	Mechanism 1 for the conversion of the PCU dione 5.1 to the lactam 5.2..	56
Figure 5.2	Gas phase Gibbs free energy for the mechanism proposed in Figure 5.1 ..	57

Figure 5.3	Graphical representation of the IRC reaction coordinate <i>vs</i> relative energy for structure 5.3.2	62
Figure 5.4	Graphical representation of energy <i>vs</i> reaction coordinate for structure 5.5.1 64	
Figure 5.5	Graphical representation of the IRC reaction coordinate <i>vs</i> relative energy for structure 5.5.1	65
Figure 5.6	Graphical representation of energy <i>vs</i> reaction coordinate for structure 5.5.2 66	
Figure 5.7	Graphical representation of the IRC reaction coordinate <i>vs</i> relative energy for structure 5.5.2	68
Figure 5.8	Graphical representation of the IRC reaction coordinate <i>vs</i> relative energy for structure 5.7.1	70
Figure 5.9	Graphical representation of energy <i>vs</i> reaction coordinate for structure 5.7.2 (Scan 1).....	71
Figure 5.10	Graphical representation of energy <i>vs</i> reaction coordinate for structure 5.7.2 (Scan 2).....	73
Figure 5.11	Graphical representation of the IRC reaction coordinate <i>vs</i> relative energy for structure 5.7.2	76
Figure 5.12	Graphical representation of energy <i>vs</i> reaction coordinate for structure 5.10.1	77
Figure 5.13	Graphical representation of the IRC reaction coordinate <i>vs</i> relative energy for structure 5.10.1	79
Figure 5.14	Graphical representation of the IRC reaction coordinate <i>vs</i> relative energy for structure 5.10.2	81
Figure 5.15	Graphical representation of the IRC reaction coordinate <i>vs</i> relative energy for structure 5.12 TS1	83
Figure 5.16	Graphical representation of the IRC reaction coordinate <i>vs</i> relative energy for structure 5.13 TS1	85
Figure 5.17	Graphical representation of energy <i>vs</i> reaction coordinate for structure 5.13 Scan	86
Figure 5.18	Graphical representation of the IRC reaction coordinate <i>vs</i> relative energy for structure 5.13 TS2.....	87
Figure 5.19	Graphical representation of energy <i>vs</i> reaction coordinate for structure 5.12 Scan	89
Figure 5.20	Graphical representation of the IRC reaction coordinate <i>vs</i> relative energy for structure 5.12 TS2.....	90
Figure 5.21	Mechanism 2 for the conversion of the PCU dione 5.1 to the lactam 5.2..	97
Figure 5.22	Gas phase Gibbs free energy for the mechanism proposed in Figure 5.21	98
Figure 5.23	Graphical representation of relative energy <i>vs</i> optimisation step number for structure 5.15.1	101

Figure 5.24 Graphical representation of the IRC reaction coordinate <i>vs</i> relative energy for structure 5.15.1	102
Figure 5.25 Graphical representation of the IRC reaction coordinate <i>vs</i> relative energy for structure 5.15.2	104
Figure 5.26 Graphical representation of the IRC reaction coordinate <i>vs</i> relative energy for structure 5.17	107
Figure 5.27 Mechanism 3-route 1 for the conversion of the PCU dione 5.1 to the lactam 5.2	113
Figure 5.28 Gas phase Gibbs free energy for the mechanism proposed in Figure 5.27	114
Figure 5.29 Graphical representation of energy <i>vs</i> reaction coordinate for structure 5.20.1	117
Figure 5.30 Graphical representation of the IRC reaction coordinate <i>vs</i> relative energy for structure 5.20.1	119
Figure 5.31 Graphical representation of the IRC reaction coordinate <i>vs</i> relative energy for structure 5.20.2	121
Figure 5.32 Mechanism 3-route 2 for the conversion of the PCU dione 5.1 to the lactam 5.2	127
Figure 5.33 Gas phase Gibbs free energy for the mechanism proposed in Figure 5.32	128
Figure 5.34 Graphical representation of energy <i>vs</i> reaction coordinate for structure 5.24.1	132
Figure 5.35 Graphical representation of the IRC reaction coordinate <i>vs</i> relative energy for structure 5.24.1	134
Figure 5.36 Graphical representation of energy <i>vs</i> reaction coordinate for structure 5.23.2	135
Figure 5.37 Graphical representation of the IRC reaction coordinate <i>vs</i> relative energy for structure 5.24.2	137
Figure A1.1 Graphical representation of energy <i>vs</i> reaction coordinate for structure 5.3.2	151
Figure A2.1 Graphical representation of energy <i>vs</i> reaction coordinate for structure 5.17	173

LIST OF TABLES

Table 5.1	Summary of the relative ^a thermochemical data for the conversion of the PCU dione 5.1 to the lactam 5.2 in the gas phase [B3LYP/6-31+G(d)] for mechanism 1.....	55
Table 5.2	Calculated relative Gibbs free energy changes [B3LYP/6-31+G(d)] for mechanism 1.....	93
Table 5.3	Calculated relative Gibbs free energy of solvation [B3LYP/6-31+G(d)] for mechanism 1.....	95
Table 5.4	Summary of the relative ^a thermochemical data for the conversion of the PCU dione 5.1 to the lactam 5.2 in the gas phase [B3LYP/6-31+G(d)] for mechanism 2.....	96
Table 5.5	Calculated relative Gibbs free energy changes [B3LYP/6-31+G(d)] for mechanism 2.....	109
Table 5.6	Calculated relative Gibbs free energy of solvation [B3LYP/6-31+G(d)] for mechanism 2.....	110
Table 5.7	Summary of the relative ^a thermochemical data for the conversion of the PCU dione 5.1 to the lactam 5.2 in the gas phase [B3LYP/6-31+G(d)] for mechanism 3-route 1.....	112
Table 5.8	Calculated relative Gibbs free energy changes [B3LYP/6-31+G(d)] for mechanism 3-route 1.....	123
Table 5.9	Calculated relative Gibbs free energy of solvation [B3LYP/6-31+G(d)] for mechanism 3-route 1.....	124
Table 5.10	Summary of the relative ^a thermochemical data for the conversion of the PCU dione 5.1 to the lactam 5.2 in the gas phase [B3LYP/6-31+G(d)] for mechanism 3-route 2.....	126
Table 5.11	Calculated relative Gibbs free energy changes [B3LYP/6-31+G(d)] for mechanism 3-route 2.....	138
Table 5.12	Calculated relative Gibbs free energy of solvation [B3LYP/6-31+G(d)] for mechanism 3-route 2.....	139
Table A1.1	Summary of energies for mechanism 1.....	144
Table A1.2	Summary of thermodynamic properties for mechanism 1.....	148
Table A1.3	Summary of Gibbs free energies for mechanism 1.....	149
Table A1.4	Summary of Gibbs free energies for mechanism 1 continued.....	150
Table A1.5	Summary of the relative ^a energy, enthalpy and entropy in water for mechanism 1.....	154
Table A1.6	Summary of energy, enthalpy and entropy in water for mechanism 1.....	155
Table A1.7	Summary of the relative ^a energy, enthalpy and entropy in methanol for mechanism 1.....	156

Table A1.8 Summary of energy, enthalpy and entropy in methanol for mechanism 1	157
Table A1.9 Summary of the relative ^a energy, enthalpy and entropy in acetonitrile for mechanism 1	158
Table A1.10 Summary of energy, enthalpy and entropy in acetonitrile for mechanism 1	159
Table A1.11 Summary of the relative ^a energy, enthalpy and entropy in dimethyl sulphoxide for mechanism 1	160
Table A1.12 Summary of energy, enthalpy and entropy in dimethyl sulphoxide for mechanism 1	161
Table A1.13 Summary of the relative ^a energy, enthalpy and entropy in carbon tetrachloride for mechanism 1	162
Table A1.14 Summary of energy, enthalpy and entropy in carbon tetrachloride for mechanism 1	163
Table A1.15 Summary of the relative ^a energy, enthalpy and entropy in dichloromethane for mechanism 1	164
Table A1.16 Summary of energy, enthalpy and entropy in dichloromethane for mechanism 1	165
Table A2.1 Summary of energies for mechanism 2	166
Table A2.2 Summary of thermodynamic properties for mechanism 2	170
Table A2.3 Summary of Gibbs free energies for mechanism 2	171
Table A2.4 Summary of Gibbs free energies for mechanism 2 continued.....	172
Table A2.5 Summary of the relative ^a energy, enthalpy and entropy in water for mechanism 2	175
Table A2.6 Summary of energy, enthalpy and entropy in water for mechanism 2.....	176
Table A2.7 Summary of the relative ^a energy, enthalpy and entropy in methanol for mechanism 2	177
Table A2.8 Summary of energy, enthalpy and entropy in methanol for mechanism 2.....	178
Table A2.9 Summary of the relative ^a energy, enthalpy and entropy in acetonitrile for mechanism 2.....	179
Table A2.10 Summary of energy, enthalpy and entropy in acetonitrile for mechanism 2	180
Table A2.11 Summary of the relative ^a energy, enthalpy and entropy in dimethyl sulphoxide for mechanism 2.....	181
Table A2.12 Summary of energy, enthalpy and entropy in dimethyl sulphoxide for mechanism 2.....	182

Table A2.13	Summary of the relative ^a energy, enthalpy and entropy in carbon tetrachloride for mechanism 2	183
Table A2.14	Summary of energy, enthalpy and entropy in carbon tetrachloride for mechanism 2	184
Table A2.15	Summary of the relative ^a energy, enthalpy and entropy in dichloromethane for mechanism 2	185
Table A2.16	Summary of energy, enthalpy and entropy in dichloromethane for mechanism 2	186
Table A3.1	Summary of energies for mechanism 3-route 1	187
Table A3.2	Summary of thermodynamic properties for mechanism 3-route 1	191
Table A3.3	Summary of Gibbs free energies for mechanism 3-route 1	192
Table A3.4	Summary of Gibbs free energies for mechanism 3-route 1 continued	193
Table A3.5	Summary of the relative ^a energy, enthalpy and entropy in water for mechanism 3-route 1	194
Table A3.6	Summary of energy, enthalpy and entropy in water for mechanism 3-route 1	195
Table A3.7	Summary of the relative ^a energy, enthalpy and entropy in methanol for mechanism 3-route 1	196
Table A3.8	Summary of energy, enthalpy and entropy in methanol for mechanism 3-route 1	197
Table A3.9	Summary of the relative ^a energy, enthalpy and entropy in acetonitrile for mechanism 3-route 1	198
Table A3.10	Summary of energy, enthalpy and entropy in acetonitrile for mechanism 3-route 1	199
Table A3.11	Summary of the relative ^a energy, enthalpy and entropy in dimethyl sulphoxide for mechanism 3-route 1	200
Table A3.12	Summary of energy, enthalpy and entropy in dimethyl sulphoxide for mechanism 3-route 1	201
Table A3.13	Summary of the relative ^a energy, enthalpy and entropy in carbon tetrachloride for mechanism 3-route 1	202
Table A3.14	Summary of energy, enthalpy and entropy in carbon tetrachloride for mechanism 3-route 1	203
Table A3.15	Summary of the relative ^a energy, enthalpy and entropy in dichloromethane for mechanism 3-route 1	204
Table A3.16	Summary of energy, enthalpy and entropy in dichloromethane for mechanism 3-route 1	205
Table A3.17	Summary of energies for mechanism 3-route 2	206
Table A3.18	Summary of thermodynamic properties for mechanism 3-route 2	210

Table A3.19	Summary of Gibbs free energies for mechanism 3-route 2.....	211
Table A3.20	Summary of Gibbs free energies for mechanism 3-route 2 continued	212
Table A3.21	Summary of the relative ^a energy, enthalpy and entropy in water for mechanism 3-route 2	213
Table A3.22	Summary of energy, enthalpy and entropy in water for mechanism 3-route 2	214
Table A3.23	Summary of the relative ^a energy, enthalpy and entropy in methanol for mechanism 3-route 2	215
Table A3.24	Summary of energy, enthalpy and entropy in methanol for mechanism 3-route 2	216
Table A3.25	Summary of the relative ^a energy, enthalpy and entropy in acetonitrile for mechanism 3-route 2	217
Table A3.26	Summary of energy, enthalpy and entropy in acetonitrile for mechanism 3-route 2	218
Table A3.27	Summary of the relative ^a energy, enthalpy and entropy in dimethyl sulphoxide for mechanism 3-route 2.....	219
Table A3.28	Summary of energy, enthalpy and entropy in dimethyl sulphoxide for mechanism 3-route 2	220
Table A3.29	Summary of the relative ^a energy, enthalpy and entropy in carbon tetrachloride for mechanism 3-route 2	221
Table A3.30	Summary of energy, enthalpy and entropy in carbon tetrachloride for mechanism 3-route 2	222
Table A3.31	Summary of the relative ^a energy, enthalpy and entropy in dichloromethane for mechanism 3-route 2.....	223
Table A3.32	Summary of energy, enthalpy and entropy in dichloromethane for mechanism 3-route 2	224

CHAPTER 1

INTRODUCTION

With the Nobel Prize for chemistry being jointly awarded to John A. Pople (for his work in the development of computational methods in quantum chemistry) and Walter Kohn (for his work on the development of the Density Functional Theory) in 1998¹, computational chemistry has become one of the strongholds of modern industrial and academic chemistry that makes use of established chemical theory and mathematical codes which is solved with computational or software to study chemical systems.

1.1 Computational Chemistry

The ever-increasing power of modern computers coupled with the development of new theoretical approaches are used for accurate and precise prediction of molecular properties.² Interestingly computational chemistry accounts for about a third of the computing usage worldwide. Computer methods are used extensively to solve chemical problems that would be difficult or even impossible experimentally.³

With the recent advancement of sophisticated computer hardware and software, computer-aided molecular design (CAMD) has become a subject worthy of discussion not only to theoretical chemists but also to experimental chemists.³ The broader goal of computational chemistry is not only in the characterisation and the prediction of chemical structures and their stabilities but also in the prediction of NMR, IR and UV spectra, the calculation of thermodynamic data, and the simulation and modulation of reaction pathways.⁴ Computational chemists use advanced computer software that enables them to gain theoretical insight into chemical processes and to avoid time-consuming and expensive experiments.⁴ This approach, however, does not replace the traditional wet chemistry experiments but it is a powerful aid in the understanding of experimental observations and the prediction of new reaction pathways. Some methods can be used to model not only stable molecules, but also momentary, unstable intermediates and even transition-states which are required for kinetic information. In this way, chemists can provide information about molecules and reactions that may be

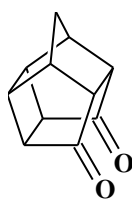
impossible to obtain experimentally. Computational chemistry is therefore both an independent research area and a vital adjunct to experimental studies.

It can be stated that computational chemistry belongs to the field of computational science and is solely based on computer models and simulation technology. The aim of computational chemistry is the determination of molecular structure and its changes including the determination of the thermodynamic properties.⁵ Reaction mechanisms that have been established by experimental kinetic data can be verified through a series of electronic structure calculations. These quantum mechanical calculations are invaluable tools which can be utilized to determine the feasibility of chemical reactions especially when more than one mechanism or reaction pathway seems to be possible.⁶

The mid nineties and the early part of the last decade were characteristic of an unrealistic expectation of the type of problems that can be solved with computational models and the ease with which it can be achieved. A much more realistic perspective has developed over the last couple of years and this project hopefully serves to shine more light on this aspect of the field of computational modeling.

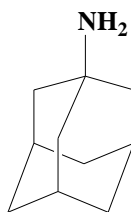
1.2 Pentacyclo-undecane (PCU) Cage Compounds

Since the publication by Cookson⁷ and co-workers in 1958 where they describe the synthesis of the pentacyclo-undecane dione **1**, the focus of many research groups⁸⁻¹³ has been the synthesis and chemistry of novel polycyclic cage compounds.



1

Davis¹⁴ and co-workers were responsible for discovering the medicinal and pharmacological properties of polycyclic cage compounds. They found that 1-amino-adamantane **3**, commonly known as amantadine, exhibits antiviral activity against a range of viruses causing influenza, hepatitis C and the herpes zoster neuralgia; thus realizing that polycyclic cage molecules also have the potential as biologically active agents.¹⁵



3

Schwab¹⁶ and co-workers later reported that amantadine was beneficial to patients with Parkinson's disease. The hydrocarbon cage of amantadine has the ability to cross the blood-brain barrier and to enter the central nervous system due to the hydrophobicity of the "cage" despite the fact that the amino group is protonated at physiological pH. Drugs containing hydrocarbon cage moieties promote their transport across cell membranes and increase their affinity for lipophilic regions in receptor molecules.¹⁷

While the hydrophobicity of the cage facilitates transport of the drug across membranes, the size and stability of the cage inculcate the drug with a structural property which results in controlled release of the active ingredients of the drug, as well as stability towards bio-degradation. In practice this translates into the slow metabolism of the drug. The important implications of this are that the duration of the intervals between drug administrations are decreased.¹⁸ It was shown that the inclusion of amantadine has given rise to longer time over which the drug is effective, greater potency of the drug and faster action. Furthermore the structural nature of the substituent influences the specificity of the drug to antibacterial¹⁹, anabolic²⁰ and analgesic action.²¹

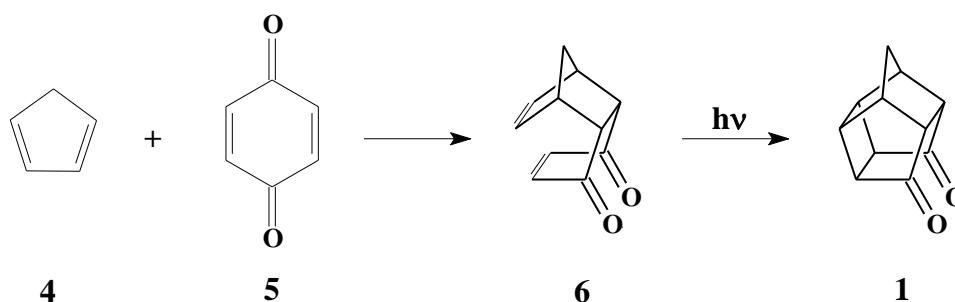
A number of cases²²⁻²⁴ have recently demonstrated the potential therapeutic value of novel pentacyclic cage compounds. These compounds have a promising potential as an important new class of medicinal and pharmaceutical agents and might extend the existing range^{25-27,13} of bio-active pentacyclo-undecane compounds. However, further investigation is required into the influence of the unique steric distribution of important functional groups around a rigid cage structure on the pharmacological activity.²⁸

Our group has also contributed to this field by investigating the PCU hydantoin as a potential epileptic agent²⁹, experimental and computational studies of the regioselective protection of hydantoins³⁰, the PCU skeleton as the basis for anti-tuberculosis drugs^{31,32}

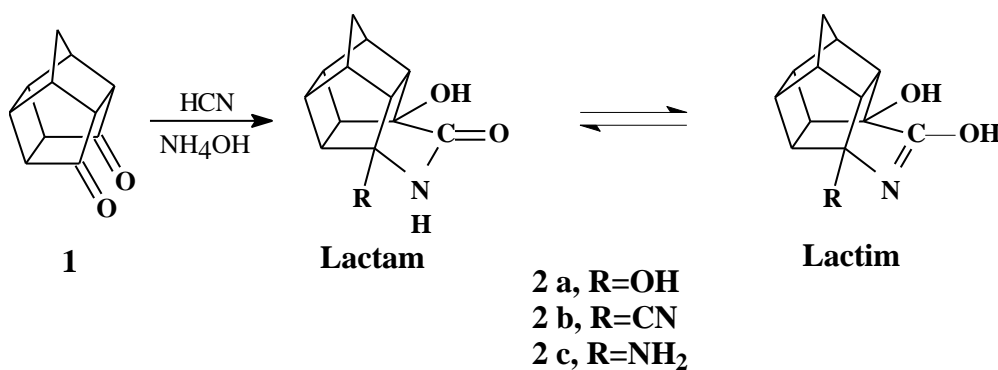
and recent unpublished reports focus on the PCU moiety as basis for novel HIV protease inhibitors.

1.3 Lactam formation

Cyclopentadiene **4** and *p*-benzoquinone **5** produce the PCU dione **1** via the Diels-Alder **6** adduct. The reaction in which the dione **1** is synthesized is the result of intramolecular photocyclisation.³³



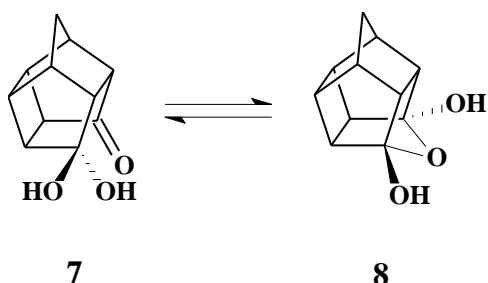
The dione **1** when treated with Strecker reagents (HCN, NH₄OH) unexpectedly produced³⁴ the δ -lactam compounds **2a-2c**. Strecker reactions normally produce cyanohydrins or amino nitriles.³⁵



The mechanism of this unique one pot conversion^{34,36-38} is not well understood in terms of the finer details. The mechanism proposed by the authors^{34,36,37} was formulated on basic chemical principles and is discussed in section 1.4. It is important to note that the derivatives of **2** are currently being investigated in our laboratory as highly active HIV-protease inhibitors.

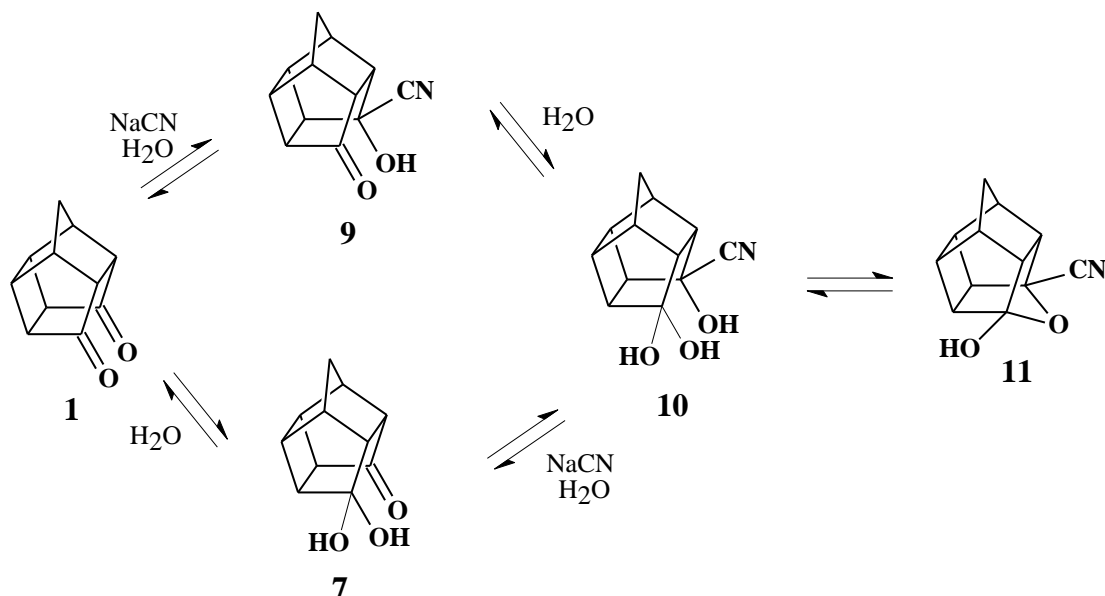
1.4 Proposed mechanisms

It was shown, in a previous study³⁹ that the dione **1** is easily hydrated to form the hydrates **7** and **8** in a 4:1 (respective) ratio.



Thus it can be expected that this trans-annular phenomenon should also play a significant role in the nucleophilic addition reactions on the carbonyl groups of the dione **1** in aqueous media. As a result, it can be assumed that both **1** and **7** (Scheme 1) can participate in the formation of the dihydroxylactam **2**.

Nucleophilic attack is expected to take place on the *exo* face of the carbonyl groups³⁸ in the dione **1** or the hydrate **7** as a result of the proximity of the groups and could lead to the formation of **10**. The cyclic ether **11** is expected to form as a result of *trans*-annular cyclisation of **10**.^{36,34,37}



Scheme 1 Conversion of the dione to the cyclic PCU ether **11**^{36,34,37}

In the experimental study, it was assumed that the cyclic ether **11** plays a prominent role in the conversion of the dione **1** to the dihydroxylactam³⁸ **2**. The “inversion” of the nitrile group was explained to proceed *via* two routes as demonstrated in Scheme 2.³⁸

Two alternative mechanisms were proposed for the conversion of the cyclic ether **11** to the hydroxy lactam **2a**.^{37,38} A summary of these mechanisms is presented in Scheme 2. Following the route on the right of the cyclic ether **11** which occurs in basic reaction conditions, ring cleavage (**11a**) of the cyclic ether **11** forms the intermediate **12** which is converted to the intermediate **13**. The electron deficient nitrile carbon atom of the *endo*-orientated cyano group in **12** is in an extremely favourable position to suffer attack from the nearby negatively charged oxygen atom. Intermediate **13** is proposed to rearrange to form intermediate **14**. Cyclisation of the intermediate **14** results in the formation of the lactim **15** and by implication the lactam **2**.³⁸ The authors^{36,38} also showed that the cyanohydrins **10** and **11** can be converted to the corresponding hydroxy lactam **8** upon treatment with aqueous NaOH, providing experimental proof for their assumption above. A subsequent and related paper by the same authors demonstrated the versatile interconversion of the three lactam products (**2a–2c**).³⁷

Following the route on the left of the cyclic ether **11** (from Scheme 1) the nucleophilic attack of the hydroxide is shown. This “inversion” of the cyano group is expected to be combined with the loss of the hydroxide group from the cyclic ether **11** leading to the formation of the cyanohydrin **16**. The reaction is performed under basic conditions, so it is likely that a second hydroxide ion can attack the freshly formed carbonyl carbon in **16**. The *endo* cyano group in **16** has an electron deficient carbon atom which is in an extremely favourable position to suffer attack from the nearby negatively charged oxygen atom thus producing the intermediate **17** and subsequently automatic conversion to **18** in aqueous media. The rearrangement of **18** to the cation **19** was postulated. This proposed rearrangement is promoted since the negative charge on the nitrogen atom of **19** is sufficiently stabilised by the adjacent carbonyl group to facilitate the rearrangement. The hydroxy group in **19** should similarly stabilize the cation and result in the formation of **2**.^{37,38}

1.5 Aim of this study

A partial study of this mechanism was completed for my MTech.⁴⁰ The study involved *ab initio* “gas phase” calculations using the 3-21+G(d) basis set and only a limited number of transition states were found. The value of this study at a lower level of theory also turned out to be largely preliminary since some of the transition states found at the lower level could not be reproduced at a higher level. Thus, the aim of this study is to establish a more in depth evaluation of the possible mechanisms for the formation of the PCU lactam 2.

The study will make use of the Density Functional Theory (DFT) level and also include the incorporation of solvent effects. The proposed pathways will be modified to include four- and six-membered ring transition structures. This will enable the investigation of neutral reaction species and also lower the energies of the charged species in the gaseous phase.

It has been proposed by several workers⁴¹⁻⁴⁴ that it is advantageous to use zero-point energies from DFT calculations in the calculations of thermochemical data. Therefore, first, geometries of all the molecules will be optimised using DFT employing the B3LYP method (Becke’s three-parameter non-local exchange function⁴⁵⁻⁴⁷ with the correlation functional of Lee, Yang and Parr⁴⁸) in conjunction with the 6-31+G(d) basis set. The thermochemical quantities such as changes in enthalpy of formation, entropy and Gibbs free energy for all the structures will be obtained from frequency calculations. Normal mode analysis will be carried out at the same level of theory for equilibrium or stationary points as well as transition structures and will be characterised as minima (no imaginary frequency) or as a transition structure (one imaginary frequency). The intrinsic reaction coordinate (IRC) calculation will be performed on all transition structures to confirm whether these connect to the right minima or not. The Gibbs free energy obtained from these calculations will be used to create a profile for the reaction and will determine the most feasible reaction pathway consistent with the expected reaction with one imaginary frequency.

The incorporation of solvent effects into DFT methods has received much attention due to its importance in understanding mechanisms and chemical reactions in solution.⁴⁹

The goal is to describe chemical processes in solution using theoretical methods that are proficient in illustrating the solvent effect at a level of accuracy comparable with that attainable for molecular solutes.⁵⁰

In order to achieve quantitative accuracy in the computational simulation of molecules and chemical reactions, solvent effects are of vital importance. Solute-solvent interactions modify the energy, the structure, the properties and hence the overall behaviour of molecules. Both in the case of classical simulations and in the case of quantum methods, an accurate model for the description of solvent effects should be part of any computational study. The reaction will be modeled in the presence of two polar solvents: water and methanol; two dipolar solvents: acetonitrile and dimethyl sulphoxide and in two non-polar solvents: carbon tetrachloride and dichloromethane. The solvents can be further classified as polar protic (water and methanol) and polar aprotic (acetonitrile, dimethyl sulphoxide and dichloromethane). Similarly, the Gibbs free energy will be used to determine the preferred solvent for this reaction. The Gibbs free energy of solvation will also be calculated.

CHAPTER 2

THEORETICAL TOOLS

Computational chemistry consists of two main types of computational code for simulating the structures of molecules and their reactivity at the atomic level: molecular mechanics and electronic structure theory.⁵¹ Both methods perform three basic types of calculations pertinent to this study. Firstly, they compute the energy of a particular molecular structure. Secondly, they perform geometry optimisations and thirdly, vibrational frequencies of molecules resulting from interatomic motion within the molecule, are calculated. In general smaller systems can be treated with quantum mechanics while classical methods are the method of choice for much larger systems.^{3,52-54} Frequently though, these two methods complement each other.

2.1 Molecular Mechanics

Molecular mechanics (MM) is a fast approximation for studying molecular structure, properties and motions of a molecule that is based on the laws of classical physics. The energy of the system is calculated by an empirically derived set of equations defining how the potential energy of a molecule varies with the location of its component atoms in the system often referred to as the force field equation.³

The aim of MM is to predict the energy associated with a given conformation of a molecule as described in the Figure 2.1:

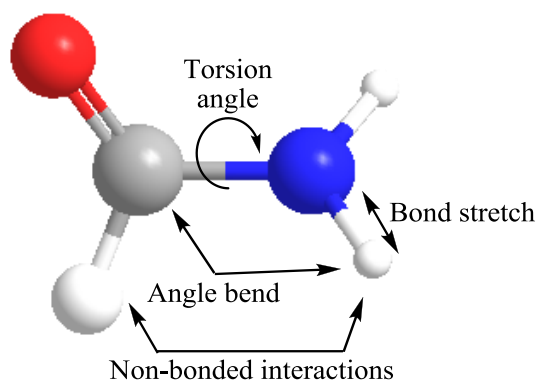


Figure 2.1 Schematic representation of energy contributions in an MM system

In general, energy arises from bond angles, bond stretching, torsion angles and non-bonded interactions. Non-bonded interactions (greater than two bonds apart) interact through van der Waals attraction, steric repulsion and electrostatic attraction or repulsion.⁵⁵

These molecular interactions are described mathematically as:

$$\begin{aligned}
 E_{Total} = & \sum_i^{bonds} E_i^{stretch} + \sum_i^{bondangles} E_i^{bend} + \sum_i^{torsionangles} E_i^{torsion} \\
 & + \sum_i^{nonbonded} \sum_j^{nonbonded} E_{ij}^{nonbonded}
 \end{aligned}
 \tag{2.1}$$

During the geometry optimisation, the bond lengths, bond angles and torsion angles are varied to yield fairly precise results for large systems containing many thousands of atoms.

However, MM have limitations as well. Firstly, a specific force field produces accurate results for a particular class of molecules. Any specific force field cannot be generally used for all molecular systems. Secondly, MM only considers the positions of nuclei and electronic motions are ignored. Although this approximation makes molecular mechanics computations quite inexpensive in terms of computational resources and time, MM cannot be used to investigate processes that involve bond formation or bond breaking.³ Consequently, this method is not suitable to describe reaction transition states.

2.2 Electronic Structure Theory

Unlike MM, electronic structure theory is based uniquely on the principles and laws of quantum mechanics. When using quantum mechanics to define the behaviour of an electron, physical constants like the speed of light, the mass and charge of the electron and nuclei and Planck's constant, are considered.^{3,51} There are three major categories of electronic structure theory: semi-empirical, *ab initio* and density functional theory methods.

2.2.1 Semi-Empirical Models

Semi-empirical (SE) methods are based on the Hartree-Fock models, but also make several approximations and obtain some parameters from empirical data. The use of empirical parameters does however allow some inclusion of electron correlation effects into these methods.^{56,57}

In Hartree-Fock calculations information such as two-electron integrals are sometimes approximated or completely ignored. In order to correct for this loss, semi-empirical methods are thus parametrised by the use of parameters, that is, their results are fitted by a set of parameters usually in such a way as to produce results that best agree with experimental data.^{4,3}

Semi-empirical methods follow what are frequently termed empirical methods where the two-electron part of the Hamiltonian is not explicitly included. For π -electron systems, the Hückel method proposed by Erich Hückel⁵⁸⁻⁶⁰ is used. For all valence electron systems, the Extended Hückel method proposed by Roald Hoffman⁶¹ is used.

There are methods in semi-empirical calculations that are restricted to π -electrons. Methods such as the Pariser-Parr-Pople^{62,63} (PPP) method provide good estimates of the π -electronic excited states when parameterised well. For many years the PPP method outperformed *ab initio* excited state calculations.

There are also methods that are restricted to all valence electrons. These are by far the largest group of semi-empirical methods and they fall into several categories. The following methods were introduced by John Pople: CNDO (Complete Neglect of Differential Overlap), INDO (Intermediate Neglect of Differential Overlap) and NDDO (Neglect of Diatomic Differential Overlap). Although rarely used currently, these methods have formed the basis of later methods. In MINDO (Modified Intermediate Neglect of Differential Overlap), MNDO (Modified Neglect of Differential Overlap), AM1 (Austin Model), PM3 (Parametric Method), and SAM1 (Semi *Ab Initio* Method) methods, the objective is to use parameters to fit experimental heats of formation, dipole moments, ionization potentials and geometries. In ZINDO (Zerner Intermediate Neglect of Differential Overlap) the aim is to calculate excited states and thus predict electronic spectra.⁵⁷

Several methods have been developed using semi-empirical calculations to locate transition structures. Some of these methods include locating minima on seams of intersecting potential energy surfaces,^{64,65} transition state modeling with empirical force fields,^{66,67} the nudged elastic band approach,⁶⁸ a generalised synchronous transit method⁶⁹ and a quadratic string adapted barrier method.⁷⁰

Semi-empirical calculations are much faster than *ab initio* methods. This is achieved firstly by reducing the number of integrals and secondly by restricting basis sets to a minimal representation. However, incorrect and erratic results may be produced, if the molecule being computed is not similar enough to the molecules in the database used to parameterize the method.^{56,57}

Semi-empirical calculations have been most successful in the description of organic chemistry where only a few elements are used extensively and the molecules are of moderate size. These methods have also been devised specifically for the description of inorganic chemistry as well. Finally, when using semi-empirical methods for a particular system, it is imperative to choose an appropriate method if feasible results are to be produced.⁵⁶

2.2.2 The *Ab Initio* Method

Ab initio computations are derived directly from theoretical principles based solely on the laws of quantum mechanics and thus these methods have no inclusion of experimental parameters in these computations. Although the *ab initio* method is generally more accurate than MM, it requires far greater computational power making it a rather expensive method.⁵⁵

Ab initio methods provide an approximate solution to the Schrödinger equation (2.2) $\hat{H}\Psi = E\Psi$. These solutions are usually mathematical approximations that generate the energy and other related properties of a stationary state of a molecule.⁵⁵

$$\hat{H}\Psi = E\Psi$$

(2.2)

where E is the numerical energy, Ψ corresponds to the wavefunction for the molecular state and H is the Hamiltonian, a differential operator. H is expressed as:

$$\hat{H} = -\frac{\hbar^2}{8\pi^2} \sum_A \frac{1}{M_A} \bar{v}_A^2 - \frac{\hbar^2}{8\pi^2 m} \sum_a \bar{v}_a^2 - e^2 \sum_A \sum_a \frac{Z_a}{r_{Aa}} + e^2 \sum_A \sum_{>B} \frac{Z_A Z_B}{R_{AB}} + e^2 \sum_a \sum_{>b} \frac{1}{r_{ab}} \quad (2.3)$$

where M denotes nuclear mass, a electrons and A nuclei. R_{AB} represents the distance between nuclei, r_{ab} that between electrons and r_{Aa} that between nuclei and electrons. The Hamiltonian is representative of the kinetic and potential energy of the molecule. The first two terms of the Hamiltonian represent the kinetic energy and describe the motions of the nuclei and electrons. The next three terms describe Coulombic interactions between particles that represent the potential energy.⁵⁵ The first step in obtaining a solution to the Schrödinger equation is simplifying the general molecular problem in quantum mechanics by separating the nuclear and electronic motions.

Born-Oppenheimer Approximation

This separation of the nuclear and electronic motions into two parts is called the adiabatic or the Born-Oppenheimer⁷¹ approximation. It is possible to separate these two motions because the nuclear masses are much greater than those of the electrons, therefore, nuclei move much slower. Hence, the electrons in a molecule adjust their distribution rapidly to changing nuclear positions.^{3,51} Thus, the electron distribution within a molecular system depends on the positions of the nuclei, and not on their velocities.

The Born-Oppenheimer approximation allows the two parts of the problem to be solved independently. It also implies that due to the sluggish movement of the nuclei they (nuclei) may be regarded as fixed and their motion may be neglected. Thus an electronic Hamiltonian that neglects the kinetic energy term of the nuclei can be constructed.³ The electronic Hamiltonian is represented as follows:

$$\hat{H} = -\frac{\hbar^2}{8\pi^2 m} \sum_a \bar{v}_a^2 - e^2 \sum_A \sum_a \frac{Z_a}{r_{Aa}} + e^2 \sum_a \sum_{>b} \frac{1}{r_{ab}} \quad (2.4)$$

This electronic Hamiltonian is then used in the Schrödinger to give:

$$\hat{H}^{elec}\Psi^{elec} = E^{elec}\Psi^{elec} \quad (2.5)$$

Hartree-Fock Theory

Although the separation of the nuclear and electronic motion by the Born-Oppenheimer approximation simplifies the Schrödinger equation, an exact solution is only possible for the smallest and simplest of molecular systems. The Hartree-Fock (HF) calculation is the most common type of *ab initio* calculation that makes use of a number of simplifying assumptions to make an approximate solution possible for a large range of molecules.^{3,57}

It should be noted that HF theory which is based on the variational method in quantum mechanics assumes that electrons move independently of each other. The first approximation thus considers Ψ which is interpreted as the probability or density of the electrons within the system. Molecular orbital theory breaks Ψ up into a combination of molecular orbitals. The resulting equation is symmetric - there is no sign change.^{4,3} Therefore this is an inadequate wavefunction.

To solve the problem of the antisymmetric equation, the second approximation uses a total wavefunction that is represented by a single Slater determinant.⁷² However, before the determinant is formed, electron spin will have to be accounted for. Closed shell calculations describe molecular orbitals as occupying a maximum of two electrons of opposite spin. The spin functions are represented as α and β .⁵⁷ The total wavefunction that defines the molecular orbitals for a system with electrons of opposite spin is presented as follows:

$$\Psi = \frac{1}{\sqrt{N!}} \begin{vmatrix} \chi_{1(1)} & \chi_{2(1)} & \chi_{n(1)} \\ \chi_{1(2)} & \chi_{2(2)} & \chi_{n(2)} \\ \chi_{1(N)} & \chi_{2(N)} & \chi_{n(N)} \end{vmatrix} \quad (2.6)$$

χ_i describes the individual spin orbitals which are a product of the molecular orbital, ψ_i , and a spin of α or β .³

The molecular orbitals are further restricted and the next approximation involves expressing them to be linear combinations of a set of N known one electron functions $\phi_1(x,y,z), \phi_2(x,y,z), \dots, \phi_N(x,y,z)$. The following equation, which is also referred to as the linear combination of atomic orbitals (LCAO) approximation⁵¹, is used to define an individual molecular orbital equation:

$$\psi_i = \sum_{\mu=1}^N c_{\mu i} \phi_{\mu}. \quad (2.7)$$

The functions $\phi_1, \phi_2, \dots, \phi_N$ are known as the basis functions and constitute the basis set. The different types of basis sets will be discussed further in this chapter. $c_{\mu i}$ is the molecular expansion coefficient. The task now is to find a solution for the set of molecular expansion coefficients. Here, HF takes advantage of the variational principle that states that the ground state of any antisymmetric normalized function of the electronic coordinates (Ξ) will always be greater than the energy for the exact wavefunction³:

$$E(\Xi) > E(\Psi); \quad \Xi \neq \Psi \quad (2.8)$$

This leads to a set of algebraic equations derived by Roothaan⁷³ and Hall⁷⁴ to describe the molecular orbital expansion coefficient, $c_{\mu i}$:

$$\sum_{\nu=1}^N (F_{\mu\nu} - \epsilon_i S_{\mu\nu}) c_{\nu i} = 0 \quad \mu = 1, 2, \dots, N \quad (2.9)$$

where ϵ_i are the orbital energies, F the Fock matrix and S the overlap matrix (indicating the overlap between orbitals).^{75,72} The Fock matrix, F represents the average effects of all the electrons on each orbital.³ Its elements are:

$$F_{\mu\nu} = H_{\mu\nu}^{core} + \sum_{\lambda=1}^N \sum_{\sigma=1}^N P_{\lambda\sigma} \left[(\mu\nu|\lambda\sigma) - \frac{1}{2}(\mu\lambda|\nu\sigma) \right] \quad (2.10)$$

where $H_{\mu\nu}^{core}$ is another matrix representing the energy of a single electron in the field of bare nuclei, and P is the density matrix, defined as:

$$P_{\lambda\sigma} = 2 \sum_{i=1}^{occupied} c_{\lambda i}^* c_{\sigma i}. \quad (2.11)$$

The summation of the coefficients is over the molecular orbitals only. The factor of two indicates that two electrons occupy each molecular orbital.³

The Roothaan-Hall equations are not linear since the Fock matrix depends on the molecular orbital coefficient through the density matrix. The solution of the equation involves an iterative process and the technique is referred to as the self-consistent field (SCF) theory.³

Further modification of the Roothaan-Hall equations are necessary for open-shell systems where the electrons are not assigned to orbitals in pairs. Molecular orbital theory is applied to open-shell systems in two ways: spin-restricted Hartree-Fock (RHF) and spin-unrestricted Hartree-Fock (UHF).^{51,57} RHF and UHF are illustrated in Figure 2.2.

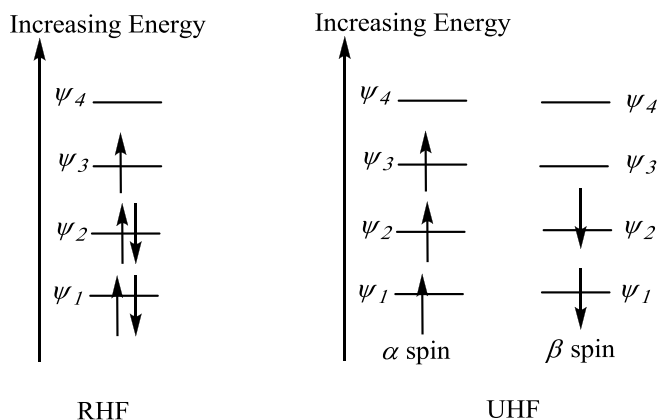


Figure 2.2 Electron configuration diagram illustrating RHF and UHF

In RHF, the set of molecular orbitals are either doubly occupied or singly occupied with an electron of α spin. In UHF, α and β electrons are assigned to different molecular orbitals. As a result of this, two sets of molecular orbital expansion coefficients are obtained. These two equations are varied independently and they result in two sets of Fock matrices and two sets of density matrices. Finally they give a solution producing two sets of orbitals.

Although the HF equations are applicable no matter how many electrons there are in a molecule, HF theory does not include full treatment of the effects of electron correlation, that is, the energy combinations arising from electrons interacting with one another especially between electrons of opposite spin.^{51,55,57}

2.2.3 Electron Correlation Methods

In HF, the major correlation effects arising from pairs of electrons with same spin, is automatically included when the wavefunction is antisymmetric. This correlation is referred to as exchange correlation. However, in HF theory the motion of electrons of opposite spin is uncorrelated. Electron correlation methods are any methods that go beyond SCF in attempting to treat this phenomenon properly. Density functional theory and Møller-Plesset models fall in this category.⁵⁵

HF models treat the motions of the individual electrons independent of one another. This leads to an overestimation of the electron-electron repulsion energy and to a high total energy. Electron correlation accounts for the coupling of electron motions and leads to a decrease of the electron-electron repulsion energy. This results in a decrease of the overall total energy.⁵⁵

Density Functional Theory (DFT) Methods

An alternative approach to electron correlation is provided by the density functional models. A theorem by Hohenberg⁷⁶ and Kohn⁷⁶ which states that the energy that is determined by the one-electron density, ρ , forms the basis for what is commonly called density functional theory (DFT). The theorem demonstrated the existence of a unique functional but however does not provide the form of this functional.⁵⁶

It must be noted, however, that it is difficult to construct a sufficiently accurate total energy functional depending only on ρ . Following on from the Hohenberg-Kohn theorem, the work by Kohn⁷⁷ and Sham⁷⁷ laid the foundation for DFT methods currently used in computational chemistry. The idea proposed by Kohn and Sham is to split the kinetic energy functional into two parts: one that can be calculated exactly and a small correction term.³ The simplified equation is:

$$E = E^T + E^V + E^J + E^{XC} \tag{2.12}$$

where E^T is the kinetic energy term as a result of the motion of the electrons; E^V is the potential energy of the nuclear-electron attraction and the repulsion between pairs of nuclei; E^J is the electron-electron repulsion as well as the Coulomb self-interaction of the electron density and E^{XC} is the exchange-correlation. The E^{XC} term is divided further into two parts referred to as the exchange functional, $E^X(\rho)$ and the correlation functional, $E^C(\rho)$:

$$E^{XC}(\rho) = E^X(\rho) + E^C(\rho) \tag{2.13}$$

All three terms are functionals of the electron density, ρ . The exchange functional and the correlation functional can be of two distinct types: local functionals that depend on only the electron density and gradient-corrected functionals that depend on both electron density and its gradient, $\bar{V}\rho$.³

For purposes of practical calculations, the Kohn and Sham functional must be supplemented by an approximation for the exchange and correlation terms. The traditional approximation, proposed by Kohn and Sham, is referred to as the local density approximation (LDA). The LDA has remained the approximation of choice for many years however, it was found that it tends to over-binding, that is, it tends to lead to too large values of molecular binding energies. This means that the exchange correlation contribution emanating from regions of low electron density is underestimated.⁵⁶

A class of corrections to the LDA has been developed that corrects this deficit to a large extent. This is usually done by introducing a dependence on the gradient of the density and the new class of corrected exchange-correlation functionals is referred to as gradient corrected or generalized gradient approximation (GGA). The Kohn-Sham equations where only the exchange correlation part of the energy must be estimated as a functional of electron density, provide viable models.^{56,57}

There are a plethora of different functionals for a variety of properties available. An evaluation of the performance of these DFT methods is also available.^{56,57} One of the earliest and most popular GGA exchange functionals was proposed by A.D. Becke⁷⁸ (referred to as B or B88) as a correction to the LDA exchange energy. The B88 exchange functional has the correct asymptotic behaviour for the energy density. There are several GGA exchange functionals available. These include PW91⁷⁹⁻⁸³ and mPW⁸⁴. Unless otherwise indicated, these exchange functionals must be combined with a correlation functional in order to produce a usable method.

There have similarly been various GGA functionals proposed for the correlation energy. One popular functional is due to Lee, Yang and Parr (LYP).⁴⁸ The LYP correlation functional is often combined with the B88 exchange functional to produce the BLYP acronym. The following correlation functionals are also available: VWN⁸⁵ (Vosko, Wilk, and Nusair), the 1980 correlation functional (III) fitting the RPA solution to the uniform electron gas often referred to as Local Spin Density (LSD) correlation; P86⁸⁶ (Perdew 86): the gradient corrections of Perdew with his 1981 local correlation functional and PBE.^{87,88} The 1996 gradient-corrected correlation functional of Perdew, Burke and Ernzerhof.

There are also a number of hybrid functionals which include a mixture of Hartree-Fock exchange with DFT exchange-correlation. Becke's three parameter hybrid functional (B3LYP) has the form devised by Becke⁸⁹ in 1993. It (B3LYP) uses the non-local correlation provided by the LYP expression and the VWN functional III for local correlation. VWN is used to provide the excess local correlation required since LYP contains a local term essentially equivalent to VWN. B3P86 specifies the same functional (VWN) with the non-local correlation provided by P86. B3PW91 also

specifies the VWN functional with the non-local correlation provided by PW91. Becke's one parameter hybrid functional (B1B95)⁹⁰ is used to specify the functional as defined in the original paper.

B3LYP with a 6-31G(d) or better basis set is *on average* the best choice of a model chemistry for most systems. It is recommended for organic molecules but is not suitable for metal containing compounds. BLYP with most basis sets is the opposite of B3LYP, that is, it is not particularly accurate with organics, but provides reasonably good energy values for metal-containing compounds. The PW91 and the PBE functionals are somewhat poorer than the other GGA functionals. PW91 can also be used for metal-containing compounds.

Thus concluding, it has been established that the major difference between DFT and molecular orbital theory is: DFT optimises the electron density and molecular orbital theory optimises the wavefunction.⁵⁶ It should be noted though that DFT is the most cost-effective method to achieve a given level of accuracy.

Even though the many successes of DFT have been reported, there are some areas where the current functionals are known to perform inadequately. A few of these shortcomings will be discussed in this section.

Weak interactions due to dispersion forces, that are part of the van der Waals type interactions, arise from electron correlation in wavefunction methods. This is poorly described by the current DFT methods.^{91,92} Loosely bound electrons, such as anions arising from systems with relatively low electron affinities, represent a problem for exchange-correlation functionals that do not include self-interaction corrections or correct for the incorrect long range behaviour of the exchange-correlation potential. However, a medium-sized basis set with a single set of diffuse functions will in many cases give a reasonable estimate of the experimental electron affinity.⁹³ It should be noted that the fairly good performance is in essence due to an accurate physical description, rather than a correct theoretical methodology.

For chemically bonded systems, that have a similar analysis to that of the H₂ system, where there are normal covalent bonds and steric repulsion between closed shell systems, then these are reasonably described by gradient-corrected methods.⁹⁴ Systems

involving radical cations, radical anions and atom transfer transition structures are predicted to be too stable. The dissociation of charged odd-electron systems is a problem for most DFT methods, with the dissociation energy profile displaying an artificial barrier and incorrect dissociation energy.⁵⁷

The absence of a wavefunction makes a direct description of excited states with the same symmetry as the ground state problematic. However, excited states can be calculated by time-dependent DFT (linear response) methods.⁵⁷

The exchange-correlation functional is inherently local. It depends on the density and possibly its derivatives at a given point. This causes DFT methods to be inherently unsuitable for describing charge transfer systems.⁵⁷

Another major shortcoming of the DFT methods when compared with *ab initio*, is that the correct energy and geometry can be approached by increasing the level of theory and improving the basis set. This is not yet possible with DFT methods. B3LYP was found to work well with most organic molecules, but the theory is not well enough understood yet to systematically improve on that. “Purists” thus criticize DFT for this reason.

Møller-Plesset Models

The “many body perturbation theory” in mathematical physics is the foundation for the Møller-Plesset⁹⁵ model that handles electron correlation by adding higher excitations to the HF theory. It is commonly referred to by the acronym MP_n where n is the order at which the perturbation theory is truncated.^{56,3,57} In perturbation theory the Hamiltonian is divided into two parts, as follows:

$$H = H_0 + \lambda V \tag{2.14}$$

H_0 is soluble exactly. The perturbation λV is defined as:

$$\lambda V = \lambda(H - H_0) \tag{2.15}$$

where H is the total Hamiltonian and λ is a dimensionless parameter. ψ_λ and E_λ are the wavefunction and the energy for a system described by the total Hamiltonian H . This is then expanded as follows⁵⁵:

$$\psi_\lambda = \psi^{(0)} + \lambda\psi^{(1)} + \lambda^2\psi^{(2)} + \dots \quad (2.16)$$

$$E_\lambda = E^{(0)} + \lambda E^{(1)} + \lambda^2 E^{(2)} + \dots \quad (2.17)$$

The Møller-Plesset energy to first order (MP1) does not advance beyond the HF level in determining the energy thus the second-order correction must be considered to obtain an estimate of the correlation energy.⁵⁷ MP2 is described as:

$$E^{(2)} = \sum_i^{\text{filled}} \sum_{i < j}^{\text{filled}} \sum_a^{\text{empty}} \sum_{a < b}^{\text{empty}} (\varepsilon_a + \varepsilon_b - \varepsilon_i - \varepsilon_j)^{-1} [(ij|ab)]^2 \quad (2.18)$$

where ε_i and ε_j are the energies of the filled molecular orbitals; ε_a and ε_b are the energies of the empty molecular orbitals and the integral $(ij|ab)$ justifies changes in electron-electron interactions as a result of promotion from the filled molecular orbitals to the empty molecular orbitals.⁵⁵

MP2 calculations can be done rapidly because equation (2.18) can be efficiently evaluated. The scaling factor of the MP2 method is roughly N^5 , where N is the number of basis functions. Analytic gradients and second derivatives are available for this level of theory so it can be used to explore PESs. MP2 and all orders of MP_n theory are size-consistent which is a desirable feature. MP2 on average accounts for 80-90% of the correlation energy and is the most economical method for including electron correlation. MP2 energy for systems can be calculated at a cost similar to or less than what is required for calculating the HF energy.⁵⁶

To improve convergence higher orders of perturbation theory can be used. At third order only matrix elements involving doubly excited determinants need to be evaluated

thus making MP3 not too much more expensive than MP2. However there is evidence that suggests MP3 calculations offer little improvement over MP2.⁵⁶

At the MP4 level, integrals involving triply and quadruply excited determinants appear. The evaluation of the terms involving triples is the most costly and scales as N^7 . If the triples are ignored, the method scales more favourably. However their application is limited to very small systems due to the extreme computational cost.⁵⁷

2.2.4 Basis Sets

A basis set is often described as a set of mathematical functions from which the wavefunction is constructed. As stated in section 2.2.2, each molecular orbital in Hartree-Fock theory is expressed as a linear combination of basis functions, the coefficients for which are determined from the iterative solution of the Hartree-Fock SCF equations. The wavefunction ϕ_i , can be expanded in terms of a set of atomic orbitals, χ_μ in the linear combination of atomic orbitals (LCAO) method, to give:

$$\phi_i = \sum_{\mu=1}^N c_{\mu i} \chi_\mu \tag{2.19}$$

where $c_{\mu i}$ is the molecular orbital expansion coefficient, and χ_μ is the basis function of the atomic orbital. The coefficient $c_{\mu i}$ is varied to obtain the wavefunction ϕ_i , which will give the lowest energy in the Schrödinger equation. Hartree-Fock theory makes use of the variation principle to solve for the set of molecular orbital coefficients. A situation is reached when the energy is no longer decreased and the best single determinant wavefunction is obtained. When this occurs, changing the wavefunction ϕ_i , by an infinitesimal amount will not alter the energy. The number and quality of the atomic orbitals χ_μ determine the quality of the molecular orbital $c_{\mu i}$. If there are many electrons in a molecule then the number of atomic integrals required increases rapidly and can be as many as several million for quite small molecules. For this reason a computer with a peak performance of at least 3.3 TeraFlops is essential.⁵¹

The two types of atomic basis functions commonly used in electronic structure calculations are Slater-type atomic orbitals (STOs) and Gaussian-type atomic orbitals (GTOs). The Gaussian series of programs deals, as the name implies, almost exclusively with Gaussian-type orbitals.^{51,55} Since STOs are not well suited to numerical work, their use in practical molecular orbital calculations has been limited. Almost all modern *ab initio* calculations employ GTO basis sets. These basis sets, in which each orbital is made up of a number of Gaussian probability functions, has considerable advantages over STOs.

Minimal Basis Sets

The simplest atomic orbital representation is referred to as a minimal basis set and these contain the minimum number of basis functions needed for each atom. The series of minimal basis sets consists of expansions of Slater-type orbitals (STOs). Usually this is a single ($1s$) function for hydrogen and five functions for lithium to neon ($1s$, $2s$, $2p_x$, $2p_y$, $2p_z$). The STO-3G basis set is expanded in terms of three Gaussians. Minimal basis sets are characterised by fixed-size atomic-type orbitals. This is a shortcoming since they therefore do not have the capability to expand or contract because the exponent is fixed.⁵¹

Split Valence Basis Sets

This shortcoming is resolved by increasing the number of basis functions per atom thus making the basis set larger. By including two sets of isotropic p -functions in the representation, one tightly held to the nucleus and the other relatively diffuse, it allows for independent variation of the radial parts of the two sets of p -functions. Thus this produces more contracted or more diffuse functions that would be suitable for the descriptions of the s - and p -systems. A basis set formed by doubling all functions in a minimal representation is known as a double-zeta basis, while one in which only the basis functions for the outer valence shells are doubled, is known as a split-valence basis set.^{51,55}

The simplest split-valence basis sets are 3-21G and 6-31G. In the 3-21G basis set each inner shell atomic orbital is represented by a single function written in terms of three Gaussians. The basis functions representing the inner and outer valence atomic orbitals are written in terms of expansions of 2 and 1. Similarly, the 6-31G basis sets are

constructed. Higher level valence shell splitting such as the 6-311G basis set, is also possible.⁵⁵

Polarised Basis Sets

Split valence basis sets allow orbitals to change their size but not their shape. Polarised basis sets remove this limitation by adding orbitals with angular momentum. For example, polarised basis sets add *p*-functions to hydrogen atoms, *d*-functions to the main groups and *f*-functions to transition metals.^{51,55,57}

The 6-31G(d) basis set, which is among the simplest of polarised basis sets, was originally proposed for first-row atoms and later extended to second-row elements. The 6-31G(d) basis set is constructed by the addition of a set of six second order (*d*-type) Gaussian primitives to the split valence 6-31G basis set description of each heavy (non-hydrogen) atom.⁵⁵

The 6-31G(d) basis set described above does not however, allow for any polarisation of the *s*-orbitals of either hydrogen or helium atoms. The 6-31G(2d) basis set is identical to 6-31G(d) except for the addition of a single set of Gaussian *p*-type functions to each hydrogen and helium atom.⁵⁵

The 3-21G(d) basis set is constructed directly from the corresponding 3-21G representations by the addition of a complete set of six second-order Gaussian primitives. Although the resulting representations contain the same number of atomic basis functions per second-row atom as the 6-31G(d) polarised basis set previously described, these are made up of significantly fewer Gaussians (three instead of six for each inner-shell atomic orbital, and two Gaussians instead of three for the inner part of the valence description).⁵¹

The basis sets that have been discussed thus far are more suitable for molecules in which electrons are tightly held to the nuclear centers than they are for species with significant electron density far removed from those centers. In these cases the basis sets often need to be supplemented by diffuse functions.⁵⁵

Basis Sets Incorporating Diffuse Functions

Calculations involving anions pose special problems since the electron affinities of the corresponding neutral molecules are typically quite low, thus the extra electron in the anion is only weakly bound. One way to overcome problems associated with anion calculations is to include in the basis representation one or more sets of highly diffuse functions (designated by “+”). These are then able to adequately describe the long-range behaviour of molecular orbitals with energies close to the ionization limit.^{51,55,57}

The 3-21+G(d) and 6-31+G(d) basis set are constructed from the underlying 3-21G(d) and 6-31G(d) representations by the addition of a single set of diffuse Gaussian *s*- and *p*-type functions. For elements with lone pairs, the effects of diffuse and polarisation functions are complementary to some extent. In protonation reactions and hydrogen bonding, where the energies of processes involving changes in the number of lone pairs are a common feature, the diffuse basis set improves the energies, even when large basis sets are used.^{55,57}

Basis sets incorporating diffuse functions produce entry level results which are relatively inexpensive in terms of computer resources and time. More importantly, this basis set can be used in calculations involving ionic species.⁵⁷

2.3. Geometry Optimisation

The separation of the nuclear and electronic degrees of freedom by the Born-Oppenheimer approximation leads to a mental picture of a chemical reaction as nuclei moving on a potential energy surface. The easiest path from one minimum to another, that is, for transforming one chemical species to another, is along the reaction path having the lowest energy which is also referred to as the minimum energy path (MEP).⁵⁶

The most common calculation performed in many computational programs is the optimisation of the molecular geometry to a minimum (minimisations or locating minima) on the potential energy surface. Optimisations to locate transition structures are handled similarly but these involve the use of different keywords.³

Potential Energy Surface (PES)

The Potential Energy Surface (PES) is the graphical description of the way the energy of molecular system varies with small changes in its structure.³ A potential energy surface is a mathematical relationship linking molecular structure and the resultant energy.⁵⁶

There are two minima on the potential energy surface of Figure 2.3. The lowest point on the potential surface is referred to as a local minimum and the global minimum is the lowest energy point anywhere on the potential energy surface. If the structure of a molecule at this minimum point is changed slightly, it leads to motion in any direction. This motion results in a higher energy. In the case of single molecules, the minima correspond to different conformations or structural isomers. For multicomponent systems the minima correspond to the reactants and products.³

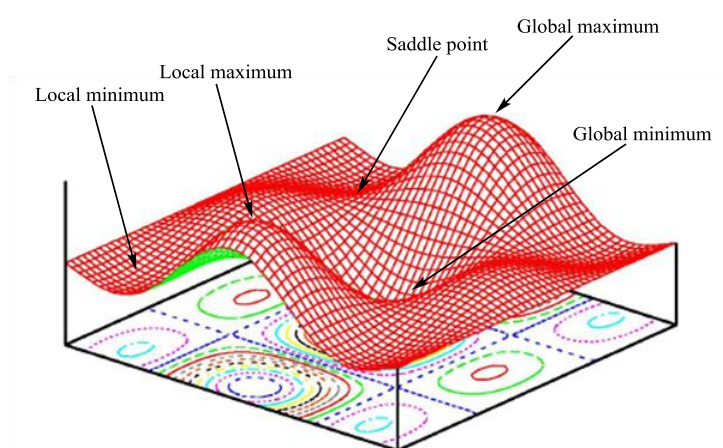


Figure 2.3 3D presentation of a typical PES⁹⁶

Peaks and ridges represent maxima on the potential energy surface. A peak is a maxima along and across the ridge. The local minimum which is a low point along a ridge is a local minimum in one direction (along the ridge) and a maximum in the other. A point which is a maximum in one direction and a minimum in the other is called a saddle point. A saddle point thus corresponds to a transition structure connecting the two equilibrium structures.³

2.3.1. Locating minima

At the minima the first derivative of the energy known as the gradient is zero. Since the gradient is the negative of the forces, the forces are also zero. The term stationary point refers to any point on the potential energy surface where the forces are zero.³ All successful optimisations locate a stationary point.

A molecular structure is specified as an input and marks the beginning of the geometry optimisation which steps along the potential energy surface. It calculates the energy and the gradient at each step and then determines how far and in which direction to make the next step. The gradient at a particular point indicates the direction (along the surface) and steepness of that slope in which the energy decreases most rapidly.³ An optimisation is complete when it has converged, that is, when the forces are zero.

2.3.2. Locating maxima

Transition structure modeling

The elucidation of reaction mechanisms is a major challenge to chemists. Generally the geometries of the reactants and products are obtained experimentally by performing a variety of analyses using spectroscopic methods such as Infra Red (IR) and Nuclear Magnetic Resonance (NMR). However, these methods provide very little information about the connecting pathways.⁵¹ A simple one-dimensional illustration of a reaction path is represented in Figure 2.4.

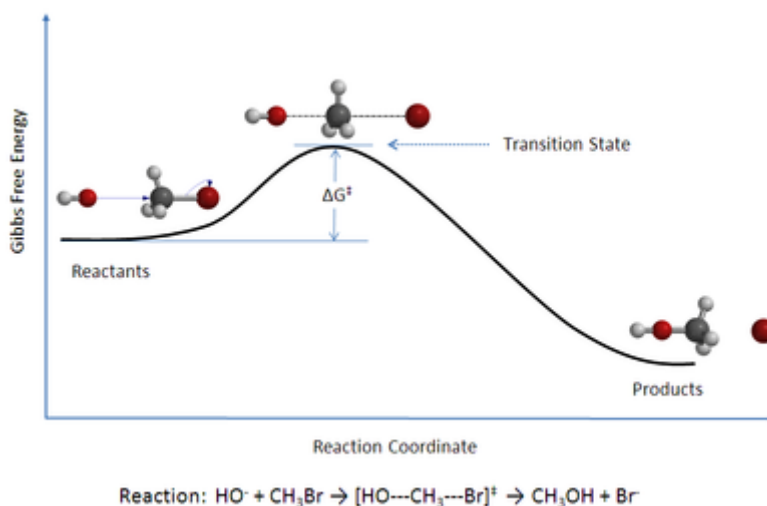


Figure 2.4 Reaction coordinate diagram for the bimolecular nucleophilic substitution ($\text{S}_{\text{N}}2$) reaction between bromomethane and the hydroxide anion⁹⁷

This means that a molecule that has reached the transition state will either proceed on to the products, or if it does not have enough kinetic energy, will fall back to the previous structure. The transition state is the configuration that connects the reactants/intermediates and products in the reaction pathway. The transition state structure with the highest energy in the reaction path is called the rate determining step of the reaction. The two terms are often used interchangeably.⁵⁷

A transition state structure is defined mathematically as the geometry which has a zero first derivative of energy with respect to moving *every* one of the nuclear coordinates and has a positive second derivative of energy of all but *one* geometric movement which has a negative curvature. This description however, describes many structures other than the specific required transition state; for example an eclipsed conformation, the intermediate point in a ring flip, a simple rotation of a methyl group or any structure with a higher symmetry than the ground state of the compound. Thus to identify a transition state structure a reliable technique is required.^{3,98}

Similar models and methods of calculation were applied to the reactants and products to examine the potential energy surface to establish whether or not a given structure corresponds to a local minimum (stationary point) or a saddle point (transition structure). The geometry and energy of a transition state structure include important pieces of information for describing reaction mechanisms. The reaction pathways can

then be established as those involving a progression from the reactants to the products over the lowest energy transition structures.⁵¹

Currently reaction mechanisms can be directly examined experimentally using femtosecond pulsed laser spectroscopy. This technique is limited to a few reactions and it will be some time before it can be applied to all of the compounds that are accessible computationally. Although short-lived reactive intermediates are sometimes detected experimentally, it is difficult to obtain information about their structures. These species (short-lived reactive intermediates) that represent shallow minima on the potential surface can thus in most cases only be characterised with computational methods.⁹⁸

Frequently predictions of transition states are based on proposed mechanisms that may be incorrect. Thus computer simulations of the geometries of transition structures are important since they can elucidate the correct geometry and consequently the correct reaction path. Furthermore, these techniques yield indirect information such as vibrational information rather than a likely geometry for the transition structure.^{51,57}

Methods available for transition structure modeling

Finding transition structures is not an easy task. There are no general techniques available for transition structure modeling. Of the many different methods that have been proposed for transition state modeling, the majority can be divided into two categories, interpolation approach and local methods. These processes assume that the reactant and product geometries are known and a transition structure is located somewhere between these two species (reactant and product). It must be noted, however, that many of the interpolation methods do not locate the transition structure but rather locate a point close to the transition structure.

Interpolation methods

In the Linear Synchronous Transit (LST) method all (Cartesian or internal) coordinates are varied linearly between the reactant and product. No optimisation is performed when the LST technique is used. This is considered as a coordinate driving method.⁹⁸

The assumption made is that all variables change linearly along the reaction path. The transition state is estimated as the highest energy structure along the interpolation line. This method, however, only works for simple systems.

In the Quadratic Synchronous Transit (QST) mode the reaction path is approximated by a parabola instead of a straight line.⁵⁷ QST techniques generally are an improvement over LST methods. The shortfall of this process is that it assumes that the reaction is a single step with a collective motion of all atoms. However, these methods can be used individually for each step in a multi-step reaction.

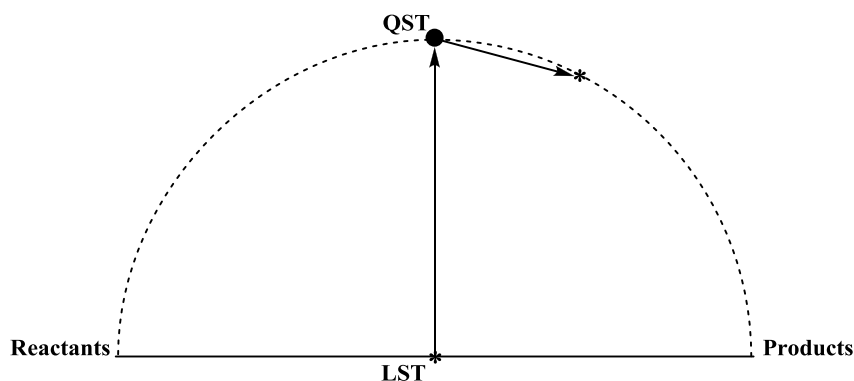


Figure 2.5 Illustration of the LST and QST methods; energy maxima and minima are denoted by * and •, respectively.⁵⁷

In certain circumstances it is better to use starting geometries that have been created manually especially for a reaction that has only one transition state but the motion does not involve bond breaking accompanied by simultaneous forming of another.⁹⁸ The LST and QST methods are illustrated in Figure 2.5.

Local methods

The local method does not require information about the reactant and/or product. The geometry of the transition structure is generated using only information about the function and its first and second derivatives at that point. Local methods require a good estimate of the transition structure in order to converge. Once the transition structure has been located, the whole reaction path can be created by tracing the intrinsic reaction coordinate (IRC).⁹⁹

Another useful technique is the pseudo reaction coordinate. This method involves much work and demands more computer time than the other techniques. However, it has the advantage of being extremely reliable. A pseudo reaction coordinate is calculated by first choosing a geometric parameter that is involved in the reaction (such as the bond

length for a bond that is being formed or broken). A series of calculations is then performed in which this parameter is fixed at various values from those in the reactants to those in the products. All the other geometric parameters are then optimised. This method does not give a true reaction coordinate but rather an approximation.⁹⁸

Computational methods employed in the Gaussian computer program

In Gaussian 09¹⁰⁰ there are two methods for modeling transition structures. The QST2 and QST3 methods have the capability of automatically producing a starting structure for a transition-state optimisation based on the reactants and products that the transition state connects.³ This is referred to as the Synchronous Transit-Guided Quasi Newton (STQN) method. This method utilizes the interpolation method, quadratic synchronous transit (QST) approach to progress closer to the quadratic region of the transition state. It then employs a quasi-Newton or eigenvector-following algorithm to complete the optimisation.¹⁰¹ The QST2 method needs two molecule specifications, that is, the reactants and products. The QST3 method, on the other hand, needs three molecule specifications, that is, the reactants, the products and an initial structure for the transition state, respectively. The QST2 and QST3 methods were initially attempted in this study, but both did not yield favourable results.

Characterisation of transition structures

In order to determine the nature of the stationary points found, a frequency calculation is performed. The frequency (discussed in the next section) output file provides information that is vital in characterising the stationary point, namely, the number of imaginary frequencies and the normal mode corresponding to the imaginary frequencies. Imaginary frequencies are listed as negative numbers in the output file. The definition states that a structure that has n imaginary frequencies is an n^{th} order saddle point. Thus transition structures are usually characterised by one imaginary frequency since they are first-order saddle points.³ The movement of atoms associated with the one imaginary frequency should follow the atoms on the reaction path between the reactant and product.

The other method of verifying a transition structure is by performing an Intrinsic Reaction Coordinate (IRC) calculation. This calculation inspects the reaction path

leading down from a transition structure on a potential energy surface. The calculation begins at the saddle point and follows the path (a fixed number of times, the default being 6) in both directions from the transition state. The geometry of the molecular system at each point along the path is optimised. In this way, an IRC calculation definitely connects two minima on the potential energy surface by a path which passes through the transition state between them.⁹⁸

It should be noted that the calculated potential energy surfaces are sensitive to the level of theory employed and the characterisation of simple potential energy surfaces may entail the location of one or more stationary points and transition structures.⁵¹

2.4. Frequency calculations and thermochemistry

The progress in the development of useful approximate functionals and the availability of versatile software has made DFT the popular method of choice for the computation of vibrational frequencies.^{76,77,102-105}

All frequency calculations include the thermochemical analysis of the system. The calculated normal-mode vibrational frequencies have three important functions. First they are used to characterise stationary points on the molecular potential surface, that is, to distinguish local minima (real or positive frequencies) from saddle points (a single imaginary or negative frequency) as discussed above. Second, for stable but highly reactive or otherwise short-lived molecules, they provide a means of identification. Finally, these calculated normal-mode vibrational frequencies provide thermodynamic properties of stable molecules by way of statistical mechanics.

The calculation of vibrational frequencies using DFT methods is significantly aided by the availability of analytical second-derivative techniques.¹⁰⁶⁻¹⁰⁹ One major advantage of DFT based frequency calculations is that they are computationally less demanding in terms of CPU time and disk usage than the conventional *ab initio* techniques such as the MP2 method.⁹⁵ Several recent studies^{110-115,105} have proved to be much better than HF theory¹¹⁶ since the calculated vibrational frequencies using DFT methods have shown that they compare well with experimental data.

Thermochemical calculations using the Gaussian program

In the Gaussian program the total energy of the molecule, from the frequency calculation, is given as the sum of the electronic and zero-point energies ($\gamma_0 + \gamma_{ZPE}$), the sum of the electronic and thermal energies ($\gamma_0 + \gamma_{tot}$), the sum of the electronic and thermal enthalpies ($\gamma_0 + H_{corr}$) and the sum of the electronic and thermal free energies ($\gamma_0 + G_{corr}$).¹¹⁷ The portion of the frequency output file that provides the information described can be found in APPENDIX 1.

For the determination of the enthalpy of the reaction, the heat of formation $\Delta_r H^0$, will have to be calculated first using the equation:

$$\Delta_r H^0(298K) = \sum_{products} \Delta_f H^0_{prod}(298K) - \sum_{reactants} \Delta_f H^0_{react}(298K) \quad (2.20)$$

The difference of sum of the products and reactants gives the enthalpy change of the reaction. However, since the sum of the electronic and thermal enthalpies is provided, the enthalpy of the reaction is calculated as follows:

$$\Delta_r H^0(298K) = \sum_{products} (\varepsilon_0 + H_{corr}) - \sum_{reactants} (\varepsilon_0 + H_{corr}) \quad (2.21)$$

Gibbs free energy change can be calculated similarly using the equation:

$$\Delta_r G^0(298K) = \sum_{products} (\varepsilon_0 + G_{corr}) - \sum_{reactants} (\varepsilon_0 + G_{corr}) \quad (2.22)$$

Once the Gibbs free energy has been computed, the rate of the reaction can also be calculated as follows:

$$k = \frac{k_B T}{hc} e^{-\Delta_r G^0/RT} \quad (2.23)$$

where k_B is the Boltzmann constant, T is the temperature (which is a default of 298K), h is Planck's constant and c is the concentration (which is usually 1).

To calculate Gibbs free energy of formation for the reaction, the entropy term is added and gives the following equation:

$$\Delta_r G^0(298K) = \Delta_f H_{prod}^0(298K) - T \left(S^0(M, 298K) - \sum S^0(X, 298K) \right) \quad (2.24)$$

where S^0 is the entropy, M is the molecule and X is the element that makes up M .

By default this analysis is carried out at 298.15 K and 1 atmosphere of pressure, using the principal isotope for each element type.³

Reliable values for stable molecules are well established and have been presented in several collected works. Thus, heats of formation, Gibbs free energy and reaction entropies, which are widely used to investigate the structures of stationary points and reactive intermediates, may be calculated from first principles. In addition, these quantities can also be obtained for the transition structures. Kinetic isotope effects and entropies of activation are of particular interest since they provide mechanistic information.¹¹⁸ Theoretical vibrational frequencies may also be used to correct experimental thermochemical data to 0 K and to evaluate zero-point vibrational energies.⁵¹

The thermochemistry of molecules is thus of significant importance since it provides information on the stabilities and reactivities of molecules in either the gas or solvated phase.¹¹⁹

2.5. Solvation studies

Solvent effects are included in the theoretical description of chemical systems using both discrete¹²⁰⁻¹²⁶ and continuum¹²⁷⁻¹³⁰ solvent models. Discrete models utilise simulation methods such as molecular dynamics and Monte Carlo, which use a classical force field and the explicit treatment of solvent molecules.¹³¹ Discrete methods work well on problems using chemical intuition; however it requires much computational

effort even for simple systems. This makes it unfeasible to use at high levels of the quantum mechanical (QM) theory and reduces its applicability.¹³²

The second method, continuum solvent models, focuses on the use of the self-consistent reaction-field (SCRF). In the continuum models the explicit solvent structure is not considered.^{133,134} This means that the solute's electronic distribution can be treated quantitatively and polarization effects are evaluated at a low cost. This feature thus makes the SCRF method an attractive option for solvation studies.

The Continuum Model

The continuum model or reaction field theory was proposed in 1934 by Kirkwood^{135,136} and in 1936 by Onsager¹³³ to account for the electrostatic effects of solvation. In Onsager's model, the solute molecule with a dipole moment is placed in a cavity in a polarisable continuum, representing the solvent, with a dielectric constant ϵ . Although "dielectric constant" is an archaic term it is still used in Gaussian. The term "relative permittivity" is currently used and refers to the dielectric constant. The dipole moment of the solute polarises the solvent. This produces a reaction field F which interacts with the solute, thus resulting in a stabilising solvation energy. Onsager's reaction field is hence given as:

$$F = g\mu \tag{2.25}$$

where

$$g = \frac{2(\epsilon - 1)}{(2\epsilon + 1)} \frac{1}{R_0^3} \tag{2.26}$$

for a spherical cavity of radius R_0 . The solvation energy W_{solv} is then defined simply as:

$$W_{\text{solv}} = -\frac{1}{2}\mu \cdot F. \tag{2.27}$$

Kirkwood's¹³⁶ model (proposed in 1938) is a generalisation of Onsager's approach. The solute is represented in terms of a multipole expansion of its charge distribution with quadrupole and octupole as well as dipole moments. In the case of a charged solute, a monopole or Born term is also included. The solvation energy is thus written as:

$$W_{\text{solv}} = -\frac{1}{2} \sum_l \sum_{m=-l}^l M_{lm} F_{lm} \quad (2.28)$$

with

$$F_{lm} = g_l M_{lm} \quad (2.29)$$

where M_{lm} are the components of the permanent multipole moment tensor of the order l , with F_{lm} being the components of the corresponding reaction field tensor, and

$$g_l = \frac{(l+1)(\epsilon-1)}{(l+1)(\epsilon+1)} \frac{1}{R_0^{2l+1}} \quad (2.30)$$

R_0 is the cavity radius. This is also referred to as the multipole expansion reaction field (MPE) model.¹³⁷

Many other useful computational methods that are employed for solvent modelling are based on the continuum solvent model.¹³⁸ One vital asset of the continuum method is the drastic reduction in the number of degrees of freedom that is considered when treating a chemical problem in the liquid phase. Computational simulations with explicit solvent monitor a larger number of degrees of freedom and many of these have a minimal direct influence on the final results. Another advantage of the continuum model is its versatility: continuum methods have been coupled successfully to almost all molecular structure systems.¹³⁹

The SCRF technique

The self-consistent reaction field (SCRF) technique has been developed,¹⁴⁰⁻¹⁴⁶ by incorporating the essential elements of reaction field theory in conventional quantum chemical methods, such as the Hartree-Fock self-consistent field (SCF) approach. This is expressed as an equation where the term describing the interaction of the solute molecule with the reaction field \hat{H}_{RF} is added to the (unperturbed) Hamiltonian \hat{H}_0 of the free solute molecule,

$$\hat{H}_S = \hat{H}_0 + \hat{H}_{\text{RF}} \tag{2.31}$$

$$\hat{H}_{\text{RF}} = - \sum_{1,m} \hat{M}_{1^m} F_{1^m}, \tag{2.32}$$

where, \hat{M}_{1^m} are the components of multipole moments operators.

The Hartree-Fock, Møller-Plesset perturbation and density functional theory methods are then used to determine the energy, wavefunction and multipole moment in the presence of a reaction field which is described by the perturbed Hamiltonian \hat{H}_S . The process is repeated until convergence is achieved.¹⁴⁷

The SCRF approach is a simple, as well as an extremely useful technique for the study of solvation effects. SCRF methods model the solvent as a dielectric constant, ϵ : as described by the continuum model discussed in the previous section above. This cavity model, in the absence of strong intermolecular forces such as hydrogen bonding or donor-acceptor interaction, has been found to account for the effects of solvation extremely well.¹⁴⁷

The main difference between the SCRF method and the Onsager-Kirkwood approach is that SCRF accounts for the polarisability of the solute molecule, since the converged multipole moments of the solute are determined in the presence of a reaction field.¹⁴⁷

The PCM and other Continuum Models

The polarisable continuum model (PCM) was first proposed by Miertuš, Scrocco and Tomasi.¹⁴⁸ As stated in the SCRF method the solvent is represented by a continuum dielectric medium, however, a cavity is “dug” to host the solute molecule. The cavity is defined as the union of a series of interlocking atomic spheres. The shared polarisation of the solute and the dielectric is calculated by numerical integration rather than by an approximation to the analytical form used in the Onsager model.³

The PCM model calculates the free energy in solution as the sum of three terms that represent the electrostatic and dispersion-repulsion contributions to the free energy, and the cavitation energy. All three terms are calculated using a cavity determined from a surface of constant charge density around the solute molecule. The reaction field is represented through point charges, referred to as apparent solvation charges (ASCs), located on the surface of the molecular cavity.¹⁴⁹ The cavity surface is partitioned in small tiles, the tesserae, where the ASCs are located. The number of tesserae is one of the parameters that influence the accuracy of the results and the computational times.¹⁵⁰

The PCM method is frequently the chosen method for solvent modeling since it is robust and flexible. It is also easily coupled with both classical calculations, such as molecular mechanics (MM) or molecular dynamics simulations, and in the case of quantum methods such as HF¹⁵¹, DFT^{152,153} and MP2.^{154,155} The PCM method can also be applied at the multiconfigurational self-consistent field (MCSCF)¹⁵⁶ and the quadratic configuration interaction singles and doubles (QCISD)¹⁴⁵ level.

There are two isodensity surface based SCRF models. These also use a numerical representation of the solvent field. The first is the Isodensity PCM (IPCM) model which defines the cavity as an isodensity surface of the molecule. In this model an iterative process is used in which an SCF cycle is performed and converged using the current isodensity cavity thus determining this isodensity. The product of this calculation is the wavefunction which is subsequently used to process an updated isodensity surface. The cycle is repeated until the cavity shape no longer changes upon completion of the SCF.³

The second isodensity surface based SCRF model is the Self-consistent Isodensity Polarised Continuum Model (SCI-PCM). This model includes the effect of solvation in the solution of the SCF problem since the isosurface and the electron density are coupled. This procedure, which allows the effects of solvation to be folded into the iterative SCF computation rather than including an extra step afterwards, solves for the electron density which minimises the energy, including the solvation energy. The SCI-PCM method thus accounts for the full coupling between the cavity and the electron density and includes coupling terms that IPCM neglects.³

Since its proposal in 1981, the PCM has undergone a number of modifications and improvements. These include a new method for incorporating the solvent effect into *ab initio* and DFT frameworks,⁴⁹ an integral equation formalism (IEF) to the PCM method,¹⁵⁷ a plane wave implementation,¹⁵⁸ a linear scaling procedure,^{132,150} an improved iterative solution to solve the electrostatic problem,¹³⁹ and time dependent solvation.¹⁵⁹ A detailed review of continuum solvation is available.¹⁶⁰

The HF method, although a basic theory, is often used for the initial exploration of the properties of a system. The MP2 method is extremely computationally demanding and normally only practical for small systems. The MCSCF and QCISD methods are equally expensive to calculate. Thus gradient-corrected DFT methods present the possibility of accurate calculation of the electron correlation effects and are computationally efficient as well. Thus the use of DFT with the continuum models for solvation is a preferred way to proceed for the modeling of solvent effects.¹⁵⁵

CHAPTER 3

COMPUTATIONAL DETAILS

This study was performed on a series of related molecules using the Gaussian 03 (G03)¹⁶¹ program implemented on a ROCKS cluster housed at the Durban University of Technology (AMD 64L) with sixteen CPU's and at the Meraka Institute at CSIR, Pretoria on an opteron AMD 64L cluster with eight CPU's. A true 64 bit operating system was implemented on both the clusters with a parallelised version of the Gaussian 03 program. All the calculations were upgraded using Gaussian 09 (G09)¹⁰⁰ on the clusters at the Centre for High Performance Computing (CHPC), Cape Town. The IBM e1350 cluster has a AMD opteron central processing unit (CPU) with a 2.6 GHz CPU clock and 2048 CPU cores. The peak performance of this unit is 3.3 TeraFlops. The Sun Hybrid System has an Intel Nehalem Processor with a 2.93 GHz CPU clock and 2304 CPU cores. The Sun cluster has a peak performance of 24 TeraFlops.

3.1 The Gaussian 09 Program

The G09 program is one in a series of electronic structure computer programs that began with Gaussian 70, Gaussian 92, Gaussian 94 and Gaussian 98. Gaussian 03 was released in April 2003. The latest version was Gaussian 09 which made its appearance in April 2009.

The Gaussian programs are general-purpose programs capable of performing semi-empirical and *ab initio* molecular orbital calculations based on the linear combination of atomic orbitals (LCAO) approach. However, as its name implies, the program deals mainly with Gaussian-type orbitals, which have been described in detail in Chapter 2. In addition, G09 calculates energies, molecular structures, vibrational frequencies and numerous other molecular properties for systems in the ground state and excited states in the gas phase and in solution. It is thus a powerful tool for exploring substituent effects, reaction mechanisms, potential energy surfaces and excitation energies. G09 is an improvement to its predecessor G03. Fundamental algorithms and existing methods have been updated to improve the different types of calculations.

The input file of a Gaussian job consists of different sections. The first is the "Link 0 commands" section. This is used to identify the location and the name of the scratch

files as well as the amount of disk storage for the scratch file. The second is the “route” section. Here the task or the calculation to be performed is specified, that is, a single-point calculation, geometry optimisation or frequency calculation. This must be specified together with the appropriate basis set and the level of theory. The third is the “molecule specification” section. This section begins with the molecular charge and the multiplicity of the system; next the symbols of the constituent atoms and a definition of the molecular structure, either in the form of cartesian coordinates or the Z-matrix notation, which defines the molecular geometry in terms of bond lengths, bond angles and dihedral angles, is specified. In the final section of the input file additional commands can be included. This section is usually used for specific job types such as a scan calculation, freezing coordinates and others.

The 3D structures on the CD accompanying this thesis are written in the Gaussian input file format expressed with the extension *.*gjf*. The geometries of the structures can be viewed by using the GaussView program or the freeware (Molekel) program.

3.2 The GaussView Program

GaussView¹⁶² is a Graphical User Interface (GUI) program designed to simplify and extend the use of the Gaussian 09 program. However, GaussView is not directly integrated into the Gaussian 09 program system, but acts as a front-end/back-end processor to facilitate its use on a desktop workstation. GaussView provides three main benefits to Gaussian 09 users. Firstly, through its advanced visualisation facility, GaussView allows molecules to be drawn and rotated, translated and zoomed in through simple mouse operations. It also allows standard molecule file formats such as the protein data base (PDB) files to be imported.

Secondly, GaussView makes it easy to set up many types of Gaussian calculations. It makes preparing complex input easy for both routine job types and advanced methods like QST2/QST3 transition structure optimisations. GaussView can also be used to launch jobs as well if Gaussian is installed on the same computer.

Finally, GaussView is used to examine the results of Gaussian calculations using a variety of graphical techniques. The following Gaussian results can be viewed graphically: optimised molecular structures; molecular orbitals; electron density

surfaces from any computed density; electrostatic potential surfaces; surfaces for magnetic properties; atomic charges; animation of the normal modes corresponding to vibrational frequencies; IR, Raman, NMR, VCD and other spectra; animation of geometry optimisations; IRC reaction path following; potential energy surface scans and plots of the total energy.

In this study, GaussView was used to build and edit molecules; set up and submit Gaussian 09 jobs and to graphically examine all the output that Gaussian 09 produces.

3.3 The Relaxed Scan Calculation

The scan option was part of the procedure used as an aid to finding an approximate starting structure for a transition state. A scan calculation involved changing the bond length, angle or the dihedral angle from reactants to products, in a step-wise manner. The only constraint in this calculation is the required reaction coordinate (the bond length, angle or the dihedral angle). The rest of the molecule is then optimised to find the lowest possible structure and energy, subject to the imposed constraints. The energy at each step is plotted against the reaction coordinate. By inspecting the different structures at each step of the scan job, one could follow the course of the reaction. The approximate starting structure for a transition state/structure optimisation was obtained by saving the coordinates of the structure closest to the maximum on the energy *vs* reaction coordinate plot. This approximate starting structure is then submitted for a full (non-constrained) geometry optimisation. The transition structure was verified by performing a frequency calculation. If the frequency calculation produced only one negative eigenvalue, that is usually associated with the movement of atoms involved in either bond breaking or bond formation, then it was concluded that the transition structure obtained was correct. If the frequency calculation showed incorrect movement of the atoms, then the scan calculation was repeated with modifications.

3.4 Keywords used in G09

Several keywords have been used in this study. The keywords and their definitions are set out as they have been used in the calculations for the transition structure modeling (the scan calculation) and those used for solvent modeling.

OPT and TS

The OPT keyword, which requests a geometry optimisation, is used in conjunction with other keywords. The geometry is adjusted according to a mathematical algorithm to follow the energy surface “down hill” until a stationary point on the potential energy surface is found. It must be noted that the algorithm by nature would not overcome local minima and special techniques such as automatic or manual conformational searches or molecular dynamics^{163,72,164} should be employed to overcome, mainly, rotational energy barriers. This is more problematic in flexible molecules such as peptides.

The keyword used to search for a transition state is TS. The TS algorithm utilises a combination of Rational Functional Optimisation (RFO) and a linear search step to search for the lowest maximum on the energy surface between the reactant and the product. The mathematical algorithm by default uses a crude semi-empirical guess for the initial start structure to solve the transition state wavefunction. If the starting structure is too far from the real maximum on the energy surface, the search algorithm would not find the correct transition structure within the multitude of local maxima.

For the HF, DFT and semi-empirical methods, the Bery algorithm is the default algorithm for minimisations to a local minimum and optimisations to transition states and higher order saddle points.

NOEIGENTEST

The default transition state search in G09 makes use of the EigenTest. If only one imaginary frequency is found, the calculation continues to find the transition state associated with this negative eigenvalue. If more than one imaginary frequency exists, the default routine is to terminate the calculations. Since it is practically almost impossible to find a starting structure for a transition state with one and only one negative eigenvalue, the default TS calculation terminates frequently. In order to overcome this oversensitive search criterion, the "NoEigenTest" option which overrides the default search criteria in G09 is used.³

MODREDUNDANT or ModRed

This is used in the route section for a scan calculation and if coordinates are frozen or fixed. The specific coordinates that are to be constrained are specified at the end of the Cartesian coordinates in the molecule specification.

GEDIIS

In G03 this keyword specified the use of the modified GDIIS algorithm. It was recommended for use with larger systems, tighter optimisations and molecules with flat potential energy surfaces. It was the default keyword for semi-empirical calculations. This command made use of a smaller step-size down the potential energy valley. In G09 the GDIIS keyword has been replaced by the GEDIIS keyword. It utilises the GEDIIS optimisation algorithm. This is the default for minimisations when gradients are available and is particularly helpful for large, floppy molecules.

CALCFC

CalcFC specifies the force constants be computed at the first point using the current method (available for the HF, MP2, DFT and semi-empirical methods only). By default Gaussian uses a MNDO, which is a semi-empirical guess, for the solution to the wavefunction of the specified system. Since the MNDO guess is based on a rather crude or inaccurate method, the calculation could sometimes follow a wrong solution for the wavefunction. This can be corrected by starting with a better structure, that is, a structure that was optimised at a lower level of theory.

Freeze and Scan

These keywords are specified in the additional commands section at the end of the molecule specification. The freeze keyword, F, indicates that specified coordinates are to be frozen in the geometry optimisation. Scan, S, specifies a relaxed potential energy surface scan to be performed. The increment of the scan and the total number of steps also have to be indicated.

SCRF and PCM

This keyword requests that the calculation be performed in the presence of a solvent using one of the many models available. In this study, the PCM model was used. In

G03, for quantum mechanical calculations, PCM performs a reaction field calculation using the IEF-PCM model. In G09 PCM makes use of the same integral equation formalism model of IEF-PCM but some details of the formalism and the implementation have changed with respect to G03¹⁶⁵. The new algorithm for PCM solvation in G09 makes the energy a properly continuous function of the nuclear coordinates and includes efficient solvation of all SCF properties. Geometry optimisations with PCM now converge at the same rate as the corresponding gas-phase optimisations. The IEFPCM calculation with radii and non-electrostatic terms for Truhlar and coworkers' SMD solvation model¹⁶⁶ is the recommended choice for computing Gibbs free energy of solvation (ΔG_{sol}). Calculations for the system of interest in the gas phase and SCRF=SMD were performed. The difference of these energies results in Gibbs free energy of solvation. The solvents were represented in the route section as follows: water as H₂O, acetonitrile as CH₃CN, dimethyl sulphoxide as DMSO and methanol as CH₃OH. Carbon tetrachloride and dichloromethane were specified as is.

Integration Grid selection option

The method of computation and the use of the two-electron integrals and their derivatives are modified by the integral keyword. Grid specifies the integration grid to be used for the numerical integrations. In this study it was represented as Int=FineGrid.

SCF and Tight

The SCF keyword controls the functioning of the SCF procedure by specifying the behaviour and algorithms. The Tight keyword requests a normal, tight convergence in the SCF.

Specifying the molecular cavity and output options for solvation effects

By default, the program builds up the cavity using the UFF radii, that is, by putting a sphere around each solute atom. There are three United Atom (UA) models available, namely, RADII, SPHEREONH and SPHEREONACIDICH. The topological model is applied on radii optimised for the B3LYP/6-31G(d) level of theory. PCMDOC requests that the descriptions and values of all the internal PCM parameters be included in the Gaussian log file. The tesserae and the number of tesserae were specified.

The keywords listed above were used to describe the procedure or the method in which this computational study was carried out. The computational details, in the form of a computational model, are discussed in detail the next chapter.

CHAPTER 4

THE COMPUTATIONAL MODEL

In the 1990s an important change was observed in the standard theoretical model that was most commonly used in quantum chemistry. Before the introduction of DFT, *ab initio* quantum chemical calculations⁵¹ used Hartree Fock (HF) as the starting point followed by the second order Møller-Plesset (MP2) perturbation theory. The couple-cluster theory, quadratic configuration interaction and other related methods were used if a small system was being studied followed by additional calculations. Although these techniques are still used extensively, a considerable majority of papers being published today are based on applications of DFT.^{76,77} Many researchers use the popular functional defined by Becke, whose papers in 1992 and 1993⁴⁵⁻⁴⁷, contributed to this noteworthy transformation that changed the entire landscape of quantum chemistry.¹⁶⁷

Thus in this computational model, all molecular structures were first optimised at the HF level to obtain a good starting point. This was followed by an optimisation at the DFT level and lastly calculation of the energy of the system at the MP2 level. A detailed description of the computational models follows.

4.1 Computational model and calculation details for the stationary points

The starting point for all calculations in this study was to model or draw the molecules in GaussView.¹⁶² In order to remove any van der Waals contacts or overlap, the structure was “cleaned”, that is, an energy minimisation was performed in GaussView using a molecular mechanics force-field. The “clean” feature in GausView adjusts the geometry of the molecule, based on a defined set of rules, to closely match chemical intuition. The result of “cleaning” is an approximation and is not intended to be a perfect structure. The final “cleaned” structures were saved as input files for a geometry optimisation in G09.

In this study, for the calculations in the gas phase, the structures were submitted for an optimisation at the HF level first. When these were completed, the optimised structures from the HF level of calculation were saved and submitted at the DFT level. As mentioned the B3LYP functional with the 6-31+G(d) basis set is the most popular

method used for organic molecules. In a previous work on condensed versions of these PCU reactions,¹⁶⁸ the 6-31+G(d) basis set was employed for the geometry optimisations at the HF, B3LYP and MP2 levels of theory. The HF level calculations are known^{38,169} to overestimate transition state energies hence all optimisations were upgraded to DFT using B3LYP¹⁷⁰. DFT approximates the effect of electron correlation and produces superior results. The smaller 6-31+G(d) basis set produces almost the same geometries and relative energies as what could be obtained when performing these optimisations with the additional polarisation functions on hydrogen atoms. Diffuse functions are typically used as a better treatment for cases where negatively charged species are being studied because the ionic radius of an anion increases significantly as compared with the corresponding neutral species. Polarisation functions remove some limitations of the basis set by expansion of the virtual space.¹⁶⁸ When the DFT optimisation was done the output structure was taken for a frequency calculation as well as a single point (SP) MP2 calculation. A summary of the thermodynamic energies for each mechanism at the B3LYP and MP2 is presented as follows: mechanism 1 (APPENDIX 1, Table A1.1); mechanism 2 (APPENDIX 2, Table A2.1); mechanism 3-route 1 (APPENDIX 3, Table A3.1) and mechanism 3-route 2 (APPENDIX 3, Table A3.17). A frequency calculation was performed on the stationary points to obtain the thermodynamic data from the output file.

For the calculations using the different solvents, again the optimised structure of the stationary points at the DFT level was used as a starting point. However, in this calculation instead of OPT the SCRF keyword was used. Here the dielectric constant (relative permittivity) for the different solvents was specified along with the PCM model. In this study the SMD solvation model was used for computing Gibbs free energy (ΔG) and Gibbs free energy of solvation (ΔG_{sol}). Here as well the same procedure was followed: the output was optimised at the DFT level and a frequency calculation was performed to obtain the thermodynamic data.

4.2 Computational model and calculation details for the transition state structures

For the transition state structures, either the reactant or the product was used as a starting point. A scan calculation was performed to locate the maxima on the potential

energy surface. A transition state scan calculation, at the HF level, was performed which involved changing the bond lengths, bond angles or dihedral angles, using the scan keyword, from the reactant to the product or *vice versa*, in a step-wise manner. This optimisation or location for transition state uses the keywords TS, Modredundant and Noeigentest. The only constraint in this calculation is the reaction coordinate, that is, the bond lengths, bond angles or dihedral angles. The molecule is then optimised to find the lowest possible energy, subject to the imposed constraints. If there is no maximum, the constraints to the molecule are adjusted and the scan is repeated. This adjustment and scan calculation procedure is repeated several times until a maximum is obtained.

The energy of each step on the scan is plotted against the reaction coordinate in GaussView. In the discussion (Chapter 5), when a scan calculation was used in locating the transition structures, the three dimensional (3D) structures have been referred to as **Scan start** and **Scan end**. **Scan start** refers to the starting structure that was submitted for the calculation. **Scan end** corresponds to the structure that was obtained at the end of the scan calculation. The different structures at each step of the scan job were inspected so that the reaction profile could be followed. The relative energies *vs* the reaction coordinate was plotted to obtain an approximate indication of the transition structure. This approximate starting structure for a full (non-restrained) transition state search was obtained from the scan calculation by saving the coordinates of the structure closest to the maximum on the reaction profile.

The approximate starting structure is used as the input in the transition state search and is referred to as **TS start**. The same basic computational methods used for the calculation of the local minimum energies were utilised in locating the geometries of the transition state structures. The only difference is that the last part of the procedure made use of a transition state optimisation during a scan close to the maximum associated with the corresponding transition state. The optimised transition structure that was obtained is referred to **TS end**.

The structure at each step of the scan calculation was examined in GaussView to follow the course of the reaction. The coordinates of the structure at the maximum of the

energy vs reaction coordinate was saved as a starting structure (**TS start**) for a non-constrained transition structure optimisation.

A transition state optimisation using the keyword CalcFC, is then performed on this non-constrained starting transition structure where the force constant is calculated at the required level/basis set and used to start the solution to the wavefunction. This is a considerably expensive calculation in terms of resources and time, since CalcFC does the same calculation as required for a frequency calculation. The optimised output structure of this calculation is optimised further at the DFT level using the keyword GEDIIS.

A frequency calculation was carried out on the optimised DFT structure (**TS end**) to verify that there is only one negative eigenvalue. An IRC was also executed on the optimised DFT structure to verify the transition structure. An additional calculation was performed to verify that the transition structure is indeed connected to the “reagent(s)” and “product(s)”. This involved submitting the first and final structures of the IRC calculation for a non-constrained optimisation to find a minimum on the energy surface. If the first structure relaxed to the reactant(s) and the final structure optimised to the product(s), then this further verified that the structure obtained was indeed a transition structure.

It was observed for certain transition structures, that after numerous attempts of adjustments and scans, a maximum or a good starting structure for a transition state search, could not be obtained. The following procedure was then followed. A starting transition structure was created using the reactants and products. A PM3 optimisation was carried out on this constructed starting point with constraints as would have been specified in a scan calculation. Here again, if the desired output structure is not produced, the constraints to the molecule are adjusted and the PM3 optimisation is repeated in order to obtain a better starting structure.

When the PM6 optimisation produces what seemed to be a more reasonable starting structure, a constrained RHF/6-31+G(d) optimisation was performed followed by an unconstrained optimisation at the same level. If this transition state calculation worked it was upgraded to a B3LYP/6-31+G(d) unconstrained transition state optimisation.

4.3 Computational model and calculation details for the addition of solvents

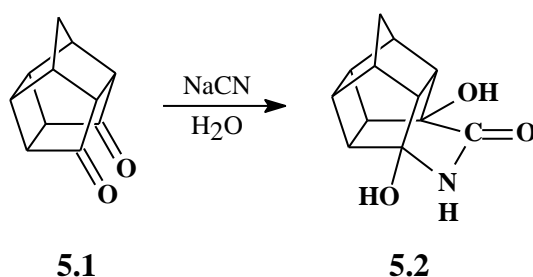
The optimised transition structure at the DFT level was used at a starting point for modeling the transition structures in the different solvents as described above. The SCRF keyword specified the dielectric constant (relative permittivity) for the different solvents together with the PCM model and the SMD solvation model. An additional command specified SCF=Tight and the integral as finegrid in the route section. The following commands were indicated at the end of the molecule specification: the topological model (RADII) with the UFF set; PCMDOC which requests that the descriptions and values of all the internal PCM parameters be included in the Gaussian log file; the tesserae (tsare) as 0.2 and the number of tesserae (tsnum) as 100.

CHAPTER 5

RESULTS AND DISCUSSION

5.1 Introduction

As explained in Chapter 1, the purpose of this study is to use computational techniques to obtain better insight into the mechanistic pathway for the one-pot conversion of pentacyclo-undecane dione **5.1** to the pentacyclo-undecane cage lactam **5.2**.



This chapter will focus on several variations of the proposed mechanistic pathways for the reaction. Mechanism 1, mechanism 2 and mechanism 3 proceed *via* two possible routes. This gives a total of six possible variations of the mechanistic pathway.

Based on the observations made during this theoretical investigation the proposed pathways were modified to include four- and six-membered ring transition state structures. This enabled the investigation of neutral reaction species, lowering the high relative energies of charged species in the gaseous phase. The relative energies for each of the mechanisms proposed in this study are depicted in the form of a reaction profile. Since the cage is very rigid, very few problems with conformational isomers of higher energies were experienced.

In this chapter, the reaction pathways will be presented followed by a table of relative energies for each mechanism and the reaction profiles. The stationary points will be identified and each transition structure will be discussed in detail. Thereafter the reaction profile for each mechanism in the various solvents will be examined and compared.

5.2 Mechanism 1

Mechanism 1 is depicted in Figure 5.1. The summary of the calculated relative thermochemical data for the structures depicted in mechanism 1 are presented in Table 5.1.

Table 5.1 Summary of the relative^a thermochemical data for the conversion of the PCU dione **5.1** to the lactam **5.2** in the gas phase [B3LYP/6-31+G(d)] for mechanism 1.

Species ^b	ΔE / kcal mol ⁻¹	ΔH / kcal mol ⁻¹	ΔG / kcal mol ⁻¹	ΔS /cal K ⁻¹ mol ⁻¹	LHVF/cm ⁻¹
5.1	0.00	0.00	0.00	0.00	102.67
5.3.1	121.66	120.86	124.78	-13.17	-122.18
5.3.2	25.85	27.71	48.33	-69.17	-272.28
5.4	0.02	1.87	13.81	-40.06	107.82
5.5.1	46.55	45.35	57.23	-39.84	-931.23
5.5.2	5.81	5.69	29.60	-80.22	-1284.30
5.6	-1.95	0.12	13.33	-44.32	120.20
5.7.1	210.91	211.04	230.73	-82.00	-464.84
5.7.2	38.95	43.18	76.50	-111.75	-332.26
5.9	-0.51	3.64	27.44	-79.85	93.40
5.10.1	43.11	43.80	68.30	-82.18	-2019.49
5.10.2	8.13	10.02	45.62	-119.40	-1400.69
5.11	-24.17	-19.10	6.59	-86.16	113.70
5.12	27.21	31.38	55.90	-82.23	-104.70
5.13	27.23	31.26	55.82	-82.37	-151.51
5.2	-46.93	-41.09	-15.97	-84.26	109.67

^a Energies relative to the energy of the starting structure **5.1**

^b Refers to the structure number in Figure 5.1

The energy in the gas phase (ΔE) (in kcal mol⁻¹), enthalpy (ΔH) (in kcal mol⁻¹) as well as Gibbs free energy (ΔG) (in kcal mol⁻¹) and entropy (ΔS) (cal K⁻¹ mol⁻¹) at 298.15 K and the lowest harmonic vibrational frequencies (LHVF) (in cm⁻¹) of the species in the formation of the PCU lactam from the PCU dione

These relative Gibbs free energy changes were used to construct the profile of the reaction in Figure 5.2. The summary of energies (Table A1.2) expressed in Hartrees and the scheme of the reaction is presented in APPENDIX 1.

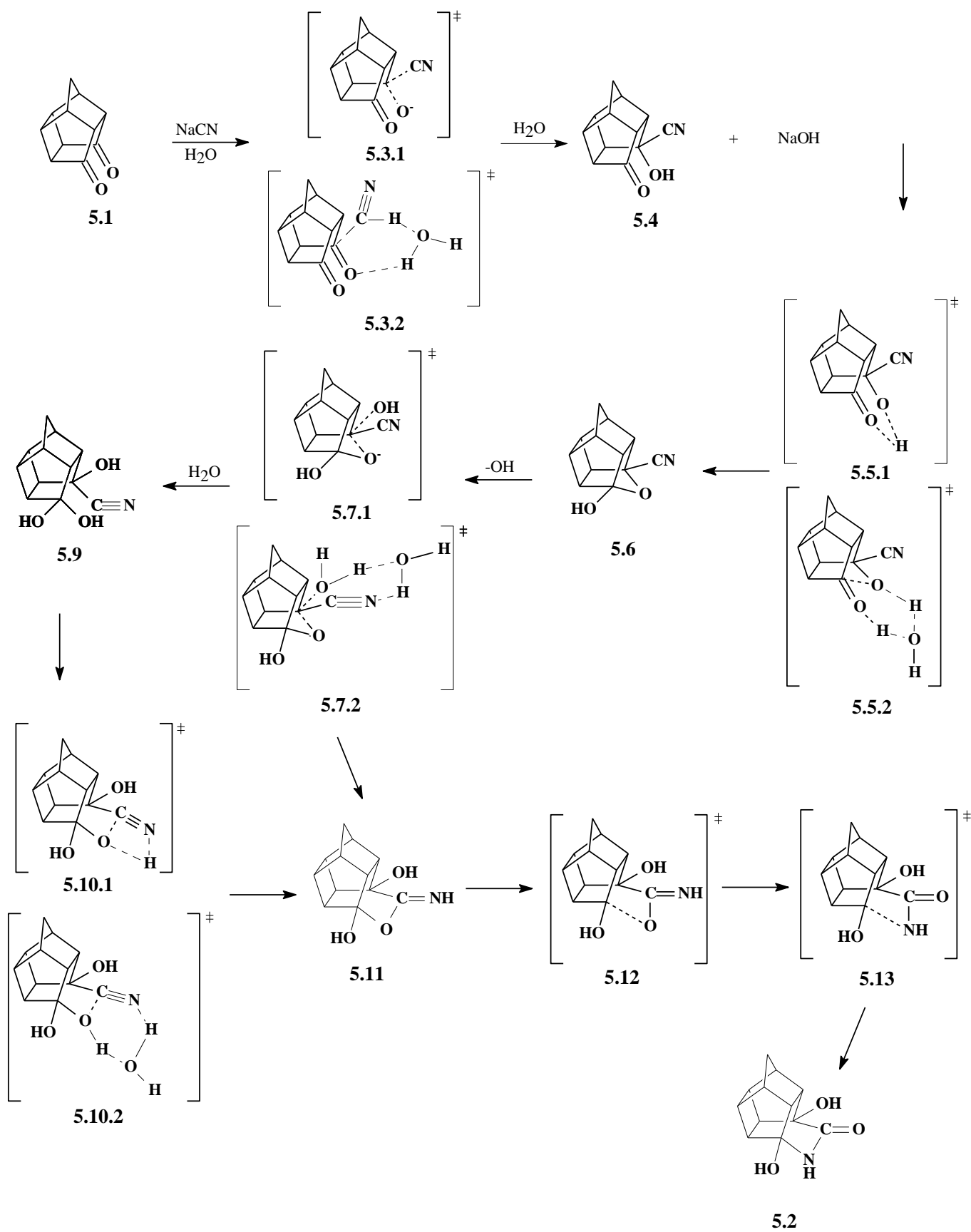


Figure 5.1 Mechanism 1 for the conversion of the PCU dione 5.1 to the lactam 5.2

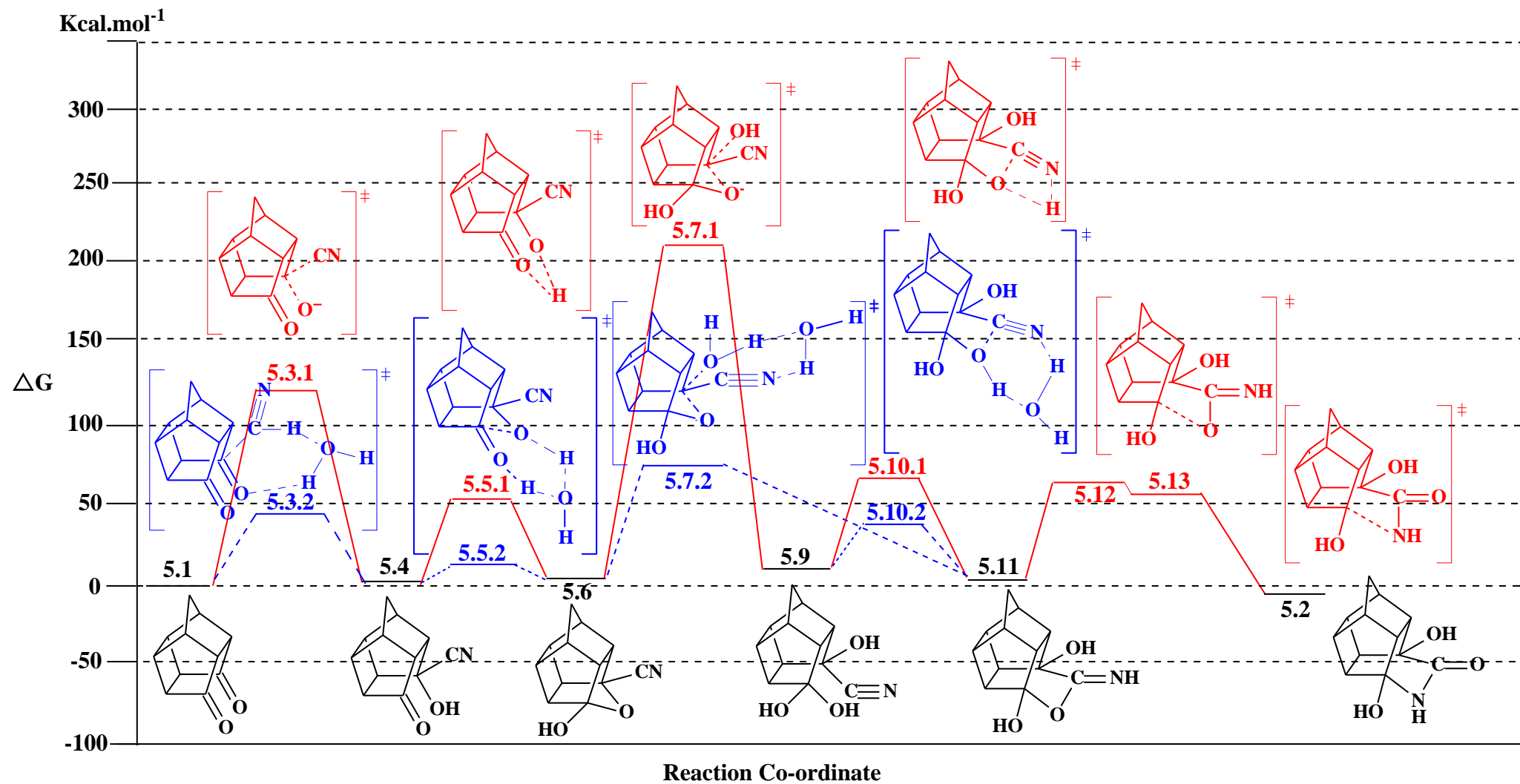
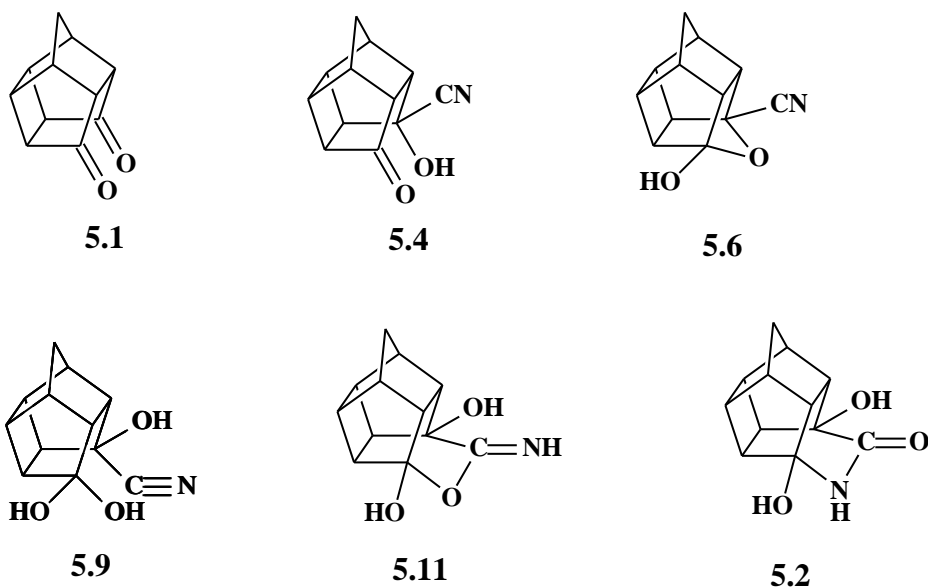


Figure 5.2 Gas phase Gibbs free energy for the mechanism proposed in Figure 5.1

The cartesian coordinates of all the 3D structures presented in this Chapter are included on the CD accompanying this Thesis.

Local minima on the energy profile

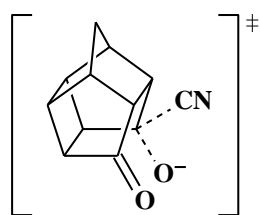
The local minima or stationary points on the energy profile of mechanism 1 were obtained from the data presented in Table 5.1 and Figure 5.2.



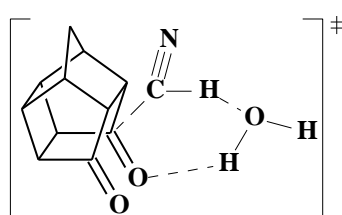
The only rotational flexibility in these structures is the C-OH groups. The absence of any negative vibrational frequencies in the calculated infrared spectra of these structures further verifies that these are local minima on the potential energy surface. The thermodynamic data were extracted from the frequency calculation and are also shown in Table 5.1.

The Transition States (TS)

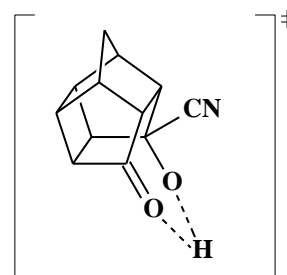
The transition states are all maximum energy structures on the energy profile (Figure 5.2). The frequency calculation of the transition states also exhibit one and one only negative frequency. The movements of the atoms associated with the negative eigenvalue were studied and they represent the movement of atoms that is expected for each specific transition state. IRC calculations were also performed and will be discussed. The inclusion of a solvent molecule in the modified transition states (to avoid the ionic character) is expected to induce a large reduction in the enthalpy energies, that is, the energy of formation despite an entropy penalty. It is clear from the results in Table 5.1 that this is worthwhile since the energy reduction from the ionic state is much more prominent.



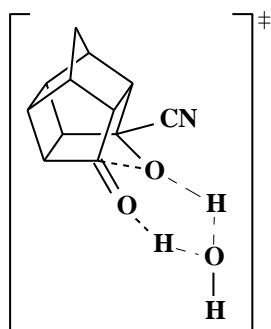
5.3.1



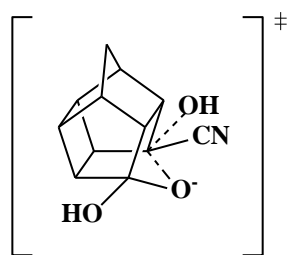
5.3.2



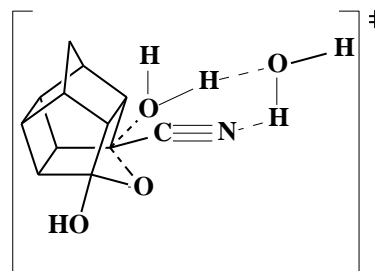
5.5.1



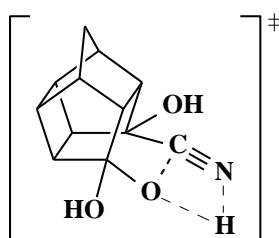
5.5.2



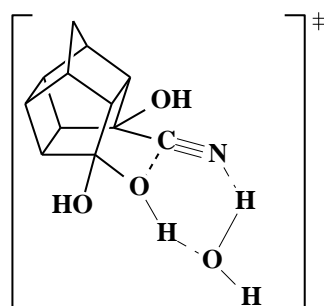
5.7.1



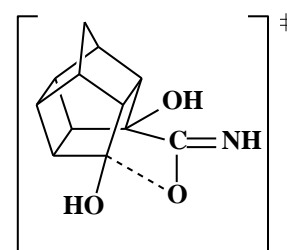
5.7.2



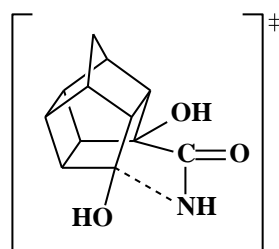
5.10.1



5.10.2



5.12

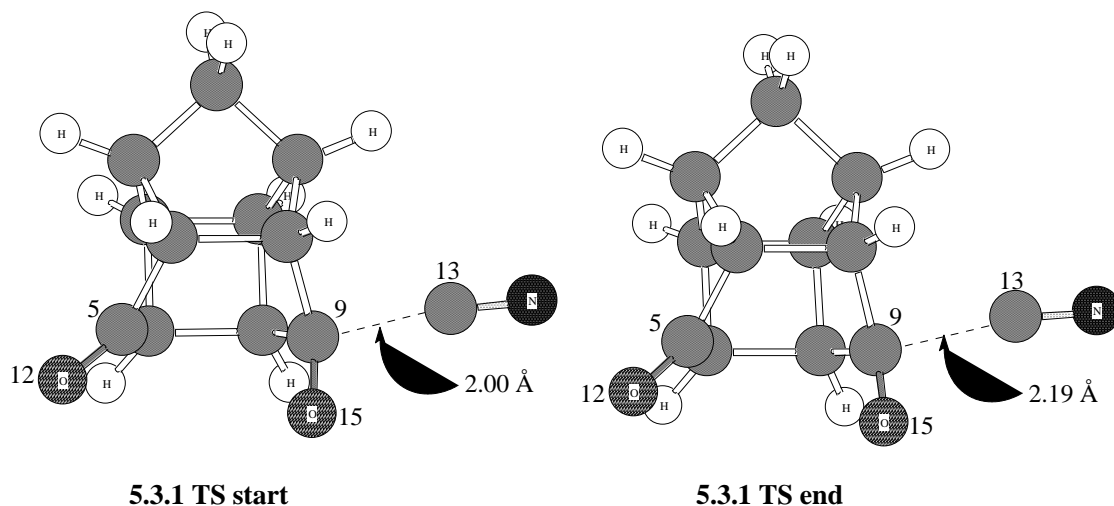


5.13

The calculated energies for the structures are also presented in the Table 5.1. The frequency output files of the different transition structures are available on the CD attached to this thesis. All the transition state structures that are presented in this discussion are at the DFT level of optimisation.

Transition state structure 5.3.1

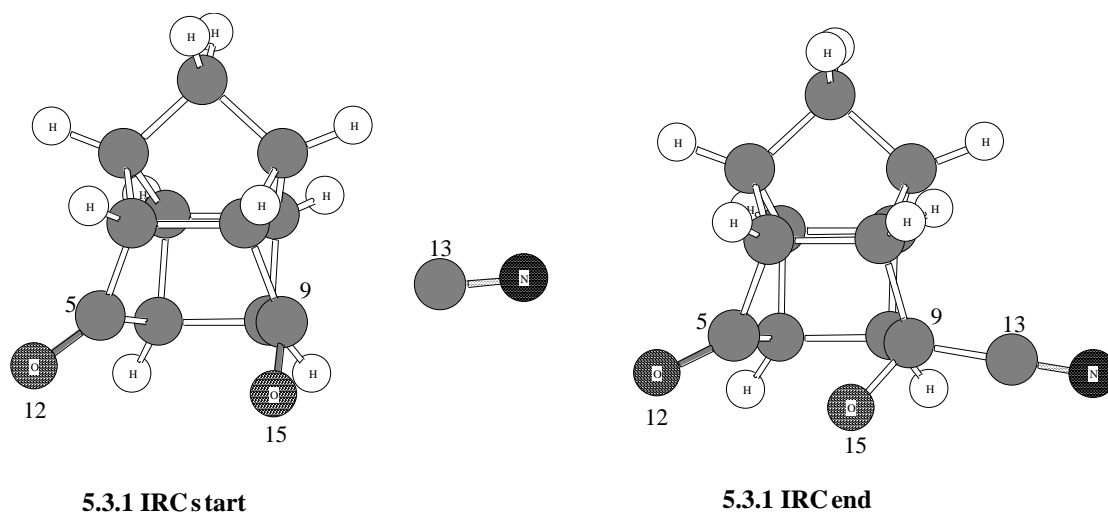
Stationary point **5.1** was used as a starting point to model transition structure **5.3.1** with a cyano group attacking the carbon (C9) on the cage. The 3D transition state start and product structures are presented:



The carbonyl carbon (C9) in **5.3.1 TS start** is moving out of plane and it is starting to become sp^3 hybridised. In **5.3.1 TS end**, at the end of the geometry optimisation, as the distance between atoms C9 and C13 has slightly increased, the CN group moved away from the cage, and the distance between atoms C9 and O15 decreased accordingly. The group attached to the carbonyl carbon (C9) becomes more planar during the course of the scan calculation.

The transition structure (**5.3.1.TS end**) was verified by performing a frequency calculation which produced one negative eigenvalue (-122.18 cm^{-1}). The frequency calculation was animated using the GaussView program with the vibration mode enabled so that the negative eigenvalue associated with that bond formation between the cyano group (C13-N14) and C9 is clearly visualized. The vibration associated with the imaginary frequency clearly shows the cyano group (C13) moving towards the cage to form/break the bond with C9. It is also clear that the C9–C13 bond is forming while O15 is moving towards C5.

The transition structure was further verified by performing an IRC calculation. The optimised transition structure was used for this calculation. The initial and final structure of the IRC calculation were optimised to determine if the respective structures proceeded to the reactant and product.



It was observed that the optimised **5.3.1 IRC start** breaks down to the reactants and **5.3.1 IRC end**, as shown in the 3D figures above, glides towards the product when optimised further. This is convincing proof that the transition structure obtained indeed connects the stationary points on either side of it on the reaction profile (structures **5.1** and **5.4** in Figure 5.2).

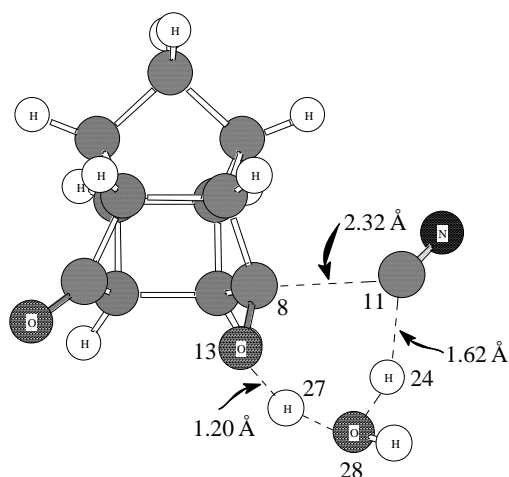
Transition state structure 5.3.2

From the gas phase reaction profile Figure 5.2 it can be seen that **5.3.1** has a relatively high energy value when compared with **5.3.2**. There are two reasons for this phenomenon. The first is that the calculation was performed in the gas phase. The second is that **5.3.1** is an ionic species and generally ionic species in the gas phase have much higher energies than when they are in the presence of a solvent such as water.

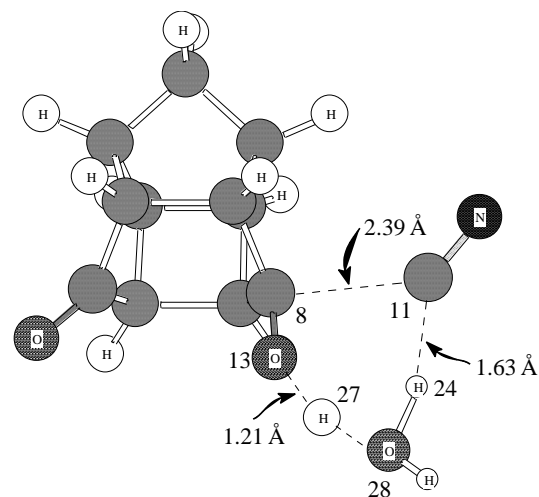
Attempts and the failure to model a 4-membered cyclic transition structure with HCN can be found in APPENDIX 1.

It was decided to do the calculation with a HCN and a H₂O molecule to form a 6-membered cyclic neutral transition structure where the hydrogen atom is transferred from HCN to O13 *via* an intermolecular mechanism. In this medium it was envisaged that the water molecule would remove a proton from HCN and donate a proton to O13 (see **5.3.2 TS1 start**).

Stationary point **5.1** was again used as a starting point to model transition structure **5.3.2**. The 3D transition state optimisation extreme structures are presented.



5.3.2 TS1 start



5.3.2 TS1 end

The transition structure (**5.3.2 TS1 end**) was verified by performing a frequency calculation which produced one negative eigenvalue at -272.28 cm^{-1} . There are three modes of vibration clearly associated with the imaginary frequency. The first vibration is the cyano group (C11) moving towards/away from the cage to form a bond with C8. The second vibration is the intramolecular hydrogen transfer between C11 and O28. The third vibration is also an intramolecular hydrogen transfer between O28 and O13.

The graphical representation of the IRC calculation for **5.3.2** is shown.

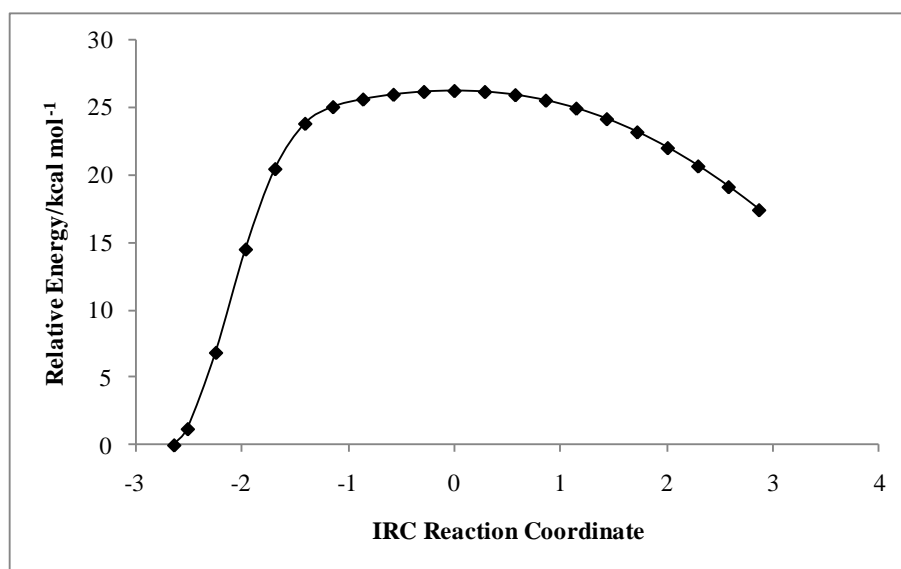


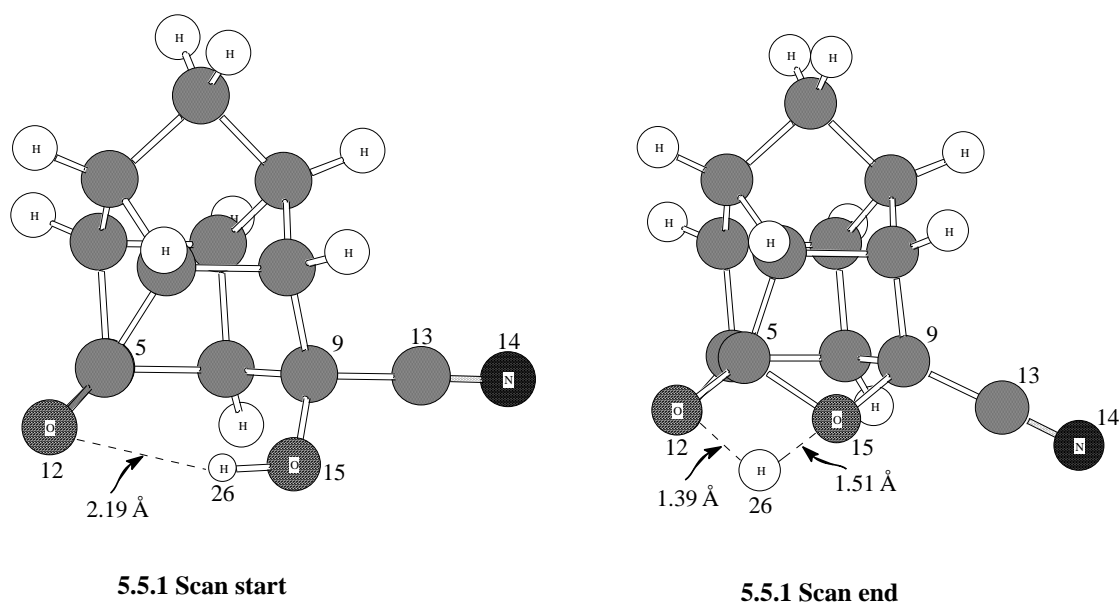
Figure 5.3 Graphical representation of the IRC reaction coordinate vs relative energy for structure 5.3.2

The structures from step 1 and step 21 of the IRC calculation were optimised. The optimised structure from step 1 fell apart to the reactants, that is, the PCU dione, HCN and H₂O. The optimised structure from step 21 yielded the products, namely, **5.4** and a H₂O molecule. This is firm proof that the transition structure obtained definitely connects the stationary points (structures **5.1** and **5.4**) on either side of the energy profile (see Figure 5.2).

A dramatic reduction in the energy for transition state **5.3.1** (relative energy 124.78 kcal mol⁻¹) was achieved by using H₂O and HCN in a six membered ring transition state **5.3.2** (relative energy 48.33 kcal mol⁻¹). It is important to note that the addition of a solvent molecule to the transition state structure comes with an entropy penalty. However, as can be seen from the free energy calculations (see Table 5.1), the gain in stability by neutralising the ionic character of the transition state weighs much more.

Transition state structure 5.5.1

The transition structure **5.5.1** involved monitoring the intramolecular transfer of the hydrogen atom (H26) between the two oxygen atoms (O12 and O15). The local minimum **5.4** was used as the starting point for a scan calculation in the determination of this transition structure. The 3D input structure (**5.5.1 Scan start**) which was used as the starting structure, as well as the output structure (**5.5.1 Scan end**), for the scan, are depicted.



The bond between O12 and H26 was scanned from 2.2 Å to 1.4 Å. It is clearly observed that the hydrogen (H26) is transferred during the scan calculation. The structure **5.5.1 Scan end** when compared to the **5.5.1 Scan start** shows that the (C9-C13-N14) group remains linear as

expected. It was also noted that atoms C5 and O15 form a bond as the distance between atoms O12 and H26 decreases as a result of the H-transfer. Atom H26 orientates itself between atoms O12 and O15. The energy profile of the scan is graphically depicted.

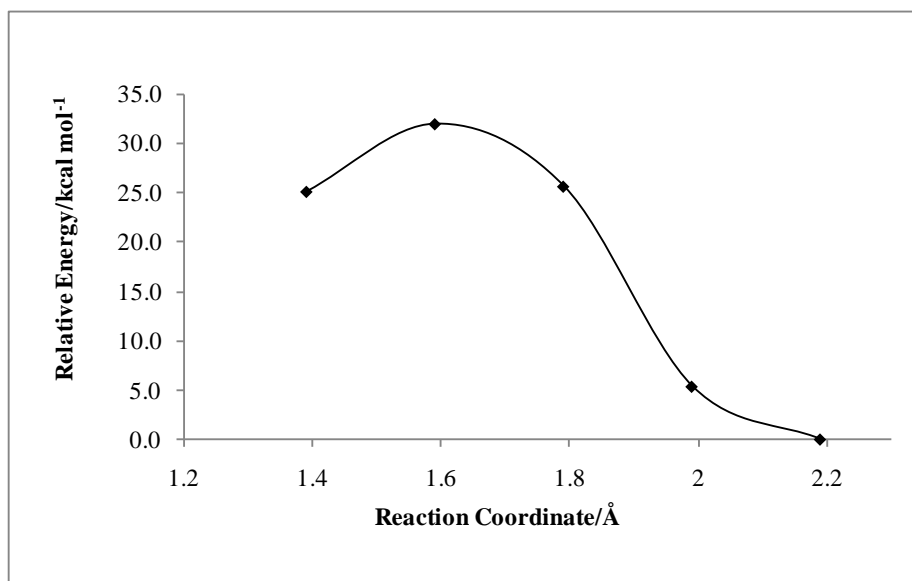
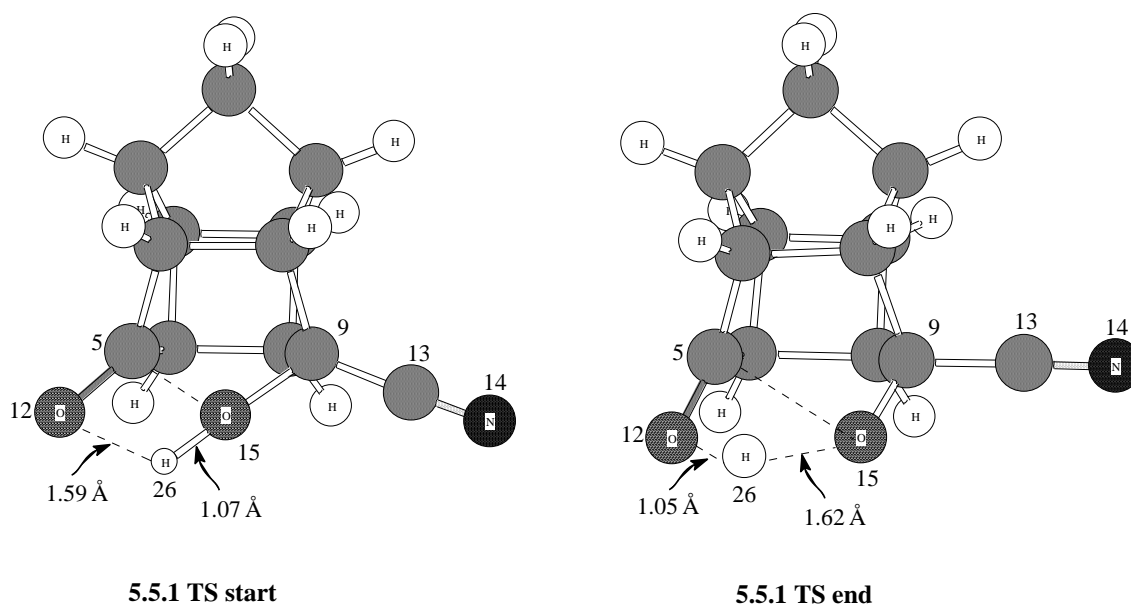


Figure 5.4 Graphical representation of energy vs reaction coordinate for structure 5.5.1

The coordinates of the structure (5.5.1 TS start) at the maximum (1.6 Å) in Figure 5.4 was submitted for a transition state optimisation. The resultant transition state structure that was obtained (5.5.1 TS end) at the end of the transition state optimisation is shown.



The transition state **5.5.1 TS end** structure was verified to be the correct transition structure since the frequency calculation produced only one negative eigenvalue and the movements of atoms associated with the negative eigenvalue correspond to the intramolecular hydrogen transfer of atom H26 between atoms O15 and O12 as well as the bond formation/dissociation between C5-O15 as discussed above.

The graphical representation of the IRC calculation for **5.5.1** is shown.

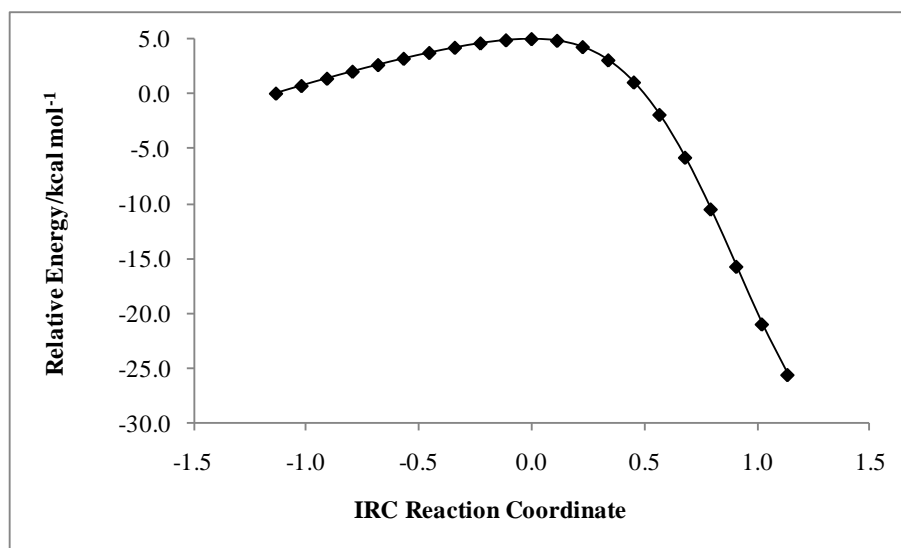


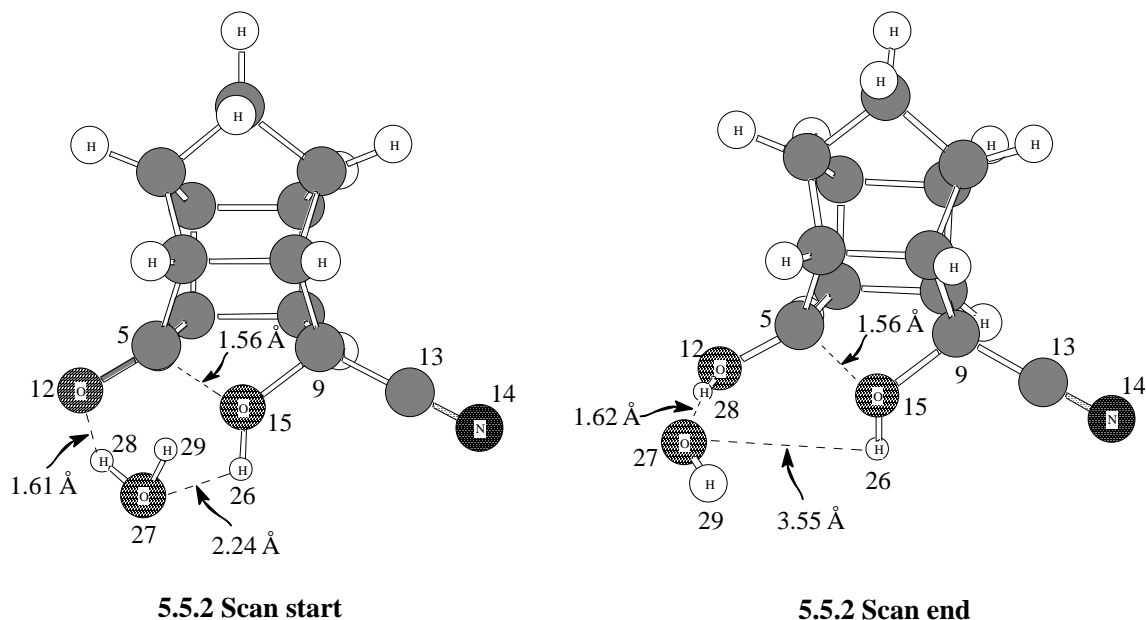
Figure 5.5 Graphical representation of the IRC reaction coordinate vs relative energy for structure **5.5.1**

The IRC calculation provided further evidence that the structure obtained was indeed the expected transition structure since the optimised structure from step 1 (IRC start) resulted in the local minimum **5.4** and step 21 (IRC end) produced the stationary point **5.6**.

Transition state structure 5.5.2

From the reaction profile in Figure 5.2 it can again be seen that **5.5.1** has a relatively high energy value also due to the ionic nature of the molecule in the gas phase. The reasons for this high energy have already been discussed in transition structure **5.3.2**. Thus it was decided to do the calculation with a H₂O molecule to form a 6-membered cyclic neutral transition structure. Here it was also envisaged that the oxygen atom from the additional H₂O molecule would remove a proton from hydroxyl group and donate a proton to O12 (see **5.5.2 Scan start**).

The local minimum **5.4**, with one additional H₂O molecule, was again used as the starting point for a scan calculation in the determination of this 6-membered transition structure. The 3D input structure (**5.5.2 Scan start**) which was used as the starting structure, as well as the final output structure (**5.5.2 Scan end**), for the scan, are represented.



The bond between O12 and H28 was scanned from 1.61 Å to 0.81 Å. The scan is graphically depicted.

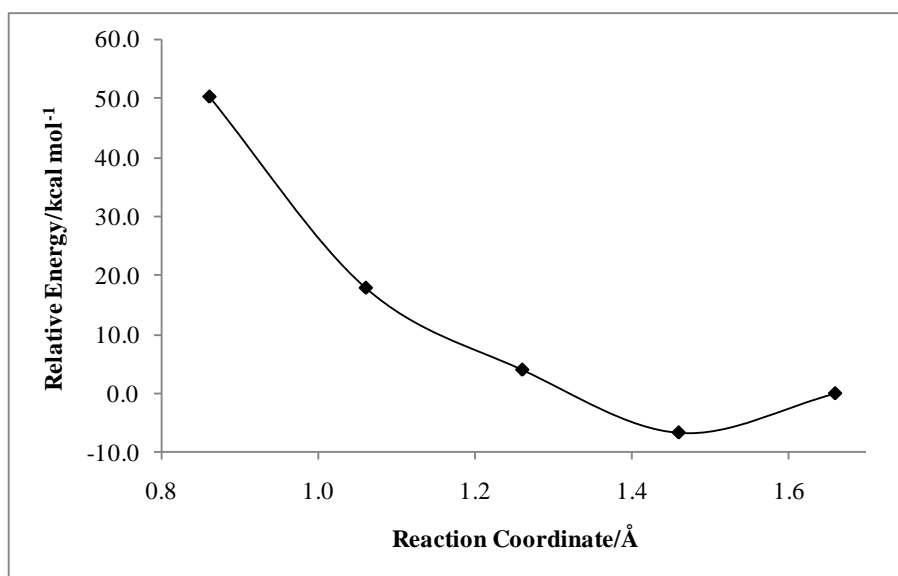
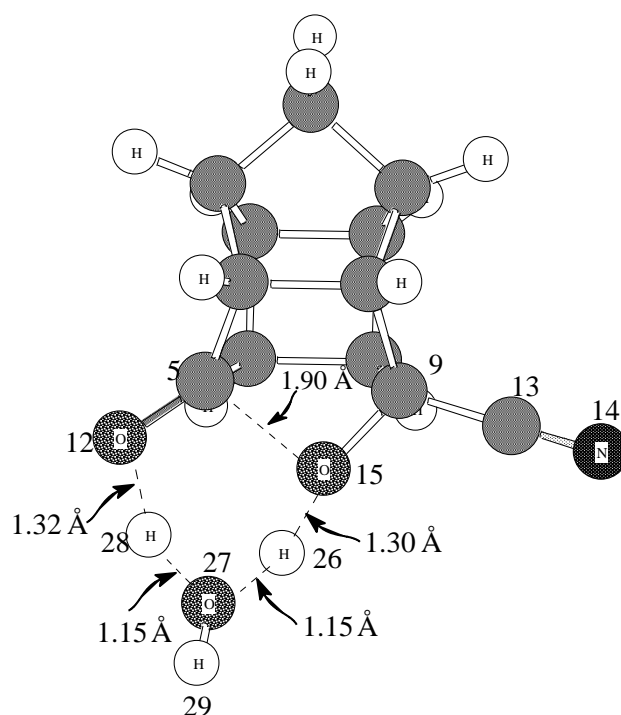


Figure 5.6 Graphical representation of energy vs reaction coordinate for structure **5.5.2**

The surface resulted in a minimum on the potential energy scan and not a maximum. The structure at each reaction coordinate was examined to determine if any could be used as a possible starting transition structure. It was observed that as the bond length between O12 and H28 decreased, the distance between H26 and O27 increased. The expected intramolecular transfer of the hydrogen atom (H26) between the two oxygen atoms (O27 and O15) was not observed. Similarly, there was no bond formation between atoms C5 and O15. However, on closer examination of the scan and in particular the structure with a distance of 1.21 Å between H28 and O12, it can be seen that only H28 is transferred during the scan calculation. At 0.81 Å, H28 is attached to O12, and H26 has not been transferred to O27. Thus, it was decided to use the structure at the reaction coordinate of 1.01 Å, which is between 1.21 Å and 0.81 Å, for an unconstrained transition state optimisation. The resultant transition structure that was obtained at the end of the transition state optimisation is **5.5.2 TS end**.



5.5.2 TS end

5.5.2 TS end was verified to be the correct transition structure since the frequency calculation produced only one negative eigenvalue of -1284.30 cm^{-1} . The movement of atoms associated with the negative eigenvalue corresponds to the intramolecular hydrogen transfer of atom H26 between atoms O15 and O27 as well as the transfer of atom H28 between atoms O12 and O27. It is also observed that there is a bond formation/dissociation between C5-O15.

The graphical representation of the IRC calculation for **5.5.2** is shown.

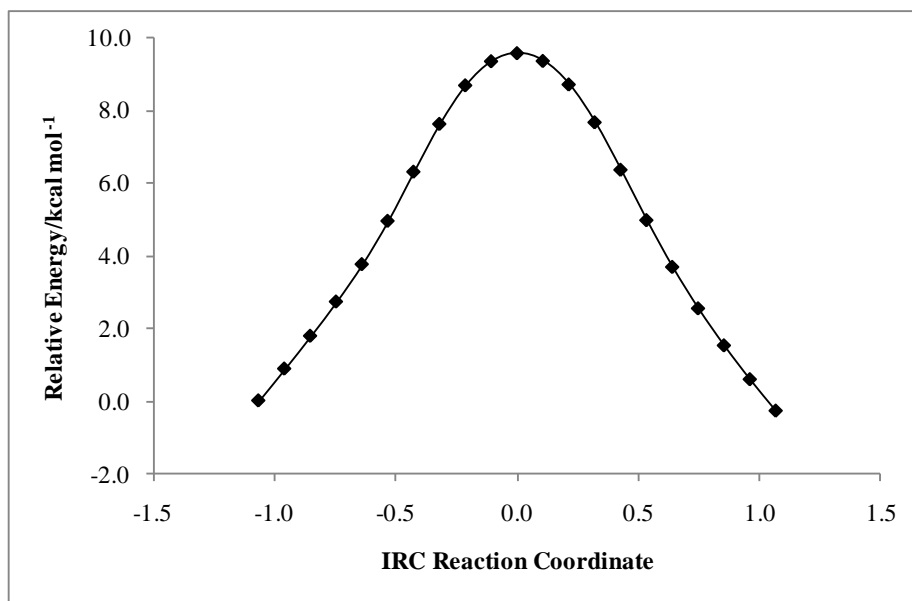
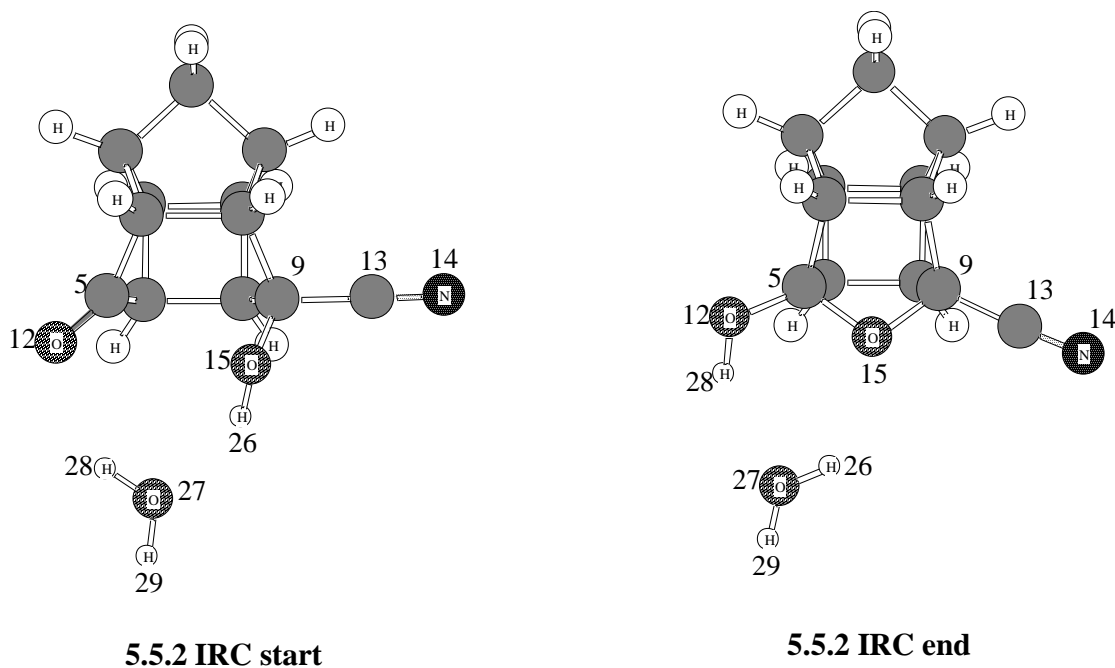


Figure 5.7 Graphical representation of the IRC reaction coordinate vs relative energy for structure **5.5.2**

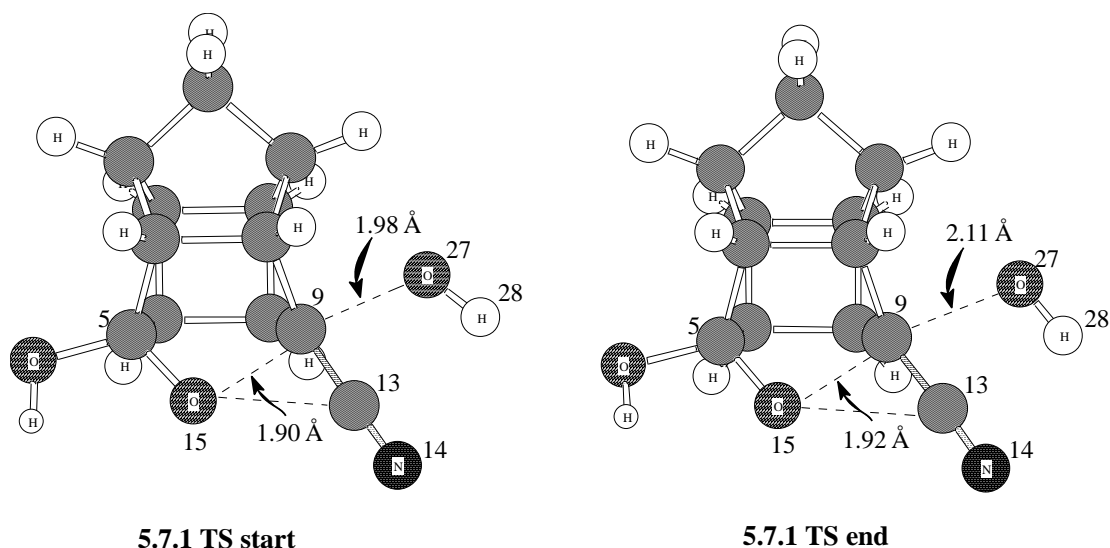
The IRC calculation provided strong evidence that the structure obtained was the correct transition structure since the optimised structure from step 1 (**5.5.2 IRC start**) resulted in the local minimum **5.4** with a H₂O molecule and step 21 (**5.5.2 IRC end**) produced the stationary point **5.6** and a H₂O molecule.



It is observed that, with the addition of a H₂O molecule for transition state **5.5.2**, a reduction in the energy by 27.63 kcal mol⁻¹ was achieved, that is, from 57.23 kcal mol⁻¹ (**5.5.1**) to 29.60 kcal mol⁻¹ (**5.5.2**). It is clear that the overall reduction in energy outweighs the entropy penalty from the additional molecule participating in the reaction.

Transition state structure 5.7.1

In structure **5.7.1** the calculations focused on monitoring the progress of the hydroxyl group (O27-H28) attaching to the cage at C9 and the breaking of the C9-O15 (ether/acetal) bond. The stationary point **5.6** with an added hydroxyl group was used as the starting structure. **5.7.1 TS start** was the input used for an *ab initio* transition state optimisation and **5.7.1 TS end** is the product of the DFT transition state optimisation.



From the two structures above, it was noted that as the ether bond between O15 and C9 breaks, there is also an increase in the bond length between C9 and O27. The transition state optimisation was also monitored to see if there would be a bond formation between O15 and C13.

The output structure above shows the correct orientation of the hydroxyl group (O27-H28). The movement of atoms associated with the negative eigenvalue at -464.84 cm⁻¹ from the frequency calculation shows that the movement of the hydroxyl group (O27-H28) forms/breaks a bond with atom C9 on the cage and the formation/dissociation of the bond between atoms O15-C9 which is expected in the transition structure.

The graphical representation of the IRC calculation for **5.7.1** is shown.

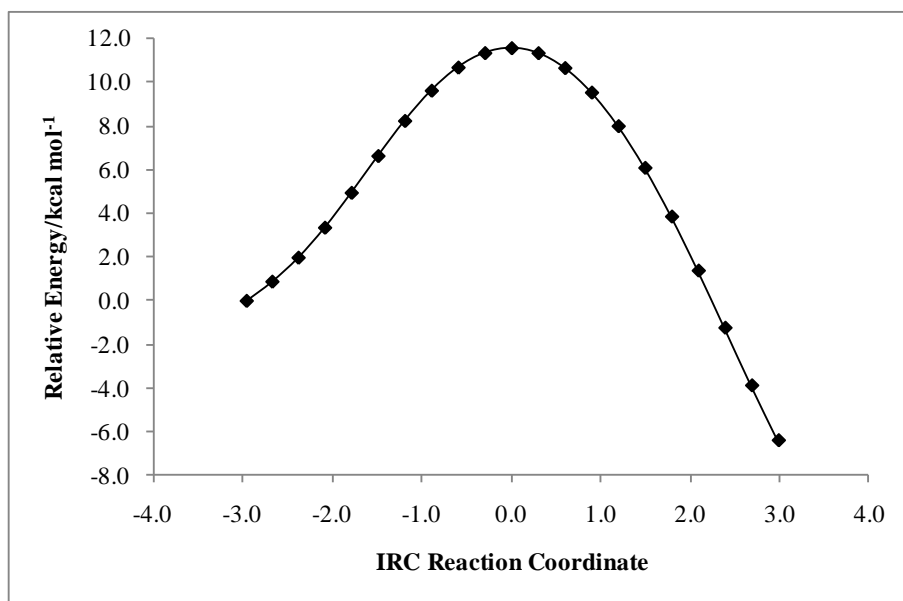
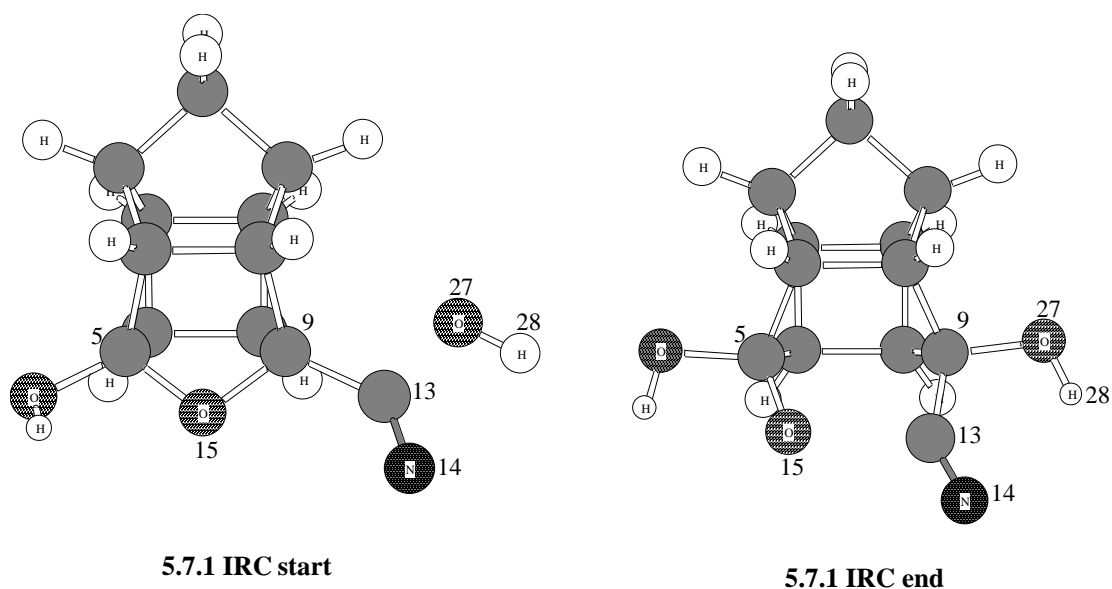


Figure 5.8 Graphical representation of the IRC reaction coordinate vs relative energy for structure 5.7.1

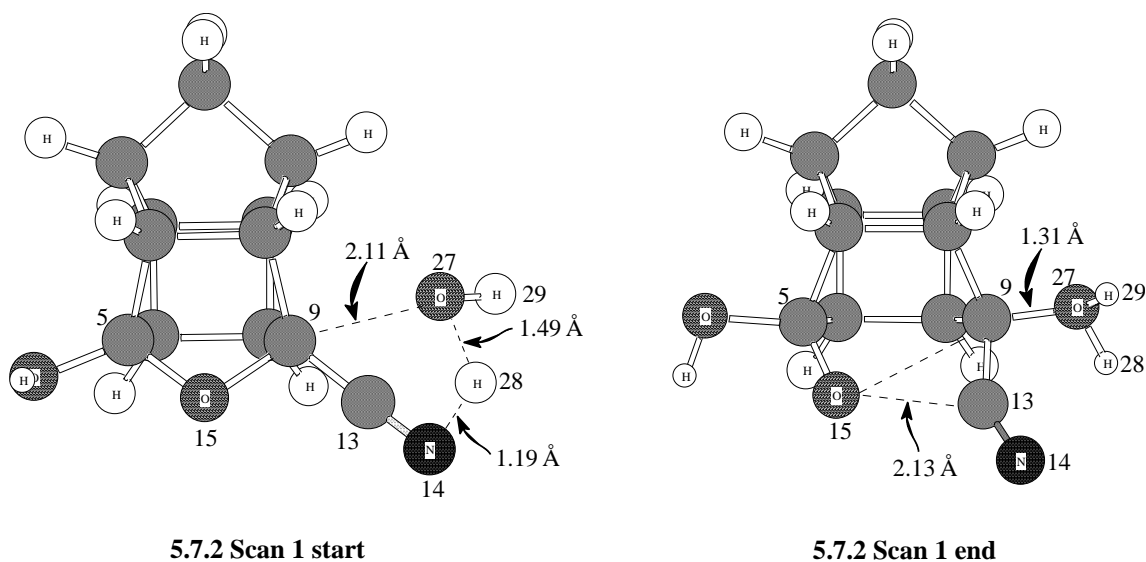
The IRC calculation proved that the structure obtained was the expected transition state structure since the optimised structure from step 1 (**5.7.1 IRC start**) relaxed to the local minimum **5.6** and a hydroxyl group and step 21 (**5.7.1 IRC end**) produced the stationary point **5.9**.



However, this transition state produced the highest energy value on the reaction profile (Figure 5.2) since O15 has a negative charge, that is, it is an ionic species in the gas phase.

Transition state structure 5.7.2

To resolve the high energy of transition structure **5.7.1**, a water molecule was added to form a 5-membered cyclic transition structure. Structure **5.6** was used as the starting point and H₂O was positioned next to C9. The 3D input structure (**5.7.2 Scan 1 start**) which was used as the starting structure, as well as the output structure (**5.7.2 Scan 1 end**), for the scan, are represented.



The bond between C9 and O27 was scanned from 2.11 Å to 1.31 Å. The scan is graphically depicted.

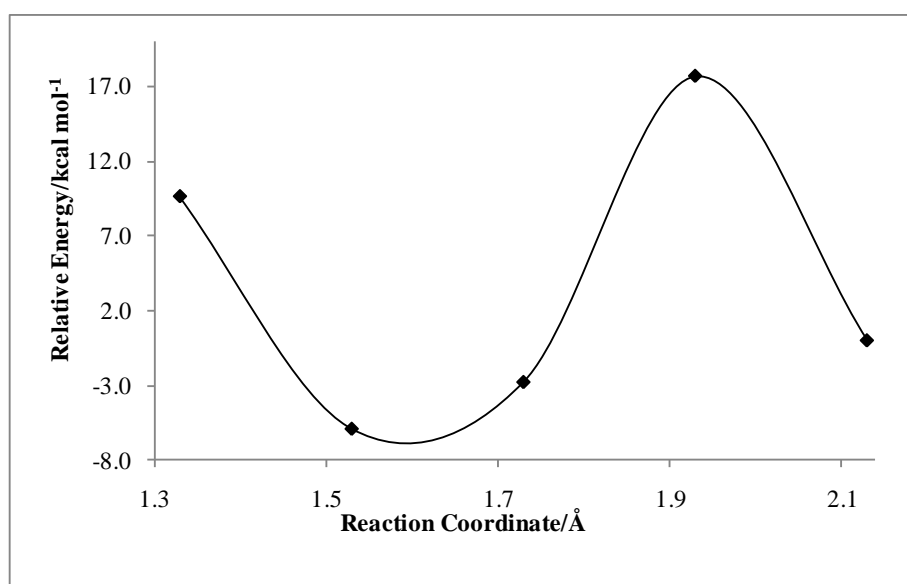
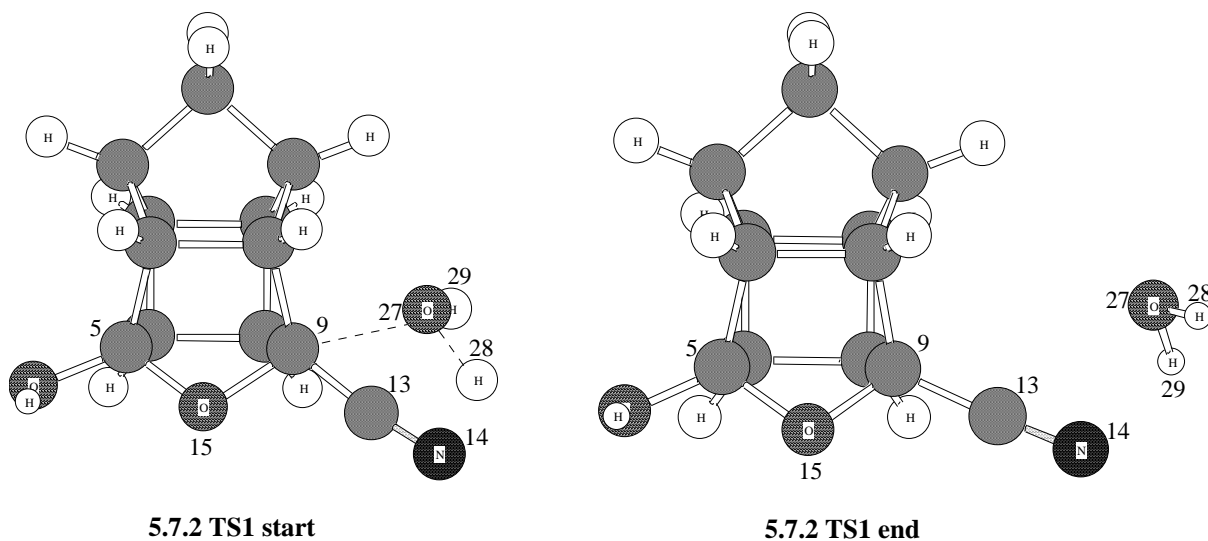
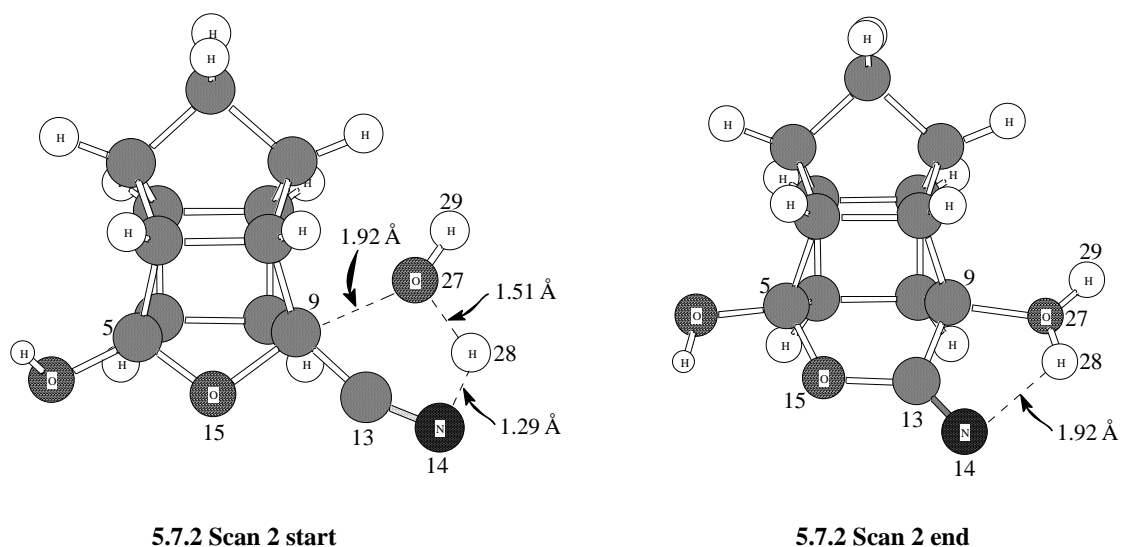


Figure 5.9 Graphical representation of energy vs reaction coordinate for structure **5.7.2 (Scan 1)**

The structure at the maximum of 1.91 Å (**5.7.2 TS1 start**) in Figure 5.9 was submitted for a transition state optimisation. The optimised 3D transition state is **5.7.2 TS1 end**.



It was expected that O27H29 would attach to C9 but this bond did not form. Instead, the water molecule moved away from the cage resulting in the formation of the reactants. The structures as 1.71 Å and 1.51 Å were also examined to see if they could be used at possible starting structures for another transition state optimisation however both these structures had already formed the products. Adjustments to the structure at 1.91 Å were made but further optimisations did not yield the correct transition structure. A second zoomed-in scan between C9 and O27 from 1.92 Å to 1.50 Å was performed. For this scan the water molecule was rotated to the back of the cage. The 3D input structure (**5.7.2 Scan 2 start**) which was used as the starting structure, as well as the output structure (**5.7.2 Scan 2 end**), for the scan, are depicted.



In this second scan, it was clearly observed that as the bond between C9 and O27 formed, the bond between C9 and O15 broke. This scan result also indicated for the first time that a direct transition from **5.6** to **5.11** could in fact be possible. The scan is graphically depicted. In **5.7.2 Scan 2 end** the bond formation between O15 and C13 is also visible; however, here again; H28 was not transferred to N14.

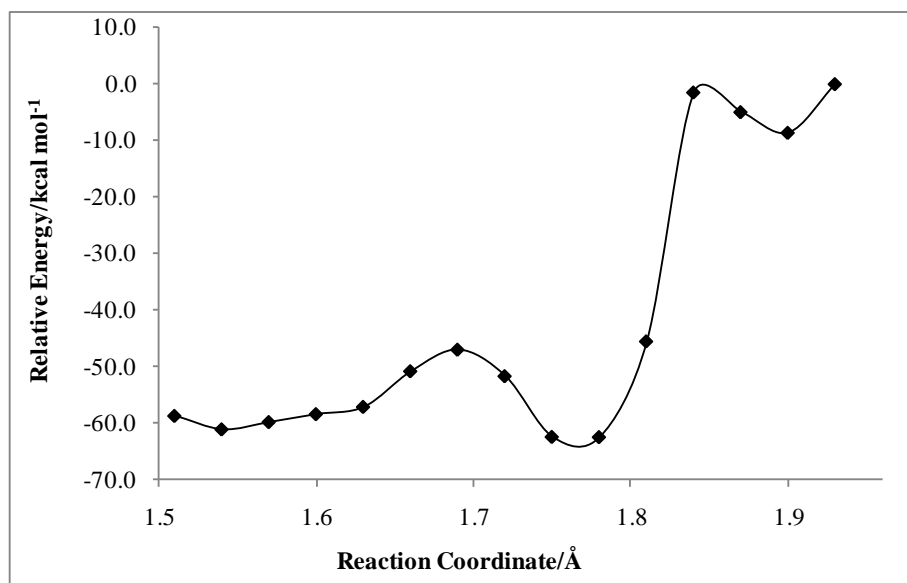
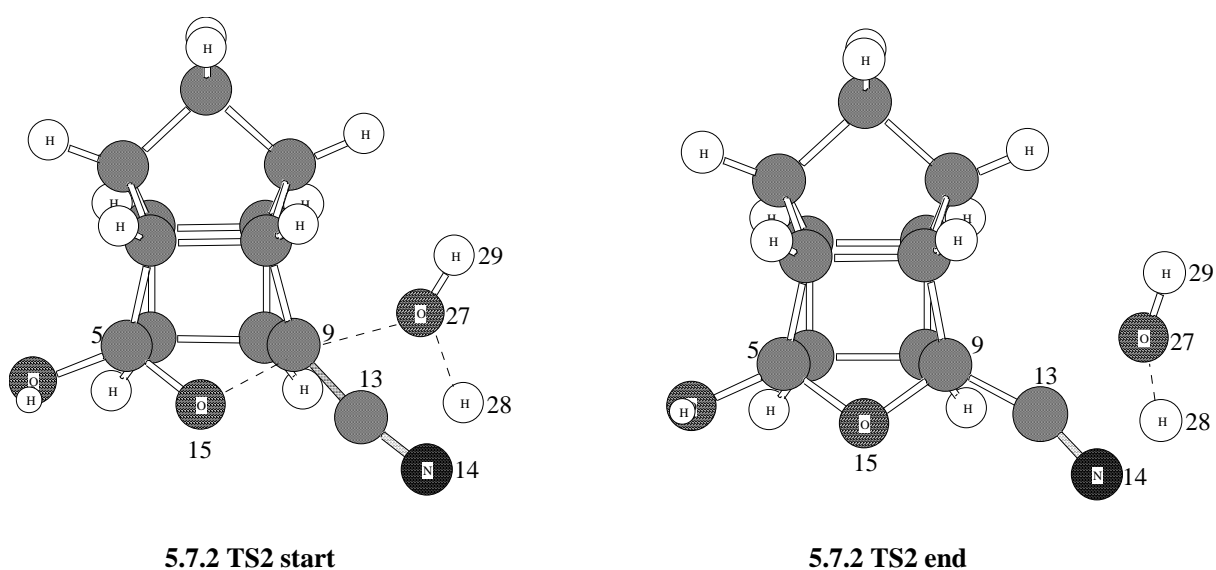


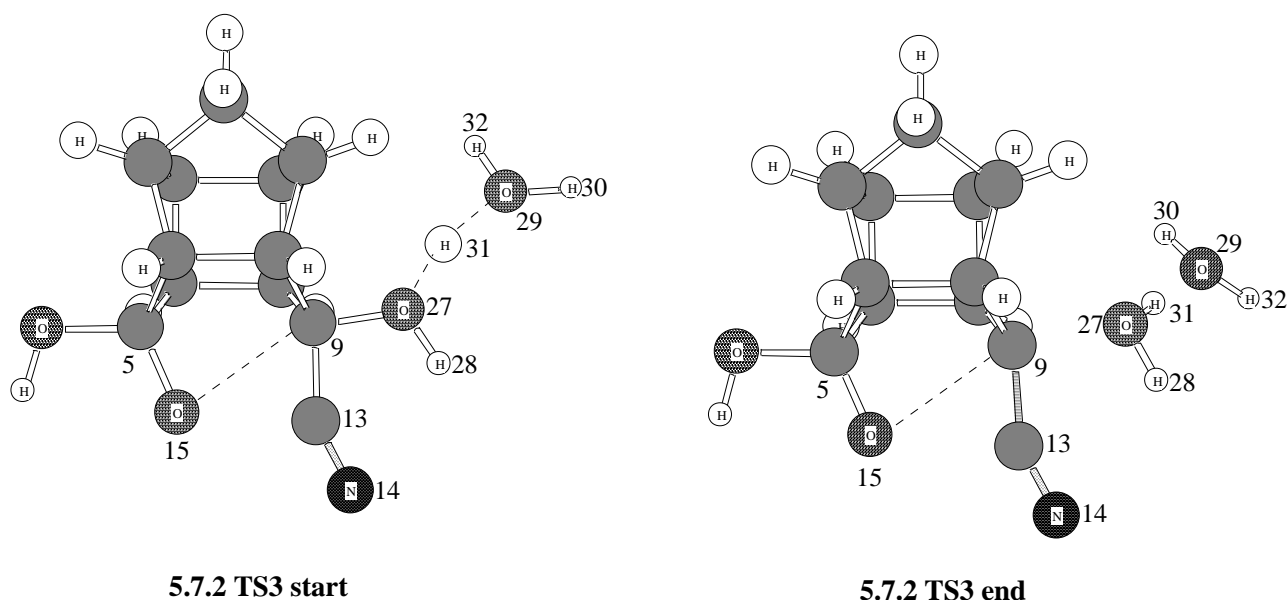
Figure 5.10 Graphical representation of energy vs reaction coordinate for structure **5.7.2 (Scan 2)**

The structure at the maximum of 1.83 Å (**5.7.2 TS2 start**) in Figure 5.10 was submitted for a transition state optimisation. The optimised 3D transition state is **5.7.2 TS2 end**.

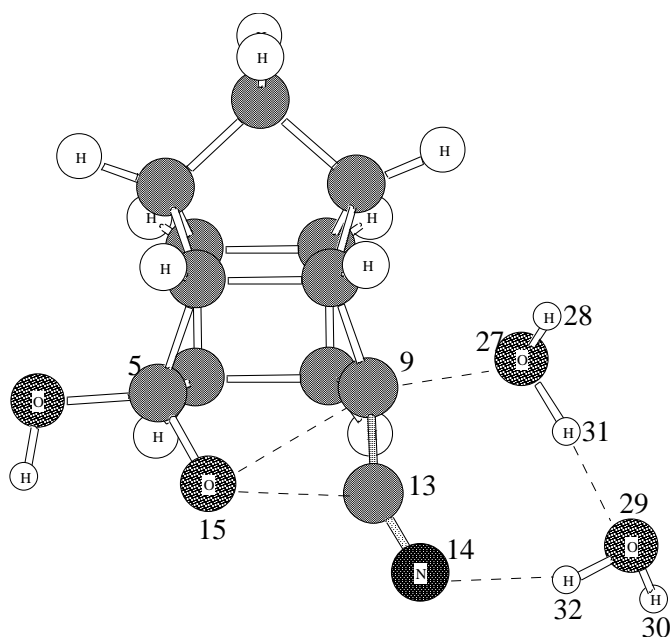


Although **5.7.2 TS2 start** was a maximum on the potential energy surface, it too, did not produce the expected 5-membered transition structure. The O27H29 group moved towards C13 but the proton H28 moved to N14. The structures at the other points on the reaction coordinate were also examined. These structures could not be used as possible starting structures for another transition state optimisation since the O27H29 group had moved too far away from C9. The bond length between C9 and O27 as well as the orientation of the water molecule (H28O27H29) to the cage were altered for several additional transition state optimisations but the transition structure could not be located.

It was thus decided to add two water molecules to **5.7.2**. The second water molecule (**5.7.2 TS3 start**) could hopefully assist with the removal of the proton (H31) from the incoming water (H28O27H31).



The 3D *ab initio* transition state optimisation input structure (**5.7.2 TS3 start**) which was used as the starting structure, as well as the output structure (**5.7.2 TS3 end**) are depicted. A linear transition structure was expected where the bond break between C9 and O15 as well as the bond formation between C9 and O27 would be observed. It would also hopefully show the intramolecular hydrogen transfer of H31 between O27 and O29. The output of the *ab initio* transition state optimisation (**5.7.2 TS3 end**) was then submitted for a DFT transition state optimisation. The output is illustrated in **5.7.2 TS4 end**.



5.7.2 TS4 end

This output, **5.7.2 TS4 end** indicates that the linear transition structure did not form. Instead a 7-membered cyclic transition structure was produced. This was verified as a plausible transition structure since the frequency calculation produced only one negative eigenvalue of -332.26 cm^{-1} . The movement of atoms associated with the negative eigenvalue corresponds to the intramolecular hydrogen transfer of atom H31 between atoms O27 and O29 as well as the transfer of atom H32 between atoms O29 and N14. The bond formation/dissociation between C9-C27, C9-O15 and O15-C13 is also observed.

The graphical representation of the IRC calculation for **5.7.2** is shown.

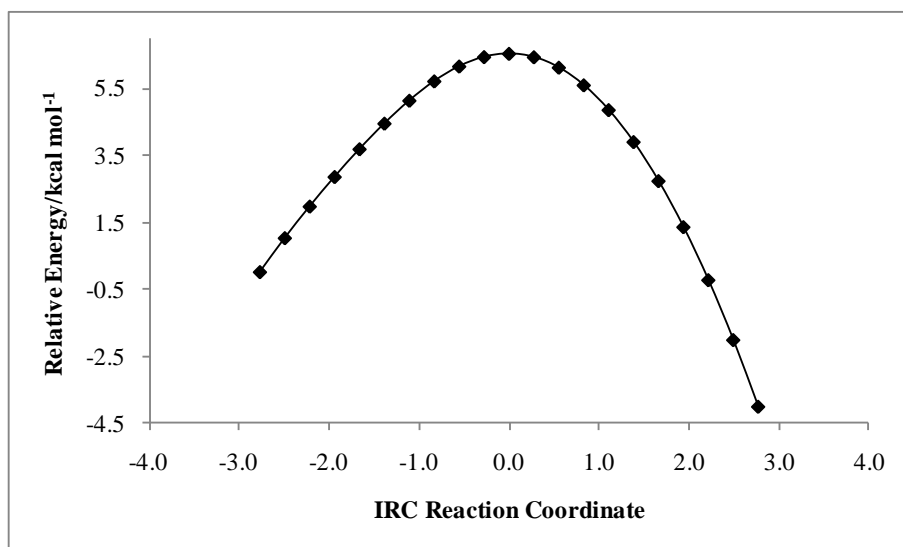
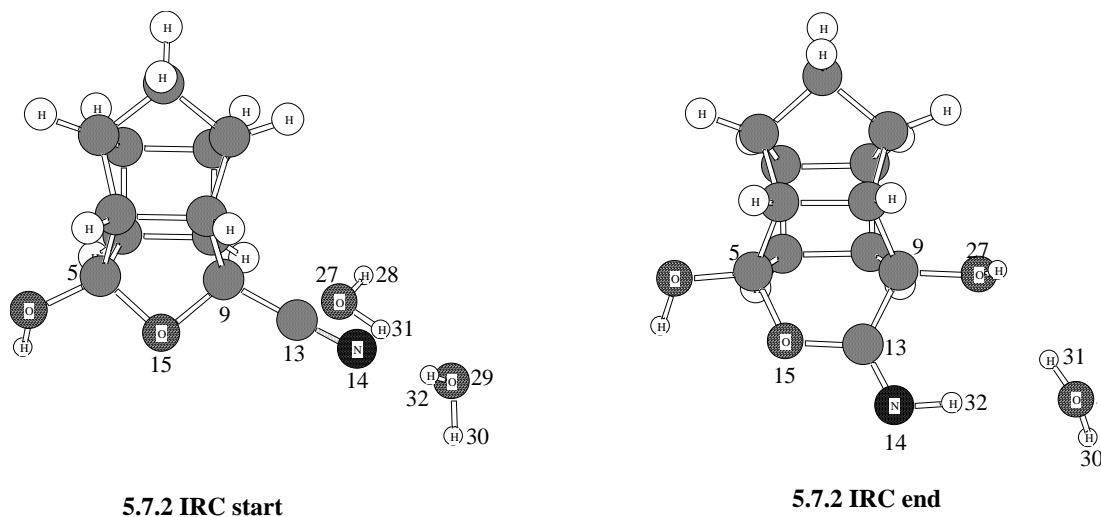


Figure 5.11 Graphical representation of the IRC reaction coordinate vs relative energy for structure 5.7.2

The IRC calculation proved that the structure obtained was definitely a viable transition structure since the optimised structure from step 1 (**5.7.2 IRC start**) resulted in the local minimum **5.6** with two water molecules and step 21 (**5.7.2 IRC end**) produced the stationary point **5.11** with one water molecule instead of **5.9**.

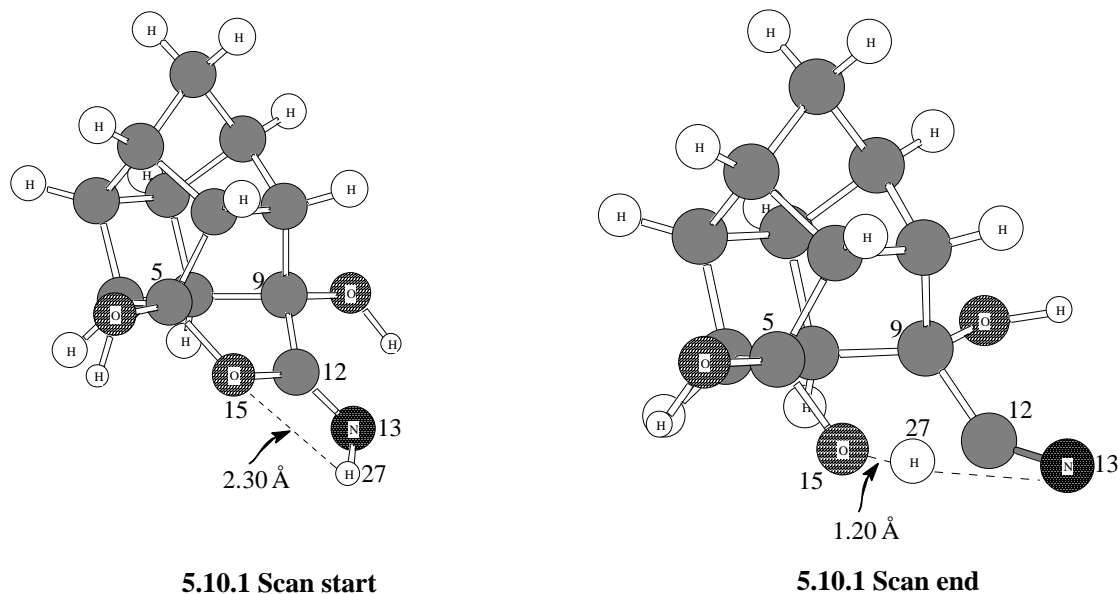


Thus, this proves that transition structure **5.7.2** can go directly from the intermediate **5.6** to **5.11** without the formation of **5.9** and **5.10**.

Transition state structure 5.10.1

The next transition structure on the reaction in profile Figure 5.2 is **5.10.1**. This involves the transition from **5.9** to **5.11**. It was decided to locate a starting structure for the transition state

by “pulling” H27 from structure **5.11** towards O15 with a relaxed scan calculation. The orientation of H27 suggested that this structure could produce a 4-membered cyclic transition state if H27 is transferred to O15. A scan was thus attempted to prove this theory. The 3D input and output structures for the scan calculation are represented.



A scan from 2.30 Å to 1.20 Å between atoms O15 and H27 was performed. It was expected that when atom H27 moved closer to O15, that the bond between atoms O15 and C12 would break. The graphical presentation of the relaxed scan is depicted below.

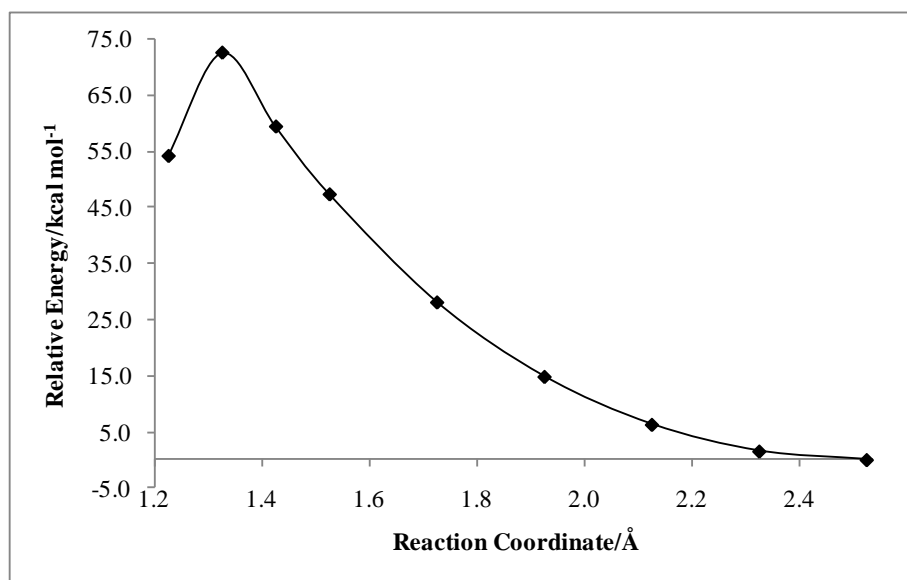
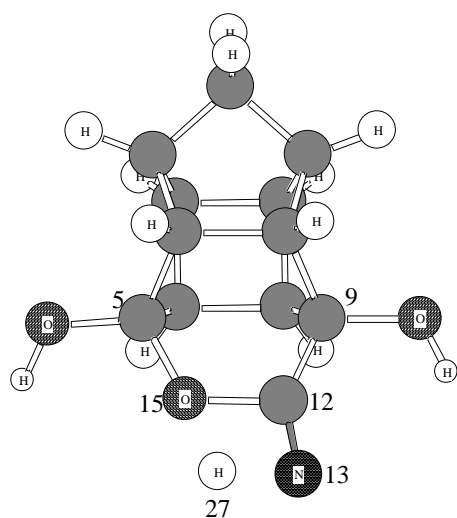
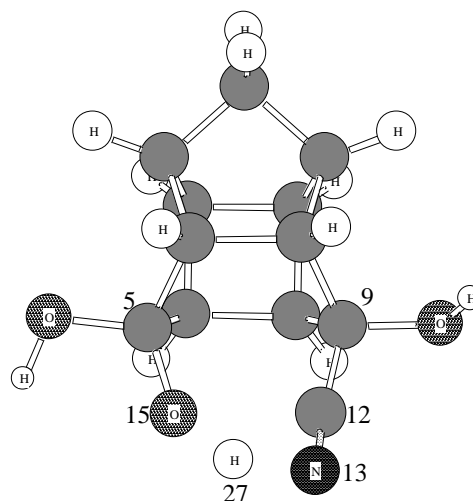


Figure 5.12 Graphical representation of energy vs reaction coordinate for structure **5.10.1**

The maximum (**5.10.1 TS1 start**) in Figure 5.12 is at 1.3 Å. Hence this structure was used as an input in a transition state optimisation. The 3D **5.10.1 TS1 end** is the output that was obtained from the unconstrained DFT transition state optimisation.



5.10.1 TS start



5.10.1 TS end

The output structure (**5.10.1 TS1 end**) clearly shows the bond break between atoms O15 and C12. The frequency calculation produced only one negative eigenvalue at -2019.49 cm^{-1} and shows the intramolecular transfer of atom H27 between O15 and N13. As atom H27 is transferred to atom O15, there is a subtle movement of the bond C12-O15, verifying that this bond breaks/forms as well.

The graphical representation of the IRC calculation for **5.10.1** is shown.

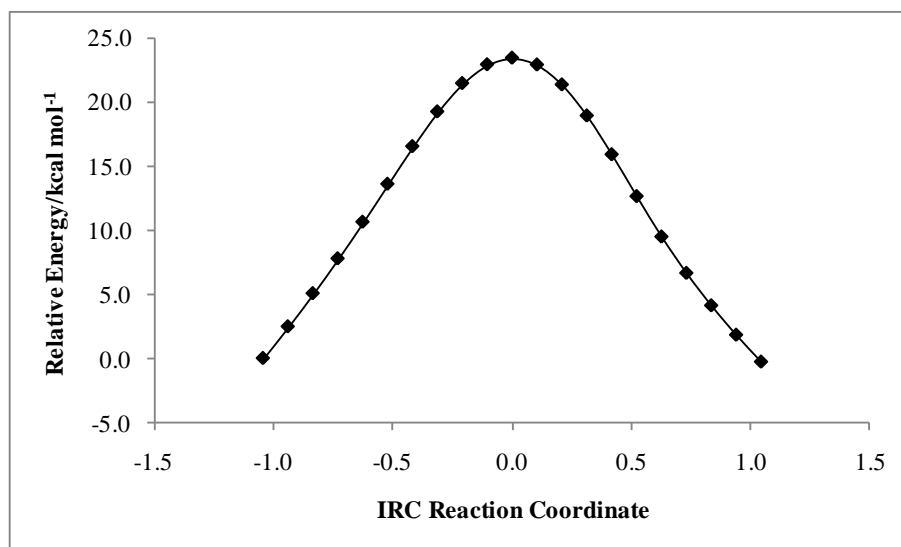
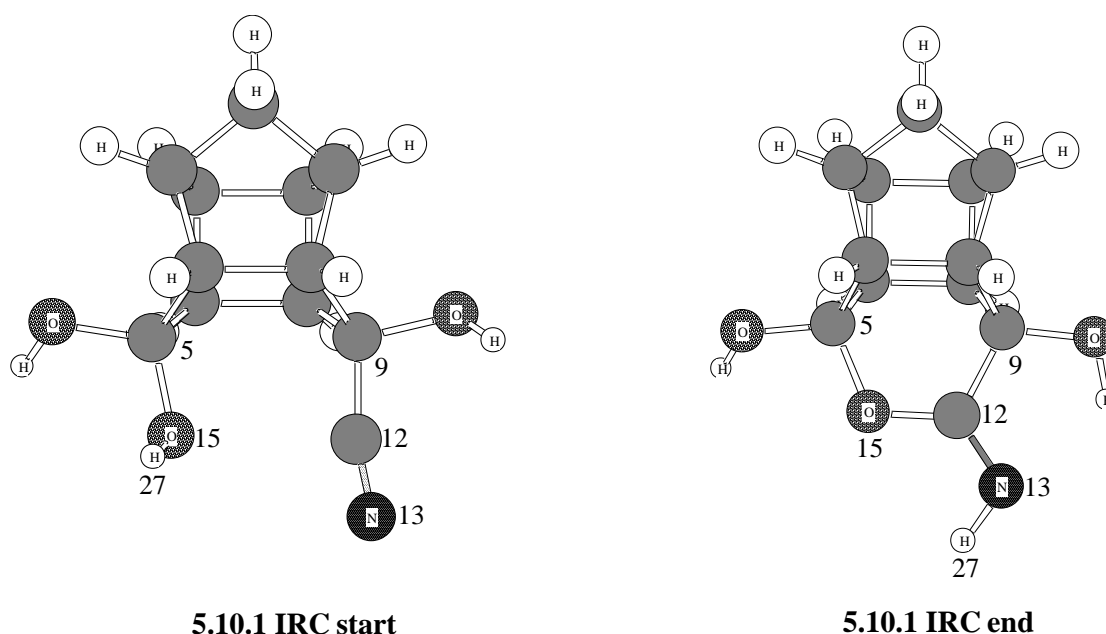


Figure 5.13 Graphical representation of the IRC reaction coordinate vs relative energy for structure 5.10.1

The IRC calculation confirmed that the structure obtained was definitely the correct transition structure since the optimised structure from step 1 (**5.10.1 IRC start**) resulted in the local minimum **5.9** and step 21 (**5.10.1 IRC end**) produced the stationary point **5.11**.

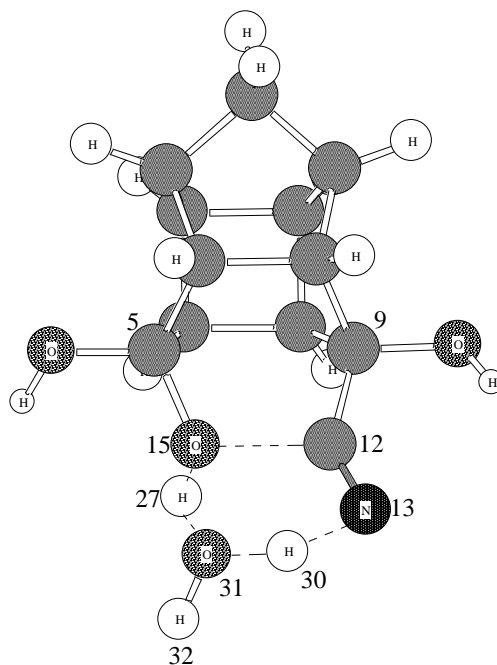


This transition state produced a relative energy value of $68.30 \text{ kcal mol}^{-1}$.

Transition state structure 5.10.2

Although the energy of **5.10.1** was not extremely high, it was decided to model the transition structure with one water molecule thus forming an intermolecular 6-membered cyclic

transition structure. Structure **5.10.1** was used as the starting point and an additional H₂O molecule was added. The 3D output structure (**5.10.2 TS end**), of the transition state optimisation is depicted.



5.10.2 TS end

The frequency calculation with a single negative eigenvalue of -1400.69 cm^{-1} verified that this is indeed a plausible transition structure. The movement of atoms corresponding to the negative eigenvalue showed the intramolecular hydrogen transfer of H30 between N13 and O31 as well as H27 between O31 and O15. There is also a small vibration indicating the formation/dissociation of the C12-O15 bond.

The graphical representation of the IRC calculation for **5.10.2** is shown.

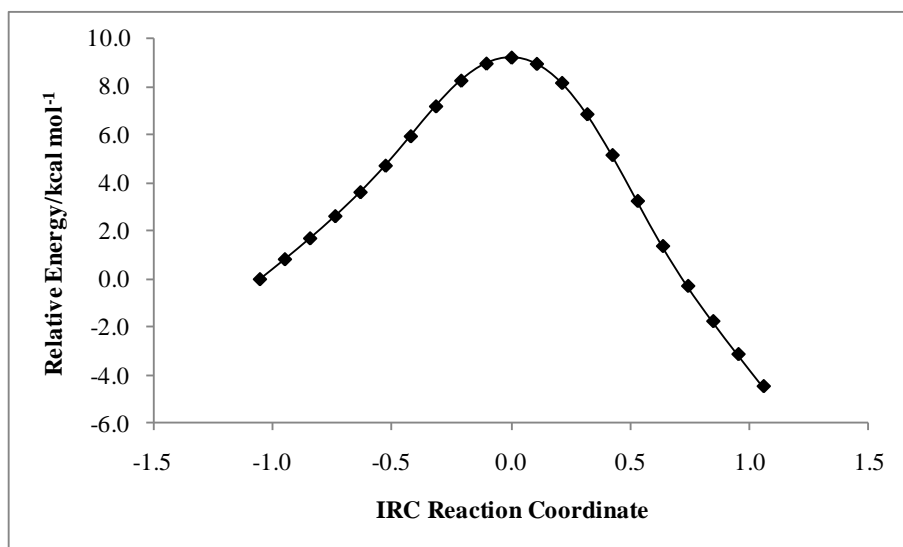
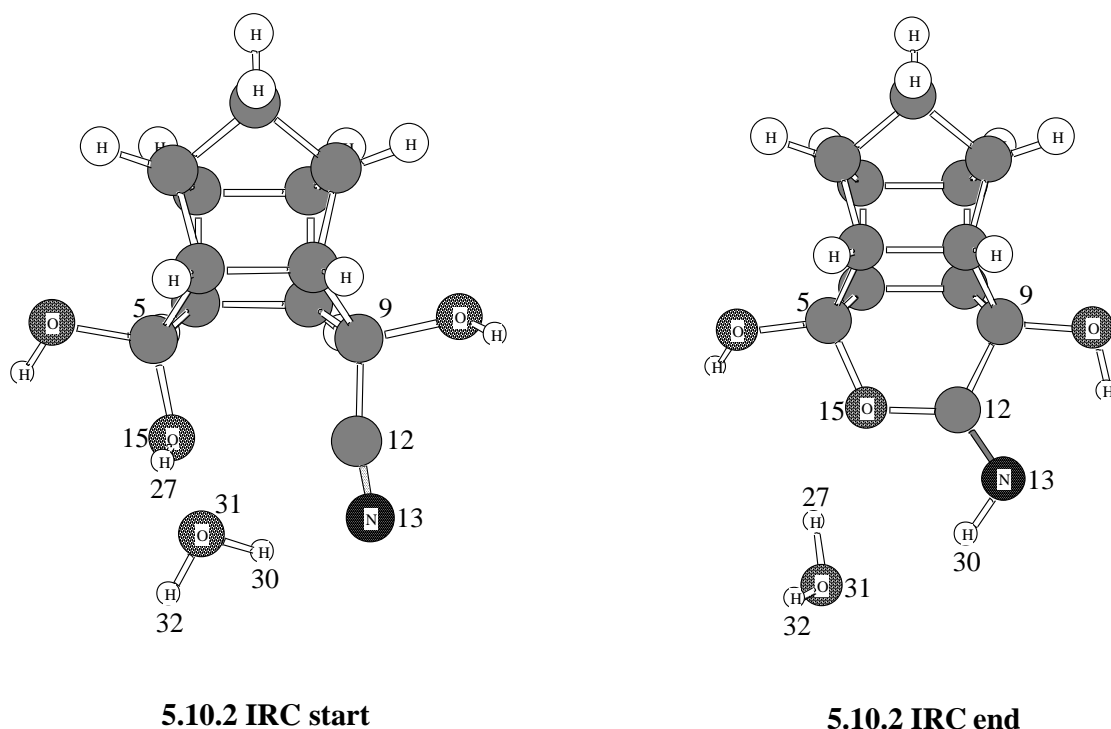


Figure 5.14 Graphical representation of the IRC reaction coordinate vs relative energy for structure 5.10.2

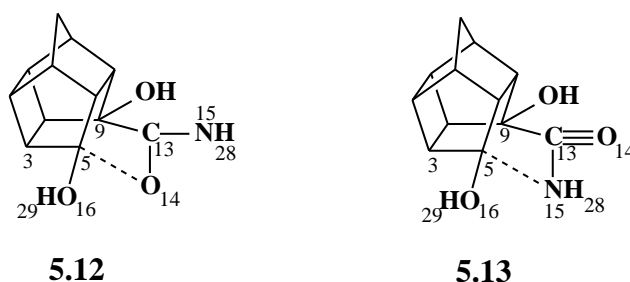
The IRC calculation verified the frequency calculation thus confirming that the structure obtained was a transition structure. The optimised structure from step 1 (**5.10.2 IRC start**) resulted in the reactants which were the local minimum **5.9** and a water molecule. The optimised structure from step 21 (**5.10.2 IRC end**) produced the stationary point **5.11** and a water molecule.



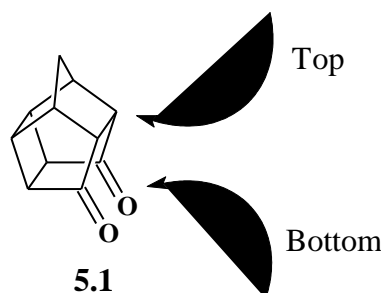
The relative energy for **5.10.2** was 45.62 kcal mol⁻¹ which is considerably lower than the energy of the 4-membered ring intramolecular transition state **5.10.1** (68.30 kcal mol⁻¹). The addition of a water molecule did result in a slight decrease in the energy of this transition structure.

Transition state structures 5.12 and 5.13

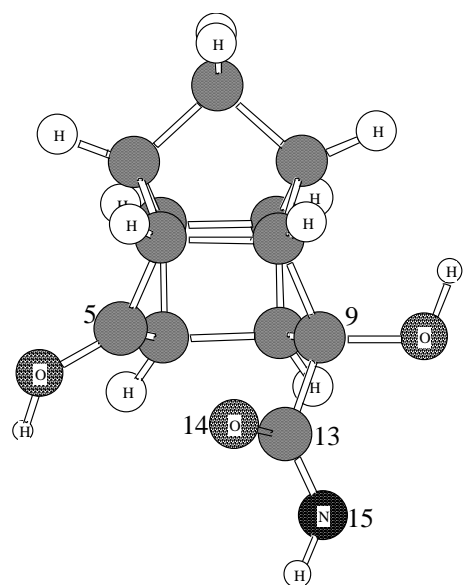
These two transition structures were calculated simultaneously. The diagrams presented depict the postulated structures for **5.12** and **5.13**.



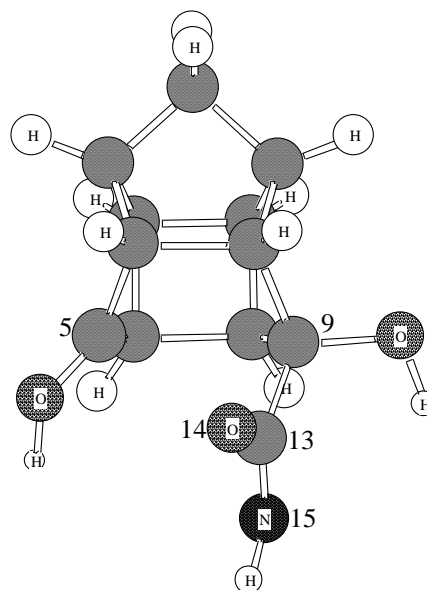
In the description of this calculation, nitrogen N15 and oxygen O14, with reference to their location on the cage, are referred to as either being at the "top" or "bottom" of the cage. "Top" is defined as closer to the CH₂ bridge at the top (shown below) and "bottom" as closer to the cyclobutane ring.



The PCU lactam **5.2** was used as a starting structure for **5.12** and **5.13**. The bond between C5 and O14 was deleted and the C9-C13 bond was rotated. It should be noted that in the resulting structure (**5.12 TS1 start**) the nitrogen N15 was positioned closer the bottom of the cage. The distance between C5 and N15 was approximately 2.7 Å. The 3D transition state input (**5.12 TS1 start**) and output (**5.12 TS1 end**) structures that were obtained for **5.12 TS1** are shown below.



5.12 TS1 start



5.12 TS1 end

The optimised output structure showed the correct orientation of the atoms thus a frequency calculation was performed. A negative eigenvalue of -104.70 cm^{-1} was obtained. When the animation of the vibration associated with the negative eigenvalue was viewed it corresponded with the C5-O14 bond breaking/formation.

The graphical representation of the IRC calculation for **5.12 TS1** is shown.

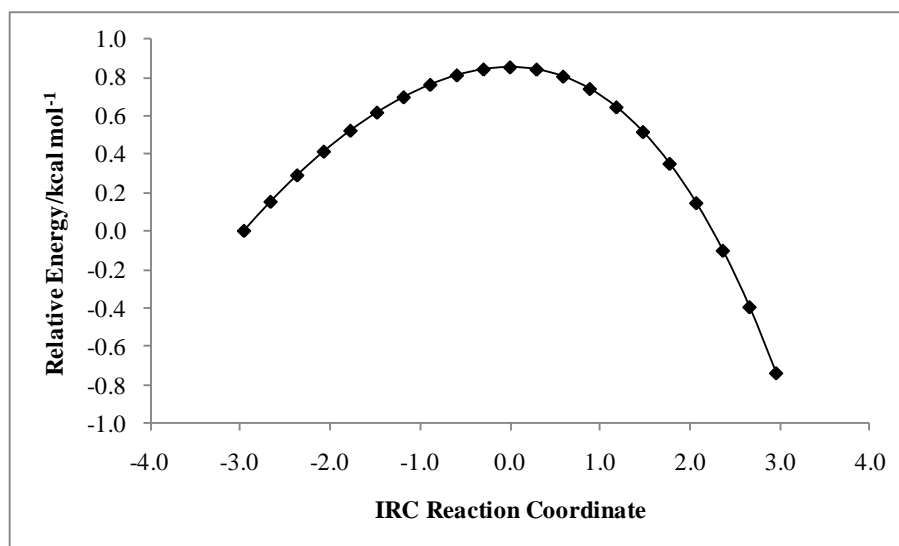
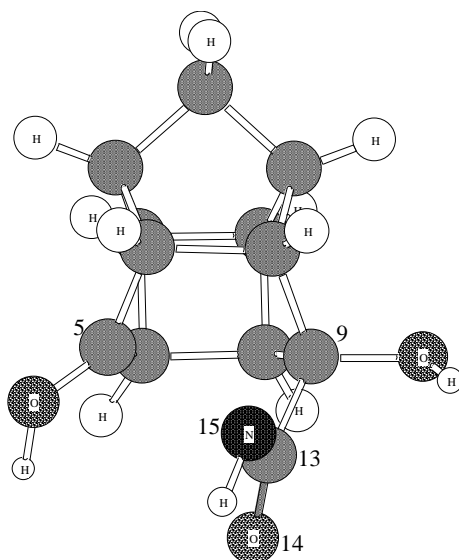


Figure 5.15 Graphical representation of the IRC reaction coordinate vs relative energy for structure **5.12 TS1**

The IRC calculation confirmed that the structure obtained was a transition structure.

For the transition structure optimisation of **5.13**, the same structure that was used as the input coordinates for **5.12 TS1 start**, was used but atoms O14 and N15 were rotated so that N15 was now positioned towards the “top” side of the cage (**5.13 TS1 end**). The same procedure that was used for the optimisation of **5.12 TS1** was carried out for **5.13 TS1**. The final optimised 3D transition state output (**5.13 TS1 end**) for **5.13 TS1** is shown.



5.13 TS1 end

The frequency calculation produced a negative eigenvalue of -151.51 cm^{-1} that corresponded with the C5-N15 bond formation/dissociation.

The graphical representation of the IRC calculation for **5.13 TS1** is shown below.

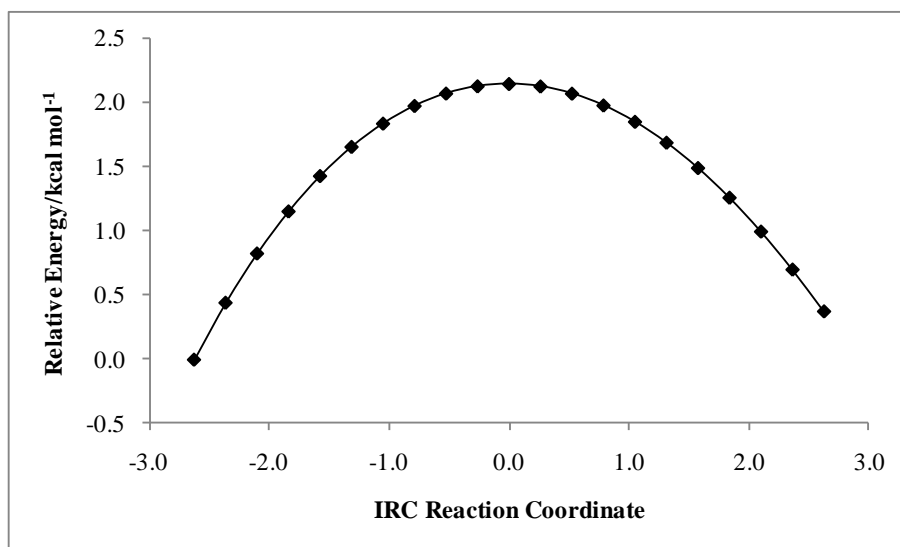
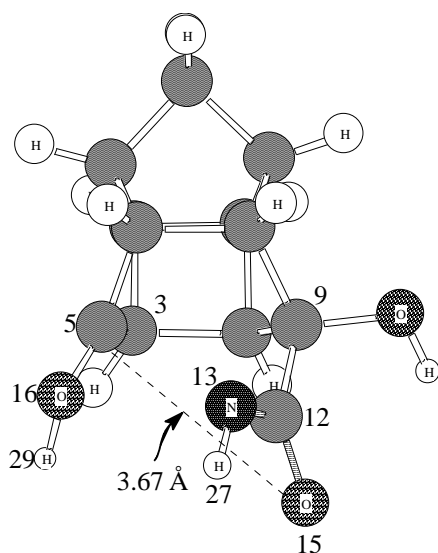


Figure 5.16 Graphical representation of the IRC reaction coordinate vs relative energy for structure 5.13 TS1

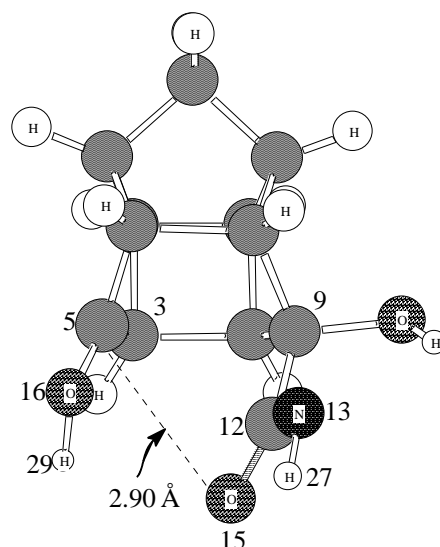
The IRC calculation confirmed that the structure obtained was a transition structure.

On closer examination of the movement of the atoms in the frequency calculations it was concluded that there is a possibility that instead of just two transition state structures, there may actually be four possible transition structures present. The two transition structures described thus far exhibit bond formation/breaking for C5-O14 (**5.12 TS1 end**) and for C5-N15 (**5.13 TS1 end**) occurring in closer proximity of the top side of the cage moiety. It might be possible that two more transition structures exist, where C5-N15 bond formation/breaking (**5.12 TS2**) and that of C5-O14 (**5.13 TS2**) occur in closer proximity to the “bottom side” of the cage. In order to confirm the absence and/or presence of these other two transition structures, a few more calculations were performed.

In **5.12 TS1** a scan to simulate the formation of a bond between N15 (at the back) and C5, was attempted. This however, resulted in the cage breaking. Instead, the **5.13 TS1 end** structure was used for a scan of the dihedral angles. The 3D input (**5.13 Scan start**) and output structures (**5.13 Scan end**) of the dihedral angle scan for **5.13** to find an approximate starting structure for **5.13 TS2** is shown.



5.13 Scan start



5.13 Scan end

The dihedral angle with atoms C9-C12-N13-O15 was frozen at an angle of 180° so that it would not affect the scan calculation. The dihedral angle with atoms C3-C5-O16-H29 was frozen at an angle of 0° away from the cyano group to prevent the hydroxide (O16-H29) from interfering in the scan calculation. The dihedral angle of C5-C9-C12-N13 was scanned from -60° to -110° thus simulating bond formation between O15, at the back of the cage, and C5. The graphical description of the scan is represented.

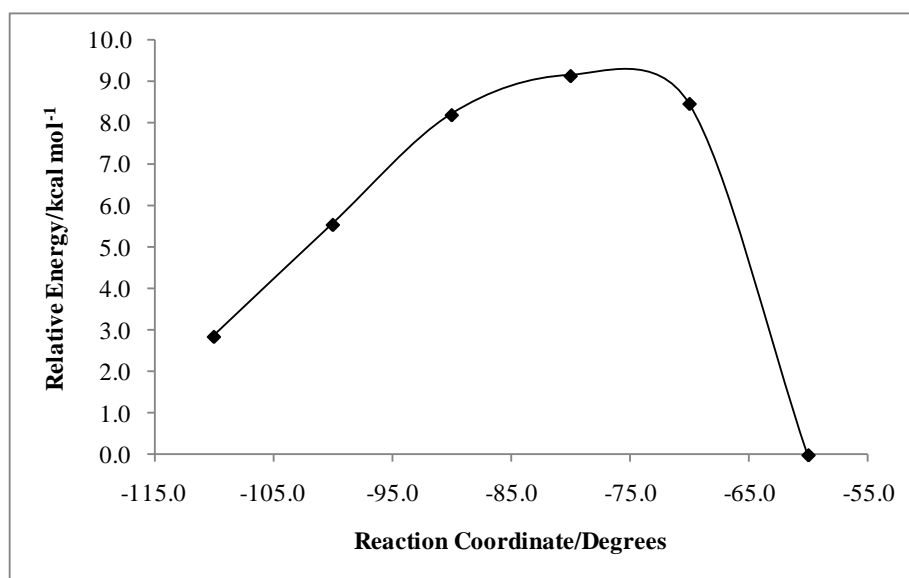
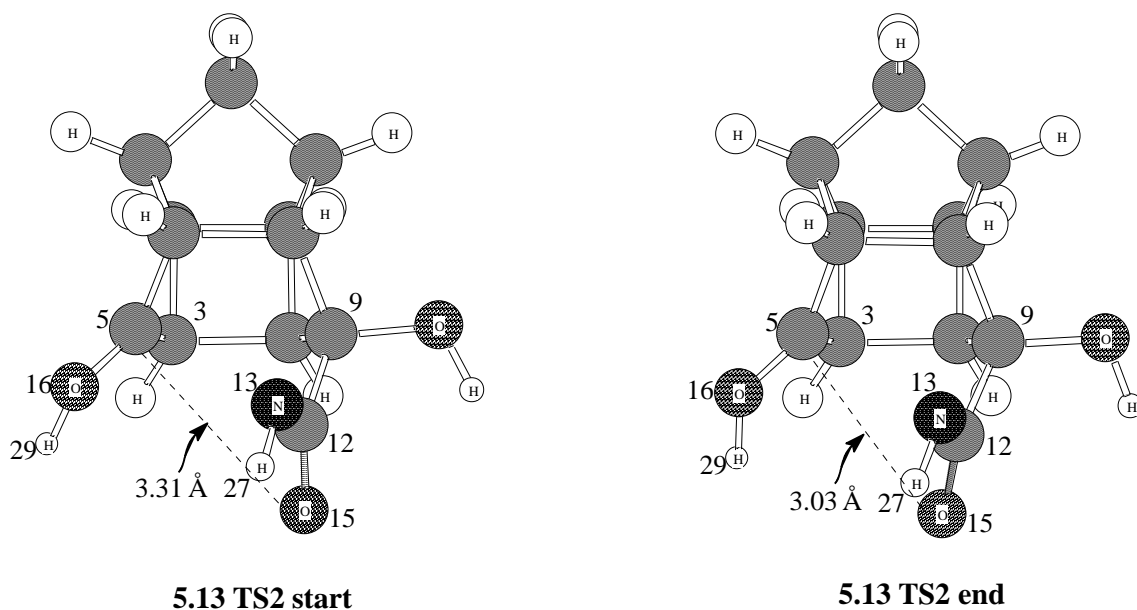


Figure 5.17 Graphical representation of energy vs reaction coordinate for structure 5.13 Scan

A maximum was observed at -80.0° . This approximate transition structure, **5.13 TS2 start**, was submitted for a DFT TS optimisation. The input **5.13 TS2 start** and output structure **5.13 TS2 end** that were obtained are shown.



The bond distance between C5-O15 once optimised was reduced to 3.03 Å. The frequency calculation produced a negative eigenvalue of -150.50 cm^{-1} which corresponds to O15 moving towards C5 to "close" the cage (bond formation) thus forming **5.11**.

The graphical representation of the IRC calculation for **5.13 TS2** is shown.

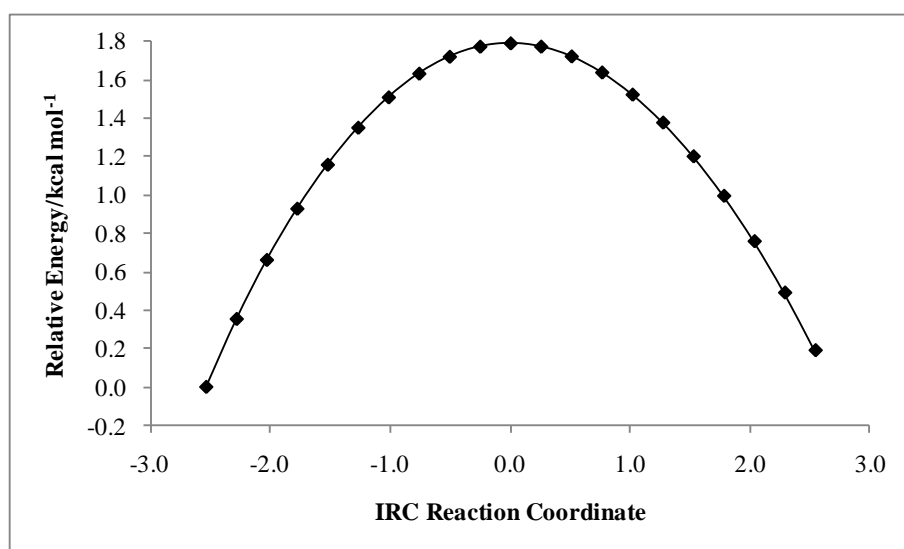
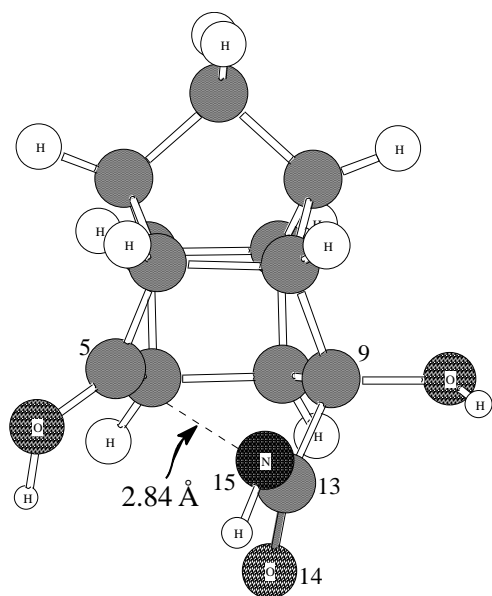


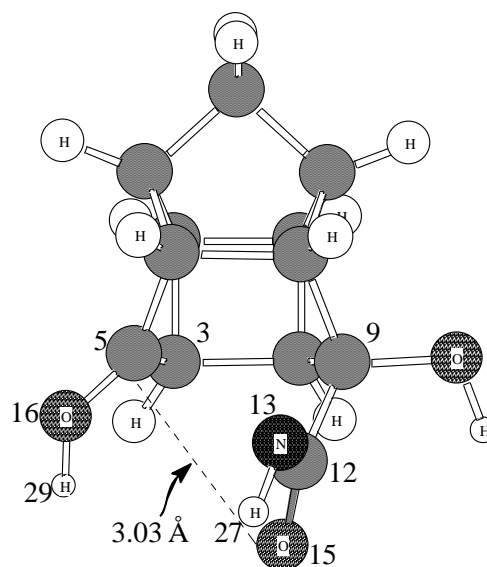
Figure 5.18 Graphical representation of the IRC reaction coordinate vs relative energy for structure **5.13 TS2**

The IRC calculation confirmed that the structure obtained was a transition structure.

Transition structure **5.13 TS1 end** which depicted bond breakage/formation between C5-N15 at the top of cage produced energy of 55.83 kcal mol⁻¹. Transition structure **5.13 TS2 end** which showed the bond breaking/forming between C5-O15 at the bottom of cage produced energy of 55.65 kcal mol⁻¹. This is an energy difference of 0.18 kcal mol⁻¹ which is relatively small. However, since **5.13 TS2 end** produced a lower energy, the conclusion would be that this is the preferred transition structure.



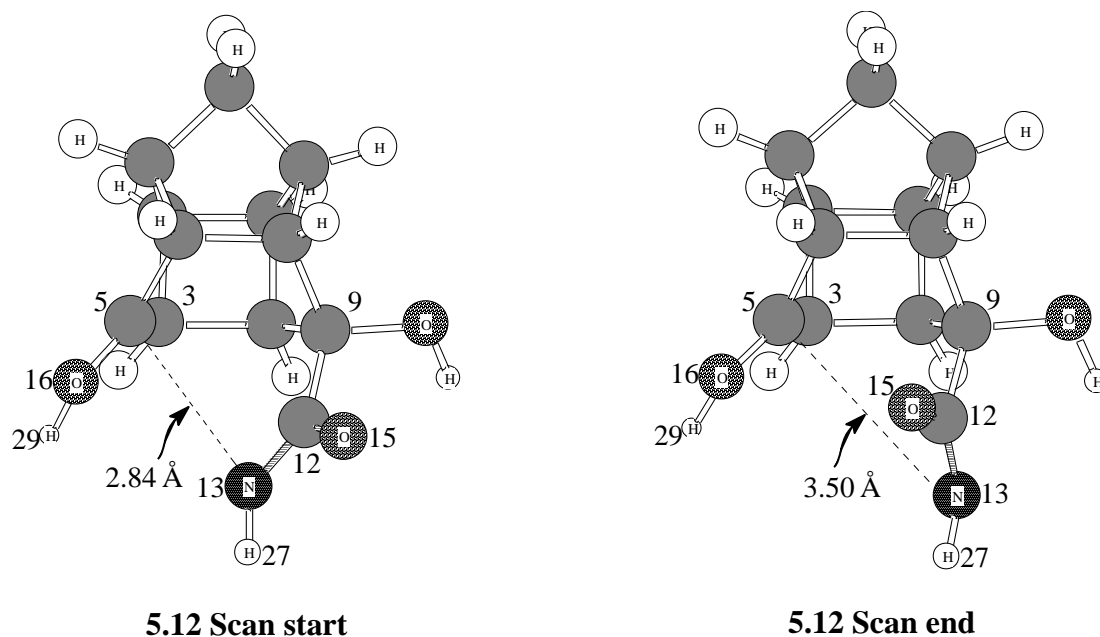
5.13 TS1 end



5.13 TS2 end

However, by inspecting the bond length involved in the transition structure, it is observed that **5.13 TS1 end** has a shorter bond length (C5-N15) than that of **5.13 TS2 end** (C5-O15). This, thus, makes **5.13 TS1 end** the transition structure *via* which the reaction proceeds. Since the energy difference between the two transition structures is fairly small, it is negligible.

The next task was to find the fourth possible transition structure where C5-N15 bond formation (**5.12 TS2**) is at the bottom of the cage. A second dihedral scan was performed by using an adjusted **5.12 TS1 end** structure as the starting point. The 3D input (**5.12 Scan start**) and output structures (**5.12 Scan end**) of the dihedral angle scan for **5.12** to find an approximate starting structure for **5.12 TS2** is shown.



The dihedral C9-C12-N13-O15 was frozen at an angle of 180° and the dihedral C3-C5-O16-H29 was frozen at an angle of 0° for the same reason as stated above. The scan of the dihedral C5-C9-C12-N13 was carried out from 60° to 110° .

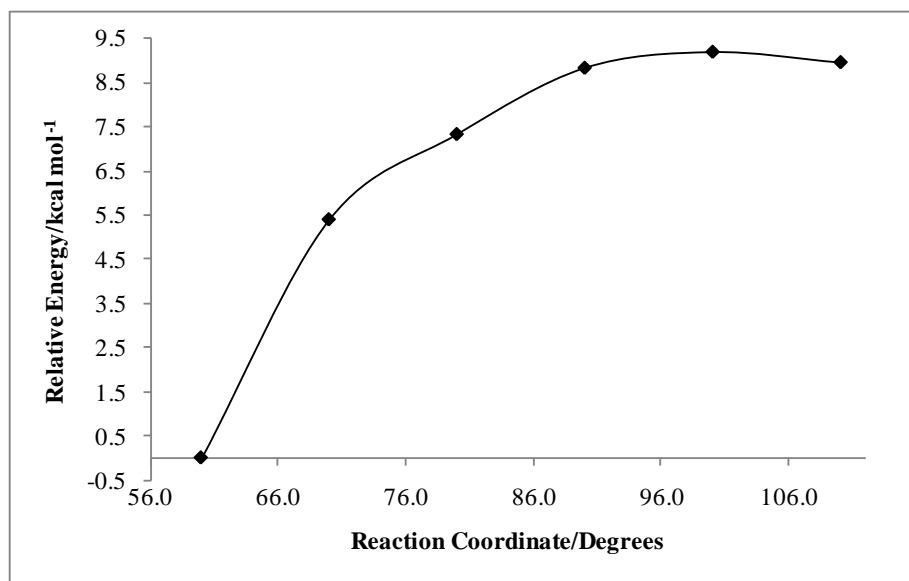
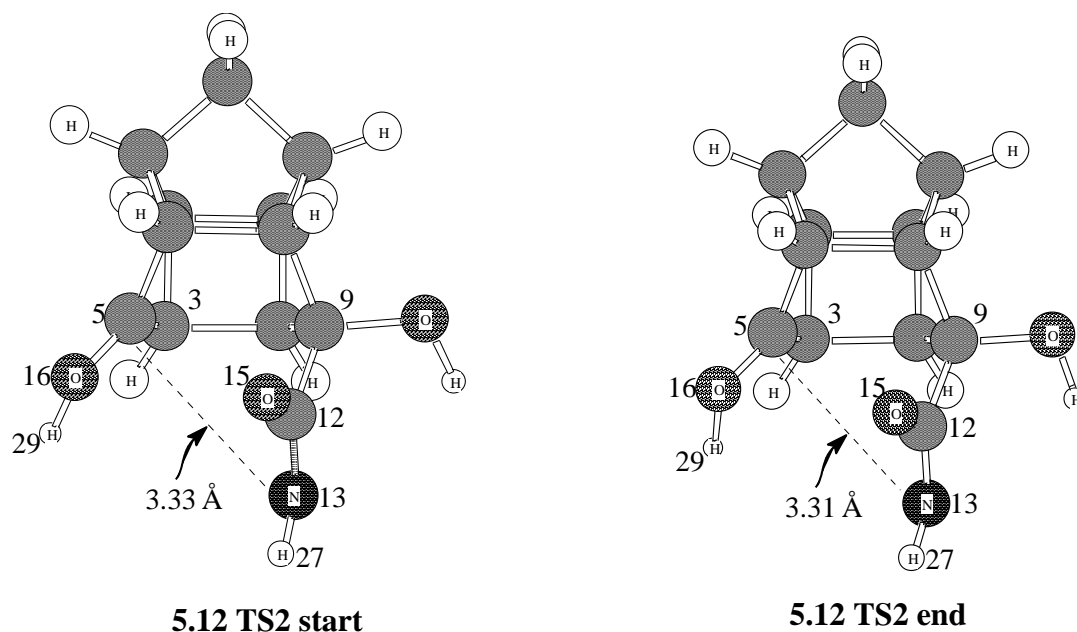


Figure 5.19 Graphical representation of energy vs reaction coordinate for structure **5.12 Scan**

As the angle was increased a maximum was observed at 100.0° . The structure at this maximum (**5.12 TS2 start**) was submitted for a transition state optimisation. The 3D input (**5.12 TS2 start**) and output structure (**5.12 TS2 end**) of the transition state optimisation are shown.



The bond length between C5-N13 at the beginning of the *ab initio* transition state optimisation was 3.33 Å. In the final DFT optimised transition structure the bond distance between C5-N13 decreased to 3.31 Å. The frequency calculation produced a negative eigenvalue of -104.68 cm^{-1} which corresponds to N13 moving to form a bond with C5 resulting in the final product, **5.2**.

The graphical representation of the IRC calculation for **5.12 TS2** is shown below.

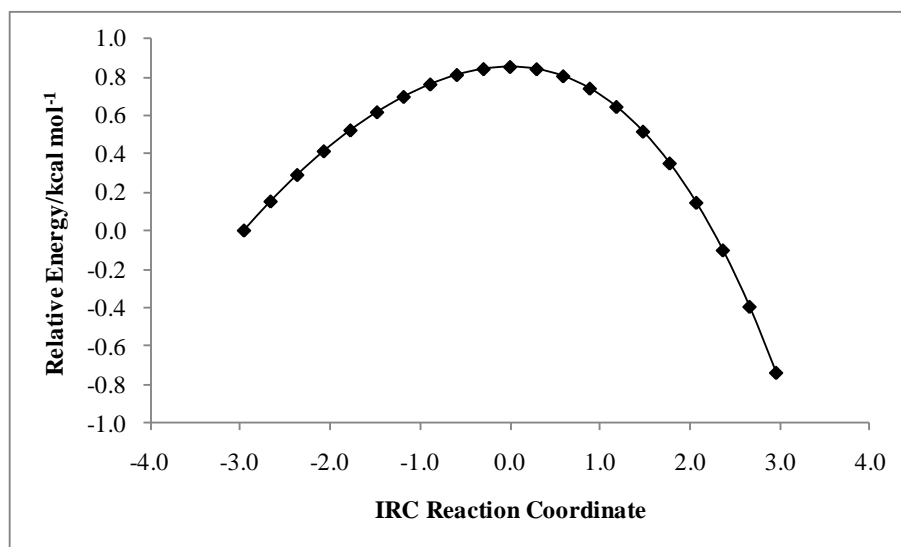
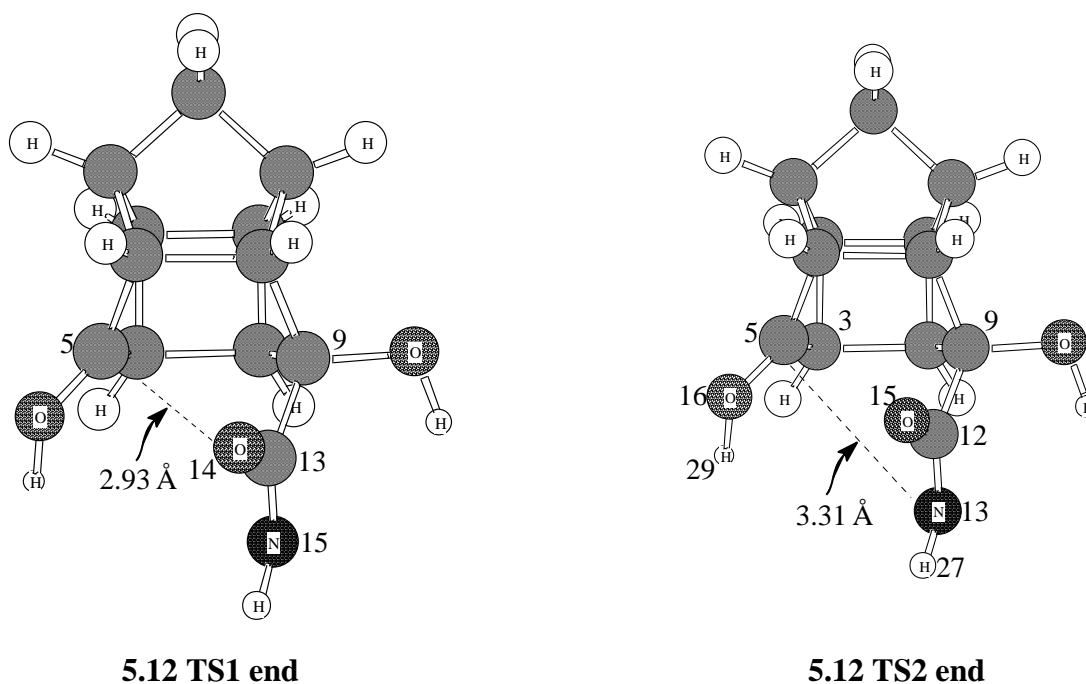


Figure 5.20 Graphical representation of the IRC reaction coordinate vs relative energy for structure **5.12 TS2**

The IRC calculation confirmed that the structure obtained was a transition structure.

Transition structure **5.12 TS1 end** showed bond breakage/formation between C5-O14 at the top of cage. Transition structure **5.12 TS2 end** depicted the bond breaking/forming between C5-N13 at the bottom of cage. Both transition structures produced energy of $55.90 \text{ kcal mol}^{-1}$. The bond lengths between the atoms that are involved in the bond breaking/forming were also compared. It was observed that the C5-O14 bond length (**5.12 TS1 end**) and the C5-O15 bond length (**5.12 TS2 end**) was 2.93 \AA . Similarly the C5-N15 bond length (**5.12 TS1 end**) and the C5-N13 bond length (**5.12 TS2 end**) was 3.31 \AA . There was no difference in the energies and geometries of the structures. This concludes that only one transition structure exists for **5.12**.



Thus for this study the energies of the transition structures **5.12 TS1 end** and **5.13 TS1 end** were used.

Martins³⁴ and co-workers showed experimentally that structures **5.4** and **5.6** are intermediates in the conversion of the dione **5.1** to the lactam **5.2**. The inseparable cyanohydrin mixture (**5.4** and **5.6**) was successfully isolated. When the mixture was treated with aqueous sodium hydroxide it yielded the hydroxylactam **5.2**. Since these compounds are found experimentally to co-exist and interchange at room temperature, the real energy barrier should be lower than the calculated Gibbs energy barrier of $29.60 \text{ kcal mol}^{-1}$ (see Figure 5.2). A possible explanation for the higher than expected energy barrier for the conversion between the cyanohydrin mixture **5.4** and **5.6**, is that the enthalpy penalty for the addition of an explicit water molecule to facilitate the intramolecular hydrogen transfer in the calculated

transition state (5.5.2) is obviously much higher than in reality for similar hydrogen transfer by solvent water molecules. The experimental results by Martins and co-workers also imply that transition state 5.7.2 should be the rate-determining step for the overall reaction which was confirmed by the theoretical results for mechanism 1. The theoretical approach followed in this investigation has therefore provided some valuable insight into this unique mechanism which correlates well with the experimental results.

5.2.1 Mechanism 1 with different solvents

In order to achieve quantitative accuracy in the computational simulation of molecules and chemical reactions, solvent effects are of vital importance. Solute-solvent interactions modify the energy, the structure, the properties and hence the overall behavior of molecules.

The reaction profile (Figure 5.2) shows that the addition of a single water molecule (5.5.2) results in the lowering of the energy by approximately 33 kcal mol⁻¹ and two water molecules (5.7.2) results in a decrease of the energy by approximately 154 kcal mol⁻¹. The use of explicit water molecules in the calculation also decreases the enthalpy penalty and hence the Gibbs free energy of the resulting substrate/solvent complex.

The effect of solvent on the overall energy of the reaction profile was investigated by modeling the reaction in the presence of two polar solvents: water and methanol; three dipolar solvents: acetonitrile, dimethyl sulphoxide and dichloromethane and in non-polar solvent: carbon tetrachloride.

Table 5.2 with the calculated relative Gibbs free energy changes for each solvent is presented. The summary of the calculated relative Gibbs free energy (Table A1.3 and Table A1.4) expressed in Hartrees is presented in APPENDIX 1. The energy (ΔE) (in kcal mol⁻¹), enthalpy (ΔH) (in kcal mol⁻¹) and entropy differences (ΔS) (cal K⁻¹ mol⁻¹) at 298.15 K in the various solvents are also presented in APPENDIX 1.

Table 5.2 Calculated relative^a Gibbs free energy changes [B3LYP/6-31+G(d)] for mechanism 1

Species ^b	ΔG						
	Gas	H ₂ O	MeOH	CH ₃ CN	DMSO	CCl ₄	DCM
5.1	0.00	0.00	0.00	0.00	0.00	0.00	0.00
5.3.1	124.78	21.02	22.21	17.13	37.23	58.57	44.54
5.3.2	48.34	51.13	12.91	50.62	50.23	6.53	50.47
5.4	13.81	17.31	17.03	24.55	25.71	20.01	22.42
5.5.1	57.23	4.58	5.19	8.25	8.47	9.55	7.71
5.5.2	29.60	23.32	10.48	14.55	14.40	10.45	13.58
5.6	13.34	19.69	19.32	26.62	28.01	20.72	24.13
5.7.1	230.73	104.38	88.29	99.18	103.67	155.31	108.44
5.7.2	76.50	67.36	69.00	16.60	17.37	13.43	15.74
5.9	27.45	36.98	36.48	44.00	45.62	37.26	41.33
5.10.1	68.31	22.09	24.83	9.95	9.81	4.52	8.59
5.10.2	45.58	38.83	15.38	16.21	15.92	9.22	14.95
5.11	6.60	19.87	20.39	26.24	27.05	17.09	23.31
5.12	55.91	17.37	8.55	9.94	9.81	4.53	8.59
5.13	55.83	38.59	18.95	9.95	9.81	4.53	8.59
5.2	-15.96	-10.14	-8.60	-6.39	-6.81	-11.37	-7.66

^a Energies relative to the energy of the starting structure **5.1**

^b Refers to the structure number in Figure 5.1

The relative Gibbs free energy (ΔG) (in kcal mol⁻¹) in water (H₂O), methanol (MeOH), acetonitrile (CH₃CN), dimethyl sulphoxide (DMSO), carbon tetrachloride (CCl₄) and dichloromethane (DCM) at 298.15 K

By examining the energy values in Table 5.2 it can be seen that for the transition structures the trend observed is that the high energy values that were obtained in the gas phase have been significantly reduced by the addition of a solvent indicating that the transition structure in medium (solvent) is more stable. The only discrepancy was found with **5.3.2** where the energy increased in solvents water, acetonitrile, dimethyl sulphoxide and dichloromethane (indicated in red). This transition state was one of two that was modeled with an HCN and an H₂O molecule. The transition state is an example of an amphiphilic molecule. A molecule that has both hydrophilic (water-loving) and lipophilic (fat-loving) properties is termed amphiphilic. It has a large hydrocarbon moiety that is lipophilic. The hydrophilic end consists of either charged groups or polar, uncharged groups. Since the molecule has lipophilic and hydrophilic portions it is extremely difficult to envisage whether the polar or

non-polar character of the molecule will dominate in a specific solvent.¹⁷¹ The theoretical results suggest that the non-polar character dominates in solvents such as water, acetonitrile, dimethyl sulphoxide and dichloromethane while the opposite is true for methanol and carbon tetrachloride.

The trend for the energy of the local minima is that the energy increased in solvent when compared to their gas phase energy values. This increase in energy is also due to the amphiphilic nature of the molecule.

The Gibbs free energy of solvation (ΔG_{sol}) is defined as the change of the Gibbs free energy when a particle of the solute is transferred from a fixed position in the gas phase into a fixed position in solution at constant temperature.¹⁷² For solvation to occur energy is required for the molecule to interact with the solvent. As these interactions occur energy is released. This released energy is termed free energy of solvation.¹⁷³ The difference of the Gibbs free energy in the gas phase and the Gibbs free energy of the solvent results in Gibbs free energy of solvation. The calculated relative Gibbs free energy of solvation for each solvent is presented in Table 5.3.

Table 5.3 Calculated relative Gibbs free energy of solvation [B3LYP/6-31+G(d)] for mechanism 1

Species ^a	ΔG_{sol}						
	Gas	H ₂ O	MeOH	CH ₃ CN	DMSO	CCl ₄	DCM
5.1	0.00	0.00	0.00	0.00	0.00	0.00	0.00
5.3.1	124.78	-103.77	-102.57	-107.66	-87.56	-66.21	-80.24
5.3.2	48.34	2.79	-35.43	2.28	1.89	-41.81	2.13
5.4	13.81	3.50	3.21	10.73	11.90	6.20	8.61
5.5.1	57.23	-52.65	-52.03	-48.97	-48.76	-47.68	-49.52
5.5.2	29.60	-6.28	-19.12	-15.06	-15.21	-19.16	-16.03
5.6	13.34	6.36	5.98	13.28	14.68	7.38	10.79
5.7.1	230.73	-126.35	-142.44	-131.55	-127.06	-75.43	-122.29
5.7.2	76.50	-9.13	-7.50	-59.90	-59.12	-63.06	-60.76
5.9	27.45	9.53	9.03	16.55	18.17	9.81	13.88
5.10.1	68.31	-46.22	-43.48	-58.36	-58.50	-63.79	-59.72
5.10.2	45.58	-6.75	-30.20	-29.37	-29.67	-36.36	-30.64
5.11	6.60	13.28	13.79	19.65	20.45	10.49	16.71
5.12	55.91	-38.54	-47.35	-45.97	-46.10	-51.38	-47.32
5.13	55.83	-17.24	-64.43	-45.89	-46.02	-51.31	-47.24
5.2	-15.96	5.82	7.36	9.57	9.15	4.59	8.30

^a Refers to the structure number in Figure 5.1

The relative Gibbs free energy of solvation (ΔG_{sol}) (in kcal mol⁻¹) in water (H₂O), methanol (MeOH), acetonitrile (CH₃CN), dimethyl sulphoxide (DMSO), carbon tetrachloride (CCl₄) and dichloromethane (DCM) at 298.15 K

The trend observed for the Gibbs free energy of solvation was that the energies decreased for most of transition structures with the exception of **5.3.2** where the energy increased. This increase in energy has been explained. The energies of the local minima also decreased when compared with their gas phase energies indicating that the solvation process is thermodynamically favoured.

5.3 Mechanism 2

Mechanism 2 is depicted in Figure 5.21. In this proposed mechanism, water molecules react with the PCU dione to form a 4 and 6-membered transition structure and then the stationary point **5.16**. **5.16** reacts with HCN and water to form the transition structure **5.17**. Although the formation of the cyclic transition structure for **5.17** and **5.3.2** is similar, it should be noted that transition structure **5.17** has a dihydroxy group and **5.3.2** has a carbonyl group. **5.17**

results in the stationary point **5.18** which is a dihydroxy cyano substituted cage. After the *trans*-annular transition structure **5.19** the mechanism follows the same path as mechanism 1.

The summary of the calculated relative thermochemical data for the structures depicted in mechanism 2 are presented in Table 5.4 below. The relative Gibbs free energy changes were used to construct the profile of the reaction in Figure 5.22. The summary of energies (Table A2.2) expressed in Hartrees and the reaction scheme is presented in APPENDIX 2.

Table 5.4 Summary of the relative^a thermochemical data for the conversion of the PCU dione **5.1** to the lactam **5.2** in the gas phase [B3LYP/6-31+G(d)] for mechanism 2

Species ^b	ΔE / kcal mol ⁻¹	ΔH / kcal mol ⁻¹	ΔG / kcal mol ⁻¹	ΔS /cal K ⁻¹ mol ⁻¹	LHVF/cm ⁻¹
5.1	0.00	0.00	0.00	0.00	102.67
5.15.1	37.94	36.29	47.90	-38.95	-1801.65
5.15.2	13.72	13.04	35.99	-76.98	-1456.41
5.16	-7.04	-4.63	7.37	-40.23	140.19
5.17	23.01	26.92	59.42	-108.98	-286.71
5.18	-12.91	-7.67	16.34	-80.52	118.79
5.19					
5.6	-1.95	0.12	13.33	-44.32	120.20
5.7.1	210.91	211.04	230.73	-82.00	-464.84
5.7.2	38.95	43.18	76.50	-111.75	-332.26
5.9	-0.51	3.64	27.44	-79.85	93.40
5.10.1	43.11	43.80	68.30	-82.18	-2019.49
5.10.2	8.13	10.02	45.62	-119.40	-1400.69
5.11	-24.17	-19.10	6.59	-86.16	113.70
5.12	27.21	31.38	55.90	-82.23	-104.70
5.13	27.23	31.26	55.82	-82.37	-151.51
5.2	-46.93	-41.09	-15.97	-84.26	109.67

^a Energies relative to the energy of the starting structure **5.1**

^b Refers to the structure number in Figure 5.21

The energies in the gas phase (ΔE) (in kcal mol⁻¹), enthalpy (ΔH) (in kcal mol⁻¹) as well as Gibbs free energy (ΔG) (in kcal mol⁻¹) and entropy (ΔS) (cal K⁻¹ mol⁻¹) at 298.15 K and the lowest harmonic vibrational frequencies (LHVF) (in cm⁻¹) of the species in the formation of the PCU lactam from the PCU dione

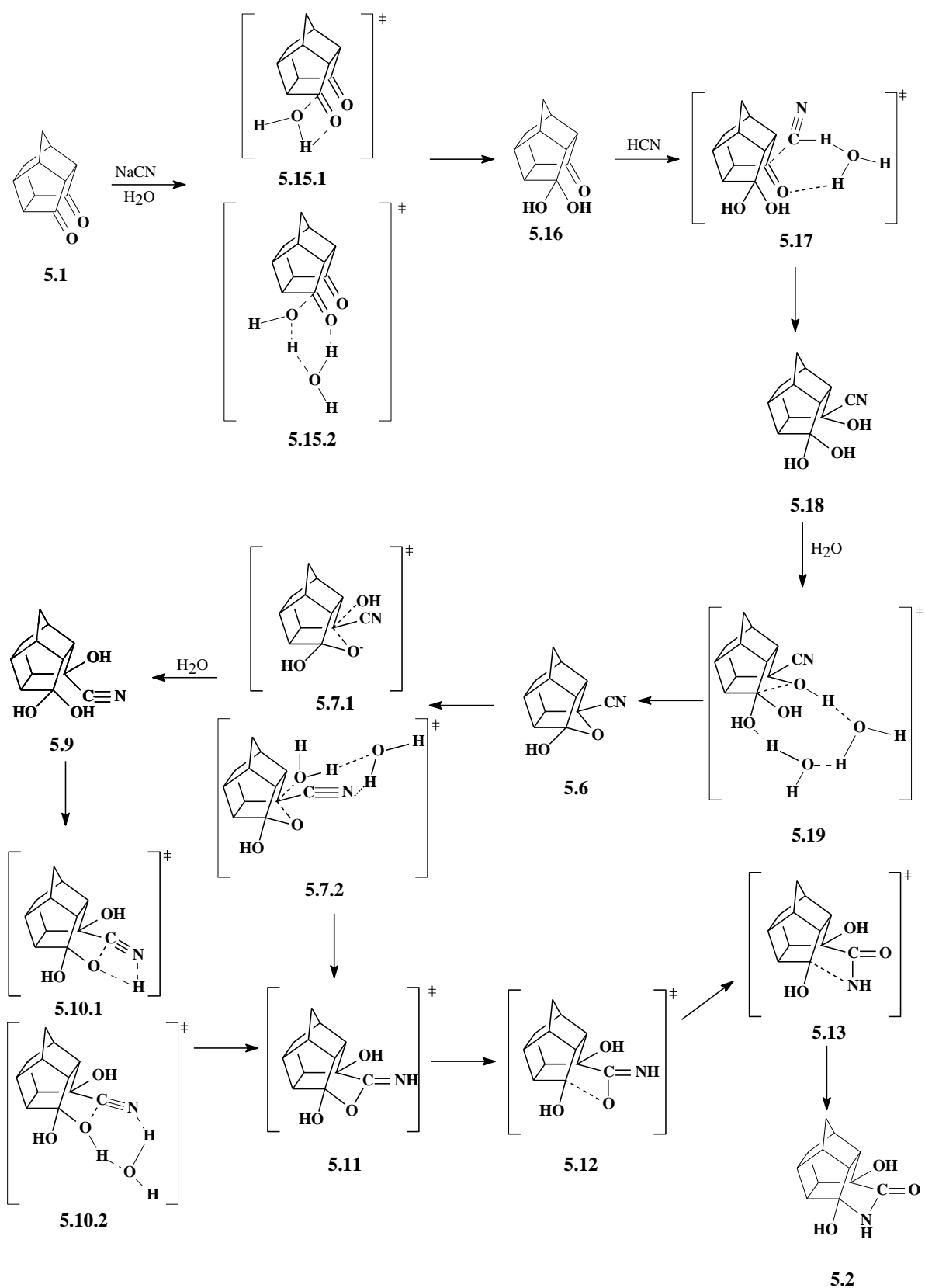


Figure 5.21 Mechanism 2 for the conversion of the PCU dione 5.1 to the lactam 5.2

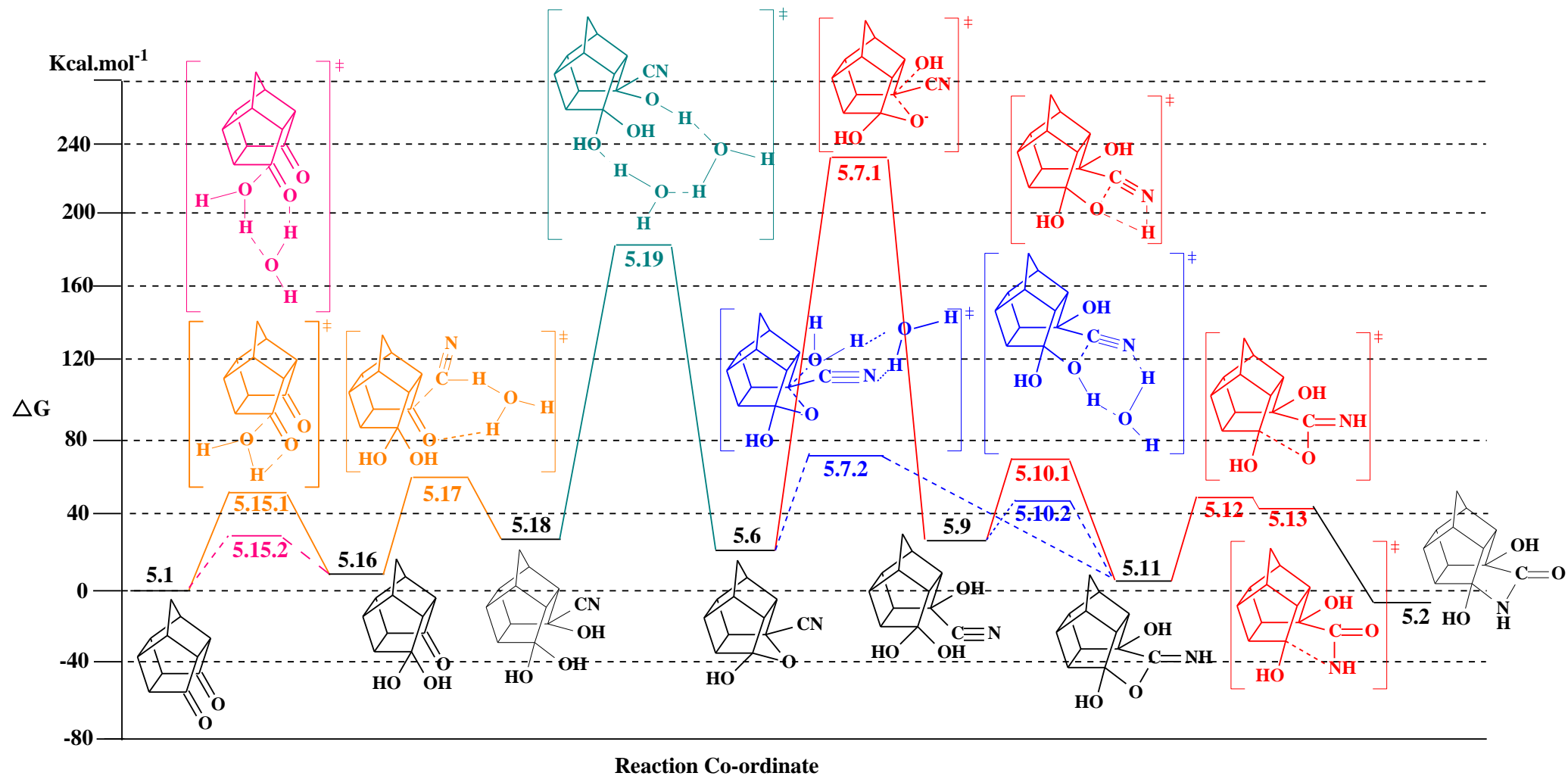
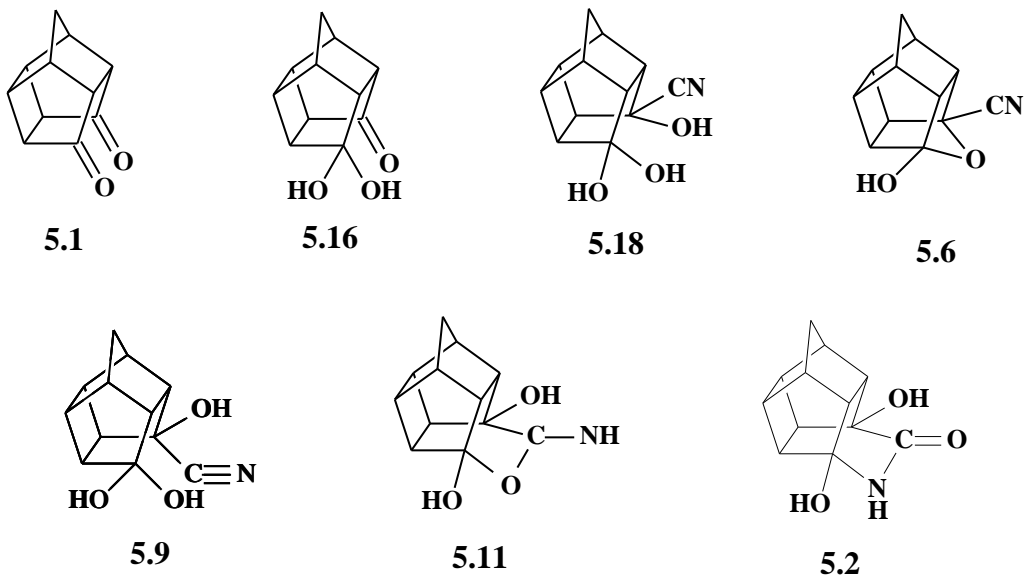


Figure 5.22 Gas phase Gibbs free energy for the mechanism proposed in Figure 5.21

Local minima on the energy profile

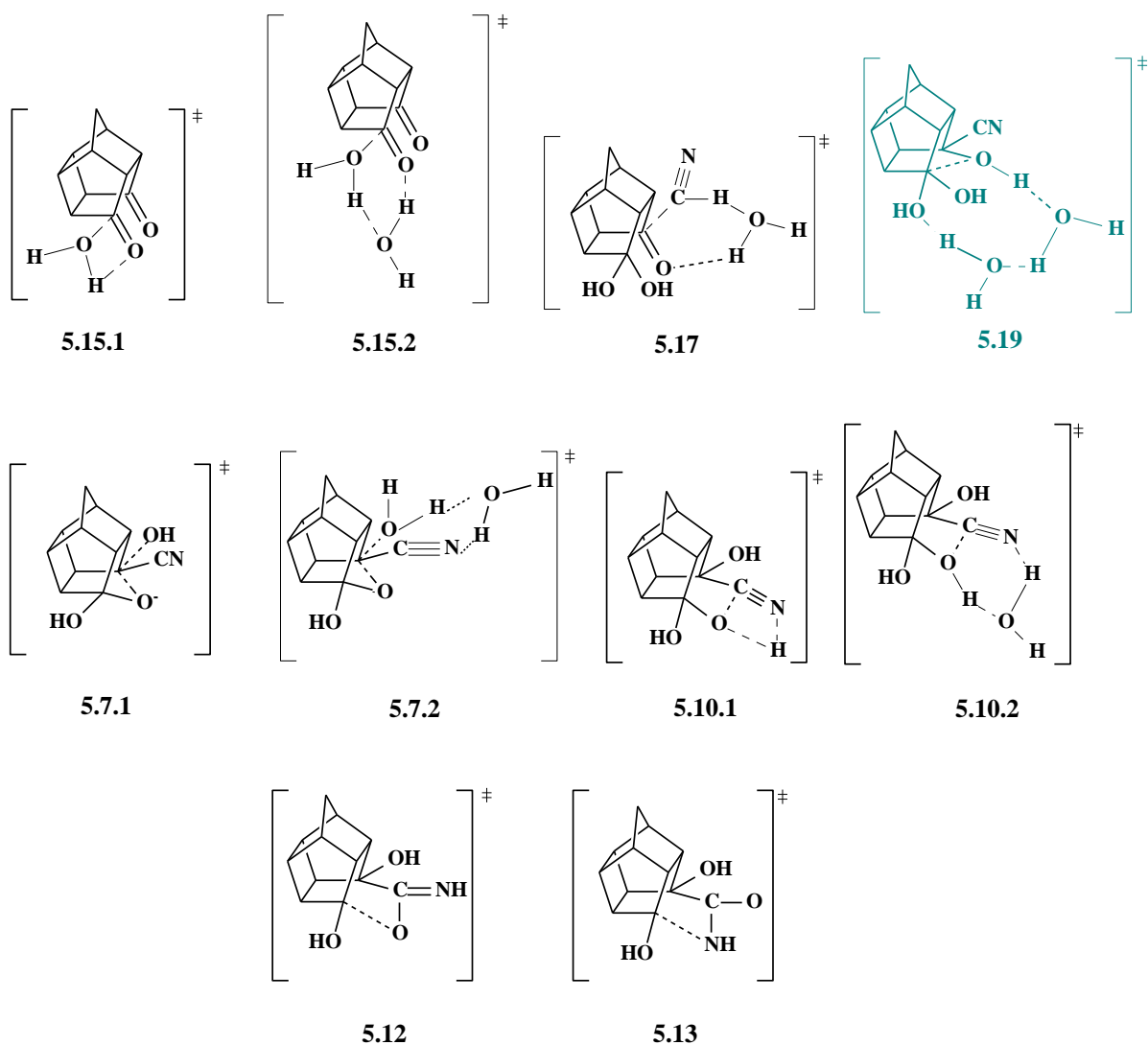
From the energy values in Table 5.4 and from their positions on the calculated energy profile in Figure 5.22, it was concluded that structures **5.1**, **5.16**, **5.18**, **5.6**, **5.9**, **5.11**, and **5.2** can be classified as local minima or stationary points on the energy profile of the reaction.



5.16 and **5.18** are the two “new” stationary points. The same procedure that was followed in mechanism 1 was carried out for mechanism 2. Geometry optimisations were done first at the *ab initio* level and then at the DFT level for each of the structures to remove any van der Waals contacts or bond overlap. The positive vibrational frequencies verified that these are local minima on the potential energy scan.

The Transition States (TS)

Structures **5.15.1**, **5.15.2**, **5.17**, **5.19**, **5.7.1**, **5.7.2**, **5.10.1**, **5.10.2**, **5.12** and **5.13** from Figure 5.22 and depicted below are characterised as the transition structures.



Here as well, the same procedure that was carried out in mechanism 1 for determining the transition structures was followed in finding transition structures **5.15.1**, **5.15.2**, **5.17** and **5.19**. The remaining four transition structures in the profile were discussed in mechanism 1.

Transition structure 5.15.1

As mentioned previously for this structure a single water molecule was added to the PCU dione to form a 4-membered cyclic transition structure. An approximate starting structure was modeled by adding a water molecule to **5.1** and an *ab initio* transition state optimisation using only 20 steps was done. The graphical representation of the transition state optimisation is shown.

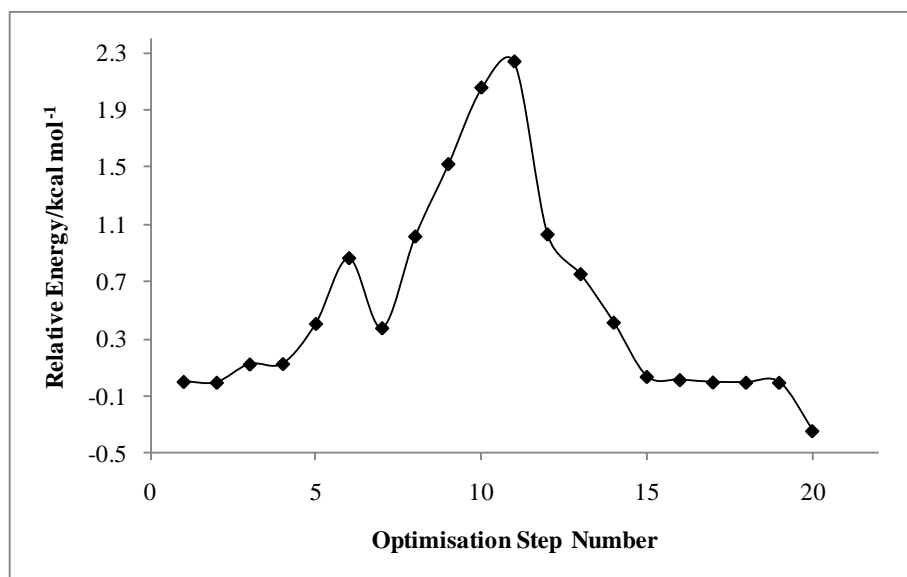
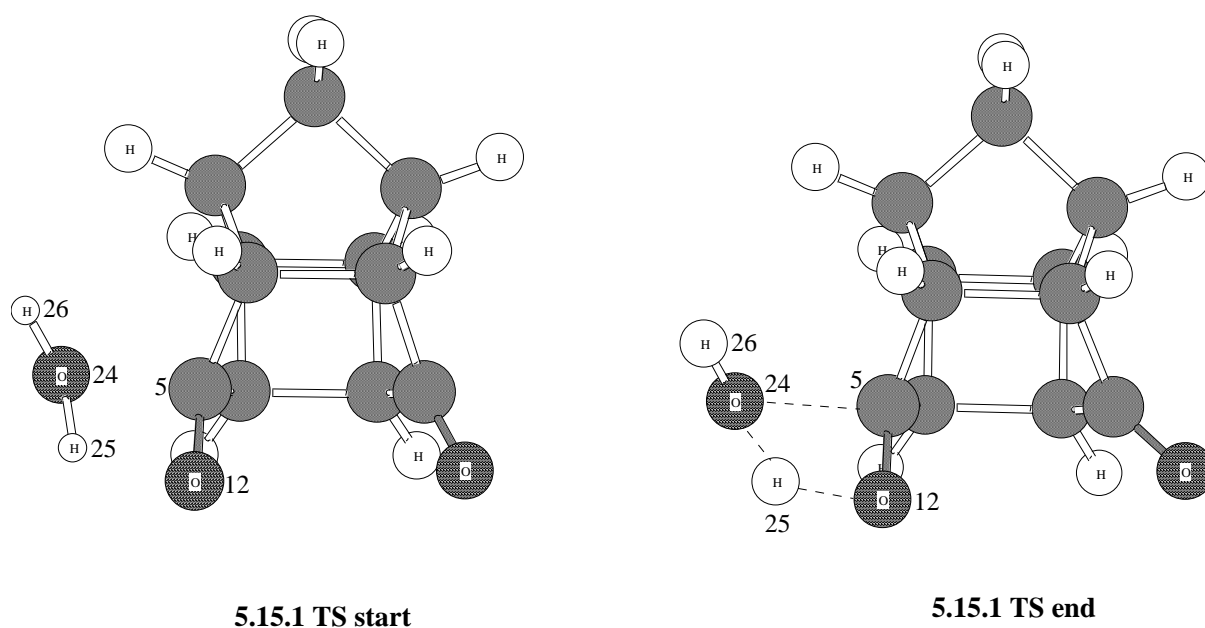


Figure 5.23 Graphical representation of relative energy vs optimisation step number for structure 5.15.1

The optimisation produced a maximum at step 11. On examination of the structure at this point, it was noted that the structure had the expected orientation of the atoms. The structure from step 11 (**5.15.1 TS1 start**) was submitted for a complete transition state optimisation at the *ab initio* level. When the optimisation had completed the output was submitted for a DFT transition state optimisation. The 3D **5.15.1 TS1 end** is the output that was obtained from the DFT transition state optimisation.



The frequency calculation produced only one negative eigenvalue of -1801.65 cm^{-1} and shows the intramolecular transfer of atom H25 between O12 and O24. As atom H25 is transferred to atom O12, the bond C5-O24 forms.

The graphical representation of the IRC calculation for **5.15.1** is shown.

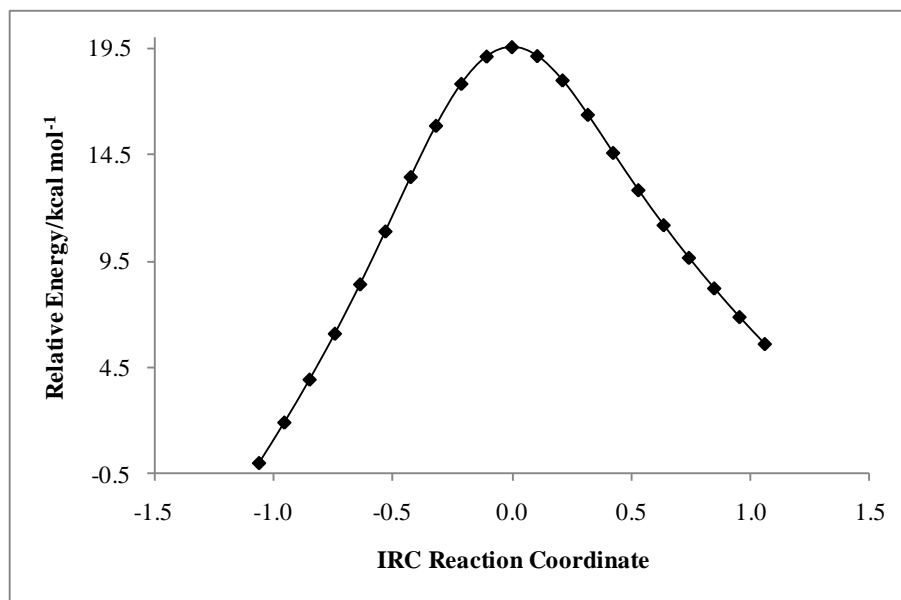
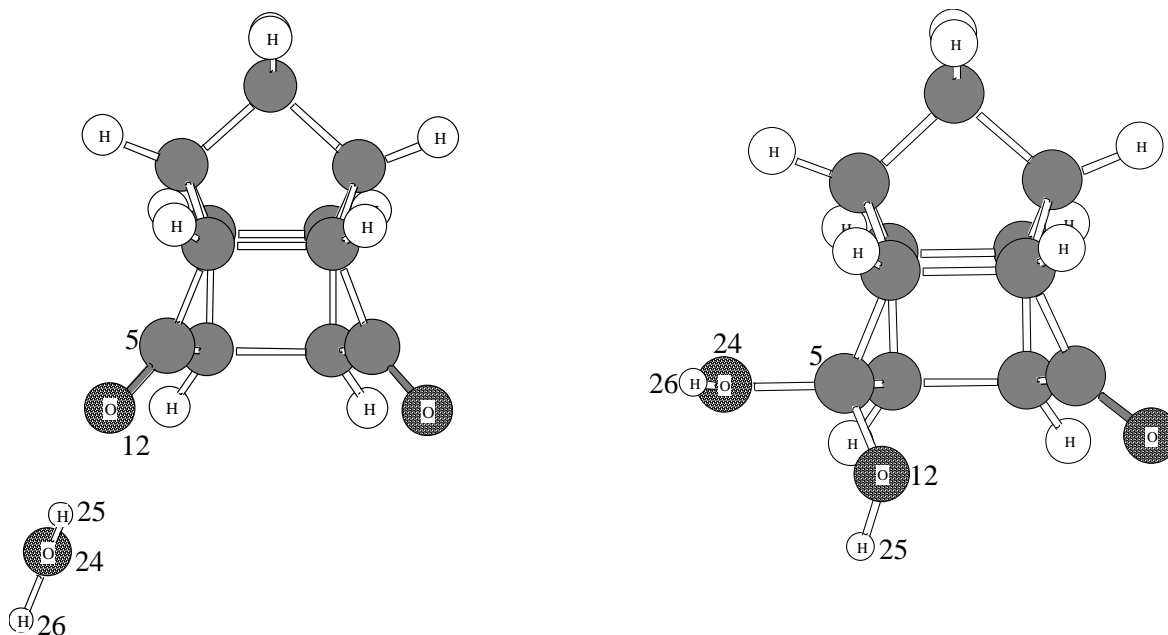


Figure 5.24 Graphical representation of the IRC reaction coordinate vs relative energy for structure **5.15.1**

The IRC calculation confirmed that the structure obtained was the expected transition structure since the optimised structure from step 1 (**5.15.1 IRC start**) resulted in the local minimum **5.1** with a water molecule and step 21 (**5.15.1 IRC end**) produced the stationary point **5.16**.



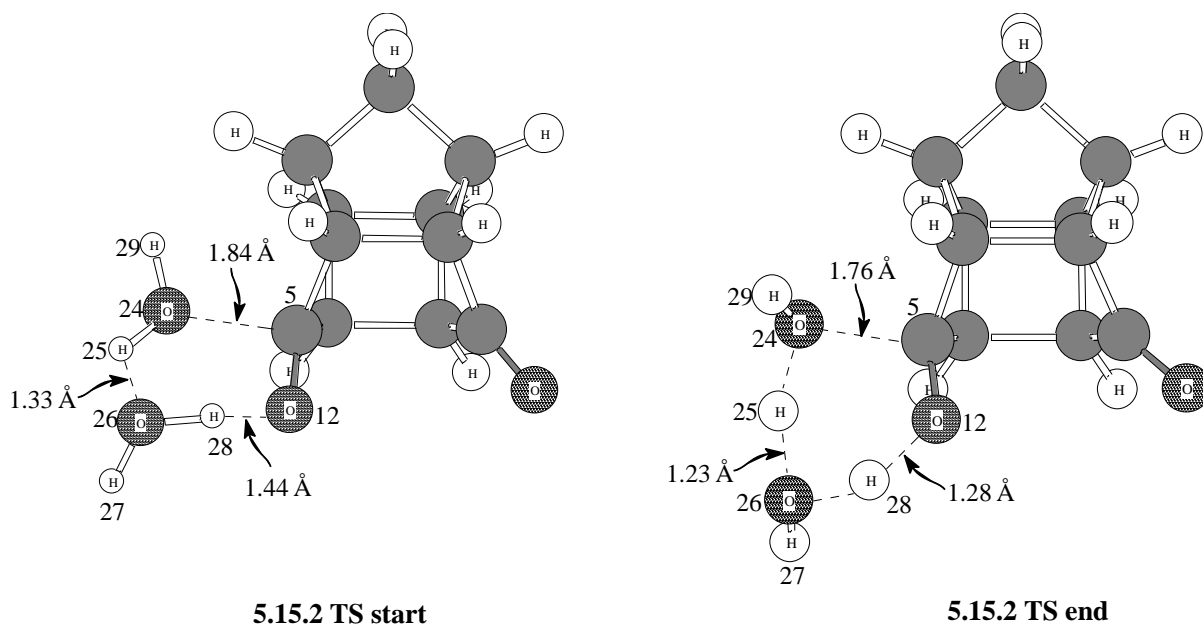
5.15.1 IRC start

5.15.1 IRC end

This transition state produced a relative energy value of $47.90 \text{ kcal mol}^{-1}$.

Transition structure 5.15.2

The transition structure **5.15.2** was modeled with two water molecules thus forming a 6-membered cyclic transition structure. **5.1** was again used as the starting point and two H_2O molecules were added. Since this is a 6-membered transition structure the bond lengths and angles were adjusted to approximately those of **5.5.2**, the 6-membered cyclic transition structure in mechanism 1. Instead of performing a scan calculation, a PM3 optimisation was done to obtain an approximate starting structure for the transition state. The following bond lengths in the input (**5.15.2 TS start**) were frozen: C5-O24 at 1.84 \AA , H25-O26 at 1.33 \AA and O12-H28 at 1.44 \AA . The 3D optimised output structure (**5.15.2 TS end**) is depicted.



The frequency calculation produced a single negative eigenvalue of -1456.41 cm^{-1} and shows the intramolecular transfer of atom H25 between O24 and O26 as well as the intramolecular transfer of atom H28 between O12 and O26. As atom H25 is transferred to atom O26, the bond C5-O24 forms and H28 is transferred to O12.

The graphical representation of the IRC calculation for **5.15.2** is shown.

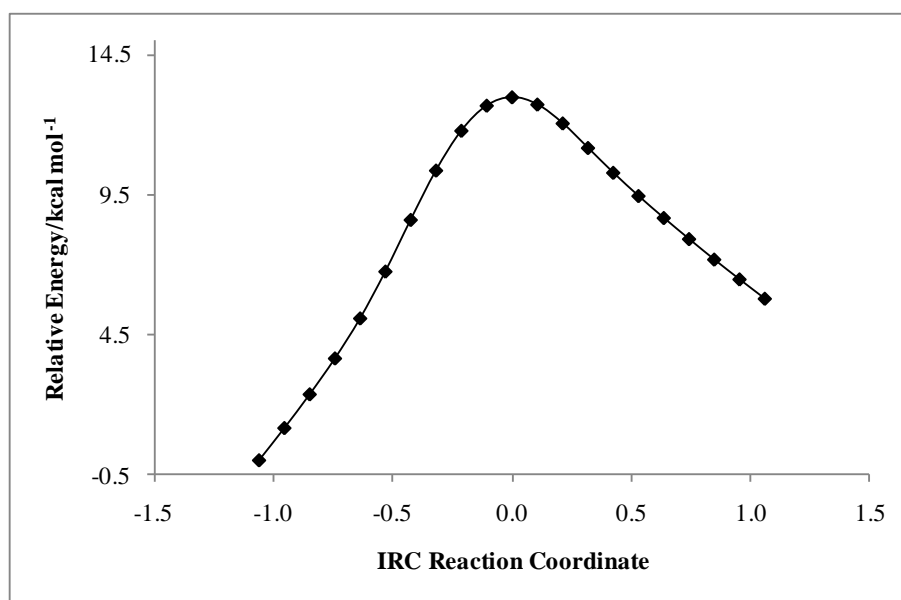
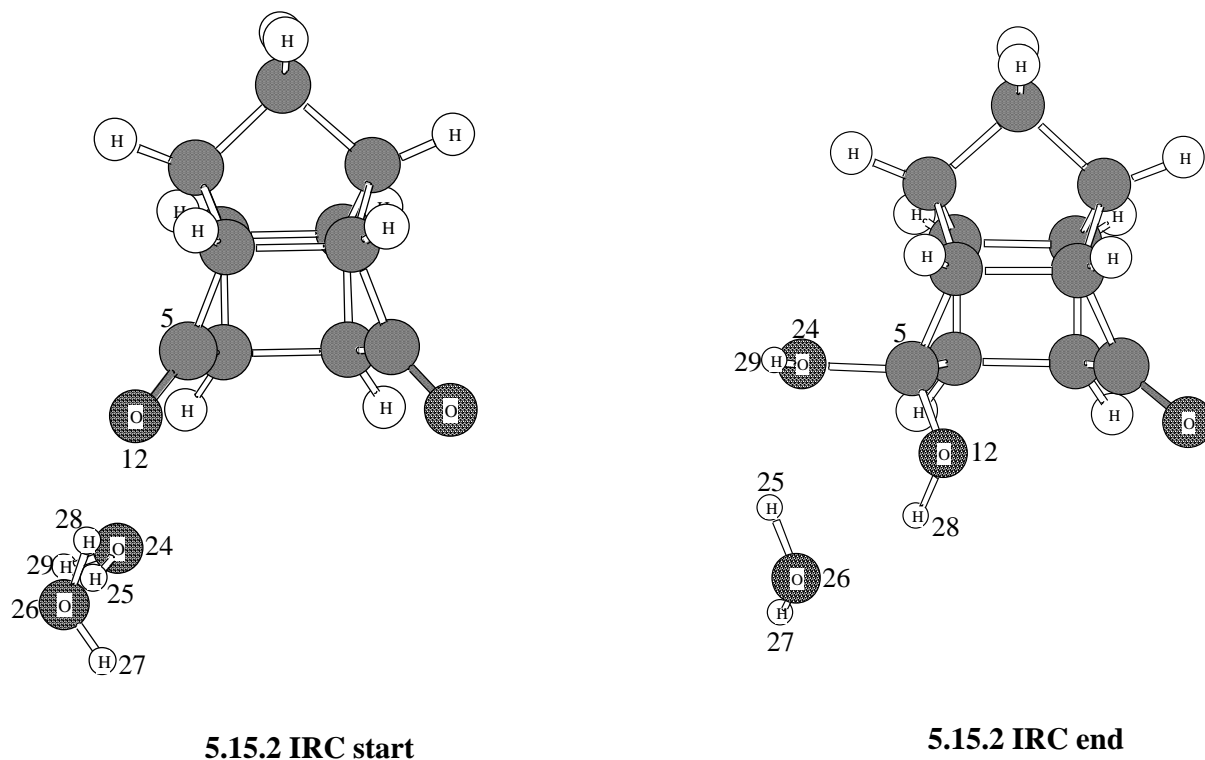


Figure 5.25 Graphical representation of the IRC reaction coordinate vs relative energy for structure 5.15.2

The IRC calculation verified the structure obtained was a transition structure since the optimised structure from step 1 (**5.15.2 IRC start**) resulted in the local minimum **5.1** with two water molecules and step 21 (**5.15.2 IRC end**) produced the stationary point **5.16** and a water molecule.

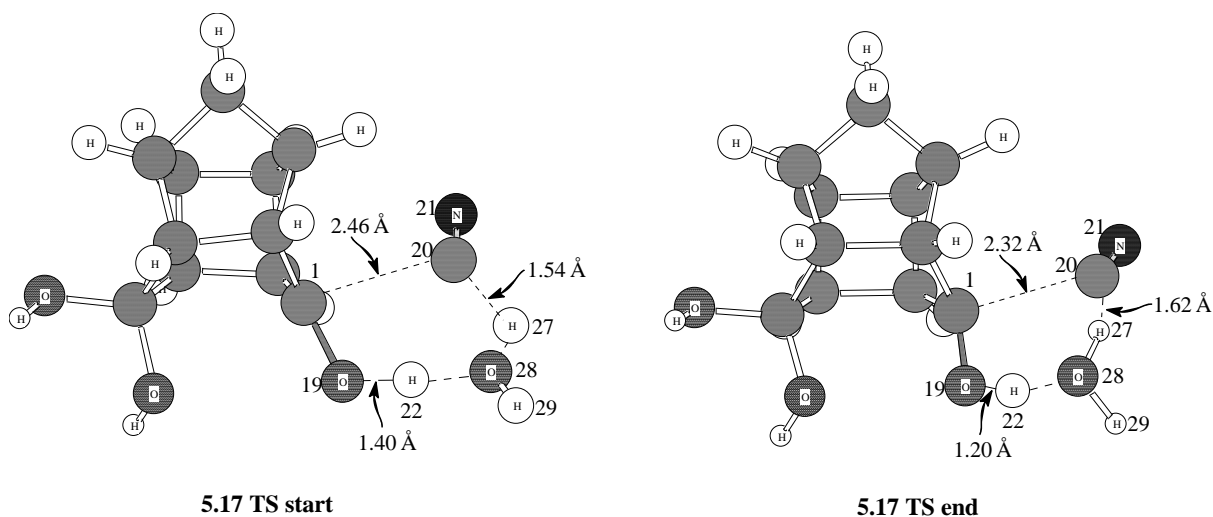


The addition of two water molecules decreased the overall energy by 11.91 kcal mol⁻¹.

Transition structure 5.17

Attempts and the failure to model a 4-membered cyclic transition structure with HCN can be found in APPENDIX 2.

Stationary point **5.16** was used as a starting point to model the transition structure. The 3D transition state optimisation is shown.



It is observed from the optimisation (**5.17 TS start**) that the bond between C20 and H27 from the HCN molecule is breaking. The H27 atom is moving towards O28 in the water molecule and H22 is being transferred to O19. There is a decrease in the bond distance from 2.46Å to 2.32Å between C1 and C20 which suggests that a bond is forming.

The transition structure (**5.17 TS end**) was verified by performing a frequency calculation which produced one negative eigenvalue of -286.71 cm^{-1} . There are three vibrations clearly associated with the imaginary frequency. The first vibration is the cyano group (C20-N21) moving towards the cage to form a bond with C1. The second vibration is the intramolecular hydrogen transfer between C20 and O28. The third vibration is also an intramolecular hydrogen transfer between O28 and O19.

The graphical representation of the IRC calculation for **5.17** is shown.

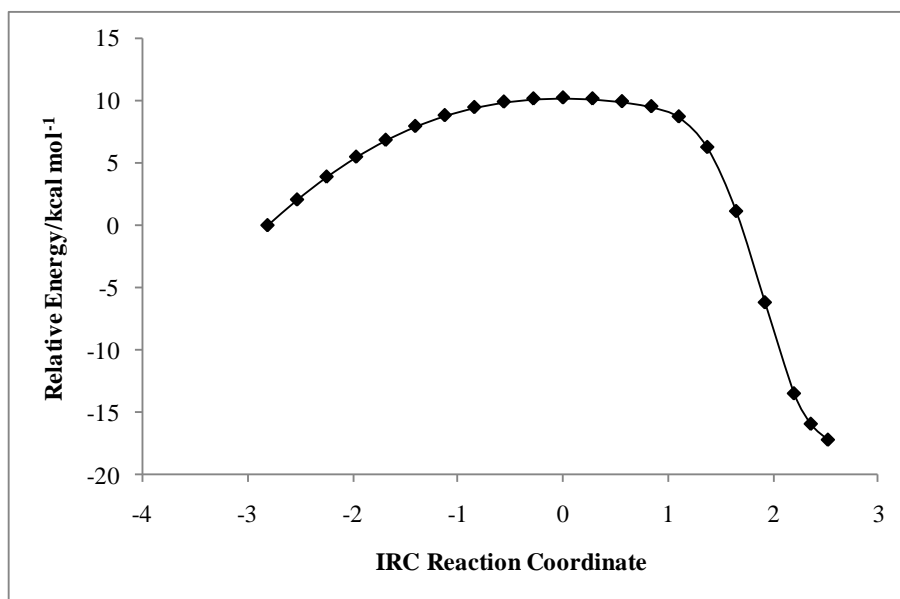


Figure 5.26 Graphical representation of the IRC reaction coordinate vs relative energy for structure 5.17

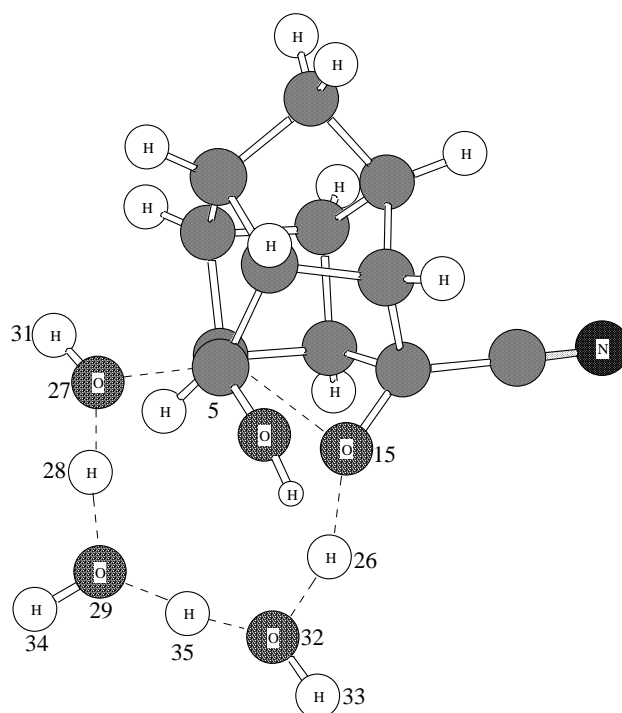
The structure from step 1 and step 21 of the IRC calculation was optimised. The optimised structure from step 1 glided towards the reactants, that is, to **5.16**, HCN and H₂O. The optimised structure from step 21 yielded the products, namely, **5.18** and a H₂O molecule. This confirms that the structure obtained was a transition structure.

Transition structure 5.19

An 8-membered transition state was attempted for this calculation. Two H₂O molecules were added to **5.18** to form the starting structure for transition state **5.19**. The first H₂O molecule (H28O29H34) donates a proton, H28, to the leaving hydroxyl group, O27H31, to form a water molecule. The second H₂O molecule (H35O32H33) accepts proton H26 from hydroxyl group O15H26 and donates the H35 proton to O29. The bond between C5 and O27 breaks. There is intramolecular hydrogen transfer between O27-O29; between O29-O32 and finally between O32-O15. This last intramolecular hydrogen transfer results in the bond formation between O15 and C5 producing **5.6**.

As mentioned, this calculation was attempted but a final transition structure could not be isolated. All the methods that were used to locate the transition structures described above and for mechanism 1 proved unsuccessful. An IRC phase calculation was also attempted but this too did not yield favourable results.

The 3D frequency output shown below produced ten negative eigenvalues but the first frequency of -1601.86 cm^{-1} corresponded correctly to the movement of the atoms described above.



5.19 Freq out

By comparing mechanism 1 and mechanism 2, it is observed that in mechanism 1 the energies of transition structures **5.3.1** ($124.78\text{ kcal mol}^{-1}$) and **5.3.2** ($48.33\text{ kcal mol}^{-1}$) were higher than the energy of **5.15.1** ($47.90\text{ kcal mol}^{-1}$) and **5.15.2** ($35.99\text{ kcal mol}^{-1}$). The conclusion would be that the preferred reaction pathway is *via* the transition structures **5.15.1** and **5.15.2**.

In mechanism 2, transition structure **5.17** ($59.42\text{ kcal mol}^{-1}$) has a higher energy than **5.5.1** ($57.23\text{ kcal mol}^{-1}$) and **5.5.2** ($29.60\text{ kcal mol}^{-1}$) from mechanism 1 despite **5.5.1** being an ionic species. This makes **5.5.2** the preferred transition structure for the reaction pathway

It is assumed that transition structure **5.19** will have a much higher energy hence ruling it out as a possible transition state in the reaction pathway. Even though **5.19** was not found, the probability that it could exist in a model that can mimic real experimental conditions, cannot be ruled out. However, due to the failure of finding this transition structure, it can also not be concluded that this proposed mechanism is in fact valid. The remainder of the pathway has been discussed in mechanism 1.

5.3.1 Mechanism 2 with different solvents

The calculated relative Gibbs free energy changes for each solvent are presented in Table 5.5. The summary of energies (Table A2.3 and Table A2.4) expressed in Hartrees is presented in APPENDIX 2. The energy (ΔE) (in kcal mol⁻¹), enthalpy (ΔH) (in kcal mol⁻¹) and entropy differences (ΔS) (cal K⁻¹ mol⁻¹) at 298.15 K in the various solvents are presented in APPENDIX 2.

Table 5.5 Calculated relative^a Gibbs free energy changes [B3LYP/6-31+G(d)] for mechanism 2

Species ^b	ΔG						
	Gas	H ₂ O	MeOH	CH ₃ CN	DMSO	CCl ₄	DCM
5.1	0.00	0.00	0.00	0.00	0.00	0.00	0.00
5.15.1	47.91	16.54	18.05	5.40	4.77	3.46	5.18
5.15.2	36.01	20.22	18.27	44.12	19.54	7.24	18.50
5.16	7.38	12.32	12.34	12.92	13.18	10.70	12.18
5.17	59.42	25.88	69.22	67.47	68.30	18.89	67.58
5.18	16.35	22.25	23.21	25.28	25.27	21.52	24.18
5.19							
5.6	13.34	19.69	19.32	26.62	28.01	20.72	24.13
5.7.1	230.73	104.38	88.29	99.18	103.67	155.31	108.44
5.7.2	76.50	67.36	69.00	16.60	17.37	13.43	15.74
5.9	27.45	36.98	36.48	44.00	45.62	37.26	41.33
5.10.1	68.31	22.09	24.83	9.95	9.81	4.52	8.59
5.10.2	45.58	38.83	15.38	16.21	15.92	9.22	14.95
5.11	6.60	19.87	20.39	26.24	27.05	17.09	23.31
5.12	55.91	17.37	8.55	9.94	9.81	4.53	8.59
5.13	55.83	38.59	18.95	9.95	9.81	4.53	8.59
5.2	-15.96	-10.14	-8.60	-6.39	-6.81	-11.37	-7.66

^a Energies relative to the energy of the starting structure **5.1**

^b Refers to the structure number in Figure 5.21

The relative Gibbs free energy (ΔG) (in kcal mol⁻¹) in water (H₂O), methanol (MeOH), acetonitrile (CH₃CN), dimethyl sulphoxide (DMSO), carbon tetrachloride (CCl₄) and dichloromethane (DCM) at 298.15 K

The 4-membered cyclic transition structure **5.15.1** followed the trend of decreased Gibbs free energy in the solvent medium. The energy of 6-membered **5.15.2** increased in acetonitrile (indicated in red). Transition structure **5.17** which is the other molecule that was modeled

with HCN and H₂O also had an increase in energy. As was discussed in the solvent modeling of mechanism 1, this increase in energy for both **5.15.2** and **5.17** is due to the amphiphilic nature of the molecule.

The local minima **5.16** and **5.18** had a similar trend where the energy increased. This increase in energy is also due to the amphiphilic nature of the molecules.

The calculated relative Gibbs free energy of solvation for each solvent is presented in Table 5.6.

Table 5.6 Calculated relative Gibbs free energy of solvation [B3LYP/6-31+G(d)] for mechanism 2

Species ^a	ΔG_{sol}						
	Gas	H ₂ O	MeOH	CH ₃ CN	DMSO	CCl ₄	DCM
5.1	0.00	0.00	0.00	0.00	0.00	0.00	0.00
5.15.1	47.91	-31.37	-29.86	-42.51	-43.14	-44.45	-42.72
5.15.2	36.01	-15.78	-17.73	8.11	-16.47	-28.76	-17.51
5.16	7.38	4.93	4.96	5.54	5.79	3.32	4.80
5.17	59.42	-33.53	9.80	8.05	8.89	-40.53	8.16
5.18	16.35	5.90	6.86	8.93	8.92	5.18	7.83
5.19							
5.6	13.34	6.36	5.98	13.28	14.68	7.38	10.79
5.7.1	230.73	-126.35	-142.44	-131.55	-127.06	-75.43	-122.29
5.7.2	76.50	-9.13	-7.50	-59.90	-59.12	-63.06	-60.76
5.9	27.45	9.53	9.03	16.55	18.17	9.81	13.88
5.10.1	68.31	-46.22	-43.48	-58.36	-58.50	-63.79	-59.72
5.10.2	45.58	-6.75	-30.20	-29.37	-29.67	-36.36	-30.64
5.11	6.60	13.28	13.79	19.65	20.45	10.49	16.71
5.12	55.91	-38.54	-47.35	-45.97	-46.10	-51.38	-47.32
5.13	55.83	-17.24	-64.43	-45.89	-46.02	-51.31	-47.24
5.2	-15.96	5.82	7.36	9.57	9.15	4.59	8.30

^a Refers to the structure number in Figure 5.21

The relative Gibbs free energy of solvation (ΔG_{sol}) (in kcal mol⁻¹) in water (H₂O), methanol (MeOH), acetonitrile (CH₃CN), dimethyl sulphoxide (DMSO), carbon tetrachloride (CCl₄) and dichloromethane (DCM) at 298.15 K

A similar trend was observed for the Gibbs free energy of solvation for mechanism 2. The energies decreased for the transition structures with the exceptions of **5.15.2** and **5.17**. The

increased energy of the local minima **5.16** and **5.18** were reversed and thus favouring solvation.

5.4 Mechanism 3 – Route 1

Mechanism 3 can potentially proceed *via* two routes. The first route is depicted in Figure 5.27. This mechanism follows the same path as that of mechanism 1 up to the stationary point **5.4**. Then instead of forming the ether, water molecules react with the carbonyl on the cage to form a 4 and 6-membered transition structure and then the stationary point **5.18**. An important point in examining this mechanism is to investigate the possibility of a linear transition state in which the *exo*-cyano group in structure **5.18** is inverted to an *endo*-cynogroup (**5.9**). The rest of the mechanism then follows the same path as that of mechanism 2.

The summary of the calculated relative thermochemical data energies for the structures depicted in mechanism 3-route 1 are presented in Table 5.7. The relative Gibbs free energy changes were used to construct the profile of the reaction in Figure 5.28. The summary of energies (Table A3.2) expressed in Hartrees and the scheme of the reaction is presented in APPENDIX 3.

Table 5.7 Summary of the relative^a thermochemical data for the conversion of the PCU dione **5.1** to the lactam **5.2** in the gas phase [B3LYP/6-31+G(d)] for mechanism 3-route 1

Species ^b	ΔE / kcal mol ⁻¹	ΔH / kcal mol ⁻¹	ΔG / kcal mol ⁻¹	ΔS /cal K ⁻¹ mol ⁻¹	LHVF/cm ⁻¹
5.1	0.00	0.00	0.00	0.00	102.67
5.3.1	121.66	120.86	124.78	-13.17	-122.18
5.3.2	38.71	27.71	48.34	-68.43	-1029.01
5.4	0.02	1.87	13.81	-40.06	107.82
5.20.1	27.42	28.70	52.54	-79.94	-1665.11
5.20.2	4.18	6.56	41.60	-117.54	-1268.92
5.18	-12.91	-7.67	16.34	-80.52	118.79
5.21					
5.9	-0.51	3.64	27.44	-79.85	93.40
5.10.1	43.11	43.80	68.30	-82.18	-2019.49
5.10.2	8.13	10.02	45.62	-119.40	-1400.69
5.11	-24.17	-19.10	6.59	-86.16	113.70
5.12	27.21	31.38	55.90	-82.23	-104.70
5.13	27.23	31.26	55.82	-82.37	-151.51
5.2	-46.93	-41.09	-15.97	-84.26	109.67

^a Energies relative to the energy of the starting structure **5.1**

^b Refers to the structure number in Figure 5.27

The energies in the gas phase (ΔE) (in kcal mol⁻¹), enthalpy (ΔH) (in kcal mol⁻¹) as well as Gibbs free energy (ΔG) (in kcal mol⁻¹) and entropy (ΔS) (cal K⁻¹ mol⁻¹) at 298.15 K and the lowest harmonic vibrational frequencies (LHVF) (in cm⁻¹) of the species in the formation of the PCU lactam from the PCU dione

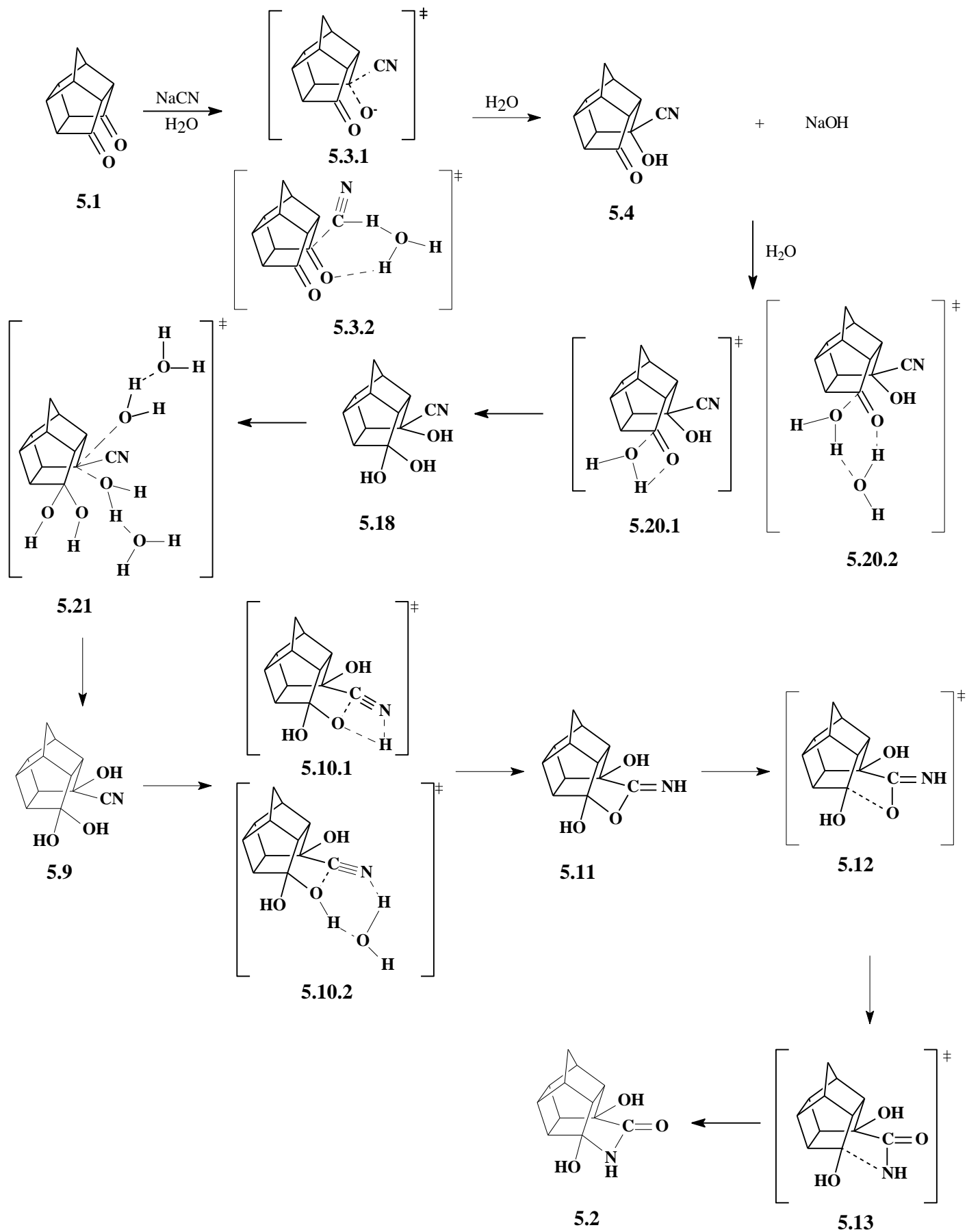


Figure 5.27 Mechanism 3-route 1 for the conversion of the PCU dione **5.1** to the lactam **5.2**

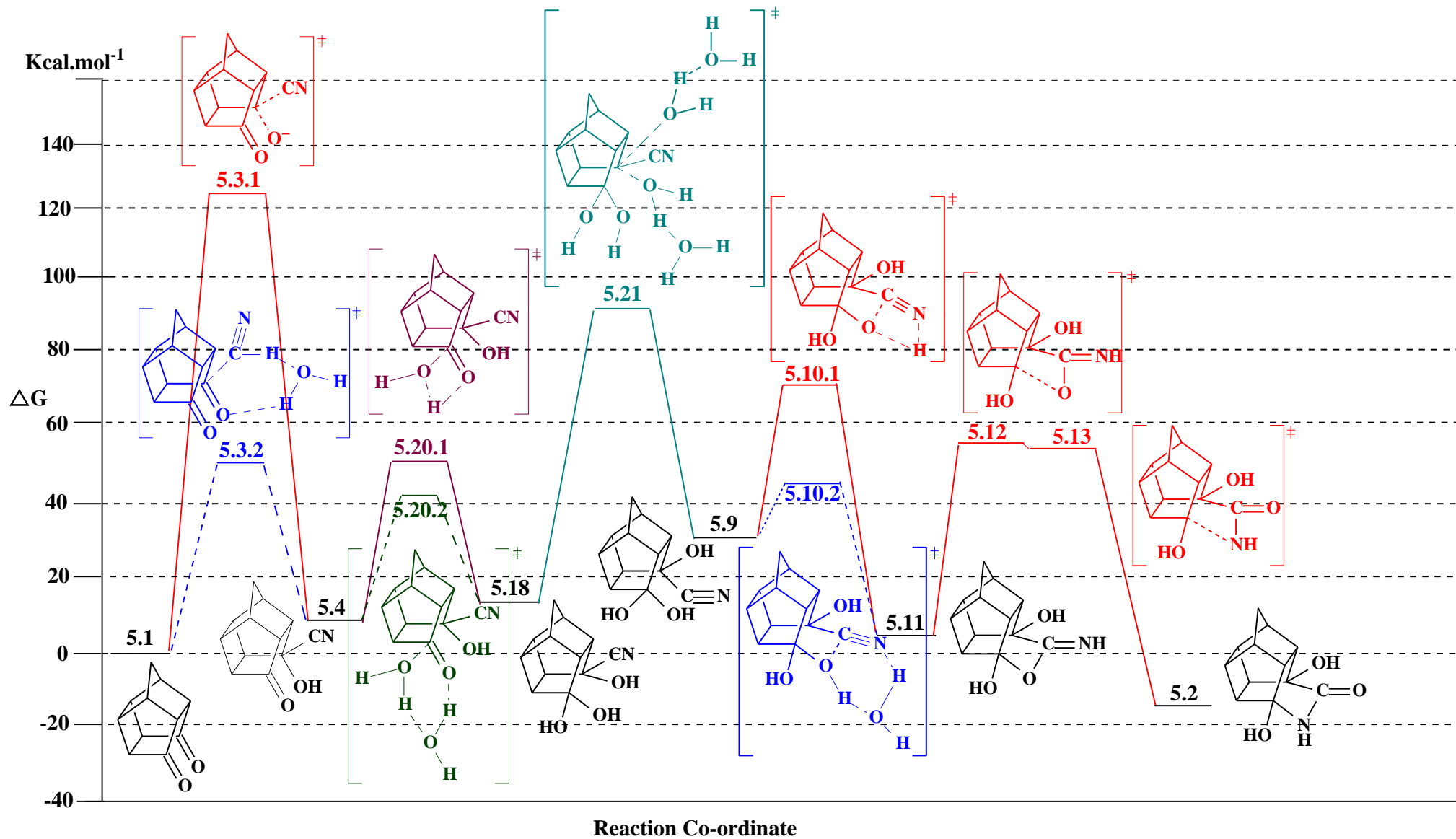
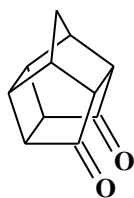


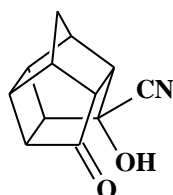
Figure 5.28 Gas phase Gibbs free energy for the mechanism proposed in Figure 5.27

Local minima on the energy profile

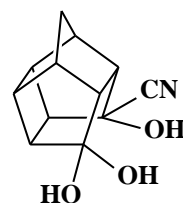
From the energy values in Table 5.7 and from their positions on the gas phase Gibbs free energy profile in Figure 5.28, it was concluded that structures **5.1**, **5.4**, **5.18**, **5.9**, **5.11**, and **5.2** are the local minima or stationary points on the energy profile of the reaction.



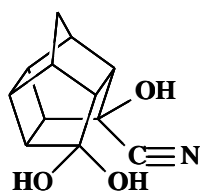
5.1



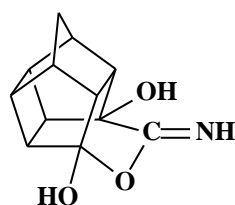
5.4



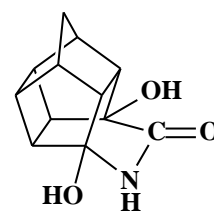
5.18



5.9



5.11

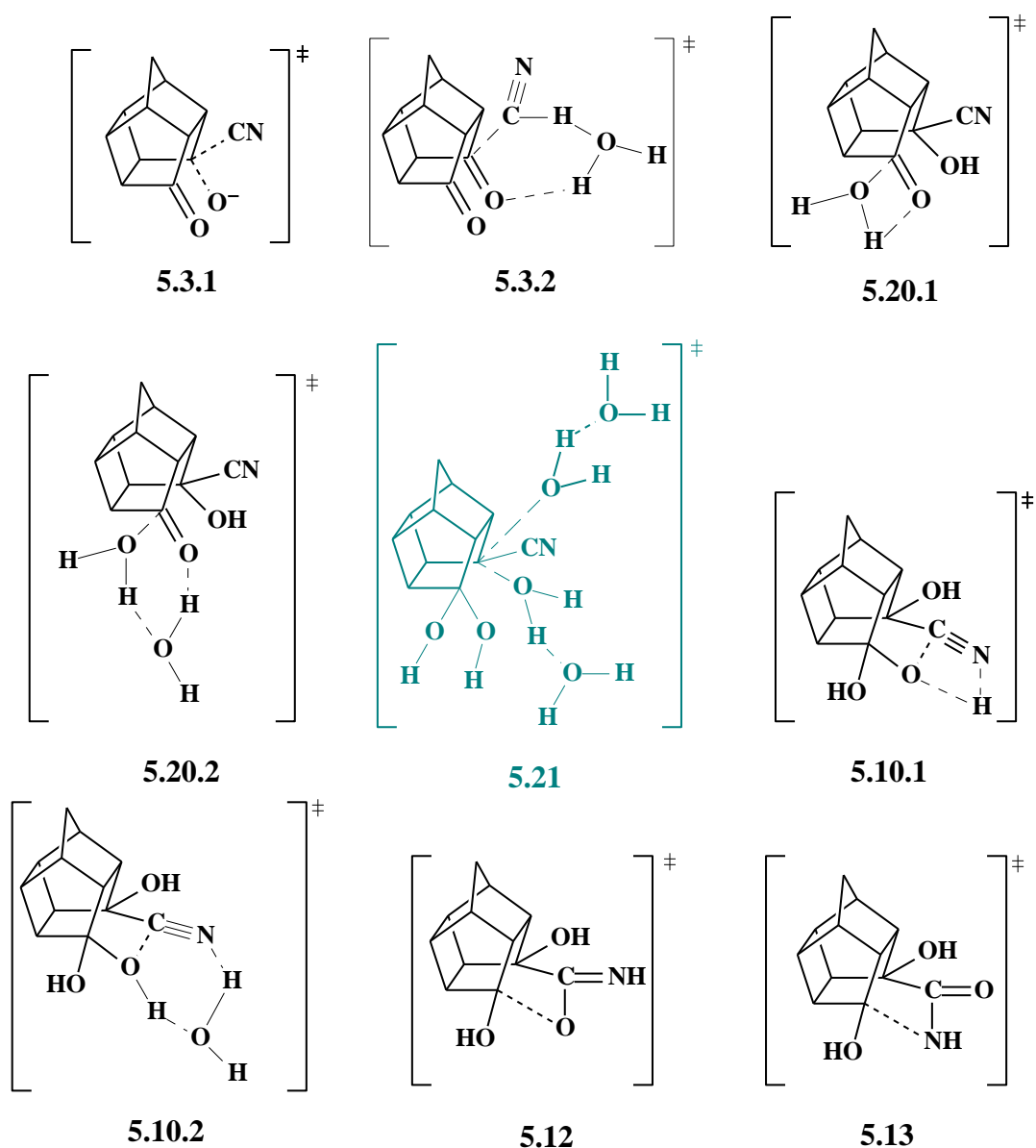


5.2

The same procedure that was followed in calculating the energies in mechanism 1 was adhered to in this mechanism as well.

The Transition States (TS)

Structures **5.3.1**, **5.3.2**, **5.20.1**, **5.20.2**, **5.21**, **5.10.1**, **5.10.2**, **5.12** and **5.13** from the mechanism in Figure 5.28 and depicted below are characterised as the transition state structures.



Here as well, the same procedure that was carried out in mechanism 1 to determine the transition state structures was followed in finding transition state structures **5.20.1** and **5.20.2**. The remaining six transition structures in this profile were discussed in mechanism 1.

Transition state structure 5.20.1

A single water molecule was added to **5.4** to form the 4-membered cyclic transition structure **5.20.1**. A scan calculation was done with O24 being moved closer to C5. The scan is graphically depicted.

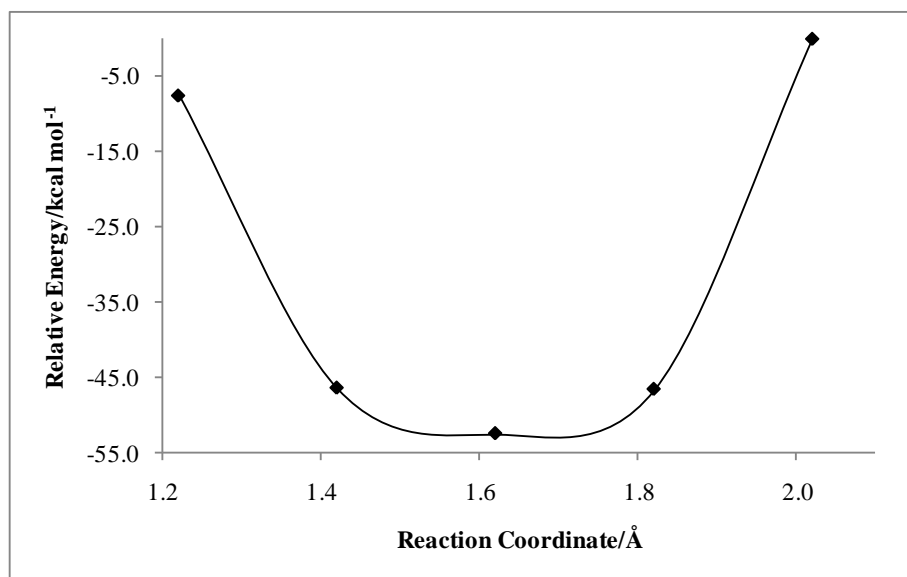
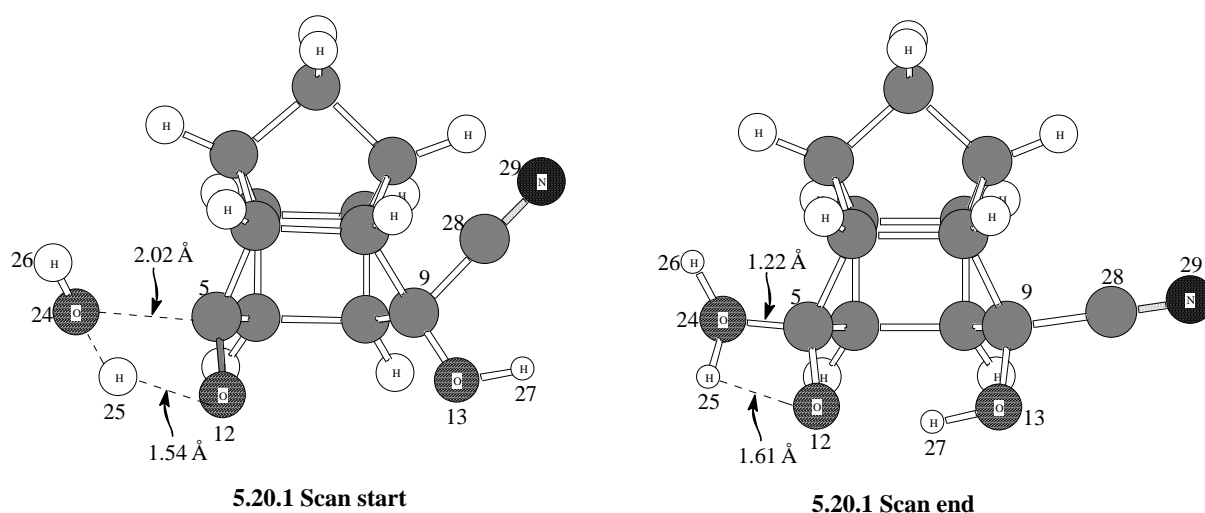


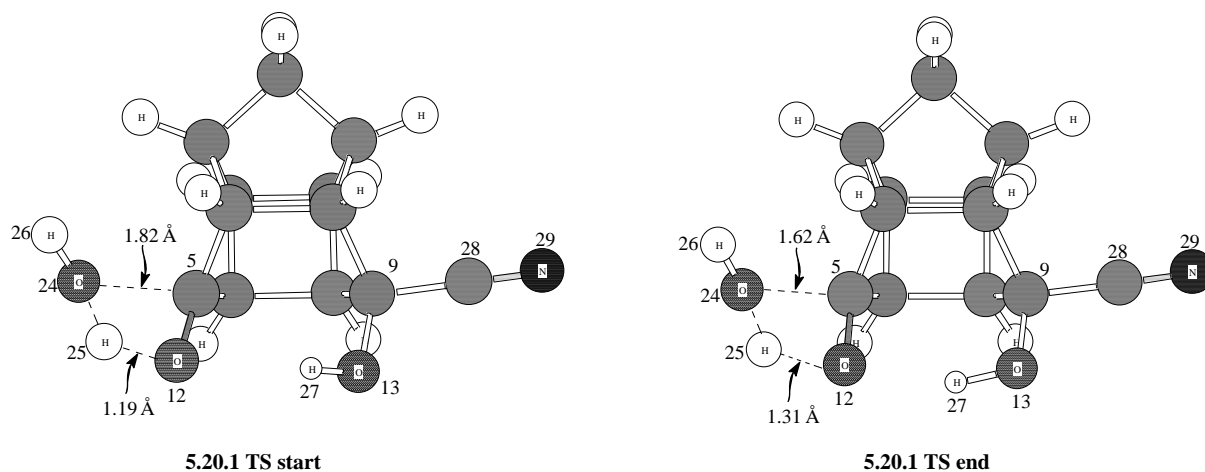
Figure 5.29 Graphical representation of energy vs reaction coordinate for structure **5.20.1**

The scan resulted in a minimum on the potential energy surface and not a maximum. The scan began with a distance of 2.02 Å between C5 and O24 and proceeded for 5 steps. The **3D Scan start** and **Scan end** structures are depicted.



As the distance between C5 and O24 decreased, H25 was not transferred to O12. Instead the distance between H25 and O12 increased. On the right of the cage, it was noted that as the C5-O24 bond formed, the C28-N29 cyano group is rotated and the hydroxyl O13-H27 is rotated from the back of the cage to the front. The structures at each reaction coordinate were examined to confirm if any had coordinates that were close to an approximate starting point for a transition state optimisation. The structure at 1.82 Å (**5.20.1 TS start**) from the scan

was used as a starting point for a transition state optimisation. The optimised 3D transition state (**5.20.1 TS end**) is shown.



The C5-O24 bond length was reduced from 1.82 Å to 1.62 Å. The O12-H25 bond length increased from 1.19 Å to 1.31 Å. This is due to the intramolecular transfer of H25 between O12 and O24.

The transition structure (**5.20.1 TS end**) was verified by performing a frequency calculation which produced one negative eigenvalue of -1665.11 cm^{-1} . There are vibrations clearly showing the bond formation of O24 with C5 and the intramolecular hydrogen transfer as mentioned above.

The graphical representation of the IRC calculation for **5.20.1** is shown.

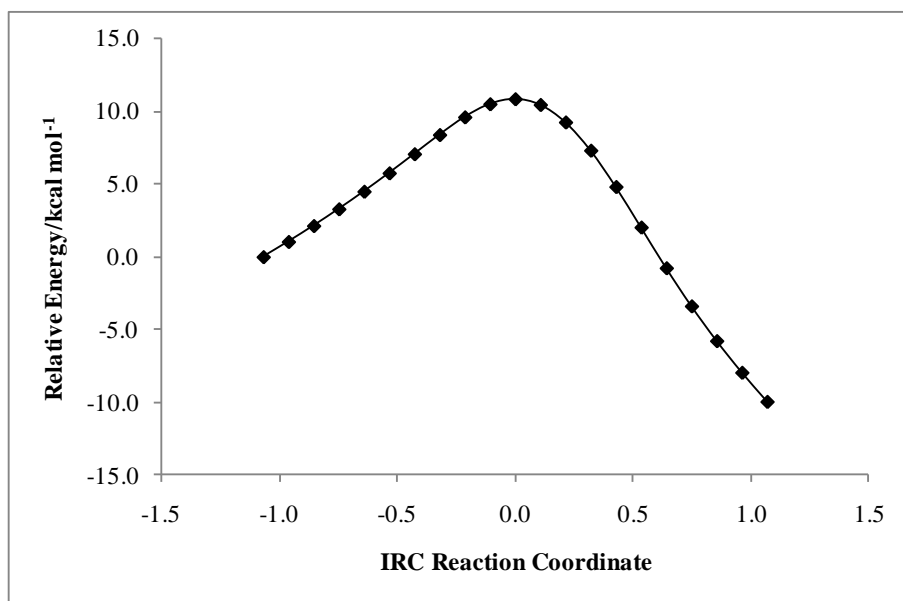
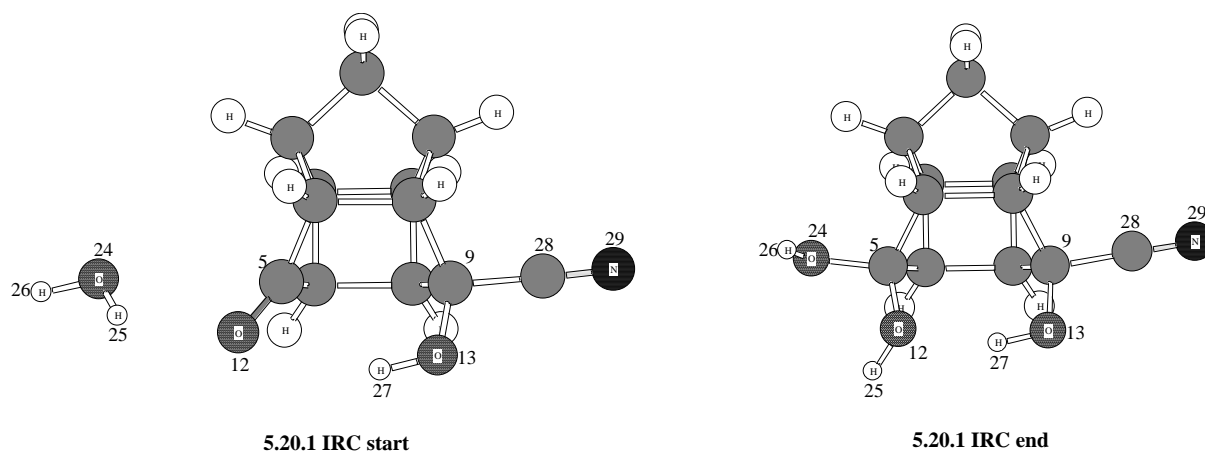


Figure 5.30 Graphical representation of the IRC reaction coordinate vs relative energy for structure 5.20.1

The IRC calculation verified the structure obtained was a transition structure since the optimised structure from step 1 (**5.20.1 IRC start**) resulted in the local minimum **5.4** with one water molecule and step 21 (**5.20.1 IRC end**) produced the stationary point **5.18**.

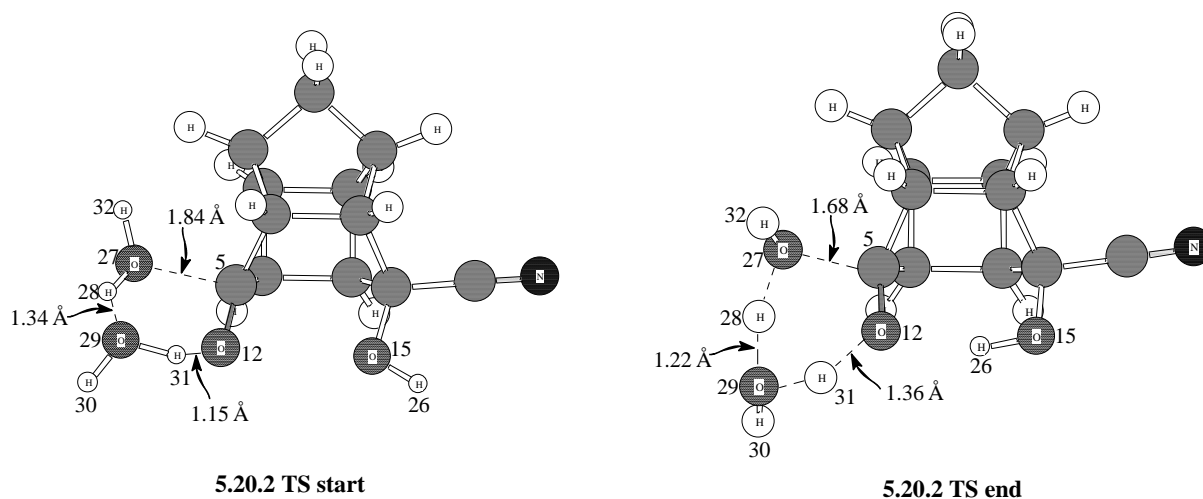


The addition of a water molecule produced a relative Gibbs free energy of 52.54 kcal mol⁻¹.

Transition state structure 5.20.2

The transition structure **5.20.2** was modeled with two water molecules thus forming a 6-membered cyclic transition structure. Local minimum structure **5.4** was again used as the starting point and two H₂O molecules were added. Since this transition structure is expected to be similar to those of **5.15.2**, the bond lengths and angles were adjusted to approximately

that of **5.15.2**. Instead of performing a scan calculation, a PM3 optimisation was done to obtain an approximate starting structure for the transition state. The following coordinates were frozen: C5-O27 at 1.84 Å, H28-O29 at 1.34 Å and O12-H31 at 1.15 Å. Once optimised, the output was submitted for an unconstrained DFT transition state optimisation. The 3D input (**5.20.2 TS start**) and output structures (**5.20.2 TS end**), of the transition state optimisation are depicted.



The frequency calculation produced a single negative eigenvalue of -1268.92 cm^{-1} and shows the intramolecular transfer of atom H28 between O27 and O29 as well as the intramolecular transfer of atom H31 between O12 and O29. As atom H28 is transferred to atom O29, the bond C5-O27 forms and H31 is transferred to O12.

The graphical representation of the IRC calculation for **5.20.2** is shown.

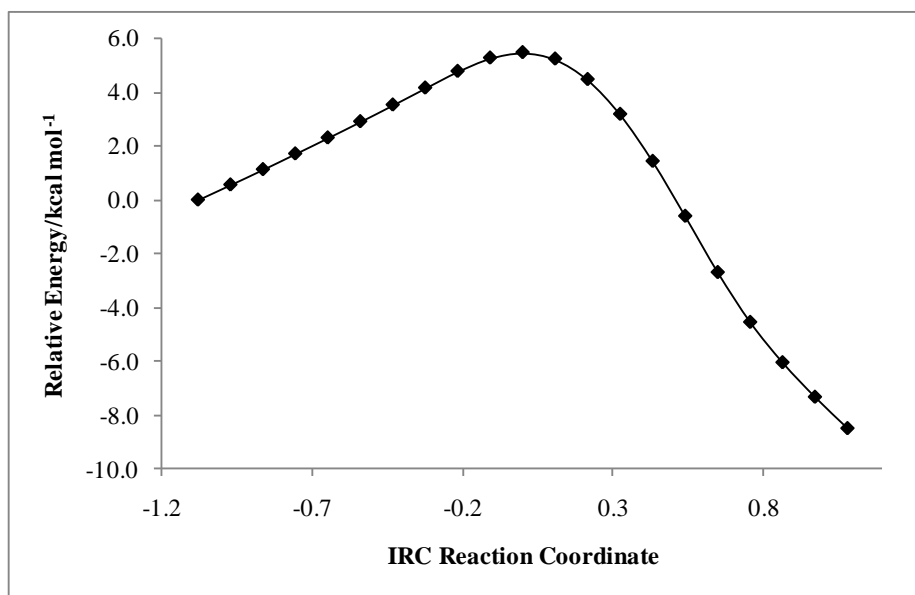
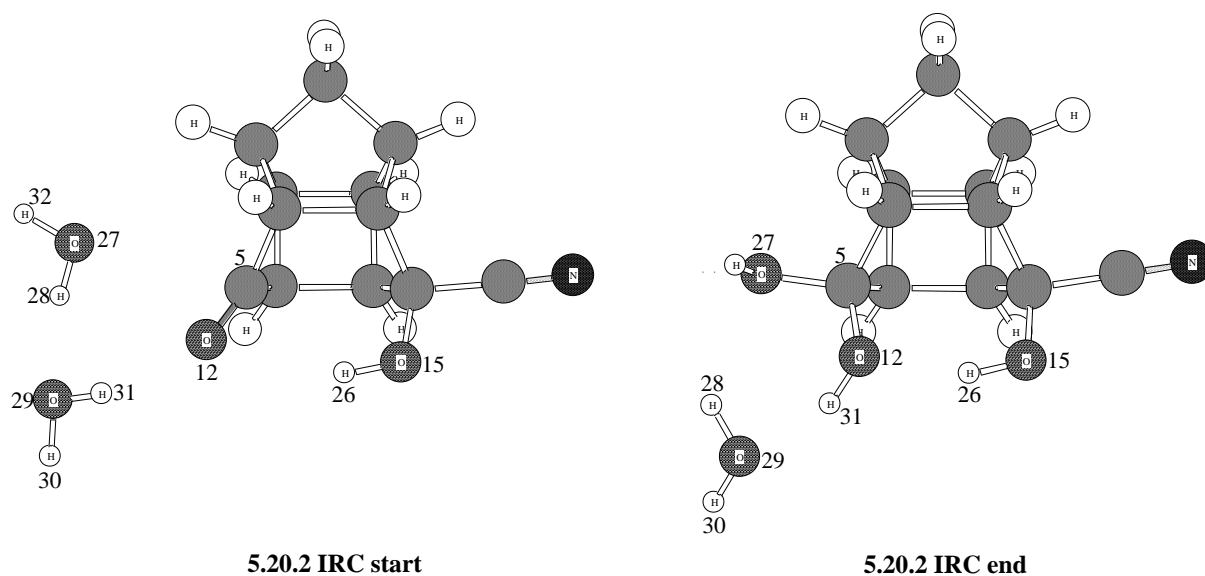


Figure 5.31 Graphical representation of the IRC reaction coordinate vs relative energy for structure 5.20.2

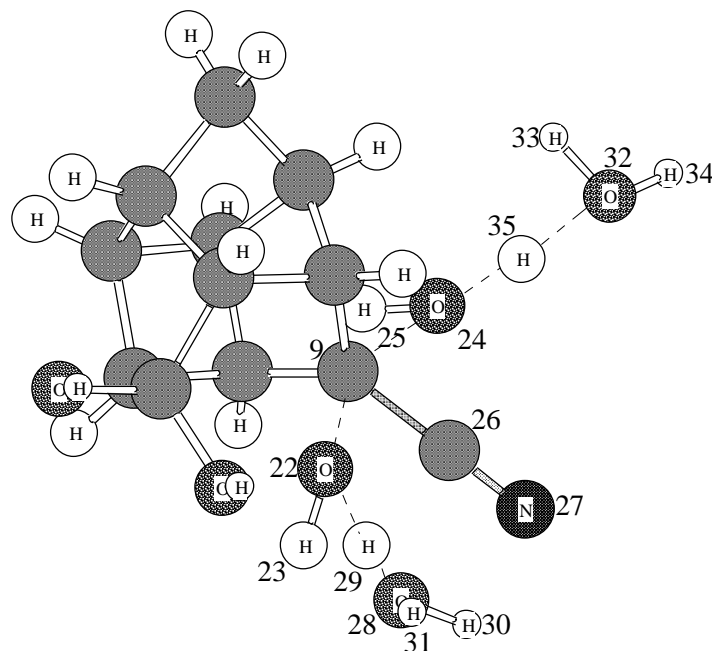
The IRC calculation verified the structure obtained was a transition structure since the optimised structure from step 1 (**5.20.2 IRC start**) resulted in the local minimum **5.4** with two water molecules and step 21 (**5.20.2 IRC end**) produced the stationary point **5.18** and a water molecule.



The addition of two water molecules decreased the overall energy by 10.94 kcal mol⁻¹.

Transition state structure 5.21

Two water molecules and an H_3O^+ ion were added to **5.18** to form the *trans*-annular or linear transition structure **5.21**. The 3D frequency output is shown.



5.21 Freq out

This calculation was attempted but a final transition structure could not be found. All the methods that were used to locate the previous transition structures described for mechanism 1 and mechanism 2 proved to be ineffective. An IRC phase calculation was attempted. The maximum on the minimum energy path was used for a frequency calculation. Although this frequency calculation did not yield favourable results since it produced many negative eigenvalues, it did show the expected movements of the atoms described below.

The hydronium ion $\text{H}_2\text{9O}_2\text{8H}_3\text{0H}_3\text{1}$ donates the $\text{H}_2\text{9}$ proton to the $\text{O}_2\text{2H}_2\text{3}$ hydroxy group at the bottom of the cage to form an H_2O molecule. This results in the $\text{C}_9\text{-O}_2\text{2}$ bond breaking.

Two H_2O molecules are added from the top of the cage. There is intramolecular hydrogen transfer of $\text{H}_3\text{5}$ between $\text{O}_2\text{4}$ and $\text{O}_3\text{2}$. Due to the $\text{C}_9\text{-O}_2\text{2}$ bond break $\text{O}_2\text{4}$ forms a bond with C_9 . The resulting structure is the local minimum **5.9**.

The *trans*-annular transition structure **5.21** is expected to have a higher energy than the 8-membered cyclic transition structure **5.19** that was presented in mechanism 2. Previous

attempts¹⁶⁸ have been made to model the linear transition structures however they have not been successful.

When comparing the three mechanisms presented thus far, it was noted that transition structures **5.20.1** (52.54 kcal mol⁻¹) and **5.20.2** (41.60 kcal mol⁻¹) have lower energies than transition structures **5.7.1** (235.48 kcal mol⁻¹) and **5.7.2** (76.50 kcal mol⁻¹) in mechanism 1. Thus the favoured reaction path would be *via* the transition structures **5.20.1** and **5.20.2**.

5.4.1 Mechanism 3-route 1 with different solvents

The calculated relative Gibbs free energy changes for each solvent are presented in Table 5.8. The summary of energies (Table A3.3 and Table A3.4) expressed in Hartrees is presented in APPENDIX 3. The energy (ΔE) (in kcal mol⁻¹), enthalpy (ΔH) (in kcal mol⁻¹) and entropy (ΔS) (cal K⁻¹ mol⁻¹) at 298.15 K in the various solvents are presented in APPENDIX 3.

Table 5.8 Calculated relative^a Gibbs free energy changes [B3LYP/6-31+G(d)] for mechanism 3-route 1

Species ^b	ΔG						
	Gas	H ₂ O	MeOH	CH ₃ CN	DMSO	CCl ₄	DCM
5.1	0.00	0.00	0.00	0.00	0.00	0.00	0.00
5.3.1	124.78	21.02	22.21	17.13	37.23	58.57	44.54
5.3.2	48.34	51.13	12.91	50.62	50.23	6.53	50.47
5.4	13.81	17.31	17.03	24.55	25.71	20.01	22.42
5.20.1	52.55	10.11	11.06	13.21	24.38	10.54	12.33
5.20.2	41.61	28.10	28.45	29.48	30.85	25.04	27.88
5.18	16.35	22.25	23.21	25.28	25.27	51.69	24.18
5.21							
5.9	27.45	36.98	36.48	44.00	45.62	37.26	41.33
5.10.1	68.31	22.09	24.83	9.95	9.81	4.52	8.59
5.10.2	45.58	38.83	15.38	16.21	15.92	9.22	14.95
5.11	6.60	19.87	20.39	26.24	27.05	17.09	23.31
5.12	55.91	17.37	8.55	9.94	9.81	4.53	8.59
5.13	55.83	38.59	18.95	9.95	9.81	4.53	8.59
5.2	-15.96	-10.14	-8.60	-6.39	-6.81	-11.37	-7.66

^a Energies relative to the energy of the starting structure **5.1**

^b Refers to the structure number in Figure 5.27

The relative Gibbs free energy (ΔG) (in kcal mol⁻¹) in water (H₂O), methanol (MeOH), acetonitrile (CH₃CN), dimethyl sulphoxide (DMSO), carbon tetrachloride (CCl₄) and dichloromethane (DCM) at 298.15 K

The 4-membered **5.20.1** and 6-membered **5.20.2** cyclic transition structures that are of particular interest in this mechanism followed the trend of the previous two mechanisms where a decrease in energy in the solvent medium was achieved.

The other transition structures and stationary points in the profile have been discussed in mechanism 1 and mechanism 2.

The calculated relative Gibbs free energy of solvation for each solvent is presented in Table 5.9.

Table 5.9 Calculated relative Gibbs free energy of solvation [B3LYP/6-31+G(d)] for mechanism 3-route 1

Species ^a	ΔG_{sol}						
	Gas	H ₂ O	MeOH	CH ₃ CN	DMSO	CCl ₄	DCM
5.1	0.00	0.00	0.00	0.00	0.00	0.00	0.00
5.3.1	124.78	-103.77	-102.57	-107.66	-87.56	-66.21	-80.24
5.3.2	48.34	2.79	-35.43	2.28	1.89	-41.81	2.13
5.4	13.81	3.50	3.21	10.73	11.90	6.20	8.61
5.20.1	52.55	-42.44	-41.49	-39.34	-28.17	-42.01	-40.21
5.20.2	41.61	-13.51	-13.16	-12.13	-10.76	-16.57	-13.73
5.18	16.35	5.90	6.86	8.93	8.92	35.34	7.83
5.21							
5.9	27.45	9.53	9.03	16.55	18.17	9.81	13.88
5.10.1	68.31	-46.22	-43.48	-58.36	-58.50	-63.79	-59.72
5.10.2	45.58	-6.75	-30.20	-29.37	-29.67	-36.36	-30.64
5.11	6.60	13.28	13.79	19.65	20.45	10.49	16.71
5.12	55.91	-38.54	-47.35	-45.97	-46.10	-51.38	-47.32
5.13	55.83	-17.24	-64.43	-45.89	-46.02	-51.31	-47.24
5.2	-15.96	5.82	7.36	9.57	9.15	4.59	8.30

^a Refers to the structure number in Figure 5.27

The relative Gibbs free energy of solvation (ΔG_{sol}) (in kcal mol⁻¹) in water (H₂O), methanol (MeOH), acetonitrile (CH₃CN), dimethyl sulphoxide (DMSO), carbon tetrachloride (CCl₄) and dichloromethane (DCM) at 298.15 K

When compared with the gas phase energies, the trend of decreased Gibbs free energy of solvation for transition structures **5.20.1** and **5.20.2** was also observed for mechanism 3-route 1.

Stationary point **5.18** was discussed in mechanism 2. Stationary points **5.11** and **5.2** were discussed in mechanism 1.

5.5 Mechanism 3 – Route 2

The second route *via* which mechanism 3 proceeds is depicted in Figure 5.32. This mechanism follows the same path as that of mechanism 1 up to the stationary point **5.4**. Then a *trans*-annular or linear transition structure **5.22**, which is similar to **5.21**, is proposed to form. This *trans*-annular transition structure should result in the formation of the stationary point **5.23**. Water molecules react with the carbonyl on the cage in **5.23** to form 4- and 6-membered transition structures that proceed to the stationary point **5.9**. The rest of the mechanism then follows the same path as that of mechanism 3-route 1.

The summary of the calculated relative thermochemical data for the structures depicted in mechanism 3-route 2 are presented in Table 5.10. The relative Gibbs free energy changes were used to construct the profile of the reaction in Figure 5.33. The summary of energies (Table A3.18) expressed in Hartrees and the scheme of the reaction is in APPENDIX 3.

Table 5.10 Summary of the relative^a thermochemical data for the conversion of the PCU dione **5.1** to the lactam **5.2** in the gas phase [B3LYP/6-31+G(d)] for mechanism 3-route 2

Species ^b	ΔE / kcal mol ⁻¹	ΔH / kcal mol ⁻¹	ΔG / kcal mol ⁻¹	ΔS /cal K ⁻¹ mol ⁻¹	LHVF/cm ⁻¹
5.1	0.00	0.00	0.00	0.00	102.67
5.3.1	121.66	120.86	124.78	-13.17	-122.18
5.3.2	25.85	27.71	48.33	-69.17	-272.28
5.4	0.02	1.87	13.81	-40.06	107.82
5.22					
5.23	1.40	3.17	15.01	-39.70	107.36
5.24.1	33.70	34.36	57.36	-77.13	-1814.19
5.24.2	10.36	11.96	46.32	-115.24	-1484.58
5.9	-0.51	3.64	27.44	-79.85	93.40
5.10.1	43.11	43.80	68.30	-82.18	-2019.49
5.10.2	8.13	10.02	45.62	-119.40	-1400.69
5.11	-24.17	-19.10	6.59	-86.16	113.70
5.12	27.21	31.38	55.90	-82.23	-104.70
5.13	27.23	31.26	55.82	-82.37	-151.51
5.2	-46.93	-41.09	-15.97	-84.26	109.67

^a Energies relative to the energy of the starting structure **5.1**

^b Refers to the structure number in Figure 5.32

The energies in the gas phase (ΔE) (in kcal mol⁻¹), enthalpy (ΔH) (in kcal mol⁻¹) as well as Gibbs free energy (ΔG) (in kcal mol⁻¹) and entropy (ΔS) (cal K⁻¹ mol⁻¹) at 298.15 K and the lowest harmonic vibrational frequencies (LHVF) (in cm⁻¹) of the species in the formation of the PCU lactam from the PCU dione

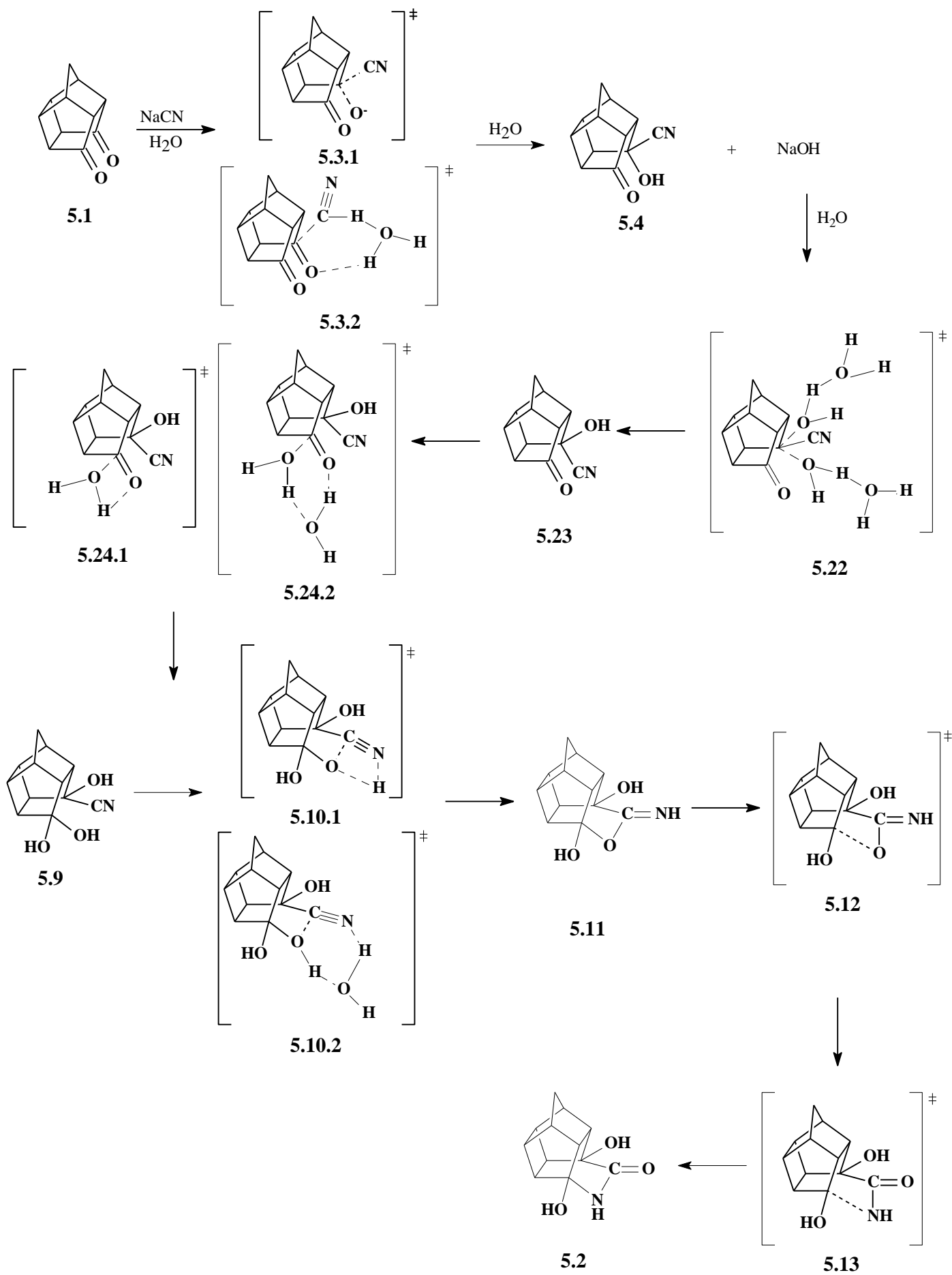


Figure 5.32 Mechanism 3-route 2 for the conversion of the PCU dione 5.1 to the lactam 5.2

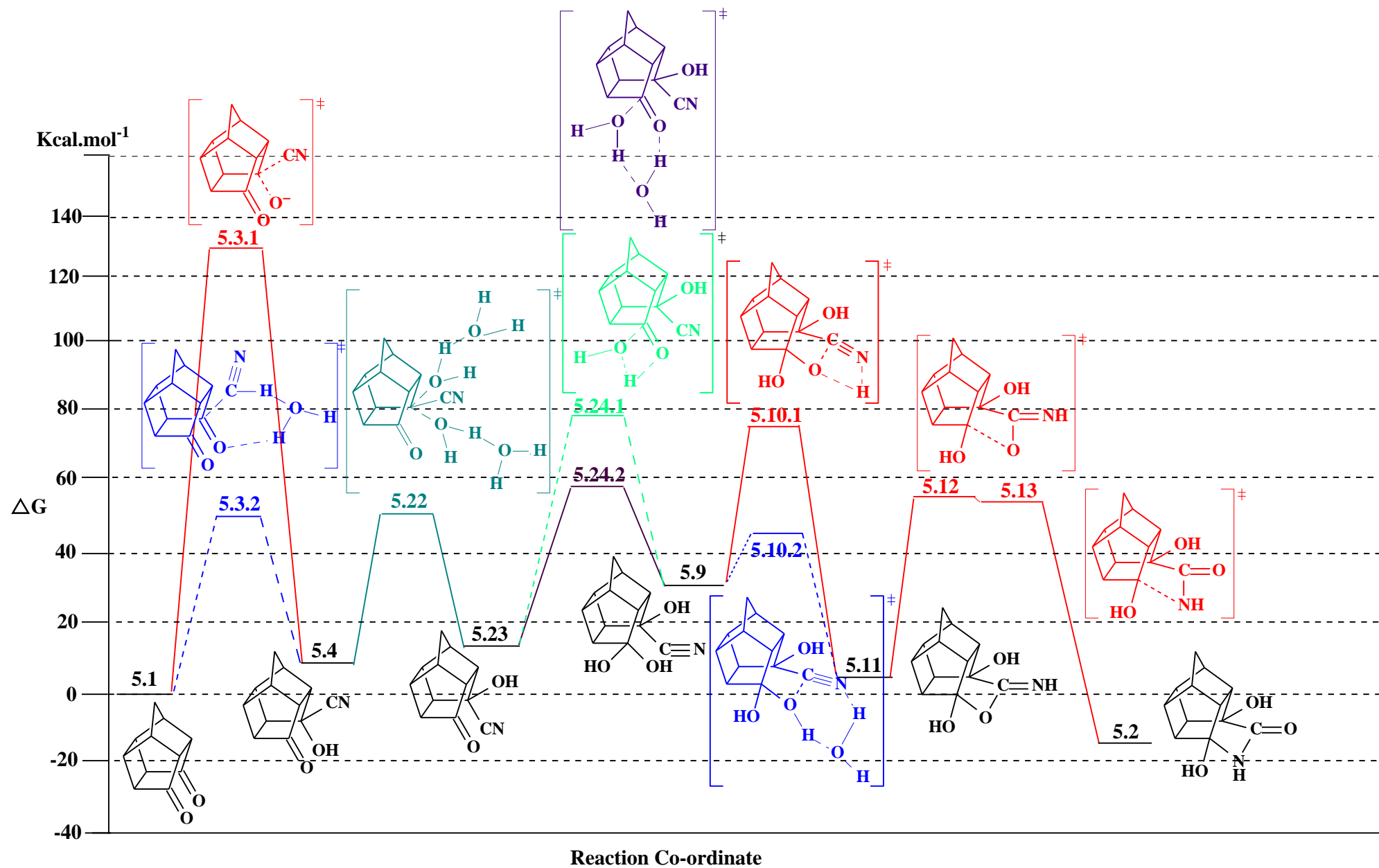
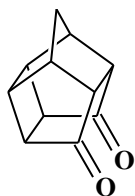


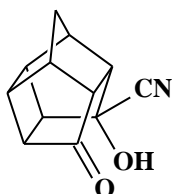
Figure 5.33 Gas phase Gibbs free energy for the mechanism proposed in Figure 5.32

Local minima on the energy profile

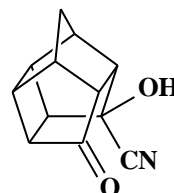
From the energy values in Table 5.10 and from their positions on the calculated Gibbs free energy profile in Figure 5.33, it was concluded that structures **5.1**, **5.4**, **5.23**, **5.9**, **5.11**, and **5.2** are the local minima or stationary points.



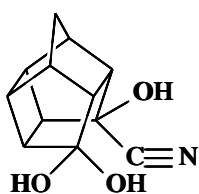
5.1



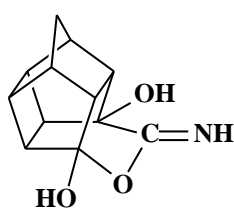
5.4



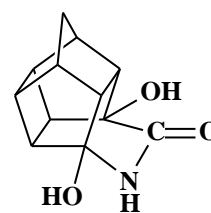
5.23



5.9



5.11

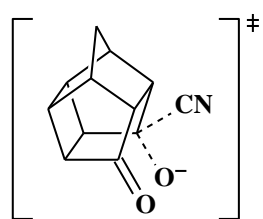


5.2

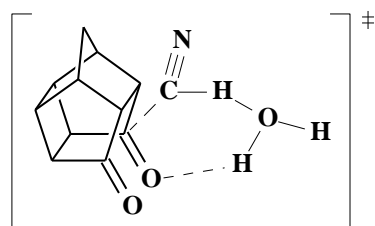
The same procedure that was employed in calculating the energies for the previous three mechanisms was followed in this mechanism as well.

The Transition States (TS)

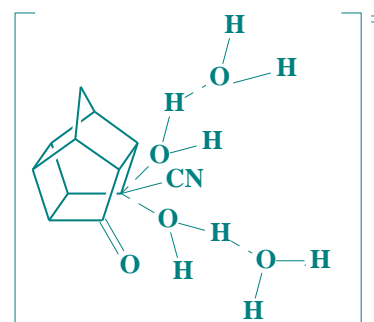
Structures **5.3.1**, **5.3.2**, **5.22**, **5.24.1**, **5.24.2**, **5.10.1**, **5.10.2**, **5.12** and **5.13** from the mechanism in Figure 5.32 and depicted below are characterised as the transition state structures.



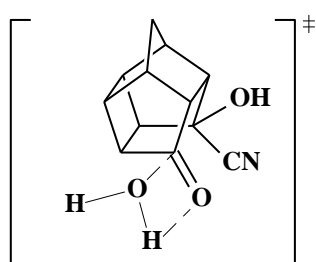
5.3.1



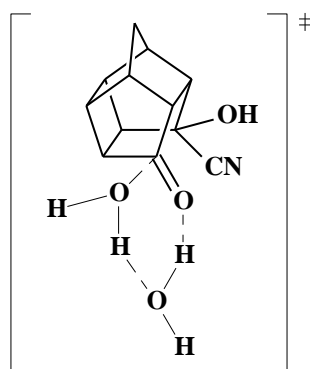
5.3.2



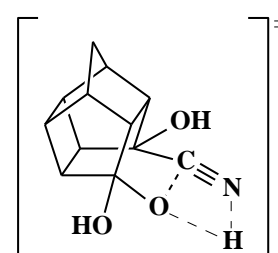
5.22



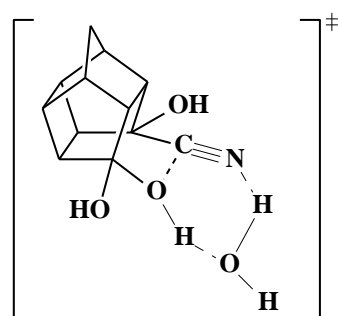
5.24.1



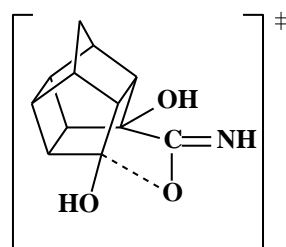
5.24.2



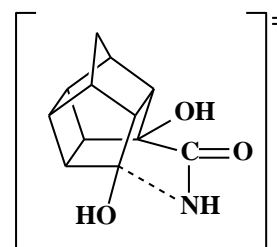
5.10.1



5.10.2



5.12

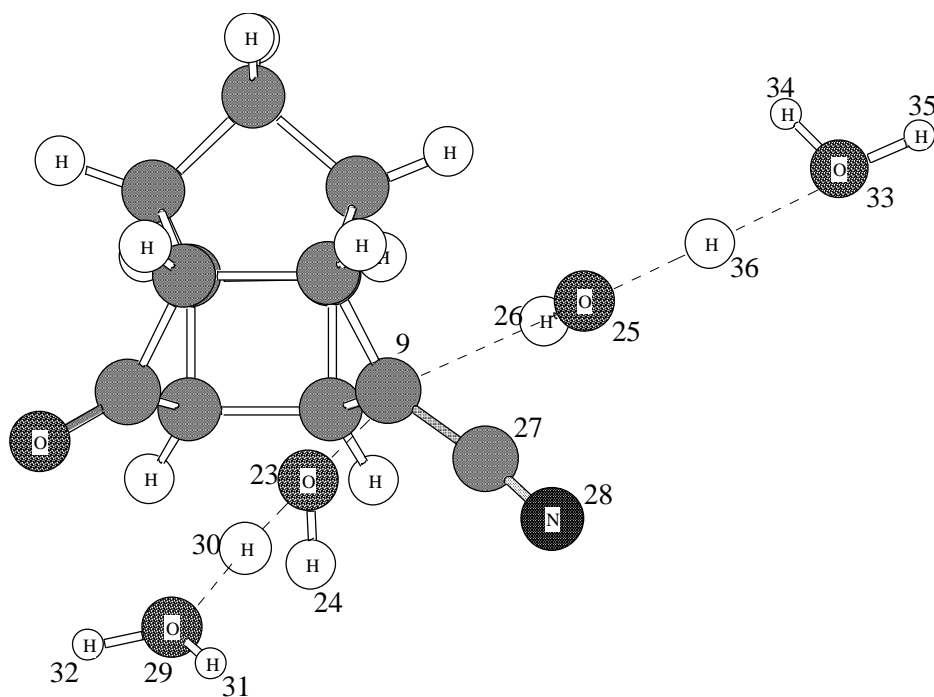


5.13

Here as well, the same procedure that was carried out in the previous mechanisms to determine the transition state structures was followed in finding transition state structures **5.22**, **5.24.1** and **5.24.2**. The remaining six transition structures in the profile have already been discussed in mechanism 1.

Transition state structure 5.22

This transition structure is similar to **5.21** which was discussed in mechanism 3-route 1. Two water molecules and an H_3O^+ ion were added to **5.4** to form the *trans*-annular transition structure **5.22**. The 3D frequency output is shown.



5.22 Freq out

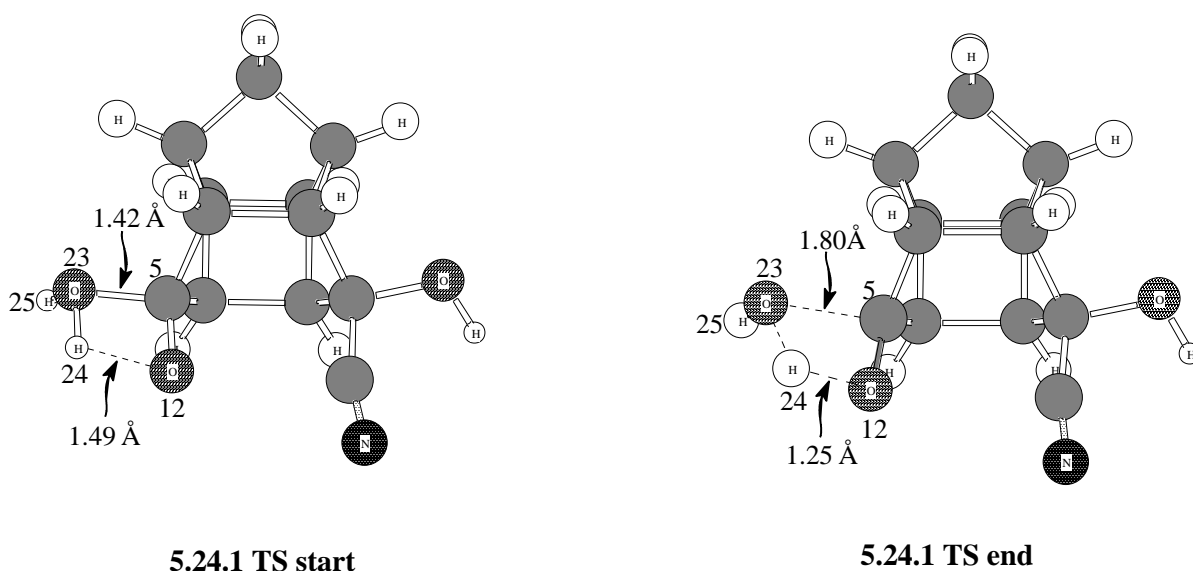
All the transition structure methods discussed were used to locate this transition structure (5.22) but all proved to be ineffective. An IRC phase calculation was performed. The maximum on the minimum energy path was used for a frequency calculation. Although this frequency calculation yielded many negative eigenvalues and could not be considered as the correct transition structure, one eigenvalue did show the expected movements of the atoms described below.

The hydronium ion H32O29H30H31 donates the H30 proton to the O23H24 hydroxy group at the bottom of the cage to form an H₂O molecule. This results in the C9-O23 bond breaking.

Two H₂O molecules are added from the top of the cage. There is intramolecular hydrogen transfer of H36 between O25 and O33. Due to the C9-O23 bond breaking O25 forms a bond with C9. The resulting structure is 5.9.

This *trans*-annular transition structure 5.22 is expected to be slightly lower in energy than the *trans*-annular transition structure 5.21 (from mechanism 3-route 1) but higher than the 8-membered cyclic transition structure 5.19 that was presented in mechanism 2.

As the distance between C5 and O23 decreased, H24 was not transferred to O12. Instead the distance between H24 and O12 increased. The structures at each reaction coordinate were examined to confirm if any of the structures had coordinates that were close to an approximate starting point for a transition state optimisation. The structure at 1.42 Å (**5.24.1 TS start**) was used as a starting point for a transition state optimisation. The optimised 3D transition state (**5.24.1 TS end**) is shown.



The C5-O23 bond length increased to 1.80 Å. The O12-H24 bond length was reduced to 1.25 Å. The transition structure (**5.24.1 TS end**) was verified by performing a frequency calculation which produced one negative eigenvalue of -1814.19 cm^{-1} . The vibrations show the bond formation of O23 with C5 and the intramolecular hydrogen transfer of H24 between O23 and O12.

The graphical representation of the IRC calculation for **5.24.1** is shown.

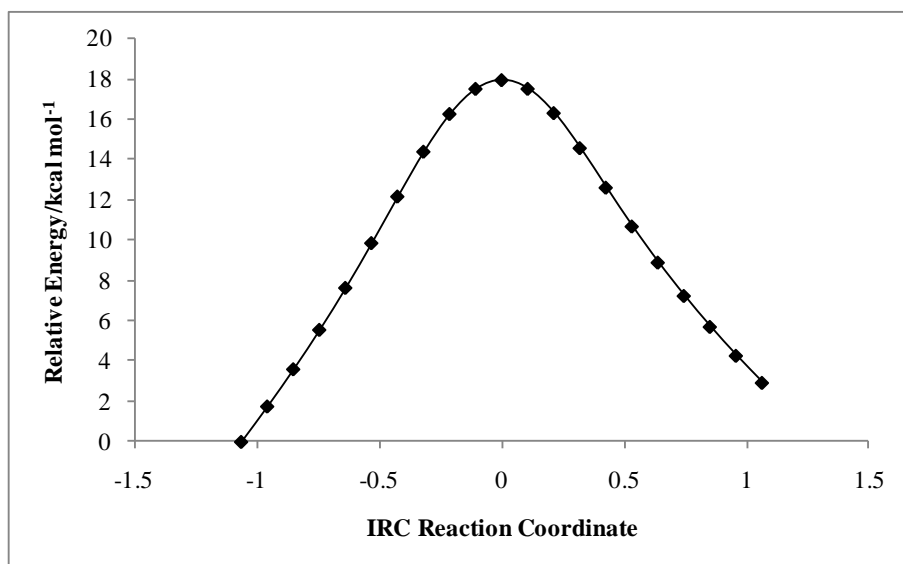
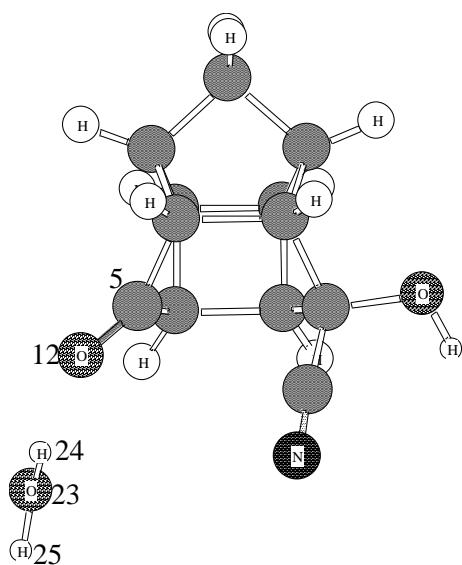
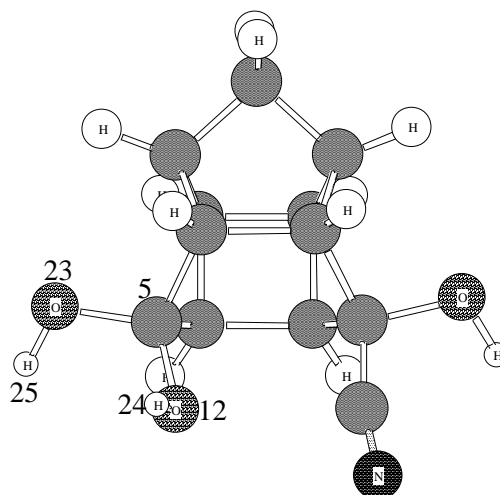


Figure 5.35 Graphical representation of the IRC reaction coordinate vs relative energy for structure 5.24.1

The IRC calculation verified the structure obtained was a transition structure since the optimised structure from step 1 (**5.24.1 IRC start**) resulted in the local minimum **5.22** with one water molecule and step 21 (**5.24.1 IRC end**) produced the stationary point **5.9**.



5.24.1 IRC start



5.24.1 IRC end

The addition of a water molecule produced a Gibbs free energy of 57.36 kcal mol⁻¹.

Transition state structure 5.24.2

The transition structure **5.24.2** was modeled with two water molecules thus forming a 6-membered cyclic transition structure. **5.4** was used as the starting point and two H₂O molecules were added. Since this transition structure involved the similar movement of atoms as that of **5.20.2**, the bond lengths and angles were adjusted to approximately those of **5.20.2**. An unconstrained scan calculation was done to obtain an approximate starting structure for the transition state. The scan is graphically depicted.

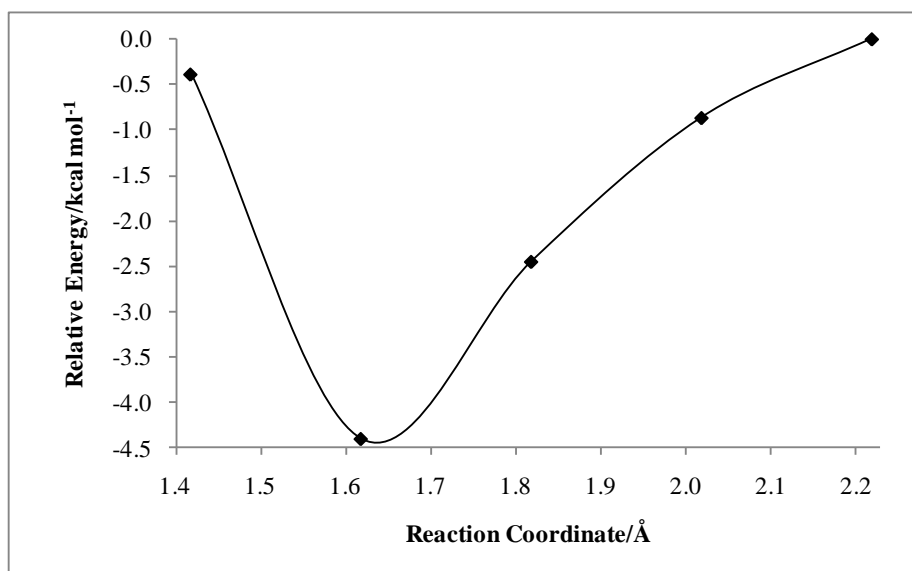
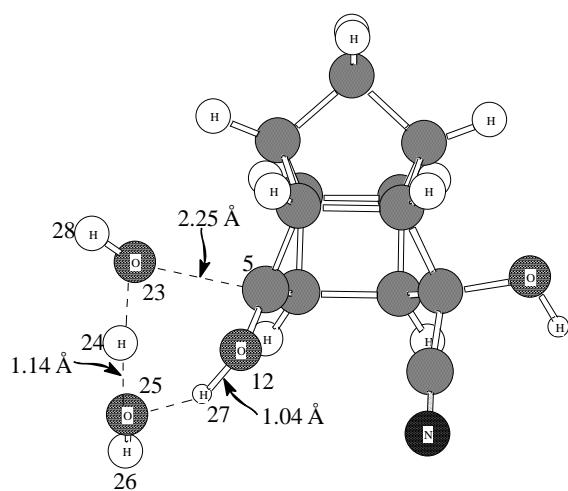
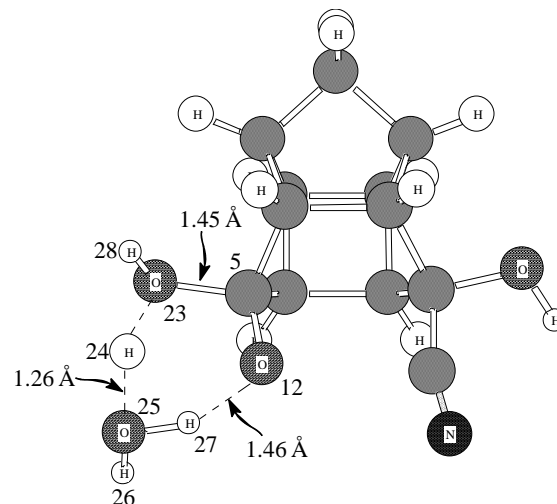


Figure 5.36 Graphical representation of energy vs reaction coordinate for structure **5.23.2**

This scan as well resulted in a minimum on the potential energy surface and not a maximum. The scan was started with a distance of 2.25 Å between C5 and O23 and proceeded for 5 steps. The 3D input (**5.24.2 Scan start**) and output structure (**5.24.2 Scan end**), of the scan calculation is depicted.

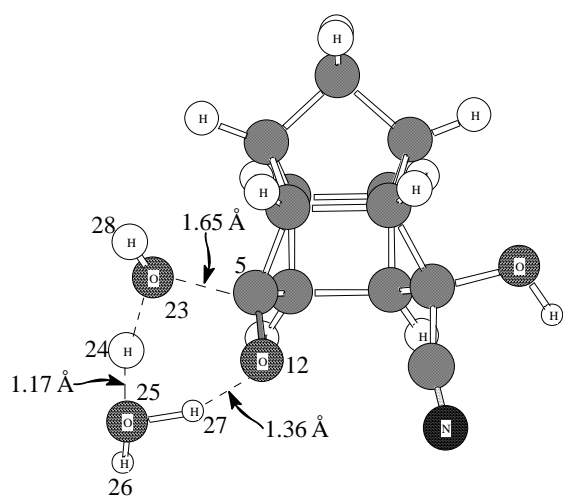


5.24.2 Scan start

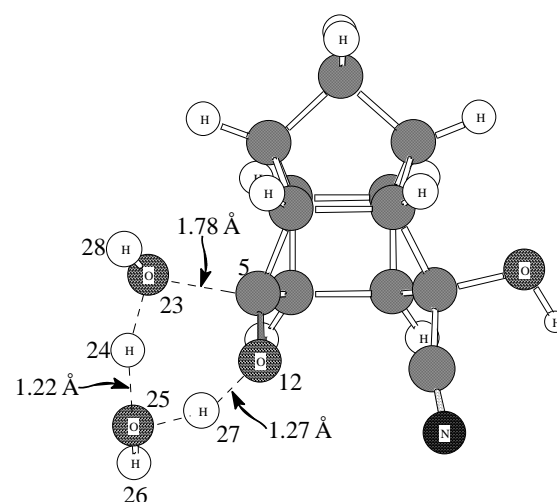


5.24.2 Scan end

As the distance between C5 and O23 decreased, H24 was not transferred to O25. Instead the distance between H24 and O25 increased. The structures at each reaction coordinate were examined to confirm if any of the structures had coordinates that were close to an approximate starting point for a transition state optimisation. The structure at 1.65 Å (**5.24.2 TS start**) was used as a starting point for a transition state optimisation. The optimised 3D transition state (**5.24.2 TS end**) is shown.



5.24.2 TS start



5.24.2 TS end

The frequency calculation produced a single negative eigenvalue of -1484.58 cm^{-1} and shows the intramolecular transfer of atom H24 between O23 and O25 as well as the intramolecular transfer of atom H27 between O12 and O25. As atom H24 is transferred to atom O25, the bond C5-O23 forms and H27 is transferred to O12.

The graphical representation of the IRC calculation for **5.24.2** is shown.

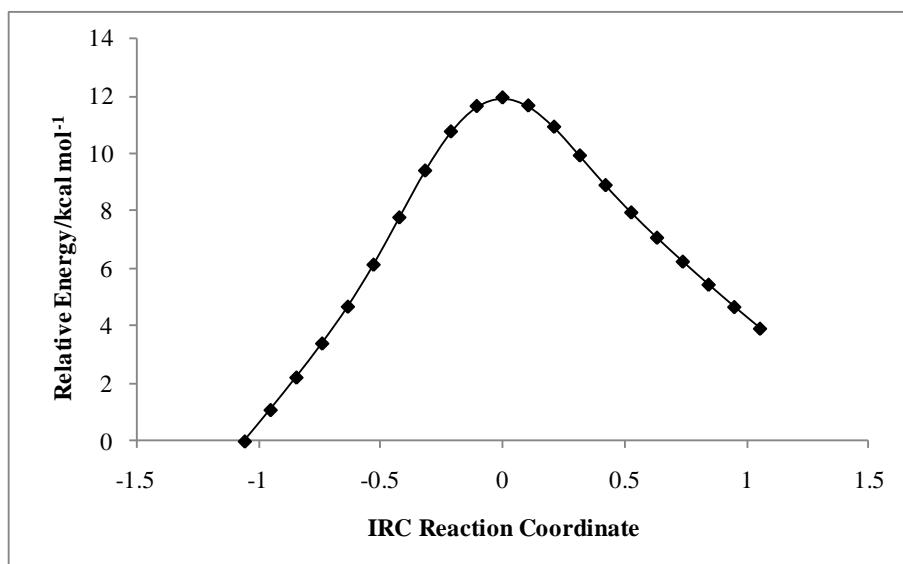
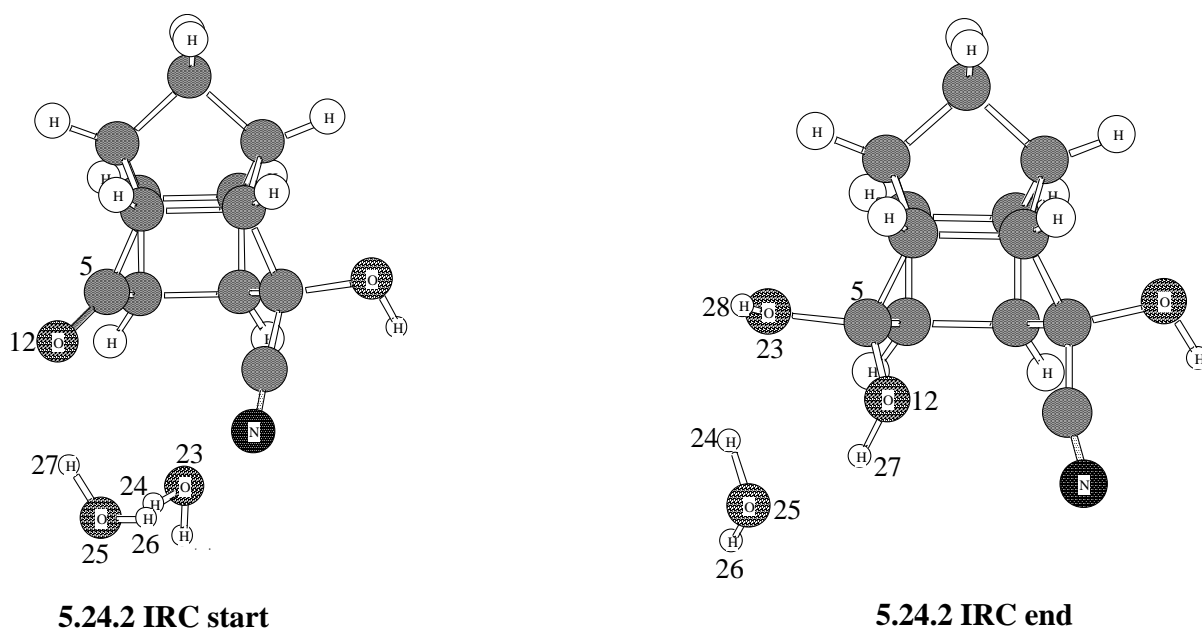


Figure 5.37 Graphical representation of the IRC reaction coordinate vs relative energy for structure 5.24.2

The IRC calculation verified the structure obtained was a transition structure since the optimised structure from step 1 (**5.24.2 IRC start**) resulted in the local minimum **5.4** with two water molecules and step 21 (**5.24.2 IRC end**) produced the stationary point **5.22** and a water molecule.



The addition of two water molecules decreased the overall energy by 11.04 kcal mol⁻¹.

By comparing the four mechanisms presented thus far, it is noted that transition structures **5.24.1** (57.36 kcal mol⁻¹) and **5.24.2** (46.32 kcal mol⁻¹) have higher energies than transition

structures **5.20.1** (52.54 kcal mol⁻¹) and **5.20.2** (41.60 kcal mol⁻¹) from mechanism 3-route 1. Thus the favoured reaction path would be *via* the transition structures **5.20.1** and **5.20.2**.

5.5.1 Mechanism 3route 2 with different solvents

The calculated relative Gibbs free energy changes for each solvent are presented in Table 5.11. The summary of energies (Table A3.19 and Table A3.20) expressed in Hartrees is presented in APPENDIX 3. The energy (ΔE) (in kcal mol⁻¹), enthalpy (ΔH) (in kcal mol⁻¹) and entropy (ΔS) (cal K⁻¹ mol⁻¹) at 298.15 K in the various solvents are presented in APPENDIX 3

Table 5.11 Calculated relative^a Gibbs free energy changes [B3LYP/6-31+G(d)] for mechanism 3-route 2

Species ^b	ΔG						
	Gas	H ₂ O	MeOH	CH ₃ CN	DMSO	CCl ₄	DCM
5.1	0.00	0.00	0.00	0.00	0.00	0.00	0.00
5.3.1	124.78	21.02	22.21	17.13	37.23	58.57	44.54
5.3.2	48.34	51.13	12.91	50.62	50.23	6.53	50.47
5.4	13.81	17.31	17.03	24.55	25.71	20.01	22.42
5.22							
5.23	15.01	17.96	17.67	25.25	26.40	21.21	23.35
5.24.1	57.36	11.15	12.09	14.01	14.17	12.44	36.47
5.24.2	46.32	30.75	31.04	34.53	34.65	15.70	33.23
5.9	27.45	36.98	36.48	44.00	45.62	37.26	41.33
5.10.1	68.31	22.09	24.83	9.95	9.81	4.52	8.59
5.10.2	45.58	38.83	15.38	16.21	15.92	9.22	14.95
5.11	6.60	19.87	20.39	26.24	27.05	17.09	23.31
5.12	55.91	17.37	8.55	9.94	9.81	4.53	8.59
5.13	55.83	38.59	18.95	9.95	9.81	4.53	8.59
5.2	-15.96	-10.14	-8.60	-6.39	-6.81	-11.37	-7.66

^a Energies relative to the energy of the starting structure **5.1**

^b Refers to the structure number in Figure 5.32

The relative Gibbs free energy (ΔG) (in kcal mol⁻¹) in water (H₂O), methanol (MeOH), acetonitrile (CH₃CN), dimethyl sulphoxide (DMSO), carbon tetrachloride (CCl₄) and dichloromethane (DCM) at 298.15 K

The transition structures that are of interest in this mechanism are the 4-membered **5.24.1** and 6-membered **5.24.2** cyclic transition structures that followed the trend of decreased Gibbs free energy in the solvent medium.

As per the trend that has been observed thus far the local minimum **5.23** increased in energy due to the amphiphilic nature of the molecule.

The calculated relative Gibbs free energy of solvation for each solvent is presented in Table 5.12.

Table 5.12 Calculated relative Gibbs free energy of solvation [B3LYP/6-31+G(d)] for mechanism 3-route 2

Species ^a	ΔG_{sol}						
	Gas	H ₂ O	MeOH	CH ₃ CN	DMSO	CCl ₄	DCM
5.1	0.00	0.00	0.00	0.00	0.00	0.00	0.00
5.3.1	124.78	-103.77	-102.57	-107.66	-87.56	-66.21	-80.24
5.3.2	48.34	2.79	-35.43	2.28	1.89	-41.81	2.13
5.4	13.81	3.50	3.21	10.73	11.90	6.20	8.61
5.22							
5.23	15.01	2.95	2.66	10.24	11.39	6.20	8.34
5.24.1	57.36	-46.21	-45.27	-43.35	-43.19	-44.92	-20.89
5.24.2	46.32	-15.57	-15.28	-11.79	-11.67	-30.61	-13.09
5.9	27.45	9.53	9.03	16.55	18.17	9.81	13.88
5.10.1	68.31	-46.22	-43.48	-58.36	-58.50	-63.79	-59.72
5.10.2	45.58	-6.75	-30.20	-29.37	-29.67	-36.36	-30.64
5.11	6.60	13.28	13.79	19.65	20.45	10.49	16.71
5.12	55.91	-38.54	-47.35	-45.97	-46.10	-51.38	-47.32
5.13	55.83	-17.24	-64.43	-45.89	-46.02	-51.31	-47.24
5.2	-15.96	5.82	7.36	9.57	9.15	4.59	8.30

^a Refers to the structure number in Figure 5.32

The relative Gibbs free energy of solvation (ΔG_{sol}) (in kcal mol⁻¹) in water (H₂O), methanol (MeOH), acetonitrile (CH₃CN), dimethyl sulphoxide (DMSO), carbon tetrachloride (CCl₄) and dichloromethane (DCM) at 298.15 K

The transition structures **5.24.1** and **5.24.2** as well as the local minimum **5.23** followed the trend of a decrease in energy as seen for the other mechanisms.

CHAPTER 6

CONCLUSION

The first aim of this study was an attempt to get an enhanced understanding of the conversion of the dione **1** to the lactam **2**. A total of four variations of possible mechanisms were proposed for this one-pot reaction. The energies of all 10 local minimum structures were successfully calculated. From the original 20 transition state structures presented in Chapter 5, 17 were successfully modelled in both the gas phase and six solvents. The transition state structures modelled were in the ionic form, as well as 4- and 6-membered cyclic structures. The linear and 8-membered cyclic transition state structures could not be obtained.

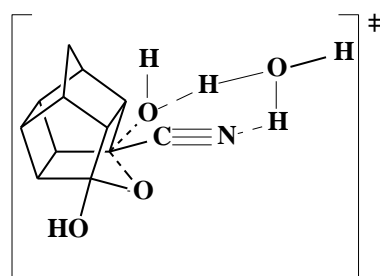
It was observed that high energies for some transition state structures were obtained in the gas phase for the four mechanisms studied. In mechanism 1, the two structures **5.3.1** and **5.7.1** which are both ionic species resulted in abnormally high energies. These high energies are the result of calculating the energy of an ionic species (-O^-) in the gas phase. In reality, the ionic species does not exist in aqueous solution since it will upon formation immediately abstract a proton from the solvent to form an alcohol (OH).

This prompted the inclusion of a water and HCN molecule to **5.3.1** and a single water molecule to **5.7.1** to form cyclic non-ionic transition structures. It should be acknowledged that this model is an over simplification of reality, but it has nevertheless provided valuable insight into the overall mechanism of the reaction.

This study has shown that the energy of an ionic transition structure decreased by approximately 76 kcal mol^{-1} for **5.3.1** and by approximately $154 \text{ kcal mol}^{-1}$ for the **5.7.1** transition structure, when explicit solvent molecules were involved in the calculation. Although this is generally accepted in organic textbooks, the theoretical results obtained in this investigation quantify the energy differences and reconfirm our basic knowledge in this regard. Since one solvent molecule lowers the energy of an ionic transition structure by as much as $159 \text{ kcal mol}^{-1}$, then the energy of the profile should also be considerably lowered by modelling the reaction in various implicit solvent systems. This was successfully achieved in all four mechanisms.

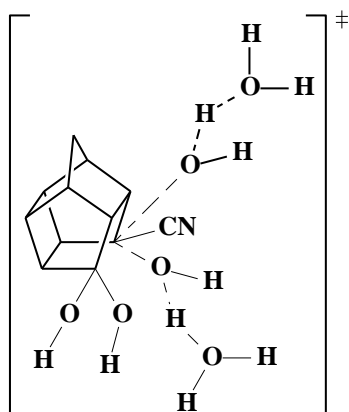
The difference of energy for the various transition structures, in the gas phase, in the four mechanisms was compared. In mechanism 1 and mechanism 2 it was observed that the

transition structure **5.7.2** has the highest Gibbs free energy of $76.50 \text{ kcal mol}^{-1}$, which makes it the rate determining step for each proposed mechanism.

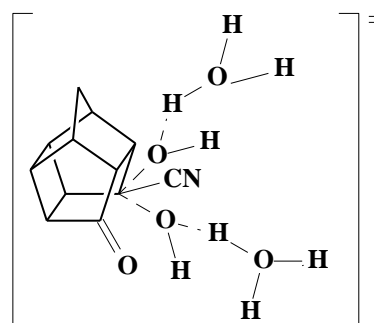


5.7.2

Modeling of the preliminary linear transition state structures of **5.21** (mechanism 3-route 1) and **5.22** (mechanism 3-route 2) was unsuccessful since these two transition structures exhibited more than one negative eigenvalue. The main reason for this is the fact that it is very difficult with the current available quantum mechanical software (and current computer hardware) to model the exact nature of proton transfer from solvent to substrate and *vice versa*. These results can therefore not be used for any definite conclusions.



5.21



5.22

However, one of these negative eigenvalues represents the expected movement of atoms for the specific transition state. In future, it is likely that a quantum chemical molecular dynamics simulation (QM/MD) of the substrate in a solvent box will be able to find the evading linear transition states.

Arising from this, it is concluded that transition state structure **5.7.2** is the rate determining step and the transition state for this one-pot reaction. This compound is also the only stable intermediate that could be isolated by experiment.³⁴ The theoretical results therefore seem to be in line with experiment.

The rate-determining step, in reality, should involve an activation energy of slightly lower than 15 kcal mol^{-1} since the real experimental reaction occurs at $10 \text{ }^\circ\text{C}$ and lower; molecules at room temperature have enough inherent energy to overcome processes up to about 15 kcal mol^{-1} . The computational model used in this study produced an activation energy of $43.77 \text{ kcal mol}^{-1}$ and this is still considerably removed from reality since the reaction should not occur at room temperature if the energy barrier of the rate-determining step (**5.7.2**) is much higher than 15 kcal mol^{-1} .

The second aim of this study was to predict the path of the one-pot reaction of the dione to the cage lactam. It is impossible to state exactly which transition structures are definitely part of this reaction since some of the transition structures cannot be experimentally isolated. It may be possible that the transition structures modeled in this study do form some of the intermediates in the reaction since the Gibbs free energy values indicate this possibility. However, the profile with the lowest rate determining step will ultimately be the preferred reaction pathway. When all four mechanisms are compared, the energies favour mechanism 1, thus making it the most likely reaction pathway.

The experimentally proposed conversions presented in Scheme 1 and Scheme 2 provided a strong basis in proposing the four mechanisms that have been discussed in this study. This theoretical study presents several transition structures and intermediates which have not been considered by the experimentalists.³⁴ Furthermore the computational calculations have shown that the proposed schemes relate well to the experimental results.

APPENDIX 1

Thermochemical data for 5.1 extracted from the frequency output file

Zero-point correction= (Hartree/Particle)				0.187781
Thermal correction to Energy=				0.195781
Thermal correction to Enthalpy=				0.196726
Thermal correction to Gibbs Free Energy=				0.154704
Sum of electronic and zero-point Energies=				-575.420533
Sum of electronic and thermal Energies=				-575.412532
Sum of electronic and thermal Enthalpies=				-575.411588
Sum of electronic and thermal Free Energies=				-575.453610
	E (Thermal)	CV	S	
	KCal/Mol	Cal/Mol-Kelvin	Cal/Mol-Kelvin	
Total	122.855	35.592	88.442	

Energy for 5.1 extracted from the frequency output file

SCF Done: E(RB3LYP) = -575.608313791

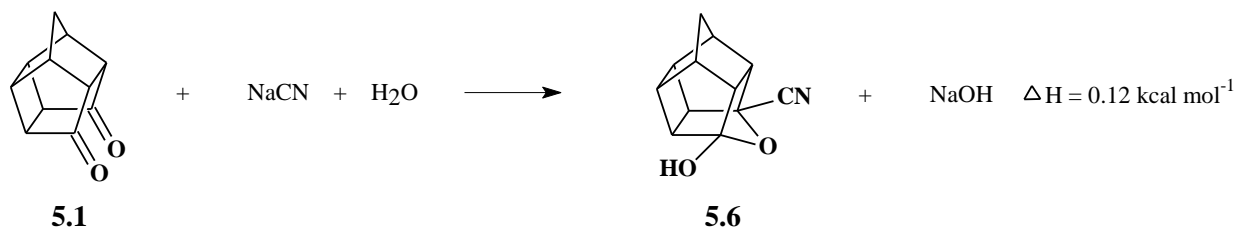
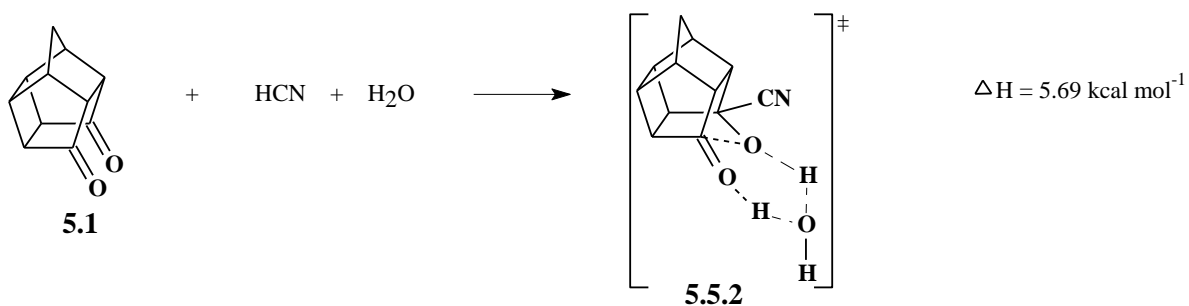
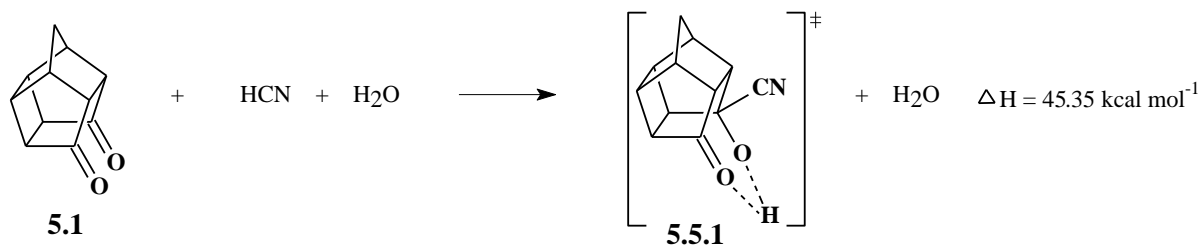
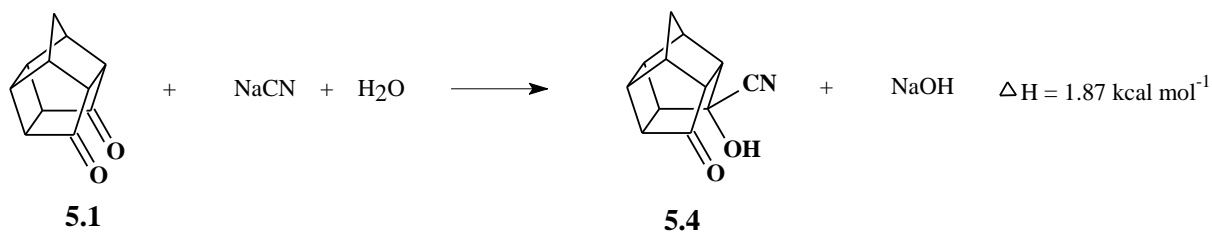
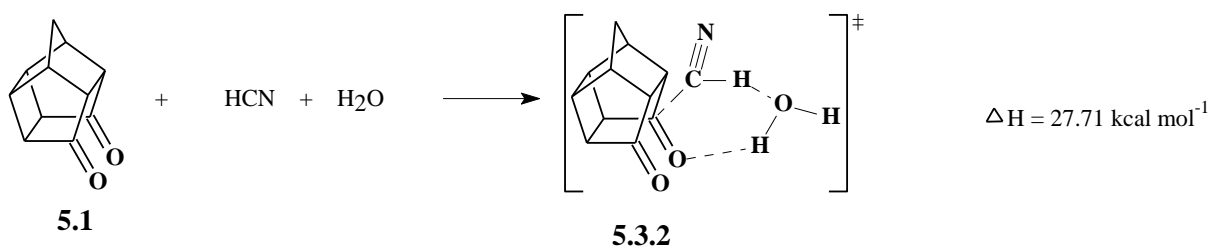
Table A1.1 Summary of energies for mechanism 1

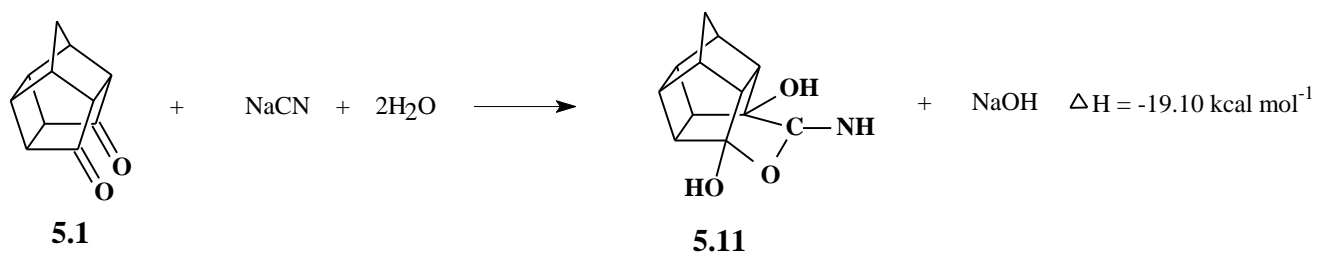
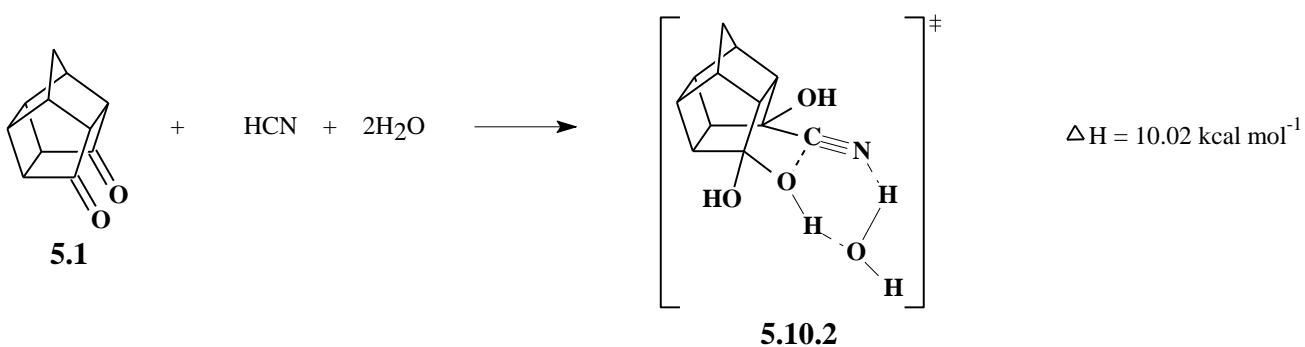
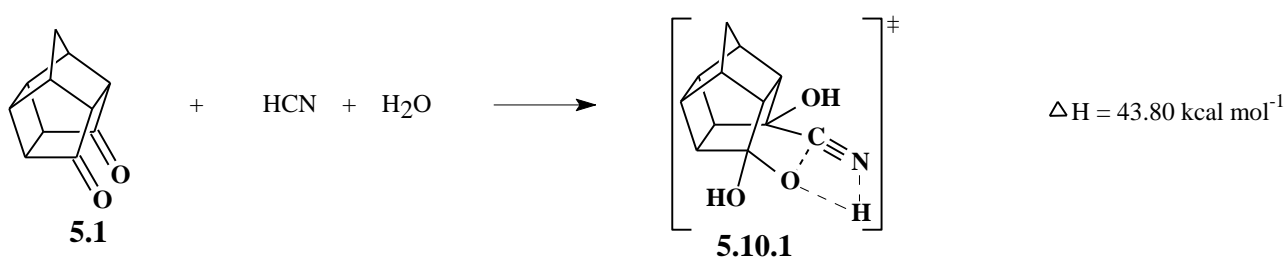
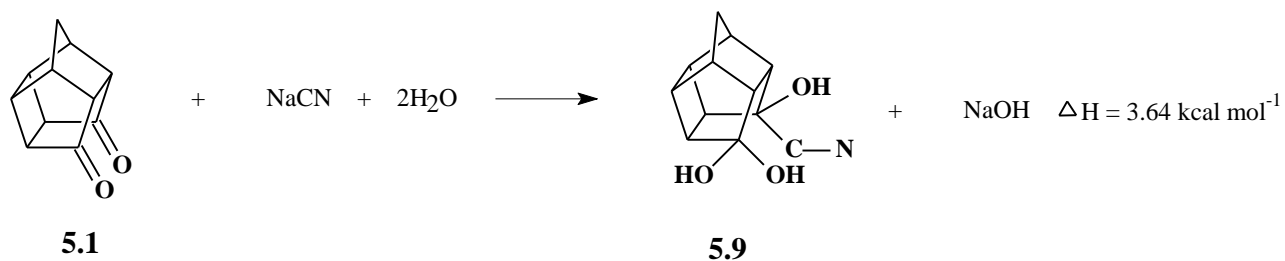
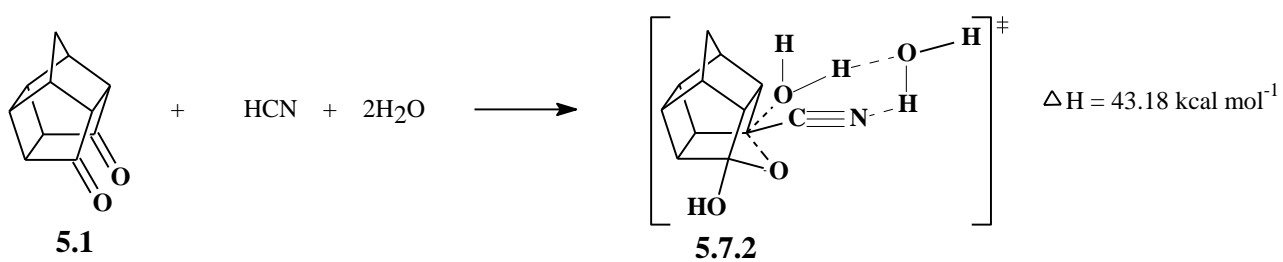
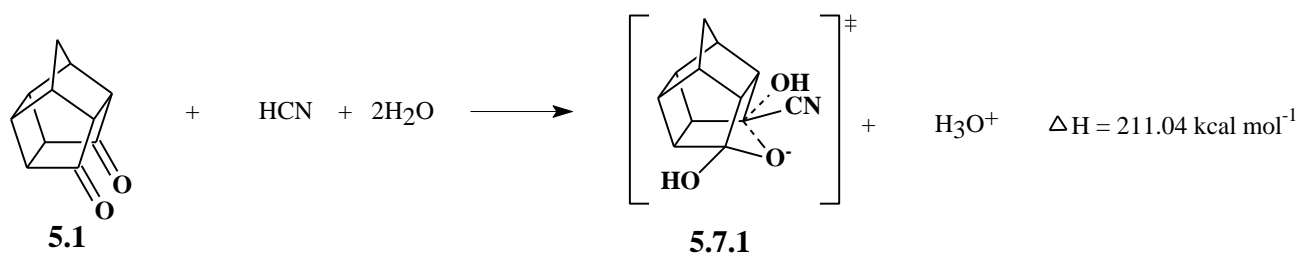
Structure number ^a	Energies ^b (B3LYP/6-31+G(d))		Energies ^b (MP2/6-31+G(d))	
	Hartrees	kcal mol ⁻¹	Hartrees	kcal mol ⁻¹
5.1	-575.6083	-361199.69	-573.8593	-360102.18
5.3.1	-668.4840	-419480.07	-666.4795	-418222.19
5.3.2	-745.3978	-467744.21	-740.9077	-464926.64
5.4	-669.0503	-419835.41	-667.0495	-418579.88
5.5.1	-668.9628	-419780.48	-666.9540	-418519.94
5.5.2	-745.4502	-467777.11	-743.2378	-466388.75
5.6	-669.0534	-419837.38	-667.0540	-418582.74
5.7.1	-744.8636	-467409.01	-742.6593	-466025.74
5.7.2	-821.8200	-515699.86	-819.3941	-514177.55
5.9	-745.4737	-467791.84	-743.2682	-466407.84
5.10.1	-745.3908	-467739.81	-743.1777	-466351.07
5.10.2	-821.8691	-515730.69	-819.4450	-514209.51
5.11	-745.5114	-467815.49	-743.2932	-466423.53
5.12	-745.4161	-467755.71	-743.1938	-466361.18
5.13	-745.4161	-467755.69	-743.1934	-466360.90
5.2	-745.5343	-467829.85	-743.3177	-466438.89
HCN	-93.4286	-58627.34	-93.1640	-58461.31
H₂O	-76.4226	-47955.89	-76.2098	-47822.35
H₃O⁺	-76.6885	-48122.73	-76.4736	-47987.93
Na⁺	-162.0812	-101707.52	-161.6593	-101442.74
NaCN	-255.1508	-160109.58	-254.4607	-159676.48
NaOH	-238.1314	-149429.72	-237.4963	-149031.17

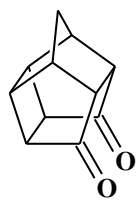
^a Refers to the structure number in Figure 5.1.

^b Energies are expressed in Hartrees and kcal mol⁻¹, performed at the DFT and MP2 level using the 6-31+G(d) level of theory.

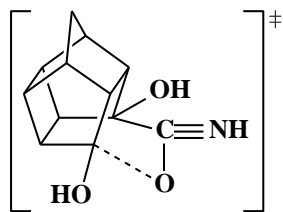
Scheme of reaction for mechanism 1





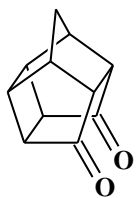


5.1

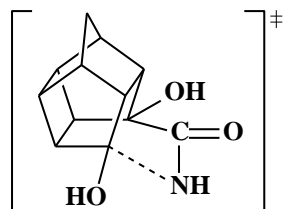


5.12

$\Delta H = 31.38 \text{ kcal mol}^{-1}$

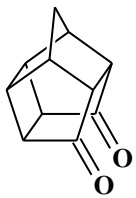


5.1

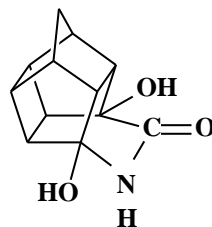


5.13

$\Delta H = 31.26 \text{ kcal mol}^{-1}$



5.1



5.2

$\Delta H = -41.09 \text{ kcal mol}^{-1}$

Table A1.2 Summary of thermodynamic properties for mechanism 1

Structure number ^a	Energies ^b (B3LYP/6-31+G(d))				
	Enthalpy (H)		Free Energy (G)		Entropy (S)
	(Hartrees)	(kcal mol ⁻¹)	(Hartrees)	(kcal mol ⁻¹)	(cal K ⁻¹ mol ⁻¹)
5.1	-575.4116	-361076.24	-575.4536	-361102.61	88.44
5.3.1	-668.2794	-419351.69	-668.3270	-419381.53	100.08
5.3.2	-745.1739	-467603.71	-745.2274	-467637.25	112.52
5.4	-668.8299	-419697.12	-668.8764	-419726.32	97.94
5.5	-668.7481	-419645.79	-668.7941	-419674.64	96.75
5.5.2	-745.2090	-467625.73	-745.2572	-467655.99	101.49
5.6	-668.8327	-419698.87	-668.8772	-419726.80	93.67
5.7.1	-744.6319	-467263.56	-744.6816	-467294.80	104.77
5.7.2	-821.5470	-515528.52	-821.6016	-515562.83	115.08
5.9	-745.2248	-467635.63	-745.2738	-467666.42	103.27
5.10.1	-745.1483	-467587.61	-745.1955	-467617.28	99.51
5.10.2	-821.5998	-515561.68	-821.6509	-515593.74	107.53
5.11	-745.2610	-467658.37	-745.3071	-467687.27	96.94
5.12	-745.1680	-467600.03	-745.2153	-467629.68	99.46
5.13	-745.1682	-467600.15	-745.2154	-467629.76	99.32
5.2	-745.2835	-467672.51	-745.3298	-467701.56	97.43
HCN	-93.4088	-58614.90	-93.4317	-58629.26	48.14
H₂O	-76.3977	-47940.28	-76.4191	-47953.73	45.12
H₃O⁺	-76.6523	-48100.07	-76.6742	-48113.79	46.01
Na⁺	-162.0789	-101706.04	-162.0957	-101716.58	35.34
NaCN	-255.1393	-160102.35	-255.1679	-160120.28	60.14
NaOH	-238.1157	-149419.88	-238.1422	-149436.48	55.71

^a Refers to the structure number in Figure 5.1.

^b Energies are expressed in Hartrees and kcal mol⁻¹, performed at the DFT level using the 6-31+G(d) level of theory.

Table A1.3 Summary of Gibbs free energies for mechanism 1

Structure number ^a	Energies ^b (B3LYP/6-31+G(d))							
	Water		Methanol		CH ₃ CN		DMSO	
	Hartrees	kcal mol ⁻¹	Hartrees	kcal mol ⁻¹	Hartrees	kcal mol ⁻¹	Hartrees	kcal mol ⁻¹
5.1	-575.4720	-361114.12	-575.4767	-361117.09	-575.4774	-361117.56	-575.4769	-361117.21
5.3.1	-668.4372	-419450.70	-668.4419	-419453.66	-668.4520	-419459.95	-668.4183	-419438.81
5.3.2	-745.2599	-467657.67	-745.3272	-467699.92	-745.2646	-467660.62	-745.2628	-467659.49
5.4	-668.8999	-419741.01	-668.9053	-419744.40	-668.9031	-419743.06	-668.9010	-419741.72
5.5	-668.8998	-419741.01	-668.9053	-419744.40	-668.9031	-419743.06	-668.9010	-419741.72
5.5.2	-745.3042	-467685.47	-745.3311	-467702.35	-745.3221	-467696.68	-745.3199	-467695.32
5.6	-668.8961	-419738.63	-668.9016	-419742.10	-668.8998	-419740.99	-668.8973	-419739.41
5.7.1	-744.7782	-467355.41	-744.8448	-467397.21	-744.8143	-467378.07	-744.8120	-467376.62
5.7.2	-821.6683	-515604.64	-821.6721	-515607.07	-821.7478	-515654.55	-821.7435	-515651.88
5.9	-745.3027	-467684.55	-745.3085	-467688.18	-745.3011	-467683.53	-745.2976	-467681.34
5.10.1	-745.3062	-467686.71	-745.3082	-467688.00	-745.3294	-467701.28	-745.3272	-467699.91
5.10.2	-821.7137	-515633.17	-821.7576	-515660.69	-821.7484	-515654.95	-821.7459	-515653.33
5.11	-745.3141	-467691.66	-745.3342	-467704.28	-745.3294	-467701.29	-745.3231	-467697.35
5.12	-745.3137	-467691.42	-745.3342	-467704.28	-745.3294	-467701.29	-745.3272	-467699.91
5.13	-745.2799	-467670.21	-745.3176	-467693.88	-745.3294	-467701.29	-745.3272	-467699.91
5.2	-745.3575	-467718.93	-745.3615	-467721.43	-745.3555	-467717.63	-745.3537	-467716.53
HCN	-93.4352	-58631.47	-93.4368	-58632.51	-93.4388	-58633.75	-93.4376	-58632.98
H₂O	-575.4720	-361114.12	-575.4767	-361117.09	-575.4774	-361117.56	-575.4769	-361117.21
H₃O⁺	-76.8310	-48212.21	-76.7966	-48190.57	-76.8019	-48193.90	-76.7940	-48188.96
Na⁺	-162.2108	-101788.79	-162.2071	-101786.48	-162.2069	-101786.38	-162.2067	-101786.23
NaCN	-255.2095	-160146.40	-255.2077	-160145.27	-255.2087	-160145.90	-255.2074	-160145.06
NaOH	-238.1883	-149465.40	-238.1863	-149464.17	-238.1729	-149455.77	-238.1707	-149454.37

^a Refers to the structure number in Figure 5.1.

^b Energies are expressed in Hartrees and kcal mol⁻¹, performed at the DFT level using the 6-31+G(d) level of theory.

Table A1.4 Summary of Gibbs free energies for mechanism 1 continued

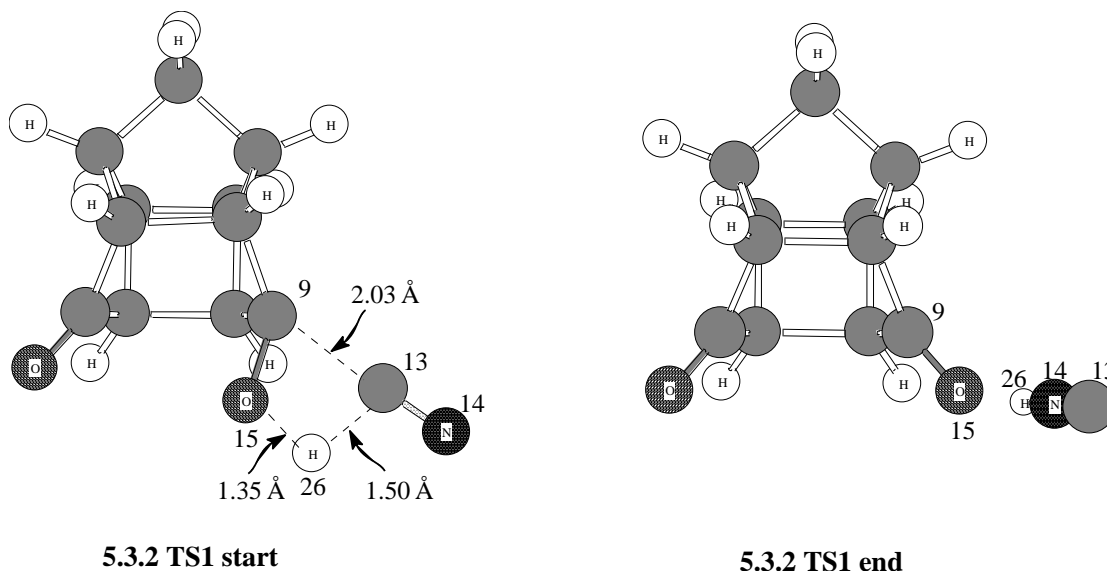
Structure number ^a	Energies ^b (B3LYP/6-31+G(d))			
	Carbon Tetrachloride		Dichloromethane	
	Hartrees	kcal mol ⁻¹	Hartrees	kcal mol ⁻¹
5.1	-575.4719	-361114.06	-575.4765	-361116.99
5.3.1	-668.4061	-419431.15	-668.4120	-419434.86
5.3.2	-745.3191	-467694.80	-745.2622	-467659.08
5.4	-668.8940	-419737.32	-668.9021	-419742.44
5.5	-668.8906	-419735.21	-668.9021	-419742.43
5.5.2	-745.3128	-467690.88	-745.3209	-467695.97
5.6	-668.8928	-419736.61	-668.8994	-419740.73
5.7.1	-744.7644	-467346.76	-744.8044	-467371.87
5.7.2	-821.7317	-515644.46	-821.7457	-515653.22
5.9	-745.2901	-467676.63	-745.3002	-467682.93
5.10.1	-745.3223	-467696.80	-745.3289	-467700.96
5.10.2	-821.7384	-515648.67	-821.7469	-515654.01
5.11	-745.3223	-467696.80	-745.3289	-467700.96
5.12	-745.3223	-467696.80	-745.3289	-467700.96
5.13	-745.3223	-467696.80	-745.3289	-467700.96
5.2	-745.3476	-467712.70	-745.3548	-467717.21
HCN	-93.4340	-58630.70	-93.4379	-58633.15
H₂O	-575.4719	-361114.06	-575.4765	-361116.99
H₃O⁺	-76.7412	-48155.83	-76.7935	-48188.65
Na⁺	-162.1586	-101756.08	-162.1977	-101780.57
NaCN	-255.1862	-160131.74	-255.2041	-160142.98
NaOH	-238.1558	-149445.04	-238.1709	-149454.52

^a Refers to the structure number in Figure 5.1.

^b Energies are expressed in Hartrees and kcal mol⁻¹, performed at the DFT level using the 6-31+G(d) level of theory.

Attempts to model Transition Structure 5.3.2 with HCN

Structure 5.1. was used as the starting point and HCN was positioned in close proximity. The 3D transition state optimisation with the HCN molecule added towards the front of the cage is illustrated in 5.3.2 TS1 start. The transition state was expected to depict C13 attaching to C9 and H26 being transferred to O15 as shown in 5.3.2 TS1 start.



The expected 4-membered transition state, however, did not form. Instead, HCN became detached when H26 attached to N14 (5.3.2 TS1 end).

A scan calculation was then attempted with C13 being scanned closer to C9. The scan is graphically depicted.

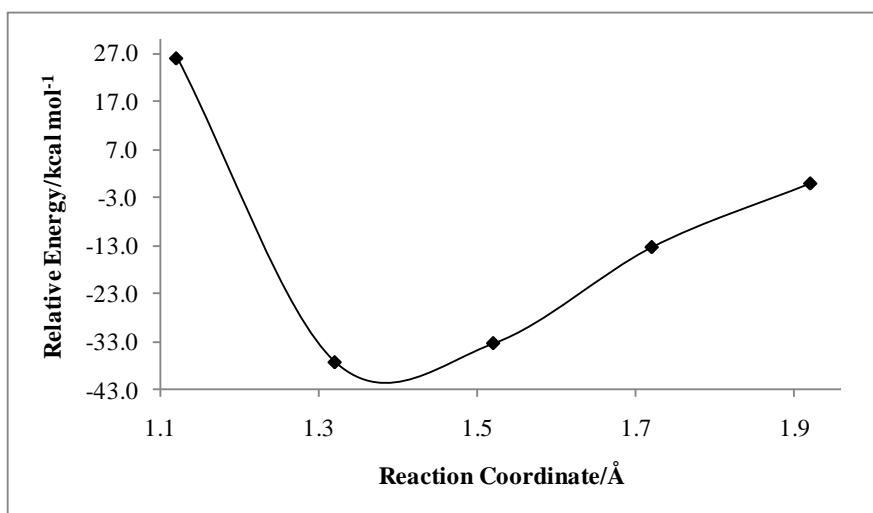
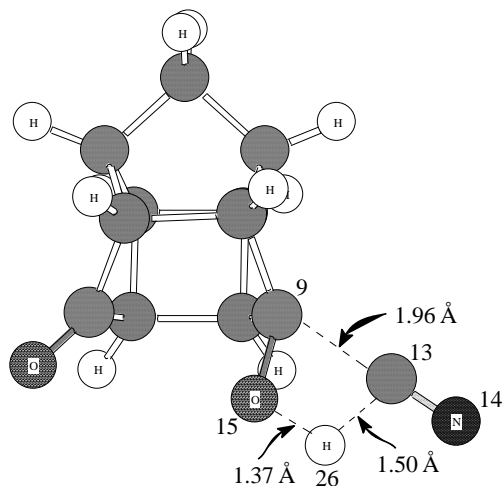
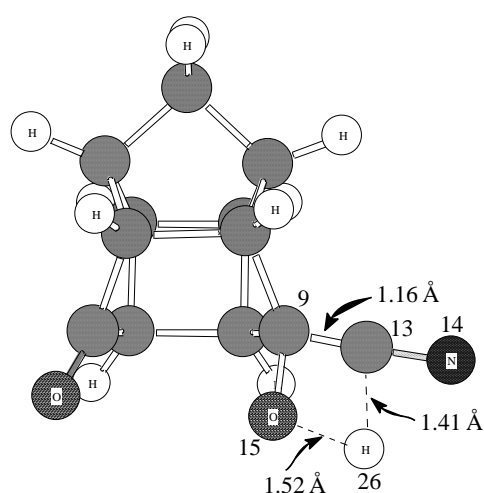


Figure A1.1 Graphical representation of energy vs reaction coordinate for structure 5.3.2

Although the scan resulted in a minimum on the potential energy surface and not a maximum, the structures at each reaction coordinate were examined. The **5.3.2 Scan start** structure and **Scan end** structure are shown. The scan was started with a distance of 1.96 Å between C9 and C13.



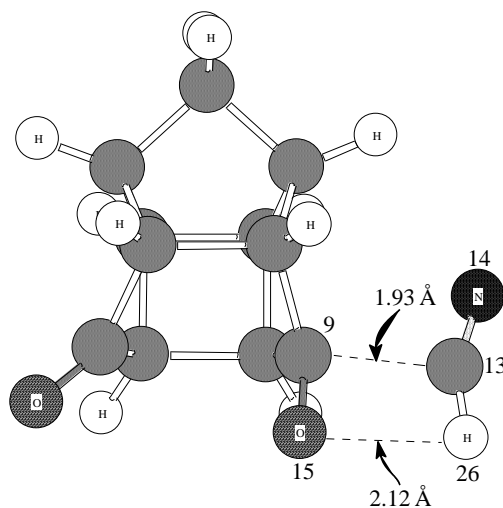
5.3.2 Scan 1 start



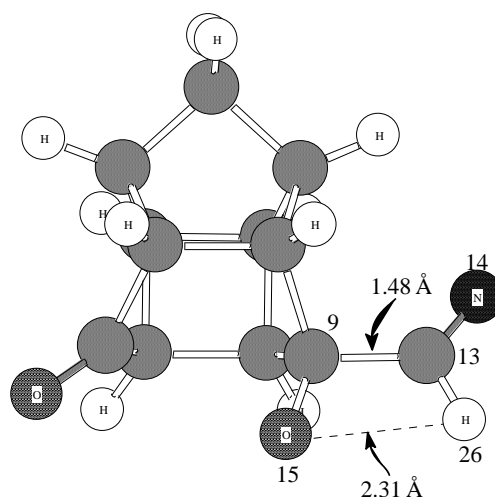
5.3.2 Scan 1 end

However, as the distance between C9 and C13 decreased, H26 was not transferred to O15. The bond distances were adjusted numerous times, even scanning C13 away from C9 but each optimisation resulted in a structure similar to **5.3.2 TS1 end** (See Chapter 5).

It was then decided to perform a scan with the HCN group orientated such that the CN was towards the back of the cage as depicted in **5.3.2 Scan 2 start**.



5.3.2 Scan 2 start



5.3.2 Scan 2 end

O13 was scanned towards C9 in 10 steps.

The scan did not produce a maximum or a minimum on the potential energy surface. The output (**5.3.2 Scan 2 end**) shows clearly that C13 formed a bond with C9 but H26 did not attach to O15. Here, as well, the bond distances were altered many times however it did not yield a good starting structure for the transition state.

Thus it was decided to do the calculation with a HCN and a H₂O molecule to form a 6-membered cyclic neutral transition structure.

Table A1.5 Summary of the relative^a energy, enthalpy and entropy in water for mechanism 1

Species ^b	$\Delta E / \text{kcal mol}^{-1}$	$\Delta H / \text{kcal mol}^{-1}$	$\Delta S / \text{cal K}^{-1} \text{mol}^{-1}$
5.1	0.00	0.00	0.00
5.3.1	27.02	18.11	-9.74
5.3.2	28.32	29.57	-72.32
5.4	3.96	5.14	-40.85
5.5.1	40.72	-7.11	-39.21
5.5.2	23.78	1.55	-73.04
5.6	5.14	6.34	-44.80
5.7.1	83.30	80.70	-79.44
5.7.2	41.12	33.82	-112.52
5.9	10.16	13.04	-80.31
5.10.1	50.13	-3.34	-85.29
5.10.2	22.55	3.98	-116.90
5.11	-10.17	-5.51	-85.13
5.12	31.15	-8.38	-86.38
5.13	16.62	15.71	-76.73
5.2	-40.84	-35.02	-83.47

^a Energies relative to the energy of the starting structure **5.1**

^b Refers to the structure number in Figure 5.1

The energies in water: (ΔE) (in kcal mol^{-1}), enthalpy (ΔH) (in kcal mol^{-1}) and entropy (ΔS) ($\text{cal K}^{-1} \text{mol}^{-1}$) at 298.15 K

Table A1.6 Summary of energy, enthalpy and entropy in water for mechanism 1

Structure number ^a	Energies ^b (B3LYP/6-31+G(d))				
	Energy (E)		Enthalpy (H)		Entropy (S)
	Hartrees	kcal mol ⁻¹	Hartrees	kcal mol ⁻¹	cal K ⁻¹ mol ⁻¹
5.1	-575.6255	-361210.45	-575.4299	-361087.70	88.61
5.3.1	-668.5766	-419538.19	-668.3875	-419419.52	104.59
5.3.2	-745.4499	-467776.87	-745.2079	-467625.02	109.51
5.4	-669.0729	-419849.60	-668.8535	-419711.95	97.47
5.5	-668.9928	-419799.31	-668.8535	-419711.95	97.46
5.5.2	-745.4571	-467781.41	-745.2525	-467653.04	108.79
5.6	-669.0710	-419848.41	-668.8516	-419710.75	93.51
5.7.1	-744.9607	-467469.95	-744.7311	-467325.82	99.23
5.7.2	-821.8668	-515729.23	-821.6139	-515570.52	114.46
5.9	-745.5004	-467808.56	-745.2537	-467653.80	103.16
5.10.1	-745.4151	-467755.06	-745.2603	-467657.92	96.53
5.10.2	-821.8964	-515747.80	-821.6614	-515600.35	-821.66
5.11	-745.5328	-467828.89	-745.2833	-467672.34	98.34
5.12	-745.4453	-467774.03	-745.2683	-467662.97	95.45
5.13	-745.4685	-467788.57	-745.2299	-467638.87	105.09
5.2	-745.4685	-467788.57	-745.2299	-467638.87	105.09
HCN	-93.4322	-58629.57	-93.4124	-58617.14	48.06
H₂O	-76.4373	-47965.16	-76.4128	-47949.75	45.15
H₃O⁺	-76.8388	-48217.10	-76.8081	-48197.81	48.30
Na⁺	-162.1963	-101779.74	-162.1940	-101778.26	35.34
NaCN	-255.1905	-160134.49	-255.1805	-160128.19	61.06
NaOH	-238.1742	-149456.55	-238.1614	-149448.55	56.50

^a Refers to the structure number in Figure 5.1.

^b Energies are expressed in Hartrees, kcal mol⁻¹ and cal K⁻¹ mol⁻¹, performed at the DFT level using the 6-31+G(d) level of theory

Table A1.7 Summary of the relative^a energy, enthalpy and entropy in methanol for mechanism 1

Species ^b	$\Delta E / \text{kcal mol}^{-1}$	$\Delta H / \text{kcal mol}^{-1}$	$\Delta S / \text{cal K}^{-1} \text{mol}^{-1}$
5.1	0.00	0.00	0.00
5.3.1	29.23	17.06	-17.27
5.3.2	29.03	-2.56	-51.88
5.4	4.07	5.26	-39.45
5.5.1	41.68	-6.50	-39.45
5.5.2	14.63	-9.23	-108.41
5.6	5.17	6.38	-43.39
5.7.1	105.65	70.69	-59.04
5.7.2	42.42	35.67	-111.78
5.9	10.06	12.91	-79.07
5.10.1	0.10	1.25	-79.07
5.10.2	23.69	-16.94	-108.41
5.11	-8.90	-4.77	-84.18
5.12	16.41	-16.47	-83.93
5.13	18.79	-33.56	-83.70
5.2	-39.11	-33.56	-83.72

^a Energies relative to the energy of the starting structure **5.1**

^b Refers to the structure number in Figure 5.1

The energies in methanol: (ΔE) (in kcal mol^{-1}), enthalpy (ΔH) (in kcal mol^{-1}) and entropy (ΔS) ($\text{cal K}^{-1} \text{mol}^{-1}$) at 298.15 K

Table A1.8 Summary of energy, enthalpy and entropy in methanol for mechanism 1

Structure number ^a	Energies ^b (B3LYP/6-31+G(d))				
	Energy (E)		Enthalpy (H)		Entropy (S)
	Hartrees	kcal mol ⁻¹	Hartrees	kcal mol ⁻¹	cal K ⁻¹ mol ⁻¹
5.1	-575.6303	-361213.47	-575.4346	-361090.66	88.63
5.3.1	-668.5801	-419540.35	-668.3959	-419424.78	96.86
5.3.2	-745.4554	-467780.33	-745.2655	-467661.17	129.96
5.4	-669.0785	-419853.09	-668.8589	-419715.33	97.49
5.5	-668.9978	-419802.46	-668.8589	-419715.34	97.48
5.5.2	-745.4783	-467794.73	-745.2761	-467667.85	115.72
5.6	-669.0767	-419851.99	-668.8571	-419714.21	93.55
5.7.1	-744.9637	-467471.79	-744.7880	-467361.53	119.67
5.7.2	-821.8715	-515732.16	-821.6174	-515572.72	115.21
5.9	-745.5064	-467812.32	-745.2596	-467657.47	103.02
5.10.1	-745.4188	-467757.40	-745.2594	-467657.37	102.73
5.10.2	-821.9013	-515750.90	-821.7012	-515625.33	118.58
5.11	-745.5364	-467831.16	-745.2877	-467675.09	97.91
5.12	-745.4755	-467792.95	-745.2877	-467675.09	97.91
5.13	-745.4717	-467790.57	-745.3149	-467692.18	98.13
5.2	-745.5640	-467848.47	-745.3149	-467692.17	98.12
HCN	-93.4339	-58630.67	-93.4140	-58618.18	48.05
H₂O	-76.4374	-47965.22	-76.4128	-47949.78	45.15
H₃O⁺	-76.8070	-48197.14	-76.7736	-48176.18	48.29
Na⁺	-162.1927	-101777.43	-162.1903	-101775.95	35.34
NaCN	-255.1890	-160133.54	-255.1788	-160127.13	60.84
NaOH	-238.1718	-149455.07	-238.1589	-149446.97	57.68

^a Refers to the structure number in Figure 5.1.

^b Energies are expressed in Hartrees, kcal mol⁻¹ and cal K⁻¹ mol⁻¹, performed at the DFT level using the 6-31+G(d) level of theory

Table A1.9 Summary of the relative^a energy, enthalpy and entropy in acetonitrile for mechanism 1

Species ^a	$\Delta E / \text{kcal mol}^{-1}$	$\Delta H / \text{kcal mol}^{-1}$	$\Delta S / \text{cal K}^{-1} \text{mol}^{-1}$
5.1	0.00	0.00	0.00
5.3.1	32.42	19.22	7.02
5.3.2	28.69	30.47	-67.56
5.4	11.01	13.01	-38.71
5.5.1	45.74	-3.42	-39.14
5.5.2	15.71	-6.61	-70.95
5.6	11.74	13.83	-42.88
5.7.1	106.06	75.12	-80.72
5.7.2	46.47	-15.77	-108.56
5.9	16.98	20.63	-78.37
5.10.1	-1.32	-15.24	-84.49
5.10.2	24.30	-16.19	-108.68
5.11	-3.85	1.18	-84.06
5.12	23.04	-15.24	-84.47
5.13	25.47	-15.24	-84.48
5.2	-36.85	-31.38	-83.78

^a Energies relative to the energy of the starting structure **5.1**

^b Refers to the structure number in Figure 5.1

The energies in acetonitrile: (ΔE) (in kcal mol^{-1}), enthalpy (ΔH) (in kcal mol^{-1}) and entropy (ΔS) ($\text{cal K}^{-1} \text{mol}^{-1}$) at 298.15 K

Table A1.10 Summary of energy, enthalpy and entropy in acetonitrile for mechanism**1**

Structure number ^a	Energies ^b (B3LYP/6-31+G(d))				
	Energy (E)		Enthalpy (H)		Entropy (S)
	Hartrees	kcal mol ⁻¹	Hartrees	kcal mol ⁻¹	cal K ⁻¹ mol ⁻¹
5.1	-575.6312	-361214.05	-575.4353	-361091.09	88.76
5.3.1	-668.5771	-419538.45	-668.3944	-419423.85	121.10
5.3.2	-745.4534	-467779.11	-745.2102	-467626.50	114.41
5.4	-669.0761	-419851.63	-668.8567	-419713.93	97.68
5.5	-668.9942	-419800.20	-668.8567	-419713.93	97.68
5.5.2	-745.4741	-467792.09	-745.2693	-467663.58	111.03
5.6	-669.0750	-419850.90	-668.8554	-419713.11	93.52
5.7.1	-744.9476	-467461.69	-744.7670	-467348.39	99.56
5.7.2	-821.8572	-515723.19	-821.6915	-515619.20	118.57
5.9	-745.4987	-467807.51	-745.2521	-467652.76	103.18
5.10.1	-745.4122	-467753.26	-745.2831	-467672.22	97.49
5.10.2	-821.8925	-515745.36	-821.6921	-515619.63	118.46
5.11	-745.5319	-467828.35	-745.2831	-467672.22	97.49
5.12	-745.4624	-467784.76	-745.2831	-467672.22	97.51
5.13	-745.4586	-467782.33	-745.2831	-467672.22	97.50
5.2	-745.5579	-467844.64	-745.3088	-467688.35	98.19
HCN	-93.4359	-58631.89	-93.4160	-58619.42	48.07
H₂O	-76.4321	-47961.86	-76.4075	-47946.46	45.16
H₃O⁺	-76.8146	-48201.90	-76.7796	-48179.93	46.85
Na⁺	-162.1925	-101777.33	-162.1901	-101775.85	35.34
NaCN	-255.1900	-160134.15	-255.1799	-160127.82	60.65
NaOH	-238.1596	-149447.42	-238.1453	-149438.43	58.17

^a Refers to the structure number in Figure 5.1.^b Energies are expressed in Hartrees, kcal mol⁻¹ and cal K⁻¹ mol⁻¹, performed at the DFT level using the 6-31+G(d) level of theory

Table A1.11 Summary of the relative^a energy, enthalpy and entropy in dimethyl sulphoxide for mechanism 1

Species ^b	$\Delta E / \text{kcal mol}^{-1}$	$\Delta H / \text{kcal mol}^{-1}$	$\Delta S / \text{cal K}^{-1} \text{mol}^{-1}$
5.1	0.00	0.00	0.00
5.3.1	32.29	32.17	-16.97
5.3.2	28.11	29.98	-67.90
5.4	12.31	14.32	-38.21
5.5.1	45.89	-3.06	-38.65
5.5.2	15.68	-6.78	-71.04
5.6	13.21	15.34	-42.50
5.7.1	110.55	79.29	-81.77
5.7.2	46.97	-16.24	-112.75
5.9	18.66	22.33	-78.10
5.10.1	-1.34	-15.29	-84.18
5.10.2	24.28	-16.46	-108.59
5.11	-3.01	2.08	-83.74
5.12	23.70	-15.29	-84.18
5.13	26.06	-15.29	-84.18
5.2	-37.15	-31.69	-83.44

^a Energies relative to the energy of the starting structure **5.1**

^b Refers to the structure number in Figure 5.1

The energies in dimethyl sulphoxide: (ΔE) (in kcal mol^{-1}), enthalpy (ΔH) (in kcal mol^{-1}) and entropy (ΔS) ($\text{cal K}^{-1} \text{mol}^{-1}$) at 298.15 K

Table A1.12 Summary of energy, enthalpy and entropy in dimethyl sulphoxide for mechanism 1

Structure number ^a	Energies ^b (B3LYP/6-31+G(d))				
	Energy (E)		Enthalpy (H)		Entropy (S)
	Hartrees	kcal mol ⁻¹	Hartrees	kcal mol ⁻¹	cal K ⁻¹ mol ⁻¹
5.1	-575.6309	-361213.88	-575.4349	-361090.86	88.36
5.3.1	-668.5759	-419537.74	-668.3723	-419409.97	96.73
5.3.2	-745.4522	-467778.36	-745.2088	-467625.60	113.68
5.4	-669.0740	-419850.31	-668.8545	-419712.57	97.77
5.5	-668.9925	-419799.12	-668.8545	-419712.57	97.77
5.5.2	-745.4720	-467790.79	-745.2674	-467662.36	110.54
5.6	-669.0726	-419849.41	-668.8529	-419711.54	93.48
5.7.1	-744.9446	-467459.80	-744.7644	-467346.72	100.30
5.7.2	-821.8536	-515720.96	-821.6894	-515617.89	113.98
5.9	-745.4954	-467805.42	-745.2487	-467650.62	103.04
5.10.1	-745.4095	-467751.53	-745.2809	-467670.87	97.40
5.10.2	-821.8898	-515743.65	-821.6897	-515618.11	118.14
5.11	-745.5299	-467827.09	-745.2809	-467670.87	97.40
5.12	-745.4593	-467782.77	-745.2809	-467670.87	97.39
5.13	-745.4555	-467780.41	-745.2809	-467670.87	97.39
5.2	-745.5562	-467843.62	-745.3071	-467687.27	98.13
HCN	-93.4346	-58631.12	-93.4148	-58618.65	48.06
H₂O	-76.4315	-47961.46	-76.4069	-47946.07	45.15
H₃O⁺	-76.8077	-48197.58	-76.7728	-48175.64	44.67
Na⁺	-162.1922	-101777.17	-162.1899	-101775.69	35.34
NaCN	-255.1887	-160133.32	-255.1786	-160126.97	60.67
NaOH	-238.1574	-149446.04	-238.1430	-149437.02	58.20

^a Refers to the structure number in Figure 5.1.

^b Energies are expressed in Hartrees, kcal mol⁻¹ and cal K⁻¹ mol⁻¹, performed at the DFT level using the 6-31+G(d) level of theory

Table A1.13 Summary of the relative^a energy, enthalpy and entropy in carbon tetrachloride for mechanism 1

Species ^b	$\Delta E / \text{kcal mol}^{-1}$	$\Delta H / \text{kcal mol}^{-1}$	$\Delta S / \text{cal K}^{-1} \text{mol}^{-1}$
5.1	0.00	0.00	0.00
5.3.1	70.79	59.46	2.97
5.3.2	27.64	-8.39	-50.05
5.4	6.26	8.15	-39.77
5.5.1	46.73	-1.65	-37.56
5.5.2	10.70	-10.91	-71.64
5.6	5.45	7.59	-44.05
5.7.1	152.48	130.74	-82.39
5.7.2	43.96	-19.41	-110.14
5.9	9.49	13.53	-79.58
5.10.1	49.47	-20.76	-84.80
5.10.2	16.95	-23.83	-110.85
5.11	-13.43	-8.47	-85.73
5.12	26.50	-20.76	-84.80
5.13	27.80	-20.76	-84.80
5.2	-41.99	-36.44	-84.08

^a Energies relative to the energy of the starting structure **5.1**

^b Refers to the structure number in Figure 5.1

The energies in carbon tetrachloride: (ΔE) (in kcal mol^{-1}), enthalpy (ΔH) (in kcal mol^{-1}) and entropy (ΔS) ($\text{cal K}^{-1} \text{mol}^{-1}$) at 298.15 K

Table A1.14 Summary of energy, enthalpy and entropy in carbon tetrachloride for mechanism 1

Structure number ^a	Energies ^b (B3LYP/6-31+G(d))				
	Energy (E)		Enthalpy (H)		Entropy (S)
	Hartrees	kcal mol ⁻¹	Hartrees	kcal mol ⁻¹	cal K ⁻¹ mol ⁻¹
5.1	-575.6262	-361210.92	-575.4298	-361087.66	88.57
5.3.1	-668.5378	-419513.83	-668.3507	-419396.39	116.58
5.3.2	-745.4401	-467770.72	-745.2565	-467655.51	131.78
5.4	-669.0675	-419846.24	-668.8475	-419708.14	97.86
5.5	-668.9827	-419792.99	-668.8435	-419705.66	99.13
5.5.2	-745.4671	-467787.67	-745.2605	-467658.03	110.19
5.6	-669.0688	-419847.04	-668.8484	-419708.71	93.58
5.7.1	-744.9125	-467439.65	-744.7170	-467316.97	99.92
5.7.2	-821.8410	-515713.06	-821.6762	-515609.63	116.83
5.9	-745.4894	-467801.65	-745.2411	-467645.87	103.18
5.10.1	-745.4053	-467748.90	-745.2762	-467667.87	97.03
5.10.2	-821.8841	-515740.07	-821.6833	-515614.05	116.12
5.11	-745.5259	-467824.58	-745.2762	-467667.87	97.03
5.12	-745.4419	-467771.86	-745.2762	-467667.87	97.03
5.13	-745.4398	-467770.57	-745.2762	-467667.87	97.03
5.2	-745.5510	-467840.36	-745.3012	-467683.55	97.75
HCN	-93.4309	-58628.79	-93.4111	-58616.35	48.12
H₂O	-76.4270	-47958.65	-76.4022	-47943.11	45.13
H₃O⁺	-76.7556	-48164.90	-76.7200	-48142.51	44.65
Na⁺	-162.1442	-101747.03	-162.1418	-101745.55	35.34
NaCN	-255.1686	-160120.72	-255.1575	-160113.74	60.38
NaOH	-238.1443	-149437.81	-238.1290	-149428.21	56.46

^a Refers to the structure number in Figure 5.1.

^b Energies are expressed in Hartrees, kcal mol⁻¹ and cal K⁻¹ mol⁻¹, performed at the DFT level using the 6-31+G(d) level of theory

Table A1.15 Summary of the relative^a energy, enthalpy and entropy in dichloromethane for mechanism 1

Species ^b	$\Delta E / \text{kcal mol}^{-1}$	$\Delta H / \text{kcal mol}^{-1}$	$\Delta S / \text{cal K}^{-1} \text{mol}^{-1}$
5.1	0.00	0.00	0.00
5.3.1	39.79	39.49	-16.93
5.3.2	28.64	30.38	-67.38
5.4	9.34	11.25	-37.47
5.5.1	45.78	-3.88	-38.86
5.5.2	14.45	-7.59	-70.98
5.6	9.63	11.70	-41.68
5.7.1	112.45	84.21	-81.28
5.7.2	45.66	-16.62	-108.52
5.9	14.53	18.31	-77.21
5.10.1	53.08	-16.56	-84.36
5.10.2	22.41	-17.65	-109.35
5.11	-6.44	-1.43	-82.97
5.12	23.35	-16.56	-84.35
5.13	25.60	-16.56	-84.35
5.2	-38.09	-32.56	-83.53

^a Energies relative to the energy of the starting structure **5.1**

^b Refers to the structure number in Figure 5.1

The energies in dichloromethane: (ΔE) (in kcal mol^{-1}), enthalpy (ΔH) (in kcal mol^{-1}) and entropy (ΔS) ($\text{cal K}^{-1} \text{mol}^{-1}$) at 298.15 K

Table A1.16 Summary of energy, enthalpy and entropy in dichloromethane for mechanism 1

Structure number ^a	Energies ^b (B3LYP/6-31+G(d))				
	Energy (E)		Enthalpy (H)		Entropy (S)
	Hartrees	kcal mol ⁻¹	Hartrees	kcal mol ⁻¹	cal K ⁻¹ mol ⁻¹
5.1	-575.6306	-361213.64	-575.4345	-361090.61	88.48
5.3.1	-668.5695	-419533.74	-668.3660	-419405.99	96.84
5.3.2	-745.4511	-467777.64	-745.2078	-467625.00	114.33
5.4	-669.0753	-419851.09	-668.8557	-419713.31	97.70
5.5	-668.9925	-419799.15	-668.8557	-419713.31	97.70
5.5.2	-745.4737	-467791.83	-745.2683	-467662.96	110.73
5.6	-669.0748	-419850.80	-668.8550	-419712.85	93.49
5.7.1	-744.9422	-467458.28	-744.7575	-467342.43	98.74
5.7.2	-821.8552	-515721.97	-821.6894	-515617.93	118.34
5.9	-745.4983	-467807.24	-745.2512	-467652.19	103.11
5.10.1	-745.4121	-467753.20	-745.2826	-467671.93	97.35
5.10.2	-821.8923	-515745.22	-821.6911	-515618.97	117.51
5.11	-745.5317	-467828.22	-745.2826	-467671.93	97.36
5.12	-745.4595	-467782.93	-745.2826	-467671.93	97.35
5.13	-745.4559	-467780.68	-745.2826	-467671.93	97.36
5.2	-745.5574	-467844.37	-745.3081	-467687.94	98.17
HCN	-93.4349	-58631.29	-93.4150	-58618.82	48.08
H₂O	-76.4313	-47961.35	-76.4067	-47945.94	45.15
H₃O⁺	-76.8067	-48196.90	-76.7712	-48174.68	46.85
Na⁺	-162.1832	-101771.52	-162.1809	-101770.04	35.34
NaCN	-255.1856	-160131.41	-255.1753	-160124.90	60.64
NaOH	-238.1573	-149445.98	-238.1429	-149436.90	59.09

^a Refers to the structure number in Figure 5.1.

^b Energies are expressed in Hartrees, kcal mol⁻¹ and cal K⁻¹ mol⁻¹, performed at the DFT level using the 6-31+G(d) level of theory

APPENDIX 2

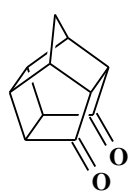
Table A2.1 Summary of energies for mechanism 2

Structure number ^a	Energies ^b (B3LYP/6-31+G(d))		Energies ^b (MP2/6-31+G(d))	
	Hartrees	kcal mol ⁻¹	Hartrees	kcal mol ⁻¹
5.1	-575.6083	-361199.69	-573.8593	-360102.18
5.15.1	-651.9704	-409117.64	-650.0121	-407888.77
5.15.2	-728.4316	-457097.74	-726.2633	-455737.15
5.16	-652.0421	-409162.62	-650.0890	-407937.01
5.17	-821.8215	-515700.81	-819.3957	-514178.61
5.18	-745.4801	-467795.83	-743.2736	-466411.24
5.19				
5.6	-669.0534	-419837.38	-667.0540	-418582.74
5.7.1	-744.8636	-467409.01	-742.6593	-466025.74
5.7.2	-821.8200	-515699.86	-819.3941	-514177.55
5.9	-745.4737	-467791.84	-743.2682	-466407.84
5.10.1	-745.3908	-467739.81	-743.1777	-466351.07
5.10.2	-821.8691	-515730.69	-819.4450	-514209.51
5.11	-745.5114	-467815.49	-743.2932	-466423.53
5.12	-745.4161	-467755.71	-743.1938	-466361.18
5.13	-745.4161	-467755.69	-743.1934	-466360.90
5.2	-745.5343	-467829.85	-743.3177	-466438.89
HCN	-93.4286	-58627.34	-93.1640	-58461.31
H₂O	-76.4226	-47955.89	-76.2098	-47822.35
H₃O⁺	-76.6885	-48122.73	-76.4736	-47987.93
Na⁺	-162.0812	-101707.52	-161.6593	-101442.74
NaCN	-255.1508	-160109.58	-254.4607	-159676.48
NaOH	-238.1314	-149429.72	-237.4963	-149031.17

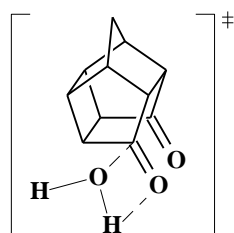
^a Refers to the structure number in Figure 5.21.

^b Energies are expressed in Hartrees and kcal mol⁻¹, performed at the DFT and MP2 level using the 6-31+G(d) level of theory.

Scheme of reaction for mechanism 2

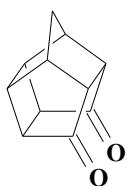


5.1

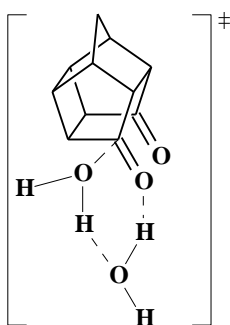


5.15.1

$\Delta H = 36.29 \text{ kcal mol}^{-1}$

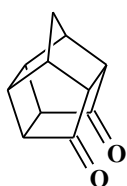


5.1



5.15.2

$\Delta H = 13.04 \text{ kcal mol}^{-1}$

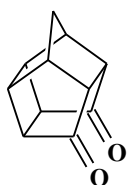


5.1

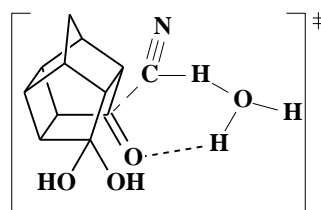


5.16

$\Delta H = -4.63 \text{ kcal mol}^{-1}$



5.1

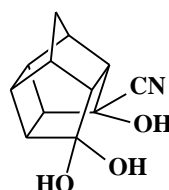


5.17

$\Delta H = 26.92 \text{ kcal mol}^{-1}$

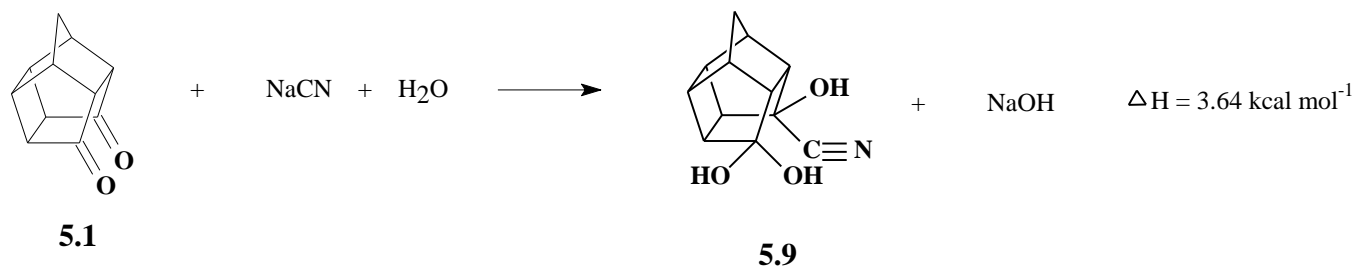
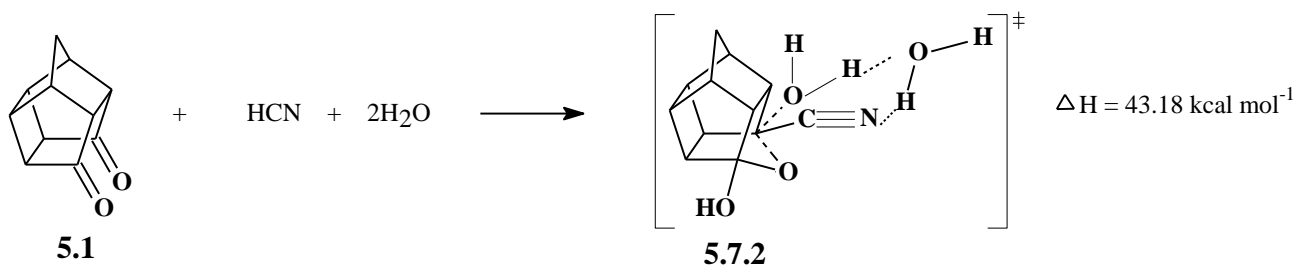
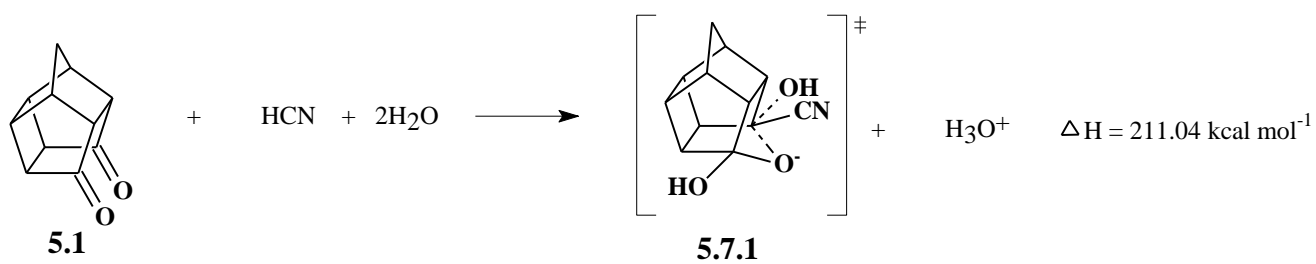
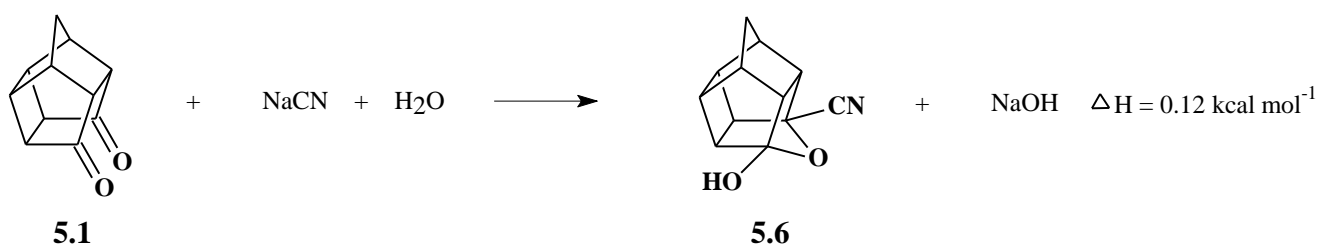
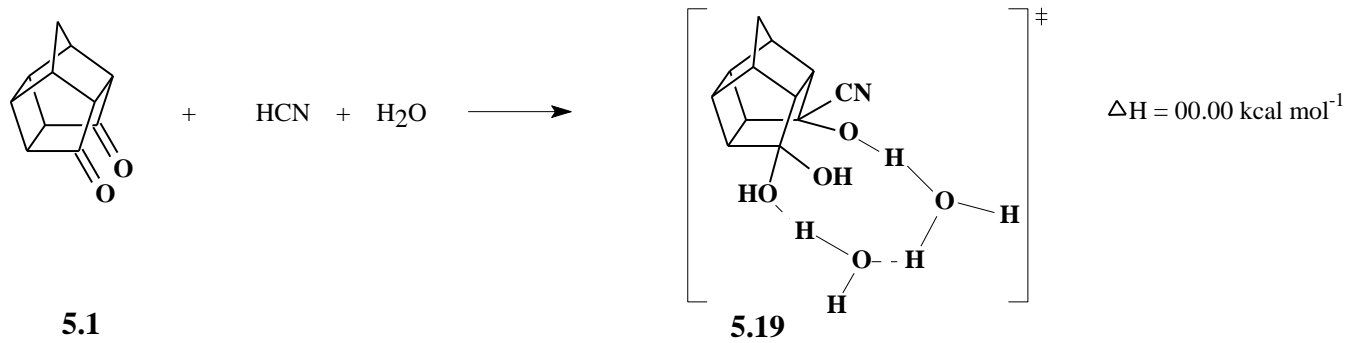


5.1



5.18

$\Delta H = -7.67 \text{ kcal mol}^{-1}$



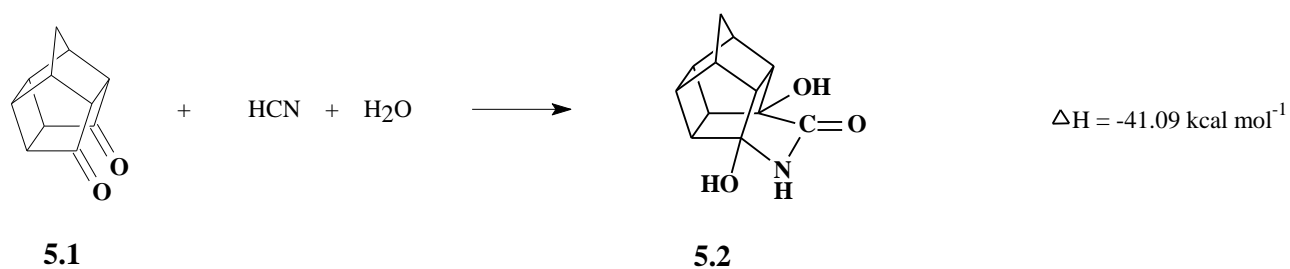
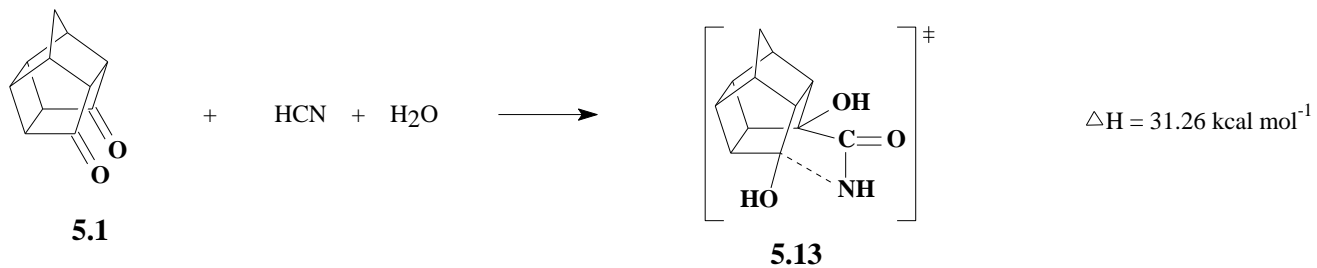
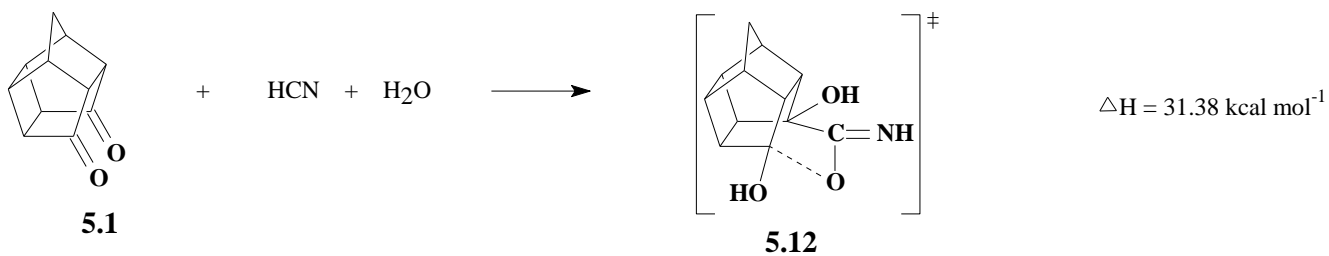
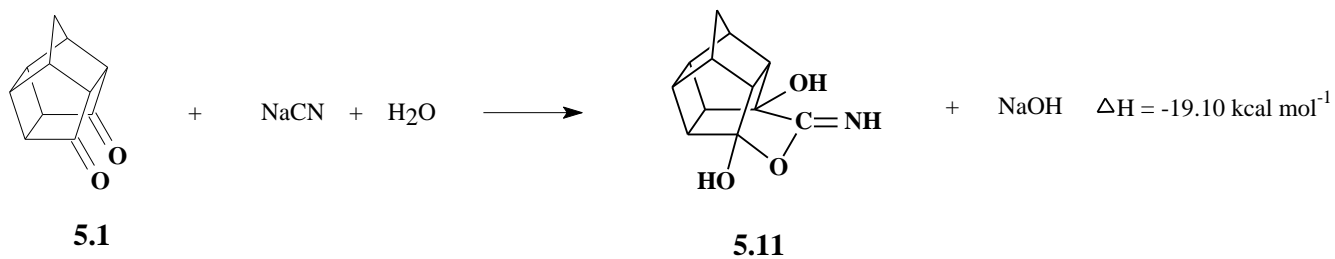
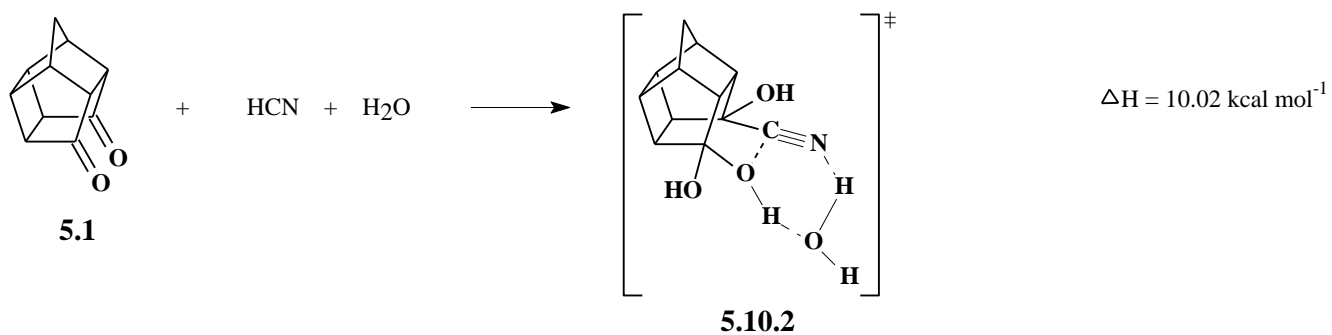
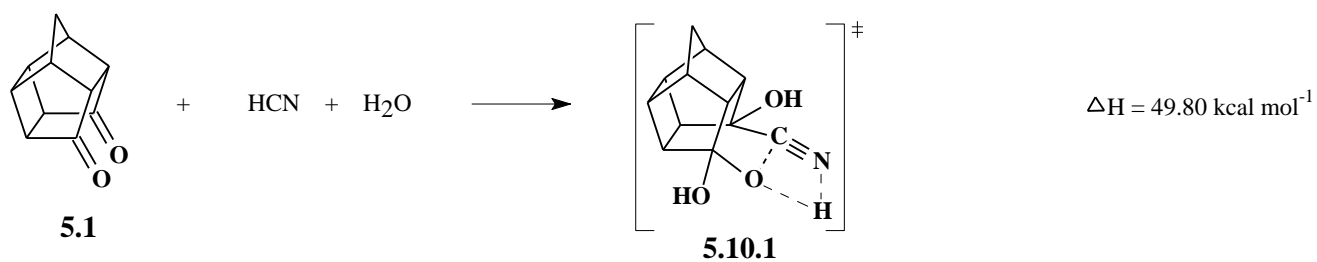


Table A2.2 Summary of thermodynamic properties for mechanism 2

Structure number ^a	Energies ^b (B3LYP/6-31+G(d))				
	Enthalpy (H)		Free Energy (G)		Entropy (S)
	(Hartrees)	(kcal mol ⁻¹)	(Hartrees)	(kcal mol ⁻¹)	(cal K ⁻¹ mol ⁻¹)
5.1	-575.4116	-361076.24	-575.4536	-361102.61	88.44
5.15.1	-651.7514	-408980.22	-651.7964	-409008.43	94.60
5.15.2	-728.1862	-456943.75	-728.2345	-456974.06	101.68
5.16	-651.8166	-409021.14	-651.8610	-409048.95	93.30
5.17	-821.5525	-515532.01	-821.6082	-515566.97	117.28
5.18	-745.2303	-467639.08	-745.2784	-467669.25	101.17
5.19					
5.6	-668.8327	-419698.87	-668.8772	-419726.80	93.67
5.7.1	-744.6319	-467263.56	-744.6816	-467294.80	104.77
5.7.2	-821.5470	-515528.52	-821.6016	-515562.83	115.08
5.9	-745.2248	-467635.63	-745.2738	-467666.42	103.27
5.10.1	-745.1483	-467587.61	-745.1955	-467617.28	99.51
5.10.2	-821.5998	-515561.68	-821.6509	-515593.74	107.53
5.11	-745.2610	-467658.37	-745.3071	-467687.27	96.94
5.12	-745.1680	-467600.03	-745.2153	-467629.68	99.46
5.13	-745.1682	-467600.15	-745.2154	-467629.76	99.32
5.2	-745.2835	-467672.51	-745.3298	-467701.56	97.43
HCN	-93.4088	-58614.90	-93.4317	-58629.26	48.14
H₂O	-76.3977	-47940.28	-76.4191	-47953.73	45.12
H₃O⁺	-76.6523	-48100.07	-76.6742	-48113.79	46.01
Na⁺	-162.0789	-101706.04	-162.0957	-101716.58	35.34
NaCN	-255.1393	-160102.35	-255.1679	-160120.28	60.14
NaOH	-238.1157	-149419.88	-238.1422	-149436.48	55.71

^a Refers to the structure number in Figure 5.21.

^b Energies are expressed in Hartrees and kcal mol⁻¹, performed at the DFT level using the 6-31+G(d) level of theory.

Table A2.3 Summary of Gibbs free energies for mechanism 2

Structure number ^a	Energies ^b (B3LYP/6-31+G(d))							
	Water		Methanol		CH ₃ CN		DMSO	
	Hartrees	kcal mol ⁻¹	Hartrees	kcal mol ⁻¹	Hartrees	kcal mol ⁻¹	Hartrees	kcal mol ⁻¹
5.1	-575.4720	-361114.12	-575.4767	-361117.09	-575.4774	-361117.56	-575.4769	-361117.21
5.15.1	-651.8798	-409060.79	-651.8822	-409062.27	-651.8978	-409072.08	-651.8977	-409071.97
5.15.2	-728.3082	-457020.32	-728.3161	-457025.29	-728.2651	-456993.28	-728.3025	-457016.73
5.16	-651.8866	-409065.01	-651.8913	-409067.98	-651.8858	-409064.56	-651.8843	-409063.56
5.17	-821.7344	-515646.12	-821.6718	-515606.85	-821.6667	-515603.69	-821.6624	-515600.95
5.18	-745.3059	-467686.55	-745.3108	-467689.63	-745.3050	-467685.95	-745.3026	-467684.45
5.19								
5.6	-668.8961	-419738.63	-668.9016	-419742.10	-668.8998	-419740.99	-668.8973	-419739.41
5.7.1	-744.7782	-467355.41	-744.8448	-467397.21	-744.8143	-467378.07	-744.8120	-467376.62
5.7.2	-821.6683	-515604.64	-821.6721	-515607.07	-821.7478	-515654.55	-821.7435	-515651.88
5.9	-745.3027	-467684.55	-745.3085	-467688.18	-745.3011	-467683.53	-745.2976	-467681.34
5.10.1	-745.3062	-467686.71	-745.3082	-467688.00	-745.3294	-467701.28	-745.3272	-467699.91
5.10.2	-821.7137	-515633.17	-821.7576	-515660.69	-821.7484	-515654.95	-821.7459	-515653.33
5.11	-745.3141	-467691.66	-745.3342	-467704.28	-745.3294	-467701.29	-745.3231	-467697.35
5.12	-745.3137	-467691.42	-745.3342	-467704.28	-745.3294	-467701.29	-745.3272	-467699.91
5.13	-745.2799	-467670.21	-745.3176	-467693.88	-745.3294	-467701.29	-745.3272	-467699.91
5.2	-745.3575	-467718.93	-745.3615	-467721.43	-745.3555	-467717.63	-745.3537	-467716.53
HCN	-93.4352	-58631.47	-93.4368	-58632.51	-93.4388	-58633.75	-93.4376	-58632.98
H₂O	-575.4720	-361114.12	-575.4767	-361117.09	-575.4774	-361117.56	-575.4769	-361117.21
H₃O⁺	-76.8310	-48212.21	-76.7966	-48190.57	-76.8019	-48193.90	-76.7940	-48188.96
Na⁺	-162.2108	-101788.79	-162.2071	-101786.48	-162.2069	-101786.38	-162.2067	-101786.23
NaCN	-255.2095	-160146.40	-255.2077	-160145.27	-255.2087	-160145.90	-255.2074	-160145.06
NaOH	-238.1883	-149465.40	-238.1863	-149464.17	-238.1729	-149455.77	-238.1707	-149454.37

^a Refers to the structure number in Figure 5.21.

^b Energies are expressed in Hartrees and kcal mol⁻¹, performed at the DFT level using the 6-31+G(d) level of theory.

Table A2.4 Summary of Gibbs free energies for mechanism 2 continued

Structure number ^a	Energies ^b (B3LYP/6-31+G(d))			
	Carbon Tetrachloride		Dichloromethane	
	Hartrees	kcal mol ⁻¹	Hartrees	kcal mol ⁻¹
5.1	-575.4719	-361114.06	-575.4765	-361116.99
5.15.1	-651.8376	-409034.31	-651.8964	-409071.21
5.15.2	-728.2493	-456983.33	-728.3034	-457017.30
5.16	-651.8341	-409032.10	-651.8853	-409064.21
5.17	-821.7230	-515639.01	-821.6631	-515601.37
5.18	-745.2471	-467649.64	-745.3040	-467685.37
5.19				
5.6	-668.8928	-419736.61	-668.8994	-419740.73
5.7.1	-744.7644	-467346.76	-744.8044	-467371.87
5.7.2	-821.7317	-515644.46	-821.7457	-515653.22
5.9	-745.2901	-467676.63	-745.3002	-467682.93
5.10.1	-745.3223	-467696.80	-745.3289	-467700.96
5.10.2	-821.7384	-515648.67	-821.7469	-515654.01
5.11	-745.3223	-467696.80	-745.3289	-467700.96
5.12	-745.3223	-467696.80	-745.3289	-467700.96
5.13	-745.3223	-467696.80	-745.3289	-467700.96
5.2	-745.3476	-467712.70	-745.3548	-467717.21
HCN	-93.4340	-58630.70	-93.4379	-58633.15
H₂O	-575.4719	-361114.06	-575.4765	-361116.99
H₃O⁺	-76.7412	-48155.83	-76.7935	-48188.65
Na⁺	-162.1586	-101756.08	-162.1977	-101780.57
NaCN	-255.1862	-160131.74	-255.2041	-160142.98
NaOH	-238.1558	-149445.04	-238.1709	-149454.52

^a Refers to the structure number in Figure 5.21.

^b Energies are expressed in Hartrees and kcal mol⁻¹, performed at the DFT level using the 6-31+G(d) level of theory.

Attempts to model Transition Structure 5.17 with HCN

A 4-membered cyclic transition structure with HCN was attempted. **5.16** was used as the starting point and HCN was added. A scan calculation was attempted with C12 being moved closer to C8. The scan is graphically depicted.

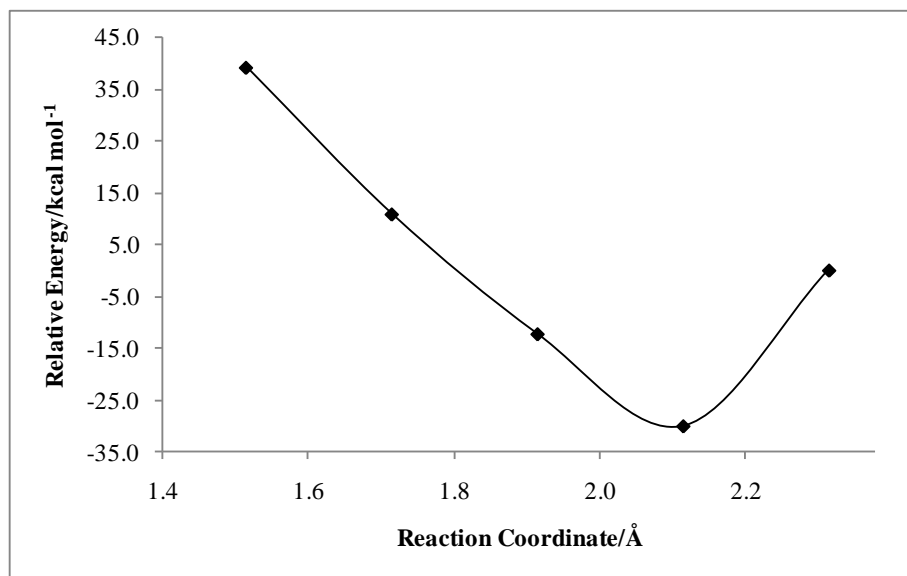
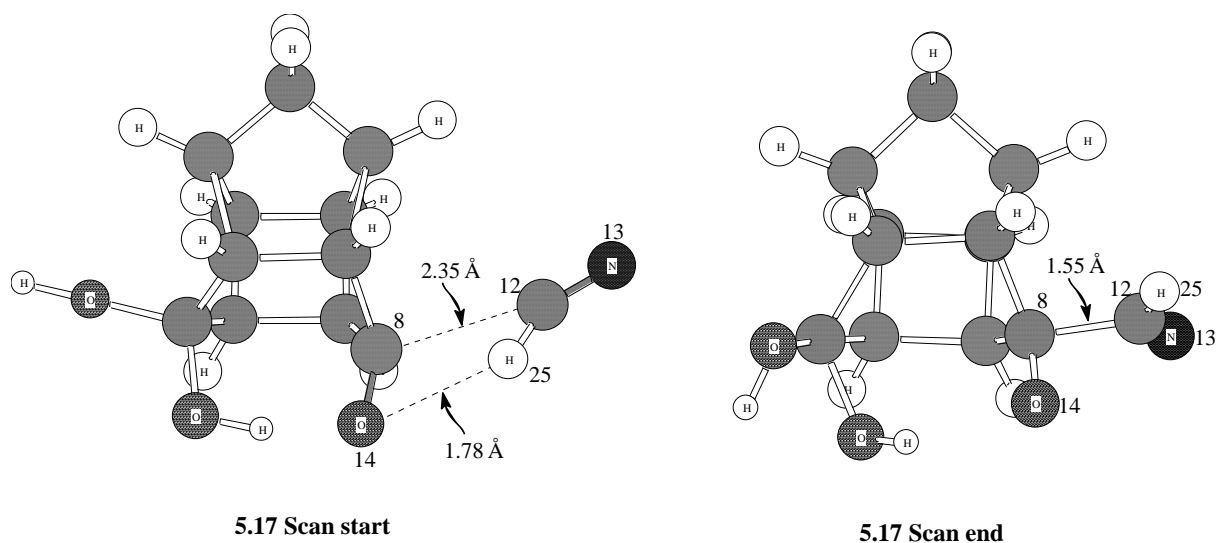


Figure A2.1 Graphical representation of energy vs reaction coordinate for structure **5.17**

The scan resulted in a minimum on the potential energy surface and not a maximum. The structures at each reaction coordinate were examined. The **5.17 Scan start** and **Scan end** structure are shown. The scan was started with a distance of 2.35 Å between C8 and C12 and proceeded for 5 steps.



As the distance between C8 and C12 decreased, it was expected that the transition state would depict H25 being transferred to O14. This did not materialise. The bond distances were adjusted for re-optimisation numerous times; however, a good approximate starting structure could not be calculated.

It was thus decided to do the calculation with a HCN and a H₂O molecule to form a 6-membered cyclic transition structure.

Table A2.5 Summary of the relative^a energy, enthalpy and entropy in water for mechanism 2

Species ^b	$\Delta E / \text{kcal mol}^{-1}$	$\Delta H / \text{kcal mol}^{-1}$	$\Delta S / \text{cal K}^{-1} \text{mol}^{-1}$
5.1	0.00	0.00	0.00
5.15.1	50.66	9.22	-24.55
5.15.2	23.53	-0.57	-69.74
5.16	-2.27	0.27	-40.40
5.17	32.28	-2.15	-94.04
5.18	-6.71	-1.73	-80.42
5.19			
5.6	5.14	6.34	-44.80
5.7.1	83.30	80.70	-79.44
5.7.2	41.12	33.82	-112.52
5.9	10.16	13.04	-80.31
5.10.1	50.13	-3.34	-85.29
5.10.2	22.55	3.98	-116.90
5.11	-10.17	-5.51	-85.13
5.12	31.15	-8.38	-86.38
5.13	16.62	15.71	-76.73
5.2	-40.84	-35.02	-83.47

^a Energies relative to the energy of the starting structure **5.1**

^b Refers to the structure number in Figure 5.21

The energies in water: (ΔE) (in kcal mol^{-1}), enthalpy (ΔH) (in kcal mol^{-1}) and entropy (ΔS) ($\text{cal K}^{-1} \text{mol}^{-1}$) at 298.15 K

Table A2.6 Summary of energy, enthalpy and entropy in water for mechanism 2

Structure number ^a	Energies ^b (B3LYP/6-31+G(d))				
	Energy (E)		Enthalpy (H)		Entropy (S)
	Hartrees	kcal mol ⁻¹	Hartrees	kcal mol ⁻¹	cal K ⁻¹ mol ⁻¹
5.1	-575.6255	-361210.45	-575.4299	-361087.70	88.61
5.15.1	-651.9821	-409124.96	-651.8279	-409028.23	109.21
5.15.2	-728.4627	-457117.25	-728.2563	-456987.77	109.174
5.16	-652.0664	-409177.89	-651.8422	-409037.17	93.363
5.17	-821.8809	-515738.07	-821.6712	-515606.49	132.934
5.18	-745.5057	-467811.90	-745.2577	-467656.31	101.405
5.19					
5.6	-669.0710	-419848.41	-668.8516	-419710.75	93.51
5.7.1	-744.9607	-467469.95	-744.7311	-467325.82	99.23
5.7.2	-821.8668	-515729.23	-821.6139	-515570.52	114.46
5.9	-745.5004	-467808.56	-745.2537	-467653.80	103.16
5.10.1	-745.4151	-467755.06	-745.2603	-467657.92	96.53
5.10.2	-821.8964	-515747.80	-821.6614	-515600.35	-821.66
5.11	-745.5328	-467828.89	-745.2833	-467672.34	98.34
5.12	-745.4453	-467774.03	-745.2683	-467662.97	95.45
5.13	-745.4685	-467788.57	-745.2299	-467638.87	105.09
5.2	-745.4685	-467788.57	-745.2299	-467638.87	105.09
HCN	-93.4322	-58629.57	-93.4124	-58617.14	48.06
H₂O	-76.4373	-47965.16	-76.4128	-47949.75	45.15
H₃O⁺	-76.8388	-48217.10	-76.8081	-48197.81	48.30
Na⁺	-162.1963	-101779.74	-162.1940	-101778.26	35.34
NaCN	-255.1905	-160134.49	-255.1805	-160128.19	61.06
NaOH	-238.1742	-149456.55	-238.1614	-149448.55	56.50

^a Refers to the structure number in Figure 5.21

^b Energies are expressed in Hartrees, kcal mol⁻¹ and cal K⁻¹ mol⁻¹, performed at the DFT level using the 6-31+G(d) level of theory

Table A2.7 Summary of the relative^a energy, enthalpy and entropy in methanol for mechanism 2

Species ^b	$\Delta E / \text{kcal mol}^{-1}$	$\Delta H / \text{kcal mol}^{-1}$	$\Delta S / \text{cal K}^{-1} \text{mol}^{-1}$
5.1	0.00	0.00	0.00
5.15.1	50.45	8.46	-32.16
5.15.2	23.45	-1.76	-69.74
5.16	-2.36	0.19	-40.76
5.17	33.25	36.71	-109.05
5.18	-5.82	-0.82	-80.57
5.19			
5.6	5.17	6.38	-43.39
5.7.1	105.65	70.69	-59.04
5.7.2	42.42	35.67	-111.78
5.9	10.06	12.91	-79.07
5.10.1	0.10	1.25	-79.07
5.10.2	23.69	-16.94	-108.41
5.11	-8.90	-4.77	-84.18
5.12	16.41	-16.47	-83.93
5.13	18.79	-33.56	-83.70
5.2	-39.11	-33.56	-83.72

^a Energies relative to the energy of the starting structure **5.1**

^b Refers to the structure number in Figure 5.21

The energies in methanol: (ΔE) (in kcal mol^{-1}), enthalpy (ΔH) (in kcal mol^{-1}) and entropy (ΔS) ($\text{cal K}^{-1} \text{mol}^{-1}$) at 298.15 K

Table A2.8 Summary of energy, enthalpy and entropy in methanol for mechanism 2

Structure number ^a	Energies ^b (B3LYP/6-31+G(d))				
	Energy (E)		Enthalpy (H)		Entropy (S)
	Hartrees	kcal mol ⁻¹	Hartrees	kcal mol ⁻¹	cal K ⁻¹ mol ⁻¹
5.1	-575.6303	-361213.47	-575.4346	-361090.66	88.63
5.15.1	-651.9873	-409128.24	-651.8339	-409031.97	101.62
5.15.2	-728.4678	-457120.47	-728.2630	-456991.97	111.76
5.16	-652.0715	-409181.05	-651.8471	-409040.25	93.02
5.17	-821.8861	-515741.34	-821.6157	-515571.69	117.94
5.18	-745.5109	-467815.18	-745.2627	-467659.43	101.26
5.19					
5.6	-669.0767	-419851.99	-668.8571	-419714.21	93.55
5.7.1	-744.9637	-467471.79	-744.7880	-467361.53	119.67
5.7.2	-821.8715	-515732.16	-821.6174	-515572.72	115.21
5.9	-745.5064	-467812.32	-745.2596	-467657.47	103.02
5.10.1	-745.4188	-467757.40	-745.2594	-467657.37	102.73
5.10.2	-821.9013	-515750.90	-821.7012	-515625.33	118.58
5.11	-745.5364	-467831.16	-745.2877	-467675.09	97.91
5.12	-745.4755	-467792.95	-745.2877	-467675.09	97.91
5.13	-745.4717	-467790.57	-745.3149	-467692.18	98.13
5.2	-745.5640	-467848.47	-745.3149	-467692.17	98.12
HCN	-93.4339	-58630.67	-93.4140	-58618.18	48.05
H₂O	-76.4374	-47965.22	-76.4128	-47949.78	45.15
H₃O⁺	-76.8070	-48197.14	-76.7736	-48176.18	48.29
Na⁺	-162.1927	-101777.43	-162.1903	-101775.95	35.34
NaCN	-255.1890	-160133.54	-255.1788	-160127.13	60.84
NaOH	-238.1718	-149455.07	-238.1589	-149446.97	57.68

^a Refers to the structure number in Figure 5.21

^b Energies are expressed in Hartrees, kcal mol⁻¹ and cal K⁻¹ mol⁻¹, performed at the DFT level using the 6-31+G(d) level of theory

Table A2.9 Summary of the relative^a energy, enthalpy and entropy in acetonitrile for mechanism 2

Species ^b	$\Delta E / \text{kcal mol}^{-1}$	$\Delta H / \text{kcal mol}^{-1}$	$\Delta S / \text{cal K}^{-1} \text{mol}^{-1}$
5.1	0.00	0.00	0.00
5.15.1	41.05	-2.10	-25.15
5.15.2	21.91	20.85	-78.03
5.16	-1.51	0.87	-40.42
5.17	33.41	37.20	-101.50
5.18	-3.86	1.19	-80.80
5.19			
5.6	11.74	13.83	-42.88
5.7.1	106.06	75.12	-80.72
5.7.2	46.47	-15.77	-108.56
5.9	16.98	20.63	-78.37
5.10.1	-1.32	-15.24	-84.49
5.10.2	24.30	-16.19	-108.68
5.11	-3.85	1.18	-84.06
5.12	23.04	-15.24	-84.47
5.13	25.47	-15.24	-84.48
5.2	-36.85	-31.38	-83.78

^a Energies relative to the energy of the starting structure **5.1**

^b Refers to the structure number in Figure 5.21

The energies in acetonitrile: (ΔE) (in kcal mol^{-1}), enthalpy (ΔH) (in kcal mol^{-1}) and entropy (ΔS) ($\text{cal K}^{-1} \text{mol}^{-1}$) at 298.15 K

Table A2.10 Summary of energy, enthalpy and entropy in acetonitrile for mechanism

2

Structure number ^a	Energies ^b (B3LYP/6-31+G(d))				
	Energy (E)		Enthalpy (H)		Entropy (S)
	Hartrees	kcal mol ⁻¹	Hartrees	kcal mol ⁻¹	cal K ⁻¹ mol ⁻¹
5.1	-575.6312	-361214.05	-575.4353	-361091.09	88.76
5.15.1	-651.9979	-409134.86	-651.8462	-409039.65	108.76
5.15.2	-728.4604	-457115.85	-728.2171	-456963.16	101.04
5.16	-652.0657	-409177.42	-651.8414	-409036.68	93.49
5.17	-821.8780	-515736.24	-821.6071	-515566.23	125.63
5.18	-745.5053	-467811.66	-745.2569	-467655.79	101.18
5.19					
5.6	-669.0750	-419850.90	-668.8554	-419713.11	93.52
5.7.1	-744.9476	-467461.69	-744.7670	-467348.39	99.56
5.7.2	-821.8572	-515723.19	-821.6915	-515619.20	118.57
5.9	-745.4987	-467807.51	-745.2521	-467652.76	103.18
5.10.1	-745.4122	-467753.26	-745.2831	-467672.22	97.49
5.10.2	-821.8925	-515745.36	-821.6921	-515619.63	118.46
5.11	-745.5319	-467828.35	-745.2831	-467672.22	97.49
5.12	-745.4624	-467784.76	-745.2831	-467672.22	97.51
5.13	-745.4586	-467782.33	-745.2831	-467672.22	97.50
5.2	-745.5579	-467844.64	-745.3088	-467688.35	98.19
HCN	-93.4359	-58631.89	-93.4160	-58619.42	48.07
H₂O	-76.4321	-47961.86	-76.4075	-47946.46	45.16
H₃O⁺	-76.8146	-48201.90	-76.7796	-48179.93	46.85
Na⁺	-162.1925	-101777.33	-162.1901	-101775.85	35.34
NaCN	-255.1900	-160134.15	-255.1799	-160127.82	60.65
NaOH	-238.1596	-149447.42	-238.1453	-149438.43	58.17

^a Refers to the structure number in Figure 5.21^b Energies are expressed in Hartrees, kcal mol⁻¹ and cal K⁻¹ mol⁻¹, performed at the DFT level using the 6-31+G(d) level of theory

Table A2.11 Summary of the relative^a energy, enthalpy and entropy in dimethyl sulphoxide for mechanism 2

Species ^b	$\Delta E / \text{kcal mol}^{-1}$	$\Delta H / \text{kcal mol}^{-1}$	$\Delta S / \text{cal K}^{-1} \text{mol}^{-1}$
5.1	0.00	0.00	0.00
5.15.1	41.00	-2.36	-23.90
5.15.2	21.76	-1.56	-70.77
5.16	-1.09	1.25	-40.00
5.17	33.00	36.78	-105.73
5.18	-3.64	1.35	-80.23
5.19			
5.6	13.21	15.34	-42.50
5.7.1	110.55	79.29	-81.77
5.7.2	46.97	-16.24	-112.75
5.9	18.66	22.33	-78.10
5.10.1	-1.34	-15.29	-84.18
5.10.2	24.28	-16.46	-108.59
5.11	-3.01	2.08	-83.74
5.12	23.70	-15.29	-84.18
5.13	26.06	-15.29	-84.18
5.2	-37.15	-31.69	-83.44

^a Energies relative to the energy of the starting structure **5.1**

^b Refers to the structure number in Figure 5.21

The energies in dimethyl sulphoxide: (ΔE) (in kcal mol^{-1}), enthalpy (ΔH) (in kcal mol^{-1}) and entropy (ΔS) ($\text{cal K}^{-1} \text{mol}^{-1}$) at 298.15 K

Table A2.12 Summary of energy, enthalpy and entropy in dimethyl sulphoxide for mechanism 2

Structure number ^a	Energies ^b (B3LYP/6-31+G(d))				
	Energy (E)		Enthalpy (H)		Entropy (S)
	Hartrees	kcal mol ⁻¹	Hartrees	kcal mol ⁻¹	cal K ⁻¹ mol ⁻¹
5.1	-575.6309	-361213.88	-575.4349	-361090.86	88.36
5.15.1	-651.9971	-409134.35	-651.8456	-409039.29	109.61
5.15.2	-728.4592	-457115.05	-728.2512	-456984.56	107.90
5.16	-652.0641	-409176.44	-651.8398	-409035.68	93.51
5.17	-821.8759	-515734.94	-821.6049	-515564.87	121.00
5.18	-745.5028	-467810.11	-745.2544	-467654.23	101.35
5.19					
5.6	-669.0726	-419849.41	-668.8529	-419711.54	93.48
5.7.1	-744.9446	-467459.80	-744.7644	-467346.72	100.30
5.7.2	-821.8536	-515720.96	-821.6894	-515617.89	113.98
5.9	-745.4954	-467805.42	-745.2487	-467650.62	103.04
5.10.1	-745.4095	-467751.53	-745.2809	-467670.87	97.40
5.10.2	-821.8898	-515743.65	-821.6897	-515618.11	118.14
5.11	-745.5299	-467827.09	-745.2809	-467670.87	97.40
5.12	-745.4593	-467782.77	-745.2809	-467670.87	97.39
5.13	-745.4555	-467780.41	-745.2809	-467670.87	97.39
5.2	-745.5562	-467843.62	-745.3071	-467687.27	98.13
HCN	-93.4346	-58631.12	-93.4148	-58618.65	48.06
H₂O	-76.43145364	-47961.46	-76.406923	-47946.07	45.153
H₃O⁺	-76.8077	-48197.58	-76.7728	-48175.64	44.67
Na⁺	-162.1922	-101777.17	-162.1899	-101775.69	35.34
NaCN	-255.1887	-160133.32	-255.1786	-160126.97	60.67
NaOH	-238.1574	-149446.04	-238.1430	-149437.02	58.20

^a Refers to the structure number in Figure 5.21

^b Energies are expressed in Hartrees, kcal mol⁻¹ and cal K⁻¹ mol⁻¹, performed at the DFT level using the 6-31+G(d) level of theory

Table A2.13 Summary of the relative^a energy, enthalpy and entropy in carbon tetrachloride for mechanism 2

Species ^b	$\Delta E / \text{kcal mol}^{-1}$	$\Delta H / \text{kcal mol}^{-1}$	$\Delta S / \text{cal K}^{-1} \text{mol}^{-1}$
5.1	0.00	0.00	0.00
5.15.1	39.98	-3.54	-23.48
5.15.2	18.20	-9.45	-56.01
5.16	-3.69	-1.34	-40.39
5.17	28.95	-8.11	-90.54
5.18	-7.67	-2.53	-80.67
5.19			
5.6	5.45	7.59	-44.05
5.7.1	152.48	130.74	-82.39
5.7.2	43.96	-19.41	-110.14
5.9	9.49	13.53	-79.58
5.10.1	49.47	-20.76	-84.80
5.10.2	16.95	-23.83	-110.85
5.11	-13.43	-8.47	-85.73
5.12	26.50	-20.76	-84.80
5.13	27.80	-20.76	-84.80
5.2	-41.99	-36.44	-84.08

^a Energies relative to the energy of the starting structure **5.1**

^b Refers to the structure number in Figure 5.21

The energies in carbon tetrachloride: (ΔE) (in kcal mol^{-1}), enthalpy (ΔH) (in kcal mol^{-1}) and entropy (ΔS) ($\text{cal K}^{-1} \text{mol}^{-1}$) at 298.15 K

Table A2.14 Summary of energy, enthalpy and entropy in carbon tetrachloride for mechanism 2

Structure number ^a	Energies ^b (B3LYP/6-31+G(d))				
	Energy (E)		Enthalpy (H)		Entropy (S)
	Hartrees	kcal mol ⁻¹	Hartrees	kcal mol ⁻¹	cal K ⁻¹ mol ⁻¹
5.1	-575.6262	-361210.92	-575.4298	-361087.66	88.57
5.15.1	-651.9895	-409129.60	-651.8376	-409034.31	110.23
5.15.2	-728.4512	-457110.03	-728.2493	-456983.33	122.83
5.16	-652.0591	-409173.26	-651.8341	-409032.10	93.32
5.17	-821.8650	-515728.07	-821.6582	-515598.34	136.42
5.18	-745.4963	-467806.04	-745.2471	-467649.64	101.16
5.19					
5.6	-669.0688	-419847.04	-668.8484	-419708.71	93.58
5.7.1	-744.9125	-467439.65	-744.7170	-467316.97	99.92
5.7.2	-821.8410	-515713.06	-821.6762	-515609.63	116.83
5.9	-745.4894	-467801.65	-745.2411	-467645.87	103.18
5.10.1	-745.4053	-467748.90	-745.2762	-467667.87	97.03
5.10.2	-821.8841	-515740.07	-821.6833	-515614.05	116.12
5.11	-745.5259	-467824.58	-745.2762	-467667.87	97.03
5.12	-745.4419	-467771.86	-745.2762	-467667.87	97.03
5.13	-745.4398	-467770.57	-745.2762	-467667.87	97.03
5.2	-745.5510	-467840.36	-745.3012	-467683.55	97.75
HCN	-93.4309	-58628.79	-93.4111	-58616.35	48.12
H₂O	-76.4270	-47958.65	-76.4022	-47943.11	45.13
H₃O⁺	-76.7556	-48164.90	-76.7200	-48142.51	44.65
Na⁺	-162.1442	-101747.03	-162.1418	-101745.55	35.34
NaCN	-255.1686	-160120.72	-255.1575	-160113.74	60.38
NaOH	-238.1443	-149437.81	-238.1290	-149428.21	56.46

^a Refers to the structure number in Figure 5.21

^b Energies are expressed in Hartrees, kcal mol⁻¹ and cal K⁻¹ mol⁻¹, performed at the DFT level using the 6-31+G(d) level of theory

Table A2.15 Summary of the relative^a energy, enthalpy and entropy in dichloromethane for mechanism 2

Species ^b	$\Delta E / \text{kcal mol}^{-1}$	$\Delta H / \text{kcal mol}^{-1}$	$\Delta S / \text{cal K}^{-1} \text{mol}^{-1}$
5.1	0.00	0.00	0.00
5.15.1	40.89	-2.34	-25.22
5.15.2	21.25	-2.41	-70.10
5.16	-2.18	0.21	-40.14
5.17	32.53	36.32	-104.84
5.18	-4.95	0.15	-80.58
5.19			
5.6	9.63	11.70	-41.68
5.7.1	112.45	84.21	-81.28
5.7.2	45.66	-16.62	-108.52
5.9	14.53	18.31	-77.21
5.10.1	53.08	-16.56	-84.36
5.10.2	22.41	-17.65	-109.35
5.11	-6.44	-1.43	-82.97
5.12	23.35	-16.56	-84.35
5.13	25.60	-16.56	-84.35
5.2	-38.09	-32.56	-83.53

^a Energies relative to the energy of the starting structure **5.1**

^b Refers to the structure number in Figure 5.21

The energies in dichloromethane: (ΔE) (in kcal mol^{-1}), enthalpy (ΔH) (in kcal mol^{-1}) and entropy (ΔS) ($\text{cal K}^{-1} \text{mol}^{-1}$) at 298.15 K

Table A2.16 Summary of energy, enthalpy and entropy in dichloromethane for mechanism 2

Structure number ^a	Energies ^b (B3LYP/6-31+G(d))				
	Energy (E)		Enthalpy (H)		Entropy (S)
	Hartrees	kcal mol ⁻¹	Hartrees	kcal mol ⁻¹	cal K ⁻¹ mol ⁻¹
5.1	-575.6306	-361213.64	-575.4345	-361090.61	88.48
5.15.1	-651.9967	-409134.10	-651.8449	-409038.89	108.41
5.15.2	-728.4592	-457115.10	-728.2518	-456984.90	108.68
5.16	-652.0653	-409177.17	-651.8409	-409036.34	93.49
5.17	-821.8762	-515735.10	-821.6051	-515565.00	122.01
5.18	-745.5046	-467811.23	-745.2560	-467655.22	101.12
5.19					
5.6	-669.0748	-419850.80	-668.8550	-419712.85	93.49
5.7.1	-744.9422	-467458.28	-744.7575	-467342.43	98.74
5.7.2	-821.8552	-515721.97	-821.6894	-515617.93	118.34
5.9	-745.4983	-467807.24	-745.2512	-467652.19	103.11
5.10.1	-745.4121	-467753.20	-745.2826	-467671.93	97.35
5.10.2	-821.8923	-515745.22	-821.6911	-515618.97	117.51
5.11	-745.5317	-467828.22	-745.2826	-467671.93	97.36
5.12	-745.4595	-467782.93	-745.2826	-467671.93	97.35
5.13	-745.4559	-467780.68	-745.2826	-467671.93	97.36
5.2	-745.5574	-467844.37	-745.3081	-467687.94	98.17
HCN	-93.4349	-58631.29	-93.4150	-58618.82	48.08
H₂O	-76.4313	-47961.35	-76.4067	-47945.94	45.15
H₃O⁺	-76.8067	-48196.90	-76.7712	-48174.68	46.85
Na⁺	-162.1832	-101771.52	-162.1809	-101770.04	35.34
NaCN	-255.1856	-160131.41	-255.1753	-160124.90	60.64
NaOH	-238.1573	-149445.98	-238.1429	-149436.90	59.09

^a Refers to the structure number in Figure 5.21

^b Energies are expressed in Hartrees, kcal mol⁻¹ and cal K⁻¹ mol⁻¹, performed at the DFT level using the 6-31+G(d) level of theory

APPENDIX 3

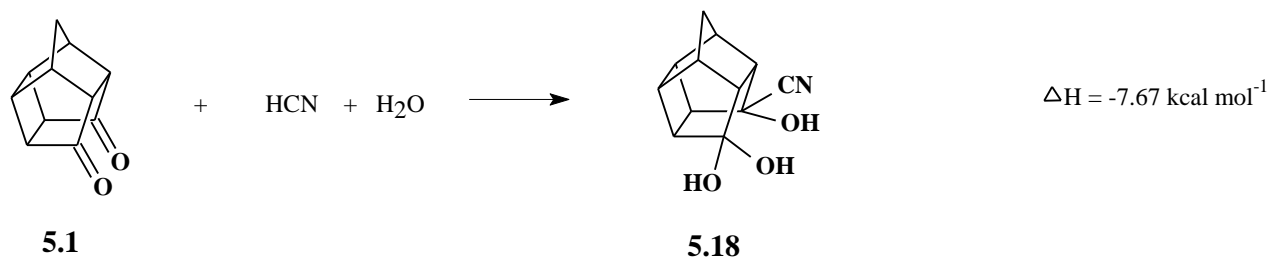
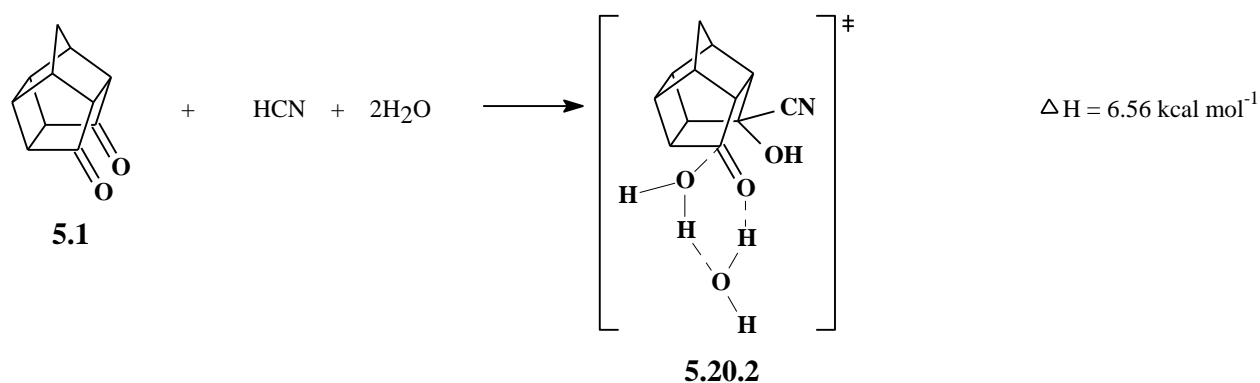
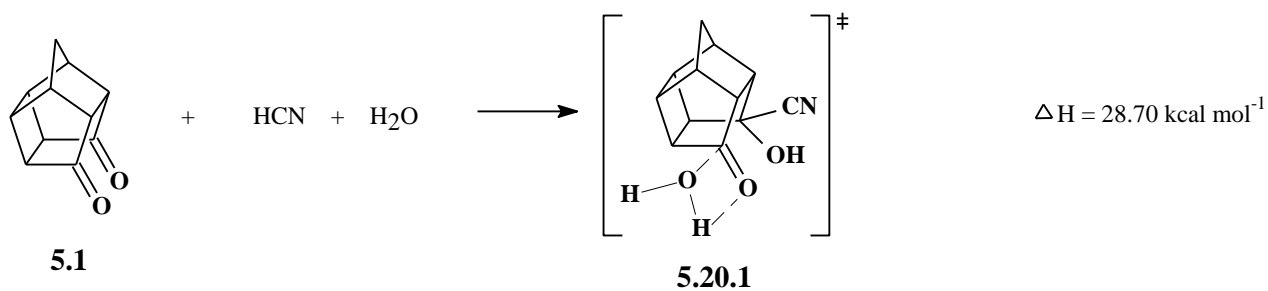
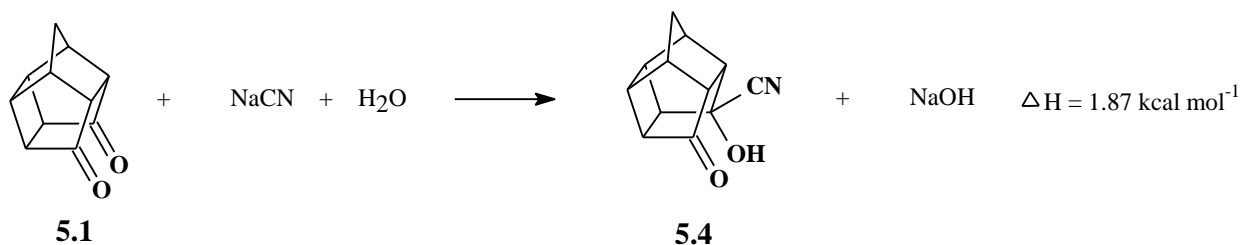
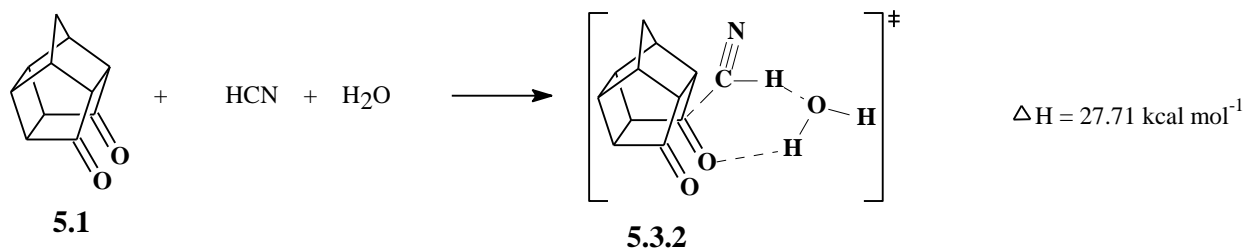
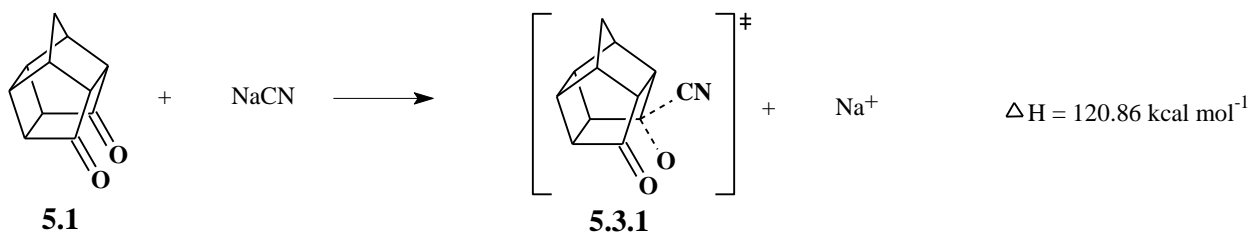
Table A3.1 Summary of energies for mechanism 3-route 1

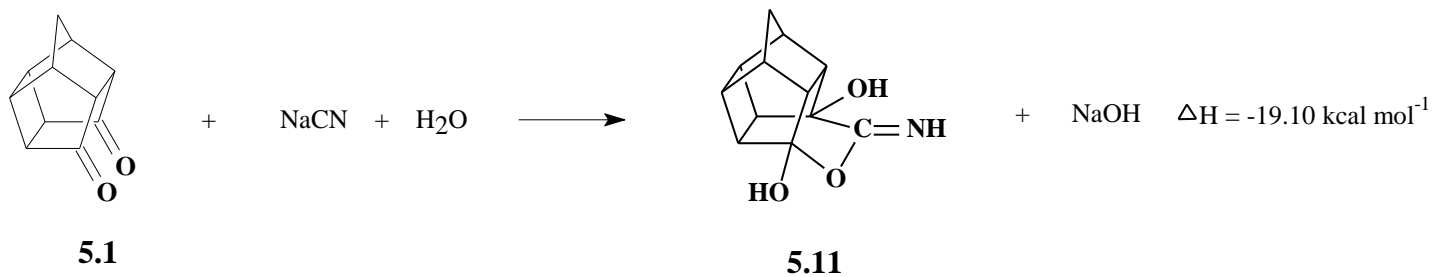
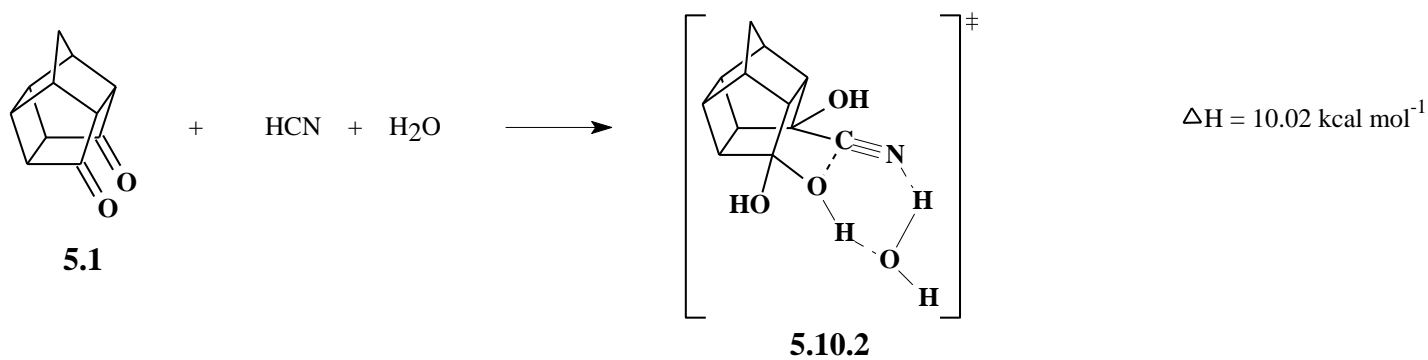
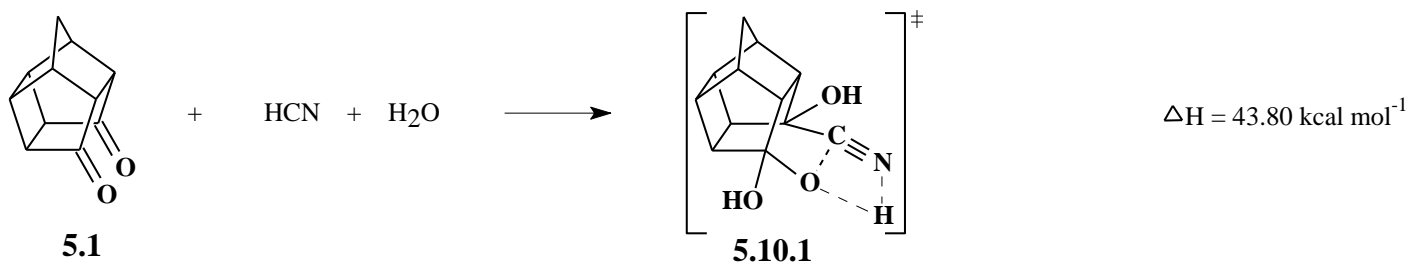
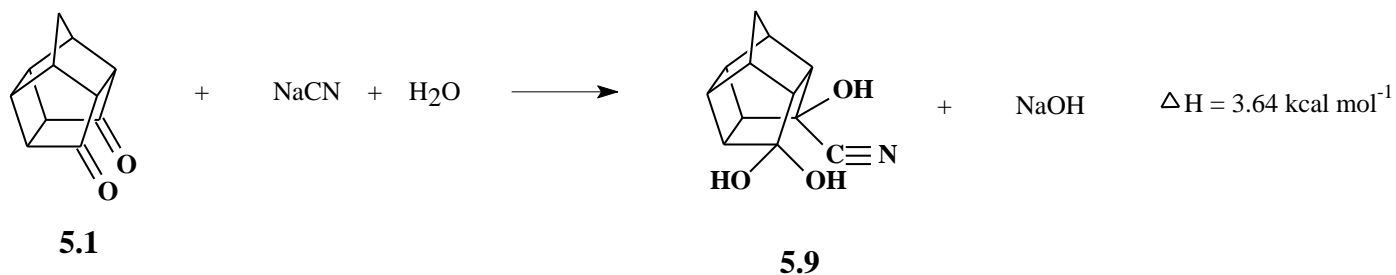
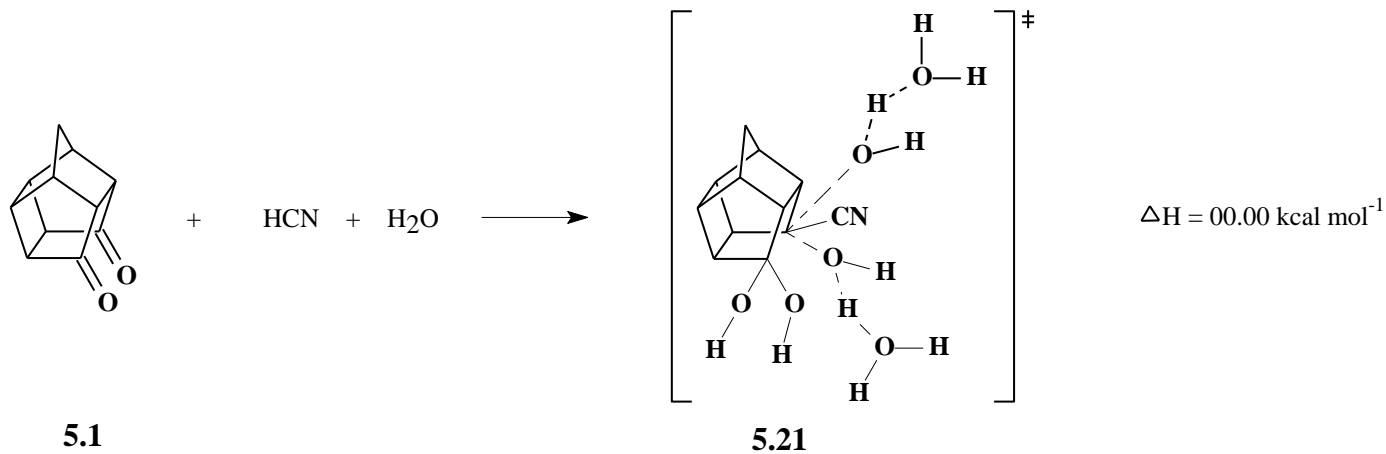
Structure number ^a	Energies ^b (B3LYP/6-31+G(d))		Energies ^a (MP2/6-31+G(d))	
	Hartrees	kcal mol ⁻¹	Hartrees	kcal mol ⁻¹
5.1	-575.6083	-361199.69	-573.8593	-360102.18
5.3.1	-668.4840	-419480.07	-666.4795	-418222.19
5.3.2	-745.3978	-467744.21	-740.9077	-464926.64
5.4	-669.0503	-419835.41	-667.0495	-418579.88
5.20.1	-745.4158	-467755.50	-743.2058	-466368.73
5.20.2	-821.8754	-515734.63	-819.4556	-514216.17
5.18	-745.4801	-467795.83	-743.2736	-466411.24
5.21				
5.9	-745.4737	-467791.84	-743.2682	-466407.84
5.10.1	-745.3908	-467739.81	-743.1777	-466351.07
5.10.2	-821.8691	-515730.69	-819.4450	-514209.51
5.11	-745.5114	-467815.49	-743.2932	-466423.53
5.12	-745.4161	-467755.71	-743.1938	-466361.18
5.13	-745.4161	-467755.69	-743.1934	-466360.90
5.2	-745.5343	-467829.85	-743.3177	-466438.89
HCN	-93.4286	-58627.34	-93.1640	-58461.31
H₂O	-76.4226	-47955.89	-76.2098	-47822.35
H₃O⁺	-76.6885	-48122.73	-76.4736	-47987.93
Na⁺	-162.0812	-101707.52	-161.6593	-101442.74
NaCN	-255.1508	-160109.58	-254.4607	-159676.48
NaOH	-238.1314	-149429.72	-237.4963	-149031.17

^a Refers to the structure number in Figure 5.27

^b Energies are expressed in Hartrees and kcal mol⁻¹, performed at the DFT and MP2 level using the 6-31+G(d) level of theory

Scheme of reaction for mechanism 3-route 1





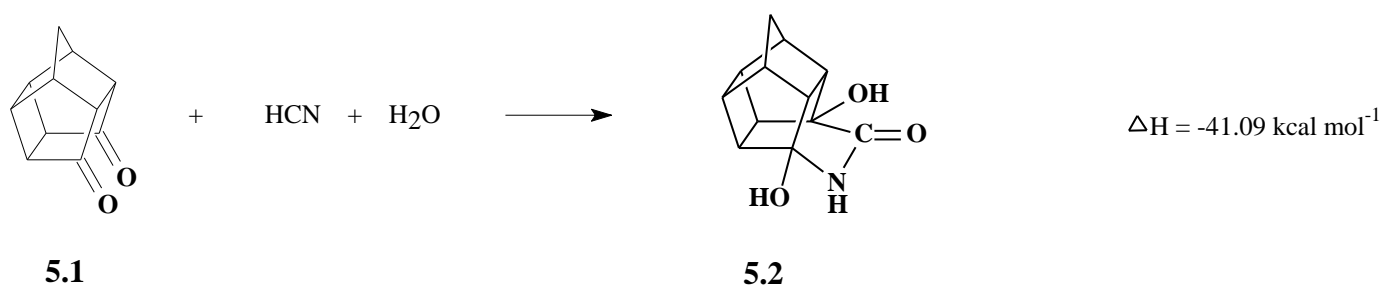
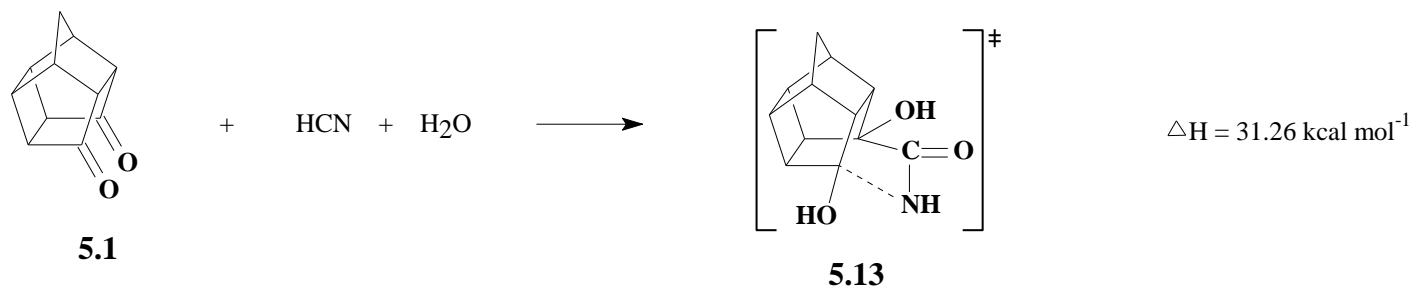
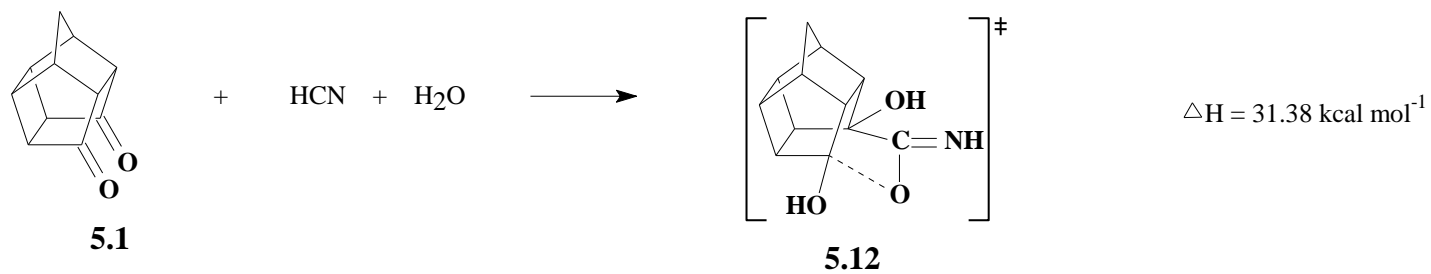


Table A3.2 Summary of thermodynamic properties for mechanism 3-route 1

Structure number ^a	Energies ^b (B3LYP/6-31+G(d))				
	Enthalpy (H)		Free Energy (G)		Entropy (S)
	(Hartrees)	(kcal mol ⁻¹)	(Hartrees)	(kcal mol ⁻¹)	(cal K ⁻¹ mol ⁻¹)
5.1	-575.4116	-361076.24	-575.4536	-361102.61	88.44
5.3.1	-668.2794	-419351.69	-668.3270	-419381.53	100.08
5.3.2	-745.1569	-467593.05	-745.2108	-467626.83	113.27
5.4	-668.8299	-419697.12	-668.8764	-419726.32	97.94
5.20.1	-745.1723	-467602.71	-745.2207	-467633.05	101.75
5.20.2	-821.6053	-515565.13	-821.6572	-515597.71	109.27
5.18	-745.2303	-467639.08	-745.2784	-467669.25	101.17
5.21					
5.9	-745.2248	-467635.63	-745.2738	-467666.42	103.27
5.10.1	-745.1483	-467587.61	-745.1955	-467617.28	99.51
5.10.2	-821.5998	-515561.68	-821.6509	-515593.74	107.53
5.11	-745.2610	-467658.37	-745.3071	-467687.27	96.94
5.12	-745.1680	-467600.03	-745.2153	-467629.68	99.46
5.13	-745.1682	-467600.15	-745.2154	-467629.76	99.32
5.2	-745.2835	-467672.51	-745.3298	-467701.56	97.43
HCN	-93.4088	-58614.90	-93.4317	-58629.26	48.14
H₂O	-76.3977	-47940.28	-76.4191	-47953.73	45.12
H₃O⁺	-76.6523	-48100.07	-76.6742	-48113.79	46.01
Na⁺	-162.0789	-101706.04	-162.0957	-101716.58	35.34
NaCN	-255.1393	-160102.35	-255.1679	-160120.28	60.14
NaOH	-238.1157	-149419.88	-238.1422	-149436.48	55.71

^a Refers to the structure number in Figure 5.27

^b Energies are expressed in Hartrees and kcal mol⁻¹, performed at the DFT level using the 6-31+G(d) level of theory

Table A3.3 Summary of Gibbs free energies for mechanism 3-route 1

Structure number ^a	Energies ^b (B3LYP/6-31+G(d))							
	Water		Methanol		CH ₃ CN		DMSO	
	Hartrees	kcal mol ⁻¹	Hartrees	kcal mol ⁻¹	Hartrees	kcal mol ⁻¹	Hartrees	kcal mol ⁻¹
5.1	-575.4720	-361114.12	-575.4767	-361117.09	-575.4774	-361117.56	-575.4769	-361117.21
5.3.1	-668.4372	-419450.70	-668.4419	-419453.66	-668.4520	-419459.95	-668.4183	-419438.81
5.3.2	-745.2599	-467657.67	-745.3272	-467699.92	-745.2646	-467660.62	-745.2628	-467659.49
5.4	-668.8999	-419741.01	-668.9053	-419744.40	-668.9031	-419743.06	-668.9010	-419741.72
5.20.1	-745.3253	-467698.69	-745.3302	-467701.77	-745.3242	-467698.03	-745.3040	-467685.34
5.20.2	-821.7308	-515643.91	-821.7368	-515647.62	-821.7273	-515641.67	-821.7221	-515638.40
5.18	-745.3059	-467686.55	-745.3108	-467689.63	-745.3050	-467685.95	-745.3026	-467684.45
5.21								
5.9	-745.3027	-467684.55	-745.3085	-467688.18	-745.3011	-467683.53	-745.2976	-467681.34
5.10.1	-745.3062	-467686.71	-745.3082	-467688.00	-745.3294	-467701.28	-745.3272	-467699.91
5.10.2	-821.7137	-515633.17	-821.7576	-515660.69	-821.7484	-515654.95	-821.7459	-515653.33
5.11	-745.3141	-467691.66	-745.3342	-467704.28	-745.3294	-467701.29	-745.3231	-467697.35
5.12	-745.3137	-467691.42	-745.3342	-467704.28	-745.3294	-467701.29	-745.3272	-467699.91
5.13	-745.2799	-467670.21	-745.3176	-467693.88	-745.3294	-467701.29	-745.3272	-467699.91
5.2	-745.3575	-467718.93	-745.3615	-467721.43	-745.3555	-467717.63	-745.3537	-467716.53
HCN	-93.4352	-58631.47	-93.4368	-58632.51	-93.4388	-58633.75	-93.4376	-58632.98
H₂O	-575.4720	-361114.12	-575.4767	-361117.09	-575.4774	-361117.56	-575.4769	-361117.21
H₃O⁺	-76.8310	-48212.21	-76.7966	-48190.57	-76.8019	-48193.90	-76.7940	-48188.96
Na⁺	-162.2108	-101788.79	-162.2071	-101786.48	-162.2069	-101786.38	-162.2067	-101786.23
NaCN	-255.2095	-160146.40	-255.2077	-160145.27	-255.2087	-160145.90	-255.2074	-160145.06
NaOH	-238.1883	-149465.40	-238.1863	-149464.17	-238.1729	-149455.77	-238.1707	-149454.37

^a Refers to the structure number in Figure 5.27

^b Energies are expressed in Hartrees and kcal mol⁻¹, performed at the DFT level using the 6-31+G(d) level of theory

Table A3.4 Summary of Gibbs free energies for mechanism 3-route 1 continued

Structure number ^a	Energies ^b (B3LYP/6-31+G(d))			
	Carbon Tetrachloride		Dichloromethane	
	Hartrees	kcal mol ⁻¹	Hartrees	kcal mol ⁻¹
5.1	-575.4719	-361114.06	-575.4765	-361116.99
5.3.1	-668.4061	-419431.15	-668.4120	-419434.86
5.3.2	-745.3191	-467694.80	-745.2622	-467659.08
5.4	-668.8940	-419737.32	-668.9021	-419742.44
5.20.1	-745.3127	-467690.79	-745.3229	-467697.21
5.20.2	-821.7132	-515632.85	-821.7263	-515641.07
5.18	-745.2471	-467649.64	-745.3040	-467685.37
5.21				
5.9	-745.2901	-467676.63	-745.3002	-467682.93
5.10.1	-745.3223	-467696.80	-745.3289	-467700.96
5.10.2	-821.7384	-515648.67	-821.7469	-515654.01
5.11	-745.3223	-467696.80	-745.3289	-467700.96
5.12	-745.3223	-467696.80	-745.3289	-467700.96
5.13	-745.3223	-467696.80	-745.3289	-467700.96
5.2	-745.3476	-467712.70	-745.3548	-467717.21
HCN	-93.4340	-58630.70	-93.4379	-58633.15
H₂O	-575.4719	-361114.06	-575.4765	-361116.99
H₃O⁺	-76.7412	-48155.83	-76.7935	-48188.65
Na⁺	-162.1586	-101756.08	-162.1977	-101780.57
NaCN	-255.1862	-160131.74	-255.2041	-160142.98
NaOH	-238.1558	-149445.04	-238.1709	-149454.52

^a Refers to the structure number in Figure 5.27

^b Energies are expressed in Hartrees and kcal mol⁻¹, performed at the DFT level using the 6-31+G(d) level of theory

Table A3.5 Summary of the relative^a energy, enthalpy and entropy in water for mechanism 3-route 1

Species ^b	$\Delta E / \text{kcal mol}^{-1}$	$\Delta H / \text{kcal mol}^{-1}$	$\Delta S / \text{cal K}^{-1} \text{mol}^{-1}$
5.1	0.00	0.00	0.00
5.3.1	27.02	18.11	-9.74
5.3.2	28.32	29.57	-72.32
5.4	3.96	5.14	-40.85
5.20.1	31.95	-8.95	-63.90
5.20.2	15.08	-4.39	-108.96
5.18	-6.71	-1.73	-80.42
5.21			
5.9	10.16	13.04	-80.31
5.10.1	50.13	-3.34	-85.29
5.10.2	22.55	3.98	-116.90
5.11	-10.17	-5.51	-85.13
5.12	31.15	-8.38	-86.38
5.13	16.62	15.71	-76.73
5.2	-40.84	-35.02	-83.47

^a Energies relative to the energy of the starting structure **5.1**

^b Refers to the structure number in Figure 5.27

The energies in water: (ΔE) (in kcal mol^{-1}), enthalpy (ΔH) (in kcal mol^{-1}) and entropy (ΔS) ($\text{cal K}^{-1} \text{mol}^{-1}$) at 298.15 K

Table A3.6 Summary of energy, enthalpy and entropy in water for mechanism 3-route 1

Structure number ^a	Energies ^b (B3LYP/6-31+G(d))				
	Energy (E)		Enthalpy (H)		Entropy (S)
	Hartrees	kcal mol ⁻¹	Hartrees	kcal mol ⁻¹	cal K ⁻¹ mol ⁻¹
5.1	-575.6255	-361210.45	-575.4299	-361087.70	88.61
5.3.1	-668.5766	-419538.19	-668.3875	-419419.52	104.59
5.3.2	-745.4499	-467776.87	-745.2079	-467625.02	109.51
5.4	-669.0729	-419849.60	-668.8535	-419711.95	97.47
5.20.1	-745.4441	-467773.24	-745.2692	-467663.53	117.93
5.20.2	-821.9083	-515755.27	-821.6748	-515608.72	118.01
5.18	-745.5057	-467811.90	-745.2577	-467656.31	101.41
5.21					
5.9	-745.5004	-467808.56	-745.2537	-467653.80	103.16
5.10.1	-745.4151	-467755.06	-745.2603	-467657.92	96.53
5.10.2	-821.8964	-515747.80	-821.6614	-515600.35	-821.66
5.11	-745.5328	-467828.89	-745.2833	-467672.34	98.34
5.12	-745.4453	-467774.03	-745.2683	-467662.97	95.45
5.13	-745.4685	-467788.57	-745.2299	-467638.87	105.09
5.2	-745.4685	-467788.57	-745.2299	-467638.87	105.09
HCN	-93.4322	-58629.57	-93.4124	-58617.14	48.06
H₂O	-76.4373	-47965.16	-76.4128	-47949.75	45.15
H₃O⁺	-76.8388	-48217.10	-76.8081	-48197.81	48.30
Na⁺	-162.1963	-101779.74	-162.1940	-101778.26	35.34
NaCN	-255.1905	-160134.49	-255.1805	-160128.19	61.06
NaOH	-238.1742	-149456.55	-238.1614	-149448.55	56.50

^a Refers to the structure number in Figure 5.27

^b Energies are expressed in Hartrees, kcal mol⁻¹ and cal K⁻¹ mol⁻¹, performed at the DFT level using the 6-31+G(d) level of theory

Table A3.7 Summary of the relative^a energy, enthalpy and entropy in methanol for mechanism 3-route 1

Species ^b	$\Delta E / \text{kcal mol}^{-1}$	$\Delta H / \text{kcal mol}^{-1}$	$\Delta S / \text{cal K}^{-1} \text{mol}^{-1}$
5.1	0.00	0.00	0.00
5.3.1	29.23	17.06	-17.27
5.3.2	29.03	-2.56	-51.88
5.4	4.07	5.26	-39.45
5.20.1	33.12	-8.04	-64.06
5.20.2	16.02	-3.52	-107.21
5.18	-5.82	-0.82	-80.57
5.21			
5.9	10.06	12.91	-79.07
5.10.1	0.10	1.25	-79.07
5.10.2	23.69	-16.94	-108.41
5.11	-8.90	-4.77	-84.18
5.12	16.41	-16.47	-83.93
5.13	18.79	-33.56	-83.70
5.2	-39.11	-33.56	-83.72

^a Energies relative to the energy of the starting structure **5.1**

^b Refers to the structure number in Figure 5.27

The energies in methanol: (ΔE) (in kcal mol^{-1}), enthalpy (ΔH) (in kcal mol^{-1}) and entropy (ΔS) ($\text{cal K}^{-1} \text{mol}^{-1}$) at 298.15 K

Table A3.8 Summary of energy, enthalpy and entropy in methanol for mechanism 3-route 1

Structure number ^a	Energies ^b (B3LYP/6-31+G(d))				
	Energy (E)		Enthalpy (H)		Entropy (S)
	Hartrees	kcal mol ⁻¹	Hartrees	kcal mol ⁻¹	cal K ⁻¹ mol ⁻¹
5.1	-575.6303	-361213.47	-575.4346	-361090.66	88.63
5.3.1	-668.5801	-419540.35	-668.3959	-419424.78	96.86
5.3.2	-745.4554	-467780.33	-745.2655	-467661.17	129.96
5.4	-669.0785	-419853.09	-668.8589	-419715.33	97.49
5.20.1	-745.4489	-467776.24	-745.2742	-467666.66	117.78
5.20.2	-821.9136	-515758.57	-821.6798	-515611.91	119.78
5.18	-745.5109	-467815.18	-745.2627	-467659.43	101.26
5.21					
5.9	-745.5064	-467812.32	-745.2596	-467657.47	103.02
5.10.1	-745.4188	-467757.40	-745.2594	-467657.37	102.73
5.10.2	-821.9013	-515750.90	-821.7012	-515625.33	118.58
5.11	-745.5364	-467831.16	-745.2877	-467675.09	97.91
5.12	-745.4755	-467792.95	-745.2877	-467675.09	97.91
5.13	-745.4717	-467790.57	-745.3149	-467692.18	98.13
5.2	-745.5640	-467848.47	-745.3149	-467692.17	98.12
HCN	-93.4339	-58630.67	-93.4140	-58618.18	48.05
H₂O	-76.4374	-47965.22	-76.4128	-47949.78	45.15
H₃O⁺	-76.8070	-48197.14	-76.7736	-48176.18	48.29
Na⁺	-162.1927	-101777.43	-162.1903	-101775.95	35.34
NaCN	-255.1890	-160133.54	-255.1788	-160127.13	60.84
NaOH	-238.1718	-149455.07	-238.1589	-149446.97	57.68

^a Refers to the structure number in Figure 5.27

^b Energies are expressed in Hartrees, kcal mol⁻¹ and cal K⁻¹ mol⁻¹, performed at the DFT level using the 6-31+G(d) level of theory

Table A3.9 Summary of the relative^a energy, enthalpy and entropy in acetonitrile for mechanism 3-route 1

Species ^b	$\Delta E / \text{kcal mol}^{-1}$	$\Delta H / \text{kcal mol}^{-1}$	$\Delta S / \text{cal K}^{-1} \text{mol}^{-1}$
5.1	0.00	0.00	0.00
5.3.1	32.42	19.22	7.02
5.3.2	28.69	30.47	-67.56
5.4	11.01	13.01	-38.71
5.20.1	34.81	-5.95	-64.26
5.20.2	16.11	-2.73	-108.03
5.18	-3.86	1.19	-80.80
5.21			
5.9	16.98	20.63	-78.37
5.10.1	-1.32	-15.24	-84.49
5.10.2	24.30	-16.19	-108.68
5.11	-3.85	1.18	-84.06
5.12	23.04	-15.24	-84.47
5.13	25.47	-15.24	-84.48
5.2	-36.85	-31.38	-83.78

^a Energies relative to the energy of the starting structure **5.1**

^b Refers to the structure number in Figure 5.27

The energies in acetonitrile: (ΔE) (in kcal mol^{-1}), enthalpy (ΔH) (in kcal mol^{-1}) and entropy (ΔS) ($\text{cal K}^{-1} \text{mol}^{-1}$) at 298.15 K

Table A3.10 Summary of energy, enthalpy and entropy in acetonitrile for mechanism 3-route 1

Structure number ^a	Energies ^b (B3LYP/6-31+G(d))				
	Energy (E)		Enthalpy (H)		Entropy (S)
	Hartrees	kcal mol ⁻¹	Hartrees	kcal mol ⁻¹	cal K ⁻¹ mol ⁻¹
5.1	-575.6312	-361214.05	-575.4353	-361091.09	88.76
5.3.1	-668.5771	-419538.45	-668.3944	-419423.85	121.10
5.3.2	-745.4534	-467779.11	-745.2102	-467626.50	114.41
5.4	-669.0761	-419851.63	-668.8567	-419713.93	97.68
5.20.1	-745.4437	-467772.99	-745.2683	-467662.93	117.72
5.20.2	-821.9056	-515753.54	-821.6707	-515606.16	119.10
5.18	-745.5053	-467811.66	-745.2569	-467655.79	101.18
5.21					
5.9	-745.4987	-467807.51	-745.2521	-467652.76	103.18
5.10.1	-745.4122	-467753.26	-745.2831	-467672.22	97.49
5.10.2	-821.8925	-515745.36	-821.6921	-515619.63	118.46
5.11	-745.5319	-467828.35	-745.2831	-467672.22	97.49
5.12	-745.4624	-467784.76	-745.2831	-467672.22	97.51
5.13	-745.4586	-467782.33	-745.2831	-467672.22	97.50
5.2	-745.5579	-467844.64	-745.3088	-467688.35	98.19
HCN	-93.4359	-58631.89	-93.4160	-58619.42	48.07
H₂O	-76.4321	-47961.86	-76.4075	-47946.46	45.16
H₃O⁺	-76.8146	-48201.90	-76.7796	-48179.93	46.85
Na⁺	-162.1925	-101777.33	-162.1901	-101775.85	35.34
NaCN	-255.1900	-160134.15	-255.1799	-160127.82	60.65
NaOH	-238.1596	-149447.42	-238.1453	-149438.43	58.17

^a Refers to the structure number in Figure 5.27

^b Energies are expressed in Hartrees, kcal mol⁻¹ and cal K⁻¹ mol⁻¹, performed at the DFT level using the 6-31+G(d) level of theory

Table A3.11 Summary of the relative^a energy, enthalpy and entropy in dimethyl sulphoxide for mechanism 3-route 1

Species ^b	$\Delta E / \text{kcal mol}^{-1}$	$\Delta H / \text{kcal mol}^{-1}$	$\Delta S / \text{cal K}^{-1} \text{mol}^{-1}$
5.1	0.00	0.00	0.00
5.3.1	32.29	32.17	-16.97
5.3.2	28.11	29.98	-67.90
5.4	12.31	14.32	-38.21
5.20.1	43.79	5.09	-64.70
5.20.2	15.83	-3.03	-113.63
5.18	-3.64	1.35	-80.23
5.21			
5.9	18.66	22.33	-78.10
5.10.1	-1.34	-15.29	-84.18
5.10.2	24.28	-16.46	-108.59
5.11	-3.01	2.08	-83.74
5.12	23.70	-15.29	-84.18
5.13	26.06	-15.29	-84.18
5.2	-37.15	-31.69	-83.44

^a Energies relative to the energy of the starting structure **5.1**

^b Refers to the structure number in Figure 5.27

The energies in dimethyl sulphoxide: (ΔE) (in kcal mol^{-1}), enthalpy (ΔH) (in kcal mol^{-1}) and entropy (ΔS) ($\text{cal K}^{-1} \text{mol}^{-1}$) at 298.15 K

Table A3.12 Summary of energy, enthalpy and entropy in dimethyl sulphoxide for mechanism 3-route 1

Structure number ^a	Energies ^b (B3LYP/6-31+G(d))				
	Energy (E)		Enthalpy (H)		Entropy (S)
	Hartrees	kcal mol ⁻¹	Hartrees	kcal mol ⁻¹	cal K ⁻¹ mol ⁻¹
5.1	-575.6309	-361213.88	-575.4349	-361090.86	88.36
5.3.1	-668.5759	-419537.74	-668.3723	-419409.97	96.73
5.3.2	-745.4522	-467778.36	-745.2088	-467625.60	113.68
5.4	-669.0740	-419850.31	-668.8545	-419712.57	97.77
5.20.1	-745.4273	-467762.68	-745.2485	-467650.49	116.88
5.20.2	-821.9033	-515752.11	-821.6683	-515604.68	113.10
5.18	-745.5028	-467810.11	-745.2544	-467654.23	101.35
5.21					
5.9	-745.4954	-467805.42	-745.2487	-467650.62	103.04
5.10.1	-745.4095	-467751.53	-745.2809	-467670.87	97.40
5.10.2	-821.8898	-515743.65	-821.6897	-515618.11	118.14
5.11	-745.5299	-467827.09	-745.2809	-467670.87	97.40
5.12	-745.4593	-467782.77	-745.2809	-467670.87	97.39
5.13	-745.4555	-467780.41	-745.2809	-467670.87	97.39
5.2	-745.5562	-467843.62	-745.3071	-467687.27	98.13
HCN	-93.4346	-58631.12	-93.4148	-58618.65	48.06
H₂O	-76.4315	-47961.46	-76.4069	-47946.07	45.15
H₃O⁺	-76.8077	-48197.58	-76.7728	-48175.64	44.67
Na⁺	-162.1922	-101777.17	-162.1899	-101775.69	35.34
NaCN	-255.1887	-160133.32	-255.1786	-160126.97	60.67
NaOH	-238.1574	-149446.04	-238.1430	-149437.02	58.20

^a Refers to the structure number in Figure 5.27

^b Energies are expressed in Hartrees, kcal mol⁻¹ and cal K⁻¹ mol⁻¹, performed at the DFT level using the 6-31+G(d) level of theory

Table A3.13 Summary of the relative^a energy, enthalpy and entropy in carbon tetrachloride for mechanism 3-route 1

Species ^b	$\Delta E / \text{kcal mol}^{-1}$	$\Delta H / \text{kcal mol}^{-1}$	$\Delta S / \text{cal K}^{-1} \text{mol}^{-1}$
5.1	0.00	0.00	0.00
5.3.1	70.79	59.46	2.97
5.3.2	27.64	-8.39	-50.05
5.4	6.26	8.15	-39.77
5.20.1	31.72	-8.30	-63.19
5.20.2	10.65	-8.20	-111.47
5.18	-7.67	-2.53	-80.67
5.21			
5.9	9.49	13.53	-79.58
5.10.1	49.47	-20.76	-84.80
5.10.2	16.95	-23.83	-110.85
5.11	-13.43	-8.47	-85.73
5.12	26.50	-20.76	-84.80
5.13	27.80	-20.76	-84.80
5.2	-41.99	-36.44	-84.08

^a Energies relative to the energy of the starting structure **5.1**

^b Refers to the structure number in Figure 5.27

The energies in carbon tetrachloride: (ΔE) (in kcal mol^{-1}), enthalpy (ΔH) (in kcal mol^{-1}) and entropy (ΔS) ($\text{cal K}^{-1} \text{mol}^{-1}$) at 298.15 K

Table A3.14 Summary of energy, enthalpy and entropy in carbon tetrachloride for mechanism 3-route 1

Structure number ^a	Energies ^b (B3LYP/6-31+G(d))				
	Energy (E)		Enthalpy (H)		Entropy (S)
	Hartrees	kcal mol ⁻¹	Hartrees	kcal mol ⁻¹	cal K ⁻¹ mol ⁻¹
5.1	-575.6262	-361210.92	-575.4298	-361087.66	88.57
5.3.1	-668.5378	-419513.83	-668.3507	-419396.39	116.58
5.3.2	-745.4401	-467770.72	-745.2565	-467655.51	131.78
5.4	-669.0675	-419846.24	-668.8475	-419708.14	97.86
5.20.1	-745.4336	-467766.65	-745.2563	-467655.42	118.643
5.20.2	-821.8941	-515746.37	-821.6583	-515598.42	115.49
5.18	-745.4963	-467806.04	-745.2471	-467649.64	101.16
5.21					
5.9	-745.4894	-467801.65	-745.2411	-467645.87	103.18
5.10.1	-745.4053	-467748.90	-745.2762	-467667.87	97.03
5.10.2	-821.8841	-515740.07	-821.6833	-515614.05	116.12
5.11	-745.5259	-467824.58	-745.2762	-467667.87	97.03
5.12	-745.4419	-467771.86	-745.2762	-467667.87	97.03
5.13	-745.4398	-467770.57	-745.2762	-467667.87	97.03
5.2	-745.5510	-467840.36	-745.3012	-467683.55	97.75
HCN	-93.4309	-58628.79	-93.4111	-58616.35	48.12
H₂O	-76.4270	-47958.65	-76.4022	-47943.11	45.13
H₃O⁺	-76.7556	-48164.90	-76.7200	-48142.51	44.65
Na⁺	-162.1442	-101747.03	-162.1418	-101745.55	35.34
NaCN	-255.1686	-160120.72	-255.1575	-160113.74	60.38
NaOH	-238.1443	-149437.81	-238.1290	-149428.21	56.46

^a Refers to the structure number in Figure 5.27

^b Energies are expressed in Hartrees, kcal mol⁻¹ and cal K⁻¹ mol⁻¹, performed at the DFT level using the 6-31+G(d) level of theory

Table A3.15 Summary of the relative^a energy, enthalpy and entropy in dichloromethane for mechanism 3-route 1

Species ^b	$\Delta E / \text{kcal mol}^{-1}$	$\Delta H / \text{kcal mol}^{-1}$	$\Delta S / \text{cal K}^{-1} \text{mol}^{-1}$
5.1	0.00	0.00	0.00
5.3.1	39.79	39.49	-16.93
5.3.2	28.64	30.38	-67.38
5.4	9.34	11.25	-37.47
5.20.1	34.08	-6.64	-63.625
5.20.2	14.95	-4.05	-107.10
5.18	-4.95	0.15	-80.58
5.21			
5.9	14.53	18.31	-77.21
5.10.1	53.08	-16.56	-84.36
5.10.2	22.41	-17.65	-109.35
5.11	-6.44	-1.43	-82.97
5.12	23.35	-16.56	-84.35
5.13	25.60	-16.56	-84.35
5.2	-38.09	-32.56	-83.53

^a Energies relative to the energy of the starting structure **5.1**

^b Refers to the structure number in Figure 5.27

The energies in dichloromethane: (ΔE) (in kcal mol^{-1}), enthalpy (ΔH) (in kcal mol^{-1}) and entropy (ΔS) ($\text{cal K}^{-1} \text{mol}^{-1}$) at 298.15 K

Table A3.16 Summary of energy, enthalpy and entropy in dichloromethane for mechanism 3-route 1

Structure number ^a	Energies ^b (B3LYP/6-31+G(d))				
	Energy (E)		Enthalpy (H)		Entropy (S)
	Hartrees	kcal mol ⁻¹	Hartrees	kcal mol ⁻¹	cal K ⁻¹ mol ⁻¹
5.1	-575.6306	-361213.64	-575.4345	-361090.61	88.48
5.3.1	-668.5695	-419533.74	-668.3660	-419405.99	96.84
5.3.2	-745.4511	-467777.64	-745.2078	-467625.00	114.33
5.4	-669.0753	-419851.09	-668.8557	-419713.31	97.70
5.20.1	-745.4424	-467772.20	-745.2668	-467662.01	118.08
5.20.2	-821.9042	-515752.68	-821.6694	-515605.37	119.76
5.18	-745.5046	-467811.23	-745.2560	-467655.22	101.12
5.21					
5.9	-745.4983	-467807.24	-745.2512	-467652.19	103.11
5.10.1	-745.4121	-467753.20	-745.2826	-467671.93	97.35
5.10.2	-821.8923	-515745.22	-821.6911	-515618.97	117.51
5.11	-745.5317	-467828.22	-745.2826	-467671.93	97.36
5.12	-745.4595	-467782.93	-745.2826	-467671.93	97.35
5.13	-745.4559	-467780.68	-745.2826	-467671.93	97.36
5.2	-745.5574	-467844.37	-745.3081	-467687.94	98.17
HCN	-93.4349	-58631.29	-93.4150	-58618.82	48.08
H₂O	-76.4313	-47961.35	-76.4067	-47945.94	45.15
H₃O⁺	-76.8067	-48196.90	-76.7712	-48174.68	46.85
Na⁺	-162.1832	-101771.52	-162.1809	-101770.04	35.34
NaCN	-255.1856	-160131.41	-255.1753	-160124.90	60.64
NaOH	-238.1573	-149445.98	-238.1429	-149436.90	59.09

^a Refers to the structure number in Figure 5.27

^b Energies are expressed in Hartrees, kcal mol⁻¹ and cal K⁻¹ mol⁻¹, performed at the DFT level using the 6-31+G(d) level of theory

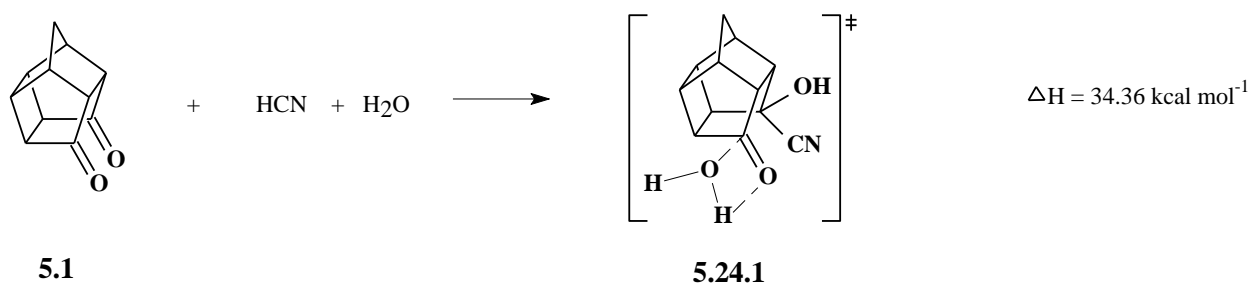
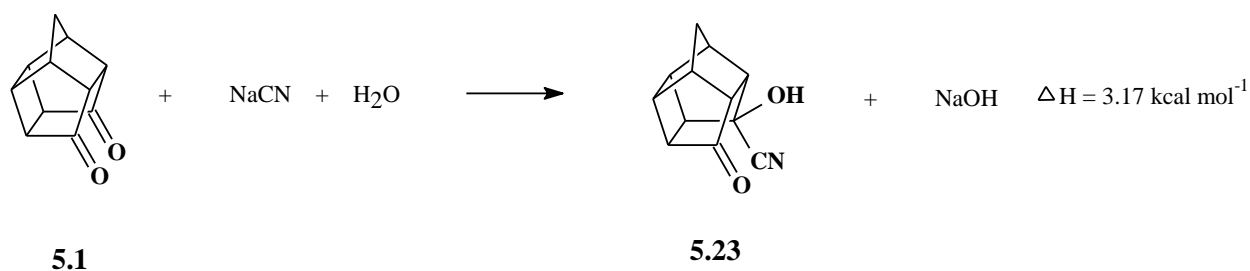
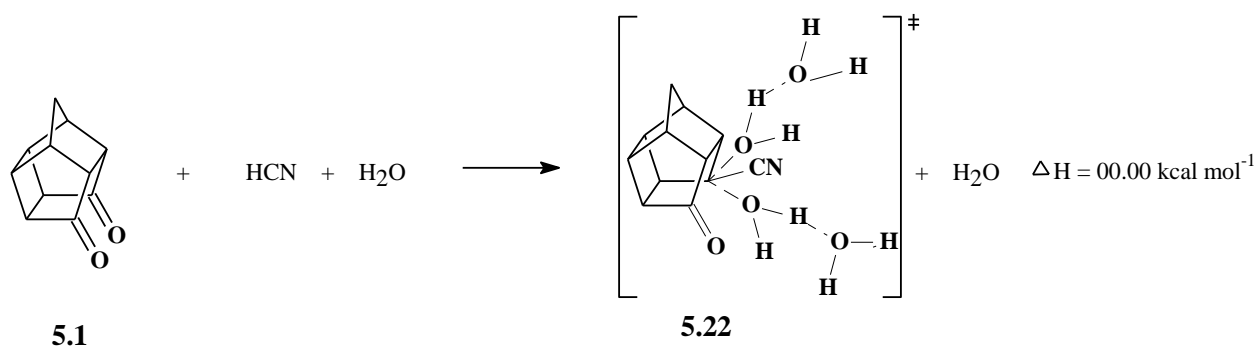
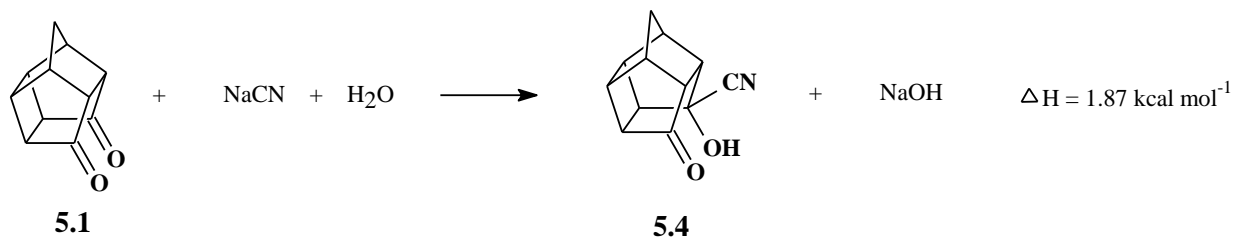
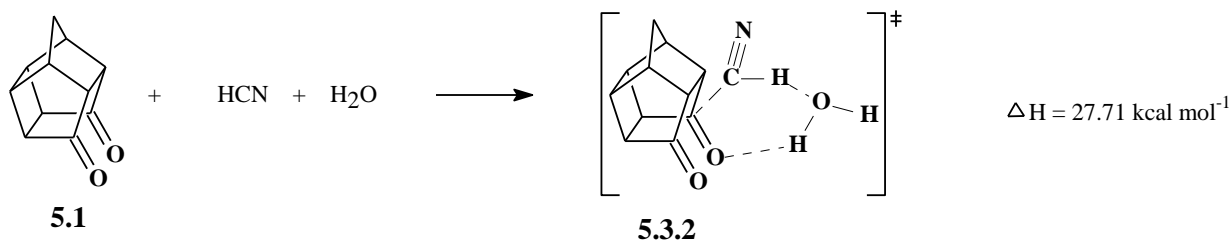
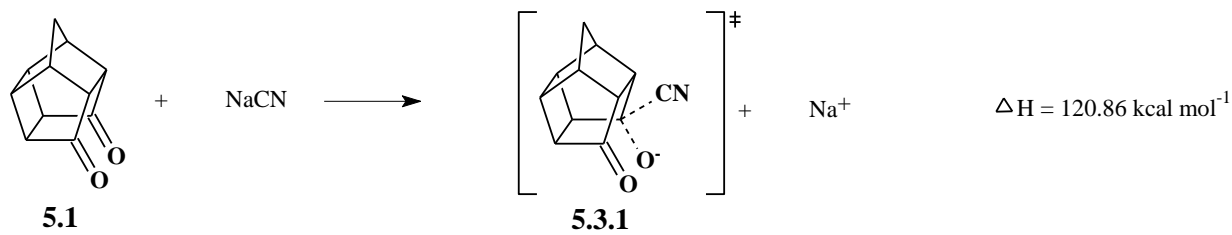
Table A3.17 Summary of energies for mechanism 3-route 2

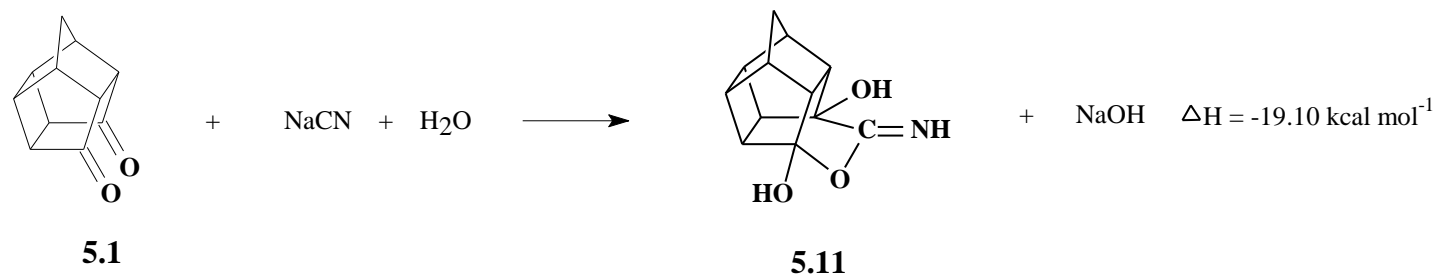
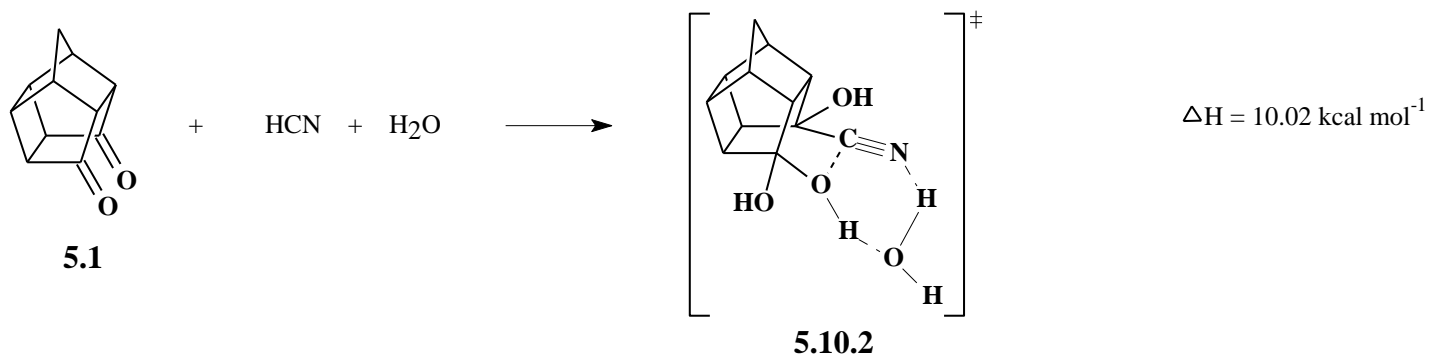
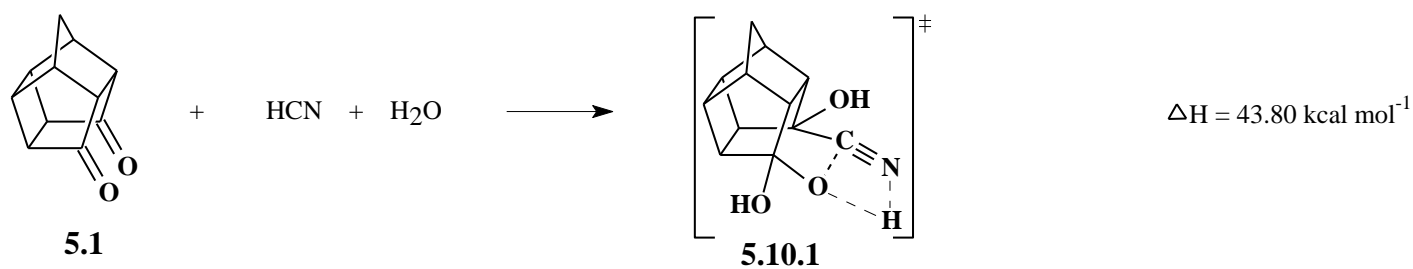
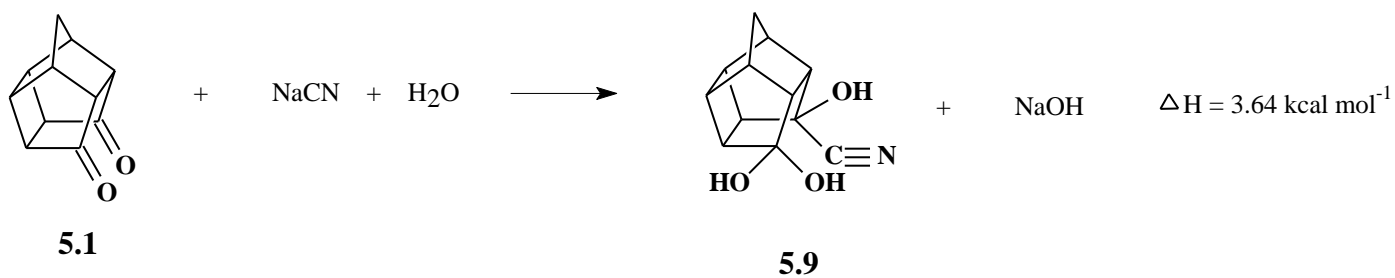
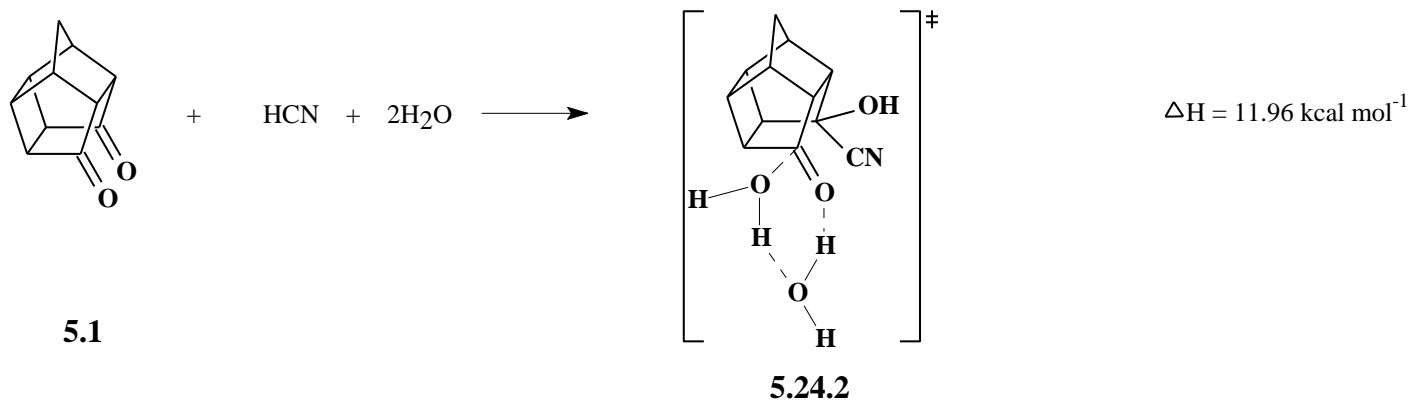
Structure number ^a	Energies ^b (B3LYP/6-31+G(d))		Energies ^a (MP2/6-31+G(d))	
	Hartrees	kcal mol ⁻¹	Hartrees	kcal mol ⁻¹
5.1	-575.6083	-361199.69	-573.8593	-360102.18
5.3.1	-668.4840	-419480.07	-666.4795	-418222.19
5.3.2	-745.3978	-467744.21	-740.9077	-464926.64
5.4	-669.0503	-419835.41	-667.0495	-418579.88
5.22				
5.23	-669.0481	-419834.03	-667.0479	-418578.91
5.24.1	-745.4058	-467749.22	-743.1956	-466362.28
5.24.2	-821.8656	-515728.45	-819.4453	-514209.74
5.9	-745.4737	-467791.84	-743.2682	-466407.84
5.10.1	-745.3908	-467739.81	-743.1777	-466351.07
5.10.2	-821.8691	-515730.69	-819.4450	-514209.51
5.11	-745.5114	-467815.49	-743.2932	-466423.53
5.12	-745.4161	-467755.71	-743.1938	-466361.18
5.13	-745.4161	-467755.69	-743.1934	-466360.90
5.2	-745.5343	-467829.85	-743.3177	-466438.89
HCN	-93.4286	-58627.34	-93.1640	-58461.31
H₂O	-76.4226	-47955.89	-76.2098	-47822.35
H₃O⁺	-76.6885	-48122.73	-76.4736	-47987.93
Na⁺	-162.0812	-101707.52	-161.6593	-101442.74
NaCN	-255.1508	-160109.58	-254.4607	-159676.48
NaOH	-238.1314	-149429.72	-237.4963	-149031.17

^a Refers to the structure number in Figure 5.32.

^b Energies are expressed in Hartrees and kcal mol⁻¹, performed at the DFT and MP2 level using the 6-31+G(d) level of theory.

Scheme of reaction for mechanism 3-route 2





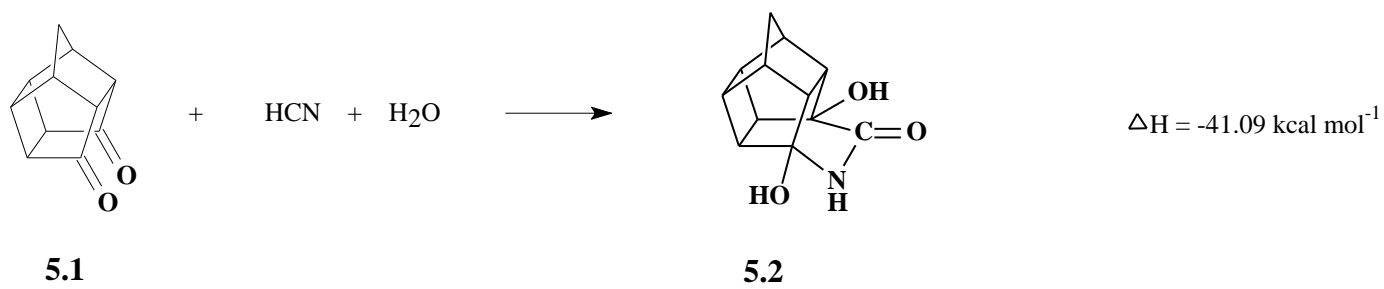
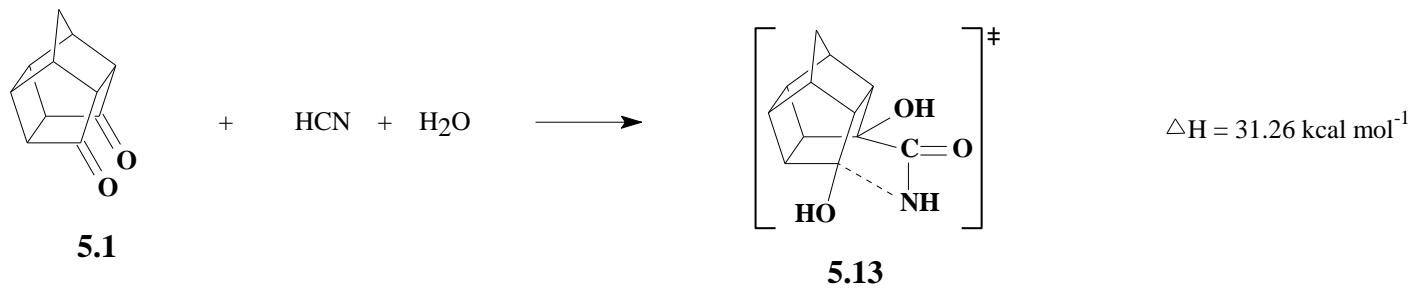
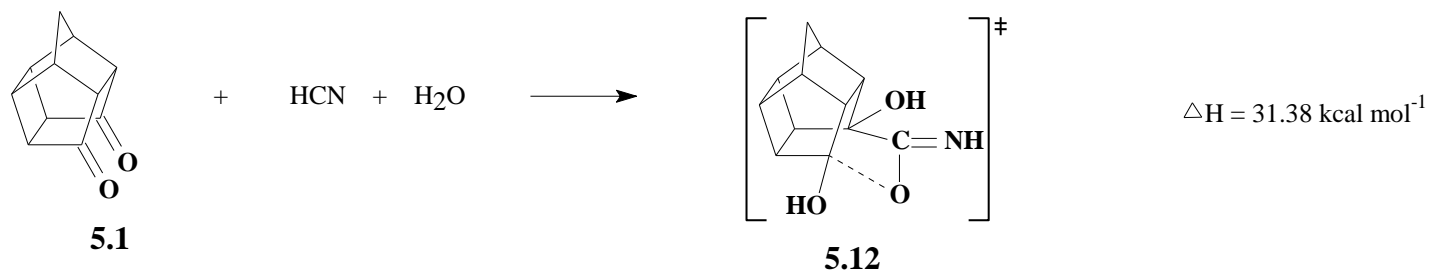


Table A3.18 Summary of thermodynamic properties for mechanism 3-route 2

Structure number ^a	Energies ^b (B3LYP/6-31+G(d))				
	Enthalpy (H)		Free Energy (G)		Entropy (S)
	(Hartrees)	(kcal mol ⁻¹)	(Hartrees)	(kcal mol ⁻¹)	(cal K ⁻¹ mol ⁻¹)
5.1	-575.4116	-361076.24	-575.4536	-361102.61	88.44
5.3.1	-668.2794	-419351.69	-668.3270	-419381.53	100.08
5.3.2	-745.1569	-467593.05	-745.2108	-467626.83	113.27
5.4	-668.8299	-419697.12	-668.8764	-419726.32	97.94
5.22					
5.23	-668.8278	-419695.82	-668.8745	-419725.13	98.30
5.24.1	-745.1633	-467597.05	-745.2130	-467628.23	104.58
5.24.2	-821.5967	-515559.73	-821.6497	-515593.00	111.60
5.9	-745.2248	-467635.63	-745.2738	-467666.42	103.27
5.10.1	-745.1483	-467587.61	-745.1955	-467617.28	99.51
5.10.2	-821.5998	-515561.68	-821.6509	-515593.74	107.53
5.11	-745.2610	-467658.37	-745.3071	-467687.27	96.94
5.12	-745.1680	-467600.03	-745.2153	-467629.68	99.46
5.13	-745.1682	-467600.15	-745.2154	-467629.76	99.32
5.2	-745.2835	-467672.51	-745.3298	-467701.56	97.43
HCN	-93.4088	-58614.90	-93.4317	-58629.26	48.14
H₂O	-76.3977	-47940.28	-76.4191	-47953.73	45.12
H₃O⁺	-76.6523	-48100.07	-76.6742	-48113.79	46.01
Na⁺	-162.0789	-101706.04	-162.0957	-101716.58	35.34
NaCN	-255.1393	-160102.35	-255.1679	-160120.28	60.14
NaOH	-238.1157	-149419.88	-238.1422	-149436.48	55.71

^a Refers to the structure number in Figure 5.32.

^b Energies are expressed in Hartrees and kcal mol⁻¹, performed at the DFT level using the 6-31+G(d) level of theory.

Table A3.19 Summary of Gibbs free energies for mechanism 3-route 2

Structure number ^a	Energies ^b (B3LYP/6-31+G(d))							
	Water		Methanol		CH ₃ CN		DMSO	
	Hartrees	kcal mol ⁻¹	Hartrees	kcal mol ⁻¹	Hartrees	kcal mol ⁻¹	Hartrees	kcal mol ⁻¹
5.1	-575.4720	-361114.12	-575.4767	-361117.09	-575.4774	-361117.56	-575.4769	-361117.21
5.3.1	-668.4372	-419450.70	-668.4419	-419453.66	-668.4520	-419459.95	-668.4183	-419438.81
5.3.2	-745.2599	-467657.67	-745.3272	-467699.92	-745.2646	-467660.62	-745.2628	-467659.49
5.4	-668.8999	-419741.01	-668.9053	-419744.40	-668.9031	-419743.06	-668.9010	-419741.72
5.22								
5.23	-668.8988	-419740.37	-668.9042	-419743.75	-668.9020	-419742.36	-668.8999	-419741.03
5.24.1	-745.3236	-467697.64	-745.3285	-467700.74	-745.3229	-467697.22	-745.3203	-467695.54
5.24.2	-821.7266	-515641.26	-821.7326	-515645.03	-821.7192	-515636.62	-821.7160	-515634.60
5.9	-745.3027	-467684.55	-745.3085	-467688.18	-745.3011	-467683.53	-745.2976	-467681.34
5.10.1	-745.3062	-467686.71	-745.3082	-467688.00	-745.3294	-467701.28	-745.3272	-467699.91
5.10.2	-821.7137	-515633.17	-821.7576	-515660.69	-821.7484	-515654.95	-821.7459	-515653.33
5.11	-745.3141	-467691.66	-745.3342	-467704.28	-745.3294	-467701.29	-745.3231	-467697.35
5.12	-745.3137	-467691.42	-745.3342	-467704.28	-745.3294	-467701.29	-745.3272	-467699.91
5.13	-745.2799	-467670.21	-745.3176	-467693.88	-745.3294	-467701.29	-745.3272	-467699.91
5.2	-745.3575	-467718.93	-745.3615	-467721.43	-745.3555	-467717.63	-745.3537	-467716.53
HCN	-93.4352	-58631.47	-93.4368	-58632.51	-93.4388	-58633.75	-93.4376	-58632.98
H₂O	-575.4720	-361114.12	-575.4767	-361117.09	-575.4774	-361117.56	-575.4769	-361117.21
H₃O⁺	-76.8310	-48212.21	-76.7966	-48190.57	-76.8019	-48193.90	-76.7940	-48188.96
Na⁺	-162.2108	-101788.79	-162.2071	-101786.48	-162.2069	-101786.38	-162.2067	-101786.23
NaCN	-255.2095	-160146.40	-255.2077	-160145.27	-255.2087	-160145.90	-255.2074	-160145.06
NaOH	-238.1883	-149465.40	-238.1863	-149464.17	-238.1729	-149455.77	-238.1707	-149454.37

^a Refers to the structure number in Figure 5.32.

^b Energies are expressed in Hartrees and kcal mol⁻¹, performed at the DFT level using the 6-31+G(d) level of theory.

Table A3.20 Summary of Gibbs free energies for mechanism 3-route 2 continued

Structure number ^a	Energies ^b (B3LYP/6-31+G(d))			
	Carbon Tetrachloride		Dichloromethane	
	Hartrees	kcal mol ⁻¹	Hartrees	kcal mol ⁻¹
5.1	-575.4719	-361114.06	-575.4765	-361116.99
5.3.1	-668.4061	-419431.15	-668.4120	-419434.86
5.3.2	-745.3191	-467694.80	-745.2622	-467659.08
5.4	-668.8940	-419737.32	-668.9021	-419742.44
5.22				
5.23	-668.8921	-419736.12	-668.9006	-419741.50
5.24.1	-745.3097	-467688.89	-745.2845	-467646.56
5.24.2	-821.7281	-515642.19	-821.7178	-515635.72
5.9	-745.2901	-467676.63	-745.3002	-467682.93
5.10.1	-745.3223	-467696.80	-745.3289	-467700.96
5.10.2	-821.7384	-515648.67	-821.7469	-515654.01
5.11	-745.3223	-467696.80	-745.3289	-467700.96
5.12	-745.3223	-467696.80	-745.3289	-467700.96
5.13	-745.3223	-467696.80	-745.3289	-467700.96
5.2	-745.3476	-467712.70	-745.3548	-467717.21
HCN	-93.4340	-58630.70	-93.4379	-58633.15
H₂O	-575.4719	-361114.06	-575.4765	-361116.99
H₃O⁺	-76.7412	-48155.83	-76.7935	-48188.65
Na⁺	-162.1586	-101756.08	-162.1977	-101780.57
NaCN	-255.1862	-160131.74	-255.2041	-160142.98
NaOH	-238.1558	-149445.04	-238.1709	-149454.52

^a Refers to the structure number in Figure 5.32.

^b Energies are expressed in Hartrees and kcal mol⁻¹, performed at the DFT level using the 6-31+G(d) level of theory.

Table A3.21 Summary of the relative^a energy, enthalpy and entropy in water for mechanism 3-route 2

Species ^b	$\Delta E / \text{kcal mol}^{-1}$	$\Delta H / \text{kcal mol}^{-1}$	$\Delta S / \text{cal K}^{-1} \text{mol}^{-1}$
5.1	0.00	0.00	0.00
5.3.1	27.02	18.11	-9.74
5.3.2	28.32	29.57	-72.32
5.4	3.96	5.14	-40.85
5.22			
5.23	5.31	5.96	-40.22
5.24.1	36.72	-7.94	-64.03
5.24.2	20.76	-1.01	-106.53
5.9	10.16	13.04	-80.31
5.10.1	50.13	-3.34	-85.29
5.10.2	22.55	3.98	-116.90
5.11	-10.17	-5.51	-85.13
5.12	31.15	-8.38	-86.38
5.13	16.62	15.71	-76.73
5.2	-40.84	-35.02	-83.47

^a Energies relative to the energy of the starting structure **5.1**

^b Refers to the structure number in Figure 5.32

The energies in water: (ΔE) (in kcal mol^{-1}), enthalpy (ΔH) (in kcal mol^{-1}) and entropy (ΔS) ($\text{cal K}^{-1} \text{mol}^{-1}$) at 298.15 K

**Table A3.22 Summary of energy, enthalpy and entropy in water for mechanism 3-
route 2**

Structure number ^a	Energies ^b (B3LYP/6-31+G(d))				
	Energy (E)		Enthalpy (H)		Entropy (S)
	Hartrees	kcal mol ⁻¹	Hartrees	kcal mol ⁻¹	cal K ⁻¹ mol ⁻¹
5.1	-575.6255	-361210.45	-575.4299	-361087.70	88.61
5.3.1	-668.5766	-419538.19	-668.3875	-419419.52	104.59
5.3.2	-745.4499	-467776.87	-745.2079	-467625.02	109.51
5.4	-669.0729	-419849.60	-668.8535	-419711.95	97.47
5.22					
5.23	-669.0707	-419848.25	-668.8522	-419711.12	98.09
5.24.1	-745.4365	-467768.47	-745.2676	-467662.52	117.79
5.24.2	-821.8992	-515749.59	-821.6694	-515605.34	120.45
5.9	-745.5004	-467808.56	-745.2537	-467653.80	103.16
5.10.1	-745.4151	-467755.06	-745.2603	-467657.92	96.53
5.10.2	-821.8964	-515747.80	-821.6614	-515600.35	-821.66
5.11	-745.5328	-467828.89	-745.2833	-467672.34	98.34
5.12	-745.4453	-467774.03	-745.2683	-467662.97	95.45
5.13	-745.4685	-467788.57	-745.2299	-467638.87	105.09
5.2	-745.4685	-467788.57	-745.2299	-467638.87	105.09
HCN	-93.4322	-58629.57	-93.4124	-58617.14	48.06
H₂O	-76.4373	-47965.16	-76.4128	-47949.75	45.15
H₃O⁺	-76.8388	-48217.10	-76.8081	-48197.81	48.30
Na⁺	-162.1963	-101779.74	-162.1940	-101778.26	35.34
NaCN	-255.1905	-160134.49	-255.1805	-160128.19	61.06
NaOH	-238.1742	-149456.55	-238.1614	-149448.55	56.50

^a Refers to the structure number in Figure 5.32

^b Energies are expressed in Hartrees, kcal mol⁻¹ and cal K⁻¹ mol⁻¹, performed at the DFT level using the 6-31+G(d) level of theory

Table A3.23 Summary of the relative^a energy, enthalpy and entropy in methanol for mechanism 3-route 2

Species ^b	$\Delta E / \text{kcal mol}^{-1}$	$\Delta H / \text{kcal mol}^{-1}$	$\Delta S / \text{cal K}^{-1} \text{mol}^{-1}$
5.1	0.00	0.00	0.00
5.3.1	29.23	17.06	-17.27
5.3.2	29.03	-2.56	-51.88
5.4	4.07	5.26	-39.45
5.22			
5.23	2.53	3.23	-38.48
5.24.1	37.40	-6.89	-63.69
5.24.2	21.32	-0.37	-105.37
5.9	10.06	12.91	-79.07
5.10.1	0.10	1.25	-79.07
5.10.2	23.69	-16.94	-108.41
5.11	-8.90	-4.77	-84.18
5.12	16.41	-16.47	-83.93
5.13	18.79	-33.56	-83.70
5.2	-39.11	-33.56	-83.72

^a Energies relative to the energy of the starting structure **5.1**

^b Refers to the structure number in Figure 5.32

The energies in methanol: (ΔE) (in kcal mol^{-1}), enthalpy (ΔH) (in kcal mol^{-1}) and entropy (ΔS) ($\text{cal K}^{-1} \text{mol}^{-1}$) at 298.15 K

**Table A3.24 Summary of energy, enthalpy and entropy in methanol for mechanism 3-
route 2**

Structure number ^a	Energies ^b (B3LYP/6-31+G(d))				
	Energy (E)		Enthalpy (H)		Entropy (S)
	Hartrees	kcal mol ⁻¹	Hartrees	kcal mol ⁻¹	cal K ⁻¹ mol ⁻¹
5.1	-575.6303	-361213.47	-575.4346	-361090.66	88.63
5.3.1	-668.5801	-419540.35	-668.3959	-419424.78	96.86
5.3.2	-745.4554	-467780.33	-745.2655	-467661.17	129.96
5.4	-669.0785	-419853.09	-668.8589	-419715.33	97.49
5.22					
5.23	-669.0761	-419851.61	-668.8575	-419714.41	98.44
5.24.1	-745.4420	-467771.96	-745.2724	-467665.51	118.15
5.24.2	-821.9051	-515753.27	-821.6748	-515608.77	121.62
5.9	-745.5064	-467812.32	-745.2596	-467657.47	103.02
5.10.1	-745.4188	-467757.40	-745.2594	-467657.37	102.73
5.10.2	-821.9013	-515750.90	-821.7012	-515625.33	118.58
5.11	-745.5364	-467831.16	-745.2877	-467675.09	97.91
5.12	-745.4755	-467792.95	-745.2877	-467675.09	97.91
5.13	-745.4717	-467790.57	-745.3149	-467692.18	98.13
5.2	-745.5640	-467848.47	-745.3149	-467692.17	98.12
HCN	-93.4339	-58630.67	-93.4140	-58618.18	48.05
H₂O	-76.4374	-47965.22	-76.4128	-47949.78	45.15
H₃O⁺	-76.8070	-48197.14	-76.7736	-48176.18	48.29
Na⁺	-162.1927	-101777.43	-162.1903	-101775.95	35.34
NaCN	-255.1890	-160133.54	-255.1788	-160127.13	60.84
NaOH	-238.1718	-149455.07	-238.1589	-149446.97	57.68

^a Refers to the structure number in Figure 5.32

^b Energies are expressed in Hartrees, kcal mol⁻¹ and cal K⁻¹ mol⁻¹, performed at the DFT level using the 6-31+G(d) level of theory

Table A3.25 Summary of the relative^a energy, enthalpy and entropy in acetonitrile for mechanism 3-route 2

Species ^b	$\Delta E / \text{kcal mol}^{-1}$	$\Delta H / \text{kcal mol}^{-1}$	$\Delta S / \text{cal K}^{-1} \text{mol}^{-1}$
5.1	0.00	0.00	0.00
5.3.1	32.42	19.22	7.02
5.3.2	28.69	30.47	-67.56
5.4	11.01	13.01	-38.71
5.22			
5.23	12.28	13.88	-38.12
5.24.1	40.44	-4.74	-62.89
5.24.2	22.36	1.86	-109.58
5.9	16.98	20.63	-78.37
5.10.1	-1.32	-15.24	-84.49
5.10.2	24.30	-16.19	-108.68
5.11	-3.85	1.18	-84.06
5.12	23.04	-15.24	-84.47
5.13	25.47	-15.24	-84.48
5.2	-36.85	-31.38	-83.78

^a Energies relative to the energy of the starting structure **5.1**

^b Refers to the structure number in Figure 5.32

The energies in acetonitrile: (ΔE) (in kcal mol^{-1}), enthalpy (ΔH) (in kcal mol^{-1}) and entropy (ΔS) ($\text{cal K}^{-1} \text{mol}^{-1}$) at 298.15 K

Table A3.26 Summary of energy, enthalpy and entropy in acetonitrile for mechanism 3-route 2

Structure number ^a	Energies ^b (B3LYP/6-31+G(d))				
	Energy (E)		Enthalpy (H)		Entropy (S)
	Hartrees	kcal mol ⁻¹	Hartrees	kcal mol ⁻¹	cal K ⁻¹ mol ⁻¹
5.1	-575.6312	-361214.05	-575.4353	-361091.09	88.76
5.3.1	-668.5771	-419538.45	-668.3944	-419423.85	121.10
5.3.2	-745.4534	-467779.11	-745.2102	-467626.50	114.41
5.4	-669.0761	-419851.63	-668.8567	-419713.93	97.68
5.22					
5.23	-669.0741	-419850.36	-668.8553	-419713.06	98.28
5.24.1	-745.4347	-467767.36	-745.2664	-467661.72	119.09
5.24.2	-821.8956	-515747.30	-821.6634	-515601.58	117.55
5.9	-745.4987	-467807.51	-745.2521	-467652.76	103.18
5.10.1	-745.4122	-467753.26	-745.2831	-467672.22	97.49
5.10.2	-821.8925	-515745.36	-821.6921	-515619.63	118.46
5.11	-745.5319	-467828.35	-745.2831	-467672.22	97.49
5.12	-745.4624	-467784.76	-745.2831	-467672.22	97.51
5.13	-745.4586	-467782.33	-745.2831	-467672.22	97.50
5.2	-745.5579	-467844.64	-745.3088	-467688.35	98.19
HCN	-93.4359	-58631.89	-93.4160	-58619.42	48.07
H₂O	-76.4321	-47961.86	-76.4075	-47946.46	45.16
H₃O⁺	-76.8146	-48201.90	-76.7796	-48179.93	46.85
Na⁺	-162.1925	-101777.33	-162.1901	-101775.85	35.34
NaCN	-255.1900	-160134.15	-255.1799	-160127.82	60.65
NaOH	-238.1596	-149447.42	-238.1453	-149438.43	58.17

^a Refers to the structure number in Figure 5.32

^b Energies are expressed in Hartrees, kcal mol⁻¹ and cal K⁻¹ mol⁻¹, performed at the DFT level using the 6-31+G(d) level of theory

Table A3.27 Summary of the relative^a energy, enthalpy and entropy in dimethyl sulphoxide for mechanism 3-route 2

Species ^b	$\Delta E / \text{kcal mol}^{-1}$	$\Delta H / \text{kcal mol}^{-1}$	$\Delta S / \text{cal K}^{-1} \text{mol}^{-1}$
5.1	0.00	0.00	0.00
5.3.1	32.29	32.17	-16.97
5.3.2	28.11	29.98	-67.90
5.4	12.31	14.32	-38.21
5.22			
5.23	13.49	15.14	-37.76
5.24.1	40.83	-4.63	-63.08
5.24.2	22.52	2.16	-108.97
5.9	18.66	22.33	-78.10
5.10.1	-1.34	-15.29	-84.18
5.10.2	24.28	-16.46	-108.59
5.11	-3.01	2.08	-83.74
5.12	23.70	-15.29	-84.18
5.13	26.06	-15.29	-84.18
5.2	-37.15	-31.69	-83.44

^a Energies relative to the energy of the starting structure **5.1**

^b Refers to the structure number in Figure 5.32

The energies in dimethyl sulphoxide: (ΔE) (in kcal mol^{-1}), enthalpy (ΔH) (in kcal mol^{-1}) and entropy (ΔS) ($\text{cal K}^{-1} \text{mol}^{-1}$) at 298.15 K

Table A3.28 Summary of energy, enthalpy and entropy in dimethyl sulphoxide for mechanism 3-route 2

Structure number ^a	Energies ^b (B3LYP/6-31+G(d))				
	Energy (E)		Enthalpy (H)		Entropy (S)
	Hartrees	kcal mol ⁻¹	Hartrees	kcal mol ⁻¹	cal K ⁻¹ mol ⁻¹
5.1	-575.6309	-361213.88	-575.4349	-361090.86	88.36
5.3.1	-668.5759	-419537.74	-668.3723	-419409.97	96.73
5.3.2	-745.4522	-467778.36	-745.2088	-467625.60	113.68
5.4	-669.0740	-419850.31	-668.8545	-419712.57	97.77
5.22					
5.23	-669.0721	-419849.13	-668.8532	-419711.74	98.22
5.24.1	-745.4320	-467765.64	-745.2640	-467660.21	118.49
5.24.2	-821.8926	-515745.41	-821.6600	-515599.49	117.76
5.9	-745.4954	-467805.42	-745.2487	-467650.62	103.04
5.10.1	-745.4095	-467751.53	-745.2809	-467670.87	97.40
5.10.2	-821.8898	-515743.65	-821.6897	-515618.11	118.14
5.11	-745.5299	-467827.09	-745.2809	-467670.87	97.40
5.12	-745.4593	-467782.77	-745.2809	-467670.87	97.39
5.13	-745.4555	-467780.41	-745.2809	-467670.87	97.39
5.2	-745.5562	-467843.62	-745.3071	-467687.27	98.13
HCN	-93.4346	-58631.12	-93.4148	-58618.65	48.06
H₂O	-76.4315	-47961.46	-76.4069	-47946.07	45.15
H₃O⁺	-76.8077	-48197.58	-76.7728	-48175.64	44.67
Na⁺	-162.1922	-101777.17	-162.1899	-101775.69	35.34
NaCN	-255.1887	-160133.32	-255.1786	-160126.97	60.67
NaOH	-238.1574	-149446.04	-238.1430	-149437.02	58.20

^a Refers to the structure number in Figure 5.32

^b Energies are expressed in Hartrees, kcal mol⁻¹ and cal K⁻¹ mol⁻¹, performed at the DFT level using the 6-31+G(d) level of theory

Table A3.29 Summary of the relative^a energy, enthalpy and entropy in carbon tetrachloride for mechanism 3-route 2

Species ^b	$\Delta E / \text{kcal mol}^{-1}$	$\Delta H / \text{kcal mol}^{-1}$	$\Delta S / \text{cal K}^{-1} \text{mol}^{-1}$
5.1	0.00	0.00	0.00
5.3.1	70.79	59.46	2.97
5.3.2	27.64	-8.39	-50.05
5.4	6.26	8.15	-39.77
5.22			
5.23	7.74	9.49	-39.31
5.24.1	38.07	-6.65	-64.01
5.24.2	17.25	-13.34	-97.41
5.9	9.49	13.53	-79.58
5.10.1	49.47	-20.76	-84.80
5.10.2	16.95	-23.83	-110.85
5.11	-13.43	-8.47	-85.73
5.12	26.50	-20.76	-84.80
5.13	27.80	-20.76	-84.80
5.2	-41.99	-36.44	-84.08

^a Energies relative to the energy of the starting structure **5.1**

^b Refers to the structure number in Figure 5.32

The energies in carbon tetrachloride: (ΔE) (in kcal mol^{-1}), enthalpy (ΔH) (in kcal mol^{-1}) and entropy (ΔS) ($\text{cal K}^{-1} \text{mol}^{-1}$) at 298.15 K

Table A3.30 Summary of energy, enthalpy and entropy in carbon tetrachloride for mechanism 3-route 2

Structure number ^a	Energies ^b (B3LYP/6-31+G(d))				
	Energy (E)		Enthalpy (H)		Entropy (S)
	Hartrees	kcal mol ⁻¹	Hartrees	kcal mol ⁻¹	cal K ⁻¹ mol ⁻¹
5.1	-575.6262	-361210.92	-575.4298	-361087.66	88.57
5.3.1	-668.5378	-419513.83	-668.3507	-419396.39	116.58
5.3.2	-745.4401	-467770.72	-745.2565	-467655.51	131.78
5.4	-669.0675	-419846.24	-668.8475	-419708.14	97.86
5.22					
5.23	-669.0652	-419844.75	-668.8453	-419706.81	98.32
5.24.1	-745.4234	-467760.29	-745.2537	-467653.76	117.82
5.24.2	-821.8836	-515739.77	-821.6665	-515603.56	129.55
5.9	-745.4894	-467801.65	-745.2411	-467645.87	103.18
5.10.1	-745.4053	-467748.90	-745.2762	-467667.87	97.03
5.10.2	-821.8841	-515740.07	-821.6833	-515614.05	116.12
5.11	-745.5259	-467824.58	-745.2762	-467667.87	97.03
5.12	-745.4419	-467771.86	-745.2762	-467667.87	97.03
5.13	-745.4398	-467770.57	-745.2762	-467667.87	97.03
5.2	-745.5510	-467840.36	-745.3012	-467683.55	97.75
HCN	-93.4309	-58628.79	-93.4111	-58616.35	48.12
H₂O	-76.4270	-47958.65	-76.4022	-47943.11	45.13
H₃O⁺	-76.7556	-48164.90	-76.7200	-48142.51	44.65
Na⁺	-162.1442	-101747.03	-162.1418	-101745.55	35.34
NaCN	-255.1686	-160120.72	-255.1575	-160113.74	60.38
NaOH	-238.1443	-149437.81	-238.1290	-149428.21	56.46

^a Refers to the structure number in Figure 5.32

^b Energies are expressed in Hartrees, kcal mol⁻¹ and cal K⁻¹ mol⁻¹, performed at the DFT level using the 6-31+G(d) level of theory

Table A3.31 Summary of the relative^a energy, enthalpy and entropy in dichloromethane for mechanism 3-route 2

Species ^b	$\Delta E / \text{kcal mol}^{-1}$	$\Delta H / \text{kcal mol}^{-1}$	$\Delta S / \text{cal K}^{-1} \text{mol}^{-1}$
5.1	0.00	0.00	0.00
5.3.1	39.79	39.49	-16.93
5.3.2	28.64	30.38	-67.38
5.4	9.34	11.25	-37.47
5.22			
5.23	10.71	12.34	-36.95
5.24.1	39.69	40.41	-75.75
5.24.2	21.11	0.63	-109.35
5.9	14.53	18.31	-77.21
5.10.1	53.08	-16.56	-84.36
5.10.2	22.41	-17.65	-109.35
5.11	-6.44	-1.43	-82.97
5.12	23.35	-16.56	-84.35
5.13	25.60	-16.56	-84.35
5.2	-38.09	-32.56	-83.53

^a Energies relative to the energy of the starting structure **5.1**

^b Refers to the structure number in Figure 5.32

The energies in dichloromethane: (ΔE) (in kcal mol^{-1}), enthalpy (ΔH) (in kcal mol^{-1}) and entropy (ΔS) ($\text{cal K}^{-1} \text{mol}^{-1}$) at 298.15 K

Table A3.32 Summary of energy, enthalpy and entropy in dichloromethane for mechanism 3-route 2

Structure number ^a	Energies ^b (B3LYP/6-31+G(d))				
	Energy (E)		Enthalpy (H)		Entropy (S)
	Hartrees	kcal mol ⁻¹	Hartrees	kcal mol ⁻¹	cal K ⁻¹ mol ⁻¹
5.1	-575.6306	-361213.64	-575.4345	-361090.61	88.48
5.3.1	-668.5695	-419533.74	-668.3660	-419405.99	96.84
5.3.2	-745.4511	-467777.64	-745.2078	-467625.00	114.33
5.4	-669.0753	-419851.09	-668.8557	-419713.31	97.70
5.22					
5.23	-669.0731	-419849.71	-668.8540	-419712.22	98.23
5.24.1	-745.4335	-467766.59	-745.1919	-467614.97	105.95
5.24.2	-821.8944	-515746.52	-821.6620	-515600.69	117.51
5.9	-745.4983	-467807.24	-745.2512	-467652.19	103.11
5.10.1	-745.4121	-467753.20	-745.2826	-467671.93	97.35
5.10.2	-821.8923	-515745.22	-821.6911	-515618.97	117.51
5.11	-745.5317	-467828.22	-745.2826	-467671.93	97.36
5.12	-745.4595	-467782.93	-745.2826	-467671.93	97.35
5.13	-745.4559	-467780.68	-745.2826	-467671.93	97.36
5.2	-745.5574	-467844.37	-745.3081	-467687.94	98.17
HCN	-93.4349	-58631.29	-93.4150	-58618.82	48.08
H₂O	-76.4313	-47961.35	-76.4067	-47945.94	45.15
H₃O⁺	-76.8067	-48196.90	-76.7712	-48174.68	46.85
Na⁺	-162.1832	-101771.52	-162.1809	-101770.04	35.34
NaCN	-255.1856	-160131.41	-255.1753	-160124.90	60.64
NaOH	-238.1573	-149445.98	-238.1429	-149436.90	59.09

^a Refers to the structure number in Figure 5.32

^b Energies are expressed in Hartrees, kcal mol⁻¹ and cal K⁻¹ mol⁻¹, performed at the DFT level using the 6-31+G(d) level of theory

REFERENCES

1. Nobelprize.org. **1998**; p. http://nobelprize.org/nobel_prizes/chemistry/laureates/1998/index.html, accessed 06/07/2009.
2. Dearing, A. *Journal of Computer-Aided Molecular Design* **1988**, 2, 179-189.
3. Foresman, J. B.; Frisch, A. *Exploring Chemistry with Electronic Structure Methods*, Second ed.; Gaussian, Inc.: Pittsburgh, PA, **1996**.
4. *HyperChem Computational Chemistry*; HyperCube, Inc.: Canada, 1996.
5. Sax, A. F. *Monatshefte für Chemie / Chemical Monthly* **2008**, 139, 299-308.
6. Tiwary, A. S.; Mukherjee, A. K. *Journal of Molecular Structure: THEOCHEM* **2009**, 909, 57-65.
7. Cookson, R. C.; Grundwell, W. H. *Indian Journal of Chemistry* **1958**, 1003-1004.
8. Darshan, R.; Haridas, V.; Madhusudanan, K. P.; Raja, R.; Nagaraj, R.; John, G. B.; Sukhaswami, M. B. *Angewandte Chemie International Edition in English* **1996**, 35, 1105-1107.
9. Griffin, G. W.; Marchand, A. P. *Chemical Reviews* **1989**, 89, 997-1010.
10. Marchand, A. P. *Advances in Theoretically Interesting Molecules*; JAI Press: Greenwich CT, **1989**.
11. Marchand, A. P. *Aldrichimica Acta* **1995**, 28, 95-104.
12. Marchand, A. P. *Chemical Reviews* **1989**, 89, 1011-1033.
13. Oliver, D. W.; Malan, S. F. *Medicinal Chemistry Research* **2008**, 17, 137-151.
14. Davies, W. L.; Grunert, R. R.; Haff, R. F.; McGahen, J. W.; Neumayer, E. M.; Paulshock, M.; Watts, J. C.; Wood, T. R.; Hermann, E. C.; Hoffman, C. E. *Science* **1964**, 144, 862-863.
15. James, B.; Viji, S.; Mathew, S.; Nair, M. S.; Lakshmanan, D.; Ajay Kumar, R. *Tetrahedron Letters* **2007**, 48, 6204-6208.
16. Schwab, R. S.; England, A. C., Jr.; Poskanzer, D. C.; Young, R. R. *JAMA* **1969**, 208, 1168-1170.
17. Neumeyer, J. L. *Principles of Medicinal Chemistry*; Lea and Febiger: London, **1989**.
18. Brookes, K. B.; Hickmott, P. W.; Jutle, K. K.; Schreyer, C. A. *South African Journal of Chemistry* **1992**, 45, 8-12.
19. Gerzon, K.; Kau, D. *Journal of Medicinal Chemistry* **1967**, 10, 189-199.
20. Rapala, R. T.; Kraay, R. J.; Gerzon, K. *Journal of Medicinal Chemistry* **1965**, 8, 580-583.
21. Voldeng, A. N.; Bradley, C. A.; Robert, D. K.; Eddie, L. K.; Fred, L. M. *Journal of Pharmaceutical Sciences* **1968**, 57, 1053-1055.

22. Aigami, K.; Inamoto, Y.; Takaishi, N.; Fujikura, Y.; Takatsuki, A.; Tamura, G. *Journal of Medicinal Chemistry* **1976**, *19*, 536-540.
23. Boeyens, J. C. A.; Cook, L. M.; Nelson, G. N.; Fourie, T. G. *South African Journal of Chemistry* **1994**, *47*, 72-5.
24. Inamoto, Y.; Aigami, K.; Kadono, T.; Nakayama, H.; Takatsuki, A.; Tamura, G. *Journal of Medicinal Chemistry* **1977**, *20*, 1371-1374.
25. Oliver, D. W.; Dekker, T. G.; Snyckers, F. O. *European Journal of Medicinal Chemistry* **1991**, *26*, 375-379.
26. Oliver, D. W.; Dekker, T. G.; Snyckers, F. O. *Arzneimittel-Forschung (Drug Research)* **1991**, *41*, 545-552.
27. Oliver, D. W.; Dekker, T. G.; Snyckers, F. O.; Fourie, T. G. *Journal of Medicinal Chemistry* **1994**, *34*, 851-854.
28. Cornelis, J. v. d. S.; Geldenhuys, W. J. *Neurotherapeutics: The Journal of the American Society for Experimental NeuroTherapeutics* **2009**, *6*, 175-186.
29. Kruger, H.; Mdluli, P. *Structural Chemistry* **2006**, *17*, 121-125.
30. Kruger, H. G.; Mdluli, P.; Power, T. D.; Raasch, T.; Singh, A. *Journal of Molecular Structure: THEOCHEM* **2006**, *771*, 165-170.
31. Onajole, O. K.; Govender, K.; Govender, P.; van Helden, P. D.; Kruger, H. G.; Maguire, G. E. M.; Muthusamy, K.; Pillay, M.; Wiid, I.; Govender, T. *European Journal of Medicinal Chemistry* **2009**, *44*, 4297-4305.
32. Onajole, O. K.; Govender, T.; Makatini, M.; Kruger, H. G. *Magnetic Resonance in Chemistry* **2008**, *46*, 1007-1014.
33. Marchand, A. P.; Allen, R. W. *The Journal of Organic Chemistry* **2002**, *39*, 1596-1596.
34. Martins, F. J. C.; Viljoen, A. M.; Kruger, H. G.; Joubert, J. A. *Tetrahedron* **1993**, *49*, 9573-9580.
35. Furniss, B. S.; Hannaford, A. J.; Smith, P. W. G.; Tatchell, A. R. *Vogel's Textbook of Practical Organic Chemistry*, 5th ed.; Longman Scientific & Technical: New York, **1989**.
36. Kruger, H. G.; Martins, F. J. C.; Viljoen, A. M.; Boeyens, J. C. A.; Cook, L. M.; Levendis, D. C. *Acta Crystallographica Section B* **1996**, *B52*, 838-841.
37. Martins, F. J. C.; Viljoen, A. M.; Kruger, H. G.; Joubert, J. A.; Wessels, P. L. *Tetrahedron* **1994**, *50*, 10783-10790.
38. Kruger, H. G. *Ph.D. Thesis, Synthesis of Pentacyclo Undecane Amino Acid Derivatives*, Potchefstroom University, **1996**.
39. Martins, F. J. C.; Viljoen, A. M.; Coetzee, M.; Fourie, L.; Wessels, L. P. *Tetrahedron*, **1991**, *47*, 9215-9224.
40. Singh, T. *MTech Thesis, Ab Initio Studies Of A Penta-Cyclo-Undecane Cage Lactam*; Durban University of Technology, **2003**.
41. Mebel, A. M.; Morokuma, K.; Lin, M. C. *The Journal of Chemical Physics* **1994**, *101*, 3916-3922.

42. Bauschlicher, C. W.; Partridge, H. *Chemical Physics Letters* **1995**, 239, 241-245.
43. Bauschlicher, J. C. W.; Partridge, H. *The Journal of Chemical Physics* **1995**, 103, 1788-1791.
44. Mebel, A. M.; Morokuma, K.; Lin, M. C. *The Journal of Chemical Physics* **1995**, 103, 7414-7421.
45. Becke, A. D. *The Journal of Chemical Physics* **1992**, 96, 2155-2160.
46. Becke, A. D. *The Journal of Chemical Physics* **1992**, 97, 9173-9177.
47. Becke, A. D. *The Journal of Chemical Physics* **1993**, 98, 5648-5652.
48. Lee, C.; Yang, W.; Parr, R. G. *Physical Review B* **1988**, 37, 785-789.
49. Truong, T. N.; Stefanovich, E. V. *Chemical Physics Letters* **1995**, 240, 253-260.
50. Cossi, M.; Barone, V.; Cammi, R.; Tomasi, J. *Chemical Physics Letters* **1996**, 255, 327-335.
51. Hehre, W. J.; Radom, L.; Schleyer, P. v. R.; Pople, J. A. *Ab Initio Molecular Orbital Theory*; John Wiley and Sons, New York, U.S.A., **1986**.
52. Hinchliffe, A. *Modeling Molecular Structure*; John Wiley & Sons, Ltd: Chichester, **1996**.
53. Hirst, D. M. *A Computational Approach to Chemistry*; Blackwell Scientific: Oxford, **1990**.
54. Schlick, T. *Molecular Modeling and Simulation: An Interdisciplinary Guide*; Springer-Verlag: New York, **2002**.
55. Hehre, W. J.; Yu, J.; Klunzinger, P. E.; Lou, L. *A Brief Guide to Molecular Mechanics and Quantum Chemical Calculations*; Wavefunction, Inc., Irvine, California, U.S.A, **1998**.
56. Cramer, C. J. *Essentials of Computational Chemistry Theories and Models*, Second ed.; John Wiley & Sons: Chichester, **2004**.
57. Jensen, F. *Introduction to Computational Chemistry* Second ed.; John Wiley and Sons, Chichester, United Kingdom, **2007**.
58. Hückel, E. *Zeitschrift für Physik A Hadrons and Nuclei* **1931**, 72, 310-337.
59. Hückel, E. *Zeitschrift für Physik A Hadrons and Nuclei* **1932**, 76, 628-648.
60. Hückel, E. *Zeitschrift für Physik A Hadrons and Nuclei* **1933**, 83, 632-668.
61. Hoffmann, R. *The Journal of Chemical Physics* **1963**, 39, 1397-1412.
62. Pariser, R.; Parr, R. G. *The Journal of Chemical Physics* **1953**, 21, 466-471.
63. Pople, J. A. *Transactions of the Faraday Society* **1953**, 49, 1375-1385.
64. Jensen, F. *Journal of the American Chemical Society* **1991**, 114, 1596-1603.
65. Jensen, F. *Journal of Computational Chemistry* **1994**, 15, 1199-1216.
66. Eksterowicz, J. E.; Houk, K. N. *Chemical Reviews* **1993**, 93, 2439-2461.

67. Jensen, F.; Norrby, P.-O. *Theoretical Chemistry Accounts: Theory, Computation, and Modeling (Theoretica Chimica Acta)* **2003**, *109*, 1-7.
68. Maragakis, P.; Andreev, S. A.; Brumer, Y.; Reichman, D. R.; Kaxiras, E. *The Journal of Chemical Physics* **2002**, *117*, 4651-4658.
69. Govind, N.; Petersen, M.; Fitzgerald, G.; King-Smith, D.; Andzelm, J. *Computational Materials Science* **2003**, *28*, 250-258.
70. Lee, D.; Lee, J.; Yoon, Y.-G. *Computer Physics Communications* **2007**, *177*, 218-218.
71. Born, M.; Oppenheimer, R. *Annalen der Physik* **1927**, *389*, 457-484.
72. Leach, A. R. *Molecular Modeling: Principles and Applications*; Addison Wesley Longman Limited: Harlow, **1996**.
73. Roothaan, C. C. J. *Reviews of Modern Physics* **1951**, *23*, 69-89.
74. Hall, G. G. *Proceedings of the Royal Society* **1951**, *A205*, 541-552.
75. Hinchliffe, A. *Chemical Modeling From Atoms to Liquids*; John Wiley & Sons, Ltd.: Chichester, **1999**.
76. Hohenberg, P.; Kohn, W. *Physical Review* **1964**, *136*, B864-B871.
77. Kohn, W.; Sham, L. J. *Physical Review* **1965**, *140*, A1133-A1138.
78. Becke, A. D. *Physical Review A* **1988**, *38*, 3098-3100.
79. Perdew, J. P. In *Electronic Structure of Solids 1991*; Ziesche, P.; Eschrig, H. Eds.; Akademie Verlag, Berlin **1991**.
80. Perdew, J. P.; Chevary, J. A.; Vosko, S. H.; Jackson, K. A.; Pederson, M. R.; Singh, D. J.; Fiolhais, C. *Physical Review B* **1992**, *46*, 6671-6687.
81. Perdew, J. P.; Chevary, J. A.; Vosko, S. H.; Jackson, K. A.; Pederson, M. R.; Singh, D. J.; Fiolhais, C. *Physical Review B* **1993**, *48*, 4978-4978.
82. Perdew, J. P.; Burke, K.; Wang, Y. *Physical Review B* **1996**, *54*, 16533-16539.
83. Burke, K.; Perdew, J. P.; Wang, Y. In *Electronic Density Functional Theory: Recent Progress and New Directions*; Dobson, J. F.; Vignale, G.; Das, M. P. Eds.; Plenum, New York, **1998**.
84. Adamo, C.; Barone, V. *Journal of Computational Chemistry* **1998**, *19*, 418-429.
85. Vosko, S. H.; Wilk, L.; Nusair, M. *Canadian Journal of Physics* **1980**, *58*, 1200-1211.
86. Perdew, J. P. *Physical Review B* **1986**, *33*, 8822-8824.
87. Perdew, J. P.; Burke, K.; Ernzerhof, M. *Physical Review Letters* **1996**, *77*, 3865-3868.
88. Perdew, J. P.; Burke, K.; Ernzerhof, M. *Physical Review Letters* **1997**, *78*, 1396-1396.
89. Becke, A. D. *Journal of Chemical Physics* **1993**, *98*, 5648-5652.
90. Becke, A. D. *Journal of Chemical Physics* **1996**, *104*, 1040-1046.

91. Meijer, E. J.; Sprik, M. *The Journal of Chemical Physics* **1996**, *105*, 8684-8689.
92. Cybulski, S. M.; Seversen, C. E. *The Journal of Chemical Physics* **2005**, *122*, 014117-9.
93. Rienstra-Kiracofe, J. C.; Tschumper, G. S.; Schaefer, H. F.; Nandi, S.; Ellison, G. B. *Chemical Reviews* **2002**, *102*, 231-282.
94. Gritsenko, O. V.; Ensing, B.; Schipper, P. R. T.; Baerends, E. J. *The Journal of Physical Chemistry A* **2000**, *104*, 8558-8565.
95. Møller, C.; Plesset, M. S. *Physical Review* **1934**, *46*, 618-622.
96. Abraham, L., **2004**; p. <http://www.lukeabraham.com/ga/downloads.html#thesis>, accessed 23/09/2009.
97. Wikipedia.org. **2009**; p. http://en.wikipedia.org/wiki/Transition_state_theory, accessed 24/09/2009.
98. Young, D., 2009; pp. <http://www.ccl.net/ccs/documents/dyoung/topics-orig/ts.html>, accessed 31/03/2009.
99. Clark, T. *A Handbook of Computational Chemistry*; John Wiley and Sons: New York, **1985**.
100. Frisch, M. J.; Trucks, G. W.; Schlegel, H. B.; Scuseria, G. E.; Robb, M. A.; Cheeseman, J. R.; Scalmani, G.; Barone, V.; Mennucci, B.; Petersson, G. A.; Nakatsuji, H.; Caricato, M.; Li, X.; Hratchian, H. P.; Izmaylov, A. F.; Bloino, J.; Zheng, G.; Sonnenberg, J. L.; Hada, M.; Ehara, M.; Toyota, K.; Fukuda, R.; Hasegawa, J.; Ishida, M.; Nakajima, T.; Honda, Y.; Kitao, O.; Nakai, H.; Vreven, T.; J. A. Montgomery, J.; Peralta, J. E.; Ogliaro, F.; Bearpark, M.; Heyd, J. J.; Brothers, E.; Kudin, K. N.; Staroverov, V. N.; Kobayashi, R.; Normand, J.; Raghavachari, K.; Rendell, A.; Burant, J. C.; Iyengar, S. S.; Tomasi, J.; Cossi, M.; Rega, N.; Millam, J. M.; Klene, M.; Knox, J. E.; Cross, J. B.; Bakken, V.; Adamo, C.; Jaramillo, J.; Gomperts, R.; Stratmann, R. E.; Yazyev, O.; Austin, A. J.; Cammi, R.; Pomelli, C.; Ochterski, J. W.; Martin, R. L.; Morokuma, K.; Zakrzewski, V. G.; Voth, G. A.; Salvador, P.; Dannenberg, J. J.; Dapprich, S.; Daniels, A. D.; Farkas, O.; Foresman, J. B.; Ortiz, J. V.; Cioslowski, J.; Fox, D. J. In *Gaussian 09*; Gaussian, Inc.: Wallingford CT, **2009**.
101. Frisch, A.; Frisch, M. J. *Gaussian 03 User's Reference*; Gaussian Inc.: Pittsburgh, PA, **2004**.
102. Labanowski, J. K.; Andzelm, J. W. *Density Functional Methods in Chemistry*; Springer-Verlag: New York, **1991**.
103. Parr, R. G.; Yang, W. *Density Functional Theory of Atoms and Molecules*; Oxford University Press: New York, **1989**.
104. Seminario, J. M.; Politzer, P. *Modern Density Functional Theory: A Tool for Chemistry*; Elsevier: Amsterdam, **1995**.
105. Ziegler, T. *Chemical Reviews* **2002**, *91*, 651-667.
106. Dunlap, B. I.; Andzelm, J. *Physical Review A* **1992**, *45*, 81-87.

107. Handy, N. C.; Tozer, D. J.; Laming, G. J.; Murray, C. W.; Amos, R. D. *Israel Journal of Chemistry* **1993**, 331-334.
108. Johnson, B. G.; Frisch, M. J. *The Journal of Chemical Physics* **1994**, *100*, 7429-7442.
109. Komornicki, A.; Fitzgerald, G. *The Journal of Chemical Physics* **1993**, *98*, 1398-1421.
110. Andzelm, J.; Wimmer, E. *The Journal of Chemical Physics* **1992**, *96*, 1280-1303.
111. Finley, J. W.; Stephens, P. J. *Journal of Molecular Structure: THEOCHEM* **1995**, *357*, 225-235.
112. Handy, N. C.; Murray, C. W.; Amos, R. D. *The Journal of Physical Chemistry* **2002**, *97*, 4392-4396.
113. Johnson, B. G.; Gill, P. M. W.; Pople, J. A. *The Journal of Chemical Physics* **1993**, *98*, 5612-5626.
114. Rauhut, G.; Pulay, P. *The Journal of Physical Chemistry* **2002**, *99*, 3093-3100.
115. Stephens, P. J.; Devlin, F. J.; Chabalowski, C. F.; Frisch, M. J. *The Journal of Physical Chemistry* **2002**, *98*, 11623-11627.
116. Wong, M. W. *Chemical Physics Letters* **1996**, *256*, 391-399.
117. Ochterski, J. W. In http://www.gaussian.com/g_whitepap/thermo.htm; Gaussian, Inc.: Wallingford CT, **2000**, accessed 29/10/2009.
118. Fabian, W. M. F. *Monatshefte für Chemie / Chemical Monthly* **2008**, *139*, 309-318.
119. Curtiss, L. A.; Raghavachari, K. *Theoretical Chemistry Accounts: Theory, Computation, and Modeling (Theoretica Chimica Acta)* **2002**, *108*, 61-70.
120. Coutinho, K.; Canuto, S. *The Journal of Chemical Physics* **2000**, *113*, 9132-9139.
121. Mennucci, B.; Martinez, J. M.; Tomasi, J. *The Journal of Physical Chemistry A* **2001**, *105*, 7287-7296.
122. Zeng, J.; Craw, J. S.; Hush, N. S.; Reimers, J. R. *The Journal of Chemical Physics* **1993**, *99*, 1482-1495.
123. Zeng, J.; Hush, N. S.; Reimers, J. R. *The Journal of Chemical Physics* **1993**, *99*, 1508-1521.
124. Zeng, J.; Woywod, C.; Hush, N. S.; Reimers, J. R. *Journal of the American Chemical Society* **2002**, *117*, 8618-8626.
125. Chesnut, D. B.; Rusiloski, B. E. *Journal of Molecular Structure: THEOCHEM* **1994**, *314*, 19-30.
126. Pecul, M.; Sadlej, J. *Chemical Physics* **1998**, *234*, 111-119.
127. Cramer, C. J.; Truhlar, D. G. *Chemical Reviews* **1999**, *99*, 2161-2200.
128. Dolney, D. M.; Hawkins, G. D.; Winget, P.; Liotard, D. A.; Cramer, C. J.; Truhlar, D. G. *Journal of Computational Chemistry* **2000**, *21*, 340-366.

129. Li, J.; Zhu, T.; Cramer, C. J.; Truhlar, D. G. *The Journal of Physical Chemistry A* **1999**, *104*, 2178-2182.
130. Tomasi, J.; Persico, M. *Chemical Reviews* **1994**, *94*, 2027-2094.
131. Arroyo, S. T.; Martín, J. A. S.; García, A. H. *Journal of Solution Chemistry* **2005**, *34*, 407-414.
132. Pomelli, C. S.; Tomasi, J. *Journal of Molecular Structure: THEOCHEM* **2001**, *537*, 97-105.
133. Onsager, L. *Journal of the American Chemical Society* **1936**, *58*, 1486-1493.
134. Rinaldi, D.; Rivail, J.-L. *Theoretical Chemistry Accounts: Theory, Computation, and Modeling (Theoretica Chimica Acta)* **1973**, *32*, 57-70.
135. Kirkwood, J. G. *The Journal of Chemical Physics* **1934**, *2*, 351-361.
136. Kirkwood, J. G.; Westheimer, F. H. *The Journal of Chemical Physics* **1938**, *6*, 506-512.
137. Tomasi, J.; Persico, M. *Chemical Reviews* **2002**, *94*, 2027-2094.
138. Tomasi, J.; Mennucci, B.; Cammi, R. *Chemical Reviews* **2005**, *105*, 2999-3094.
139. Pomelli, C. S.; Tomasi, J.; Barone, V. *Theoretical Chemistry Accounts: Theory, Computation, and Modeling (Theoretica Chimica Acta)* **2001**, *105*, 446-451.
140. Dillet, V.; Rinaldi, D.; Rivail, J.-L. *The Journal of Physical Chemistry* **1994**, *98*, 5034-5039.
141. Karelson, M. M.; Katritzky, A. R.; Zerner, M. C. *International Journal of Quantum Chemistry* **1986**, *30*, 521-527.
142. Rinaldi, D.; Ruiz-Lopez, M. F.; Rivail, J.-L. *The Journal of Chemical Physics* **1983**, *78*, 834-838.
143. Rivail, J.-L.; Rinaldi, D. *Chemical Physics* **1976**, *18*, 233-242.
144. Tapia, O.; Goscinski, O. *Molecular Physics: An International Journal at the Interface Between Chemistry and Physics* **1975**, *29*, 1653 - 1661.
145. Wong, M. W.; Frisch, M. J.; Wiberg, K. B. *Journal of the American Chemical Society* **1991**, *113*, 4776-4782.
146. Yomosa, S. *Journal of the Physical Society of Japan* **1974**, *36*, 1655-1660.
147. Lu, T. X.; Bacskey, G. B.; Haymet, A. D. J. In *Molecular Physics*; Taylor & Francis Ltd, **1996**; pp. 173-185.
148. Mierts, S.; Scrocco, E.; Tomasi, J. *Chemical Physics* **1981**, *55*, 117-129.
149. Leopoldini, M.; Marino, T.; Michelini, M.; Rivalta, I.; Russo, N.; Sicilia, E.; Toscano, M. *Theoretical Chemistry Accounts: Theory, Computation, and Modeling (Theoretica Chimica Acta)* **2007**, *117*, 765-779.
150. Scalmani, G.; Barone, V.; Kudin, K. N.; Pomelli, C. S.; Scuseria, G. E.; Frisch, M. J. *Theoretical Chemistry Accounts: Theory, Computation, and Modeling (Theoretica Chimica Acta)* **2004**, *111*, 90-100.

151. Tunon, I.; Ruiz-Lopez, M. F.; Rinaldi, D.; Bertran, J. *Journal of Computational Chemistry* **1996**, *17*, 148-155.
152. Alemán, C.; Galembeck, S. E. *Chemical Physics* **1998**, *232*, 151-159.
153. Jezierska, A.; Panek, J.; Ryng, S. *Journal of Molecular Structure: THEOCHEM* **2003**, *636*, 203-214.
154. Wong, M. W.; Wiberg, K. B.; Frisch, M. J. *Journal of the American Chemical Society* **1992**, *114*, 523-529.
155. Wang, Y.; Cheng, X.; Yang, X.; Yang, X. *Journal of Solution Chemistry* **2006**, *35*, 869-878.
156. Mikkelsen, K. V.; Cesar, A.; Agren, H.; Jensen, H. J. A. *The Journal of Chemical Physics* **1995**, *103*, 9010-9023.
157. Tomasi, J.; Mennucci, B.; Cancès, E. *Journal of Molecular Structure: THEOCHEM* **1999**, *464*, 211-226.
158. De Angelis, F.; Sgamellotti, A.; Cossi, M.; Rega, N.; Barone, V. *Chemical Physics Letters* **2000**, *328*, 302-309.
159. Mennucci, B. *Theoretical Chemistry Accounts: Theory, Computation, and Modeling (Theoretica Chimica Acta)* **2006**, *116*, 31-42.
160. Tomasi, J. *Theoretical Chemistry Accounts: Theory, Computation, and Modeling (Theoretica Chimica Acta)* **2004**, *112*, 184-203.
161. Frisch, M. J.; Trucks, G. W.; Schlegel, H. B.; Scuseria, G. E.; Robb, M. A.; Cheeseman, J. R.; J. A. Montgomery, J.; Vreven, T.; Kudin, K. N.; Burant, J. C.; Millam, J. M.; Iyengar, S. S.; Tomasi, J.; Barone, V.; Mennucci, B.; Cossi, M.; Scalmani, G.; Rega, N.; Petersson, G. A.; Nakatsuji, H.; Hada, M.; Ehara, M.; Toyota, K.; Fukuda, R.; Hasegawa, J.; Ishida, M.; Nakajima, T.; Honda, Y.; Kitao, O.; Nakai, H.; Klene, M.; Li, X.; Knox, J. E.; Hratchian, H. P.; Cross, J. B.; Adamo, C.; Jaramillo, J.; Gomperts, R.; Stratmann, R. E.; Yazyev, O.; Austin, A. J.; Cammi, R.; Pomelli, C.; Ochterski, J. W.; Ayala, P. Y.; Morokuma, K.; Voth, G. A.; Salvador, P.; Dannenberg, J. J.; Zakrzewski, V. G.; Dapprich, S.; Daniels, A. D.; Strain, M. C.; Farkas, O.; Malick, D. K.; Rabuck, A. D.; Raghavachari, K.; Foresman, J. B.; Ortiz, J. V.; Cui, Q.; Baboul, A. G.; Clifford, S.; Cioslowski, J.; Stefanov, B. B.; Liu, G.; Liashenko, A.; Piskorz, P.; Komaromi, I.; Martin, R. L.; Fox, D. J.; Keith, T.; Al-Laham, M. A.; Peng, C. Y.; Nanayakkara, A.; Challacombe, M.; Gill, P. M. W.; Johnson, B.; Chen, W.; Wong, M. W.; Gonzalez, C.; Pople, J. A. In *Gaussian 03*; Gaussian, Inc.: Wallingford CT, **2004**.
162. Dennington, R.; Keith, T.; Millam, J. In *GaussView*; Semichem Inc.: Shawnee Mission KS, **2009**.
163. Brooks, L.; Karplus, M.; Pettitt, B. M. In *Advances in Chemical Physics*; Progonine, I.; Rice, S. A. Eds.; John Wiley and Sons: New York, **1985**.
164. Lybrand, T. P. In *Reviews in Computational Chemistry*; Lipkowitz, K. B.; Boyd, D. B. Eds.; VCH Publishers, Inc.: New York, USA, **1990**.
165. Scalmani, G.; Frisch, M. J. *The Journal of Chemical Physics* **2010**, *132*, 114110-15.

166. Marenich, A. V.; Cramer, C. J.; Truhlar, D. G. *The Journal of Physical Chemistry B* **2009**, *113*, 6378-6396.
167. Raghavachari, K. *Theoretical Chemistry Accounts: Theory, Computation, and Modeling (Theoretica Chimica Acta)* **2000**, *103*, 361-363.
168. Gokul, V.; Kruger, H. G.; Govender, T.; Fourie, L.; Power, T. D. *Journal of Molecular Structure: THEOCHEM* **2004**, *672*, 119-125.
169. Power, T. D.; Sebastian, J. F. *Tetrahedron* **1998**, *54*, 8371-8392.
170. Miehlisch, B.; Savin, A.; Stoll, H.; Preuss, H. *Chemical Physics Letters* **1989**, *157*, 200-206.
171. Wikipedia.org. **2010**; p. <http://en.wikipedia.org/wiki/Amphiphile>, accessed 11/01/2011.
172. Wikipedia.org. **2011**; p. http://en.wikipedia.org/wiki/Gibbs_free_energy, accessed 10/01/2011.
173. Wikipedia.org. **2011**; p. <http://en.wikipedia.org/wiki/Solvation>, 10/01/2011.